Optically Active Dopants to Understand the Bulk and Surface Electronic Structure of II-VI Semiconductor Quantum Dots and their Heterostructures

A Thesis
Submitted for the Degree of
Doctor of Philosophy

by

G Krishna Murthy Grandhi

New Chemistry Unit
Jawaharlal Nehru Centre for Advanced Scientific Research
(A Deemed University)
Bangalore – 560064

December 2016

Dedicated to

My Parents, Family
&
My teacher Mr. K. Rama Krishna

DECLARATION

I hereby declare that the matter embodied in this thesis entitled "**Optically Active Dopants to Understand the Bulk and Surface Electronic Structure of II-VI Semiconductor Quantum Dots and their Heterostructures"** is the result of the research carried out by me at the New Chemistry Unit, Jawaharlal Nehru Centre for Advanced Scientific Research, Bangalore, India, under the supervision of Dr. Ranjani Viswanatha and it has not been submitted elsewhere for the award of any degree or diploma.

In keeping with the general practices of reporting scientific observation, due acknowledgements have been made whenever the work described is based on the findings of other investigators. Any omission which might have occurred by oversight or error in judgement is regretted.

Bangalore

……

G Krishna Murthy Grandhi

CERTIFICATE

I hereby certify that the matter embodied in this thesis entitled **"Optically Active Dopants to Understand the Bulk and Surface Electronic Structure of II-VI Semiconductor Quantum Dots and their Heterostructures"** has been carried out by Mr. G Krishna Murthy Grandhi at the New Chemistry Unit, Jawaharlal Nehru Centre for Advanced Scientific Research, Bangalore, India under my supervision and that has not been submitted elsewhere for the award of any degree or diploma.

Bangalore _____

Dr. Ranjani Viswanatha

(Research Supervisor)

Acknowledgements

First and foremost, I wish to express my sincere gratitude to my research supervisor Dr. Ranjani Viswanatha for her kind support, guidance, suggestions and invaluable encouragement that she has given to me all through the course of this investigation. I shall remain ever thankful to her for giving me enough freedom to work on various projects.

I thank Prof. C. N. R. Rao FRS, who has been a constant source of inspiration for me. I would also like to thank him as the chairman of our department (NCU) for allowing me to use the facilities in the department.

I would like to thank my collaborators K. Swathi and Prof. K. S. Narayan, CPMU, JNCASR. I thank Renu Tomar, Mahesh Krishna and Arunkumar from our lab. I thank Mr. Krishnachary Salikolimi and Prof. M. Eswaramoorthy for zeta potential measurements and Mr. K. Rajsekhar, Dr. Ramana Reddy and Mr. Ch. Arjun for their help in performing NMR measurements.

I would like to thank Department of Science and Technology (DST), International Centre for Materials Science (ICMS), Sheikh Saqr Laboratory (SSL) and JNCASR for research funding and Council of Scientific and Industrial Research (CSIR)-India for research fellowship.

I am thankful to Dr. Ranjani Viswanatha, Dr. Sebastian Peter, Prof. A. Sundaresan, Dr. Ujjal K. Gautam, Prof. T. K. Maji, Prof. Subi J. George and Prof. T. Govindaraju for their excellent courses that have been extremely helpful to this study.

I thank the timely help of technical staff namely Mr. Kannan (TEM), Mr. Karthik (TEM), Dr. Jay (TEM), Mrs. Usha (TEM), Mr. Vasu (ICP-OES and IR), Mr. Mahesh (NMR), Mr. Shiva Kumar (Absorption spectroscopy), Mr. Anil (PXRD), Mr. Peer, Mr. Mune Gowda, Mr. Naveen, Swetha and Mr. Dileep (Audio/Visual).

I am grateful to all my present and past lab mates Avijit, Suguna, Renu, Pallabi, Kushagra, Mahima, Pradeep, Amitha, Mahesh, Felix and Anur who created a wonderful working environment in the lab. I have gained a lot of scientific knowledge during the discussions with them. I thank the summer students Sai, Namitha, Ritika, Arunkumar and Raihanath for their valuable contribution to my work.

I thank Administrative staff, hostel staff, mess workers, housekeeping staff and security for providing and maintaining the various facilities that have been helped me immensely during my stay in JNCASR.

It is a pleasure to thank all my JNCASR friends Lingampalli, Shashi, Rajasekhar, Pandu, Arjun, Shivaprasad, Ramana, Pramoda, Yugandar, Vijay Simha, Manjusha and many more for their support in my Ph.D. life in JNCASR. I thank my JNCASR badminton friends (Venky, Diwakar, Suresh, Avijit, Malli, Avinash, Ravishankar, Umesh, Suseela, Manoj, Rajendar and many more) and Cricket friends (Rules Nagarjuna, Jiaul, Prem, Shiva, Deena, Matte, Narendra, Jayaram and many more). I thank Sravan and Suresh from IISc.

I would like to take this opportunity to thank my friends Madhu, Satyanarayana, Gurivi Reddy, Satish, Subramanyam, Krishna Chaitanya, Arun, Ravi and many more from M.Sc. (UoH) and Mallikarjun, Shyam, Jagadeesh, Shyam, Madhu, Konda and Vijay from my home town and all my school and college friends (Chaitanya, Kumaraswamy, Ravi, Suresh, Rajesh, Kasu, Durgas, Praveens, Mallik and many more). I thank all my well-wishers and those who have helped me directly or indirectly.

I also thank all my school and college teachers. I am highly indebted to my college teacher Mr. K. Ramakrishna who helped me a lot during college days and also without whom I would have not come this far. I thank my parents and family members from bottom of my heart for their love, blessings and affection on me. This thesis is a minor recognition to my parents and my sisters, Vasavi and Kalyani for their love and constant support throughout my career.

PREFACE

Transition metal dopants (e.g., Mn, Cu, Ni ions, etc.) introduce atomic states between the conduction band and valence band of host quantum dots. Cu doping was also well studied in the literature due to its interesting optical properties like the tunability of the Cu emission with the band gap variation. In this thesis, we have used this emission to study the bulk and surface electronic structure of quantum dots.

Chapter 1 discusses an overview of doping in quantum dots and different optical dopants that were reported in the literature. The literature pertaining to mechanism of the Cu emission in quantum dots, the oxidation state of the Cu has been discussed. The relation of Cu emission to the surface and bulk electronic structure are then deliberated.

In Chapter 2, we discuss the challenges involved in synthesizing Cu doped quantum dots and the generic synthesis procedures that were used during the work reported in this thesis. The procedures were mostly modified from the well-established literature reports of the synthesis of undoped quantum dots. The characterization techniques used in this thesis are also discussed.

Part I. Study of Bulk Electronic Structure Using Cu Emission: Quantum dot based solar cells and light emitting diodes involve charge transfer or charge extraction from the quantum dot material. The knowledge of their absolute band edge positions is necessary in making them more efficient for these applications. Apart from theoretical studies, a few experimental techniques like scanning tunneling spectroscopy, photo electron spectroscopy and cyclic voltammetry were used for this finding. However, they have limitations in determining the band edge variation and also require sophisticated instrumentation. Here, we study the bulk electronic structure of II-VI semiconductor quantum dots simply using Cu emission which involves a radiative recombination of the electron in conduction band with the hole present in the Cu d-state. This study is discussed in the next three chapters.

Chapter 3 involves determination of the variation of conduction band and valence band in II-VI semiconductor quantum dots as a function of size using Cu emission. We determined the relative band alignment of II-VI semiconductors as a function of size in the quantum confined

regime. Our experimental results are in good agreement with the theoretical data and other existing experimental data.

Chapter 4 deals with the internal structure of heterostructures. Central to the success of these materials for optoelectronic is the understanding of the photo-generated charge carrier localization. In spite of the theoretically expected prediction of the band edges of alloy or core/shell with a type I or type II structure, the actual location of the charges are often quite different leading to sub-optimal results. In this work, we have used Cu doping and its corresponding photoluminescence to differentiate an alloy from the core/shell structure. We have also studied the charge localization and the adeptness of this method has been assessed over a range of widely studied heterostructures. The electron and hole localization obtained from this method concurs with the pre-existing understanding in these well studied systems. We have also extended this method to obtain the internal structure in previously unknown heterostructures proving the usefulness of this method.

In **Chapter 5,** we have studied the temperature dependent band edge variation of II-VI quantum dots of different sizes. We have fit their band gap variation to Bose-Einstein model to obtain average energy of phonons that contribute to this shift. We have compared the variation of average phonon energy for CdS quantum dots with that of CdSe quantum dots. The band edge variation is characterized by a dominant CB shift for larger sizes with decreasing temperature while the smaller size QDs show the variation in both CB and VB. We have also studied the binding energy of the trap states as a function of temperature using Cu PL QY and average lifetime of Cu PL.

Part II. Study of Surface Electronic Structure Using Cu Emission: The surface capping ligands present around the quantum dots affect their photoluminescence efficiency. However, the role of ligand passivation is not clearly understood so far. Here, the combination of steady state and time dependent Cu emission is utilized to study the surface electronic structure of II-VI semiconductor quantum dots. As the intensity of Cu emission increases in presence of hole traps, the ratio of Cu emission to band edge emission indicates the extent of hole traps present on the quantum dot surface. Since only the photo-generated electron but not the photo-generated hole is involved in Cu emission, the non-radiative (fast) component present in the

time-dependent photoluminescence decay curve indicates the extent of electron traps present on the quantum dot surface. This is discussed in the next two chapters.

In **Chapter 6,** we study the role of commonly used ligands such as trioctylphosphine, trioctylphosphine oxide, oleic acid, dodecanethiol, 3-mercaptopropionic acid, primary amines and oleylamine in passivating II-VI semiconductor quantum dots. The role of ligands was studied during the synthesis, as well as during specific phase transfer and pyridine exchange based ligand exchange procedures. This study was utilized to plan a synthesis of highly emitting CdSe quantum dots leading to a substantial increase in the quantum yield.

Chapter 7 discusses the role of sulfide ions in passivating CdS quantum dots is studied. They passivate electron traps but trap the photo-generated hole. They have shown the conductivity of ~ 10^{-4} S cm^{-1}. The conductance behavior of these quantum dots is correlated to their surface trap states. Cu emission is used to optimize the concentration of sulfide ligands to obtain maximum conductivity for these quantum dots.

Chapter 8 discusses the applications based on Cu doped quantum dots that have not been previously studied. This is discussed in the two sections.

Section 1. NIR Phosphors: Cu doped quantum dots show tunable emission with Cu emission maxima varying from 1.9 eV to 1.35 eV. They exhibit high photoluminescence quantum yields of 25 % to 35% in NIR region and longer photoluminescence decay values of ~ 1 μs. They exhibit high thermal stability up to 100 ^{o}C in both solution and as film. The combination of all these properties makes Cu doped CdS quantum dots a NIR emitting phosphor material.

Section 2. Visible Photo-detectors: On doping Fe in Cu doped ZnS quantum dots they exhibit a broad absorption band in visible region. The doping in these quantum dots is shown to have a high photo-response in the visible region unlike their undoped counterparts that is only effective in the ultra-violet region.

TABLE OF CONTENTS

ABBREVATIONS

CB=conduction band

DDT= dodecane thiol

EPR= electron paramagnetic resonance

Fwhm= full width half maximum

ICP-OES= Inductively coupled plasma-optical emission spectroscopy

MCD= Magnetic circular dichroism

MPA=3-mercaptopropionic acid

NMR= Nuclear Magnetic Resonance

ODE=1-octadecene

PGE= photo-generated electron

PGH= photo-generated hole

PL= photoluminescence

QD= quantum dot

QY=quantum yield

SAED= Selected area electron diffraction

SILAR= successive ionic layer and adsorption reaction

TB=tight-binding

TEM= Transmission electron microscopy

TMAH= Tetramethyl ammonium hydroxide pentahyrate

TMS=tertamethylsilane

TOP= trioctylphosphine

TOPO= trioctylphosphine oxide

TPP=triphenylphosphine

TrPL=time-resolved photoluminescence

UV=ultra-violet

VB=valence band

XRD= X-ray Diffraction

Chapter 1

Introduction

Quantum dots (QDs) cover a broad and interdisciplinary area of research that has been growing rapidly worldwide in the past few decades. QDs have the potential for revolutionizing the ways in which materials and products are created and the range and nature of functionalities that can be accessed. They are already having a significant commercial impact, which will further increase in the future. QDs have extremely small size which is about 10 nm or less. Owing to their interesting characteristics, these materials find a lot of applications in many fields such as optoelectronics,[1-6] biology[7, 8] and so on. QDs have been engineered to have a quantum efficiency of radiative recombination approaching unity at room temperature, far above what has been achieved from bulk materials.[9, 10]

QD consists of a surface portion and a bulk portion. The surface-ligand chemistry of QD is known as surface electronic structure and the energy levels of QD is called bulk electronic structure. It is important to understand the both the bulk and surface electronic structure of QDs in designing them for efficient applications where both the surface-ligand chemistry and the absolute positions of CB and VB play a major role.

1.1. Electronic structure of QDs:

This section is divided into three sub-sections. The size dependent optical properties and the surface properties of the QDs will be discussed in the first two sub-sections. In the last sub-section, the other ways of improving the properties of QDs, the hetero structures will be discussed.

1.1.1. Tunability of optical spectra:

The exciton has a finite size within the crystal which is defined the Bohr exciton radius (a_B), which is a material specific property and can vary from 1 nm to about 10 nm. If the size of a semiconductor material is less than the size of the exciton, the photo-generated charge carriers become spatially confined, which increases their band gap. These QDs form a bridge between the bulk semiconductors and their molecular analogues as shown in Figure 1.1(a). In this size regime, the particles show size dependent optical properties.[11-13] For example, CdSe QDs (Eg= 1.76 eV, a_B = 9.6 nm) can emit fluorescent light throughout the visible spectrum with changing their size as shown in Figure 1.1(c).

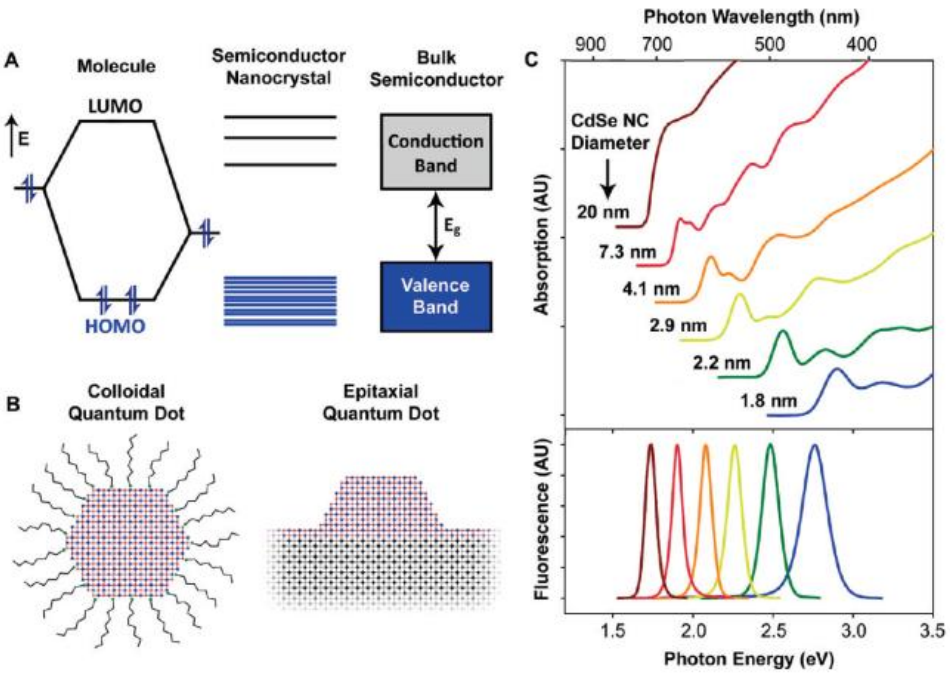

Figure 1.1. (a) *Electronic energy states of a semiconductor in the transition from discrete molecules to nano-sized crystals and bulk crystals. Blue shading denotes ground state electron occupation.* ***(b)*** *Comparison of a colloidal QD and an island like, self-assembled QD epitaxially deposited on a crystalline substrate.* ***(c)*** *Absorption (upper) and fluorescence (lower) spectra of CdSe semiconductor QDs showing size tunability. Reprinted with permission from ref [13]Copyright 2010 American Chemical Society.*

The emission properties of the QDs are strongly dependent on their surface chemistry. This makes the study of QD surface very interesting and challenging.

1.1.2. Surface properties of QDs:

The dependence of optical properties on particle size is largely a result of the internal structure of the QD. Usually, smaller QDs results in a very high surface to volume ratio. The atoms on the surface of a crystal facet are incompletely bonded within the crystal lattice, thus and leaving one or more "dangling orbital" on every atom pointed out away from the surface of QD. Most QDs are highly faceted (Figure 1.2(b)), and each surface facet contain unpassivated orbitals.[14, 15] Usually these surface energy states are within the semiconductor band gap and hence can trap charge carriers at the surface, thereby reducing the overlap between the electron and hole, increasing the probability of nonradiative decay events. In order to avoid non-radiative pathways, the surface of the QDs are usually protected by passivating ligands. to minimize surface trap states. Molecules such as oleic acid, TOP, TOPO and primary amines bind to the QD surface through ligand-metal

bonds between the basic moiety on the ligand and metal atoms on the QD surface. It gives colloidal stability to the QDs in nonpolar solvents through hydrophobic interactions with the alkyl chains on the ligands.[16] Ligands with polar end groups such as mercaptopropionic acid can be similarly used to solubilize QDs in polar solvent.

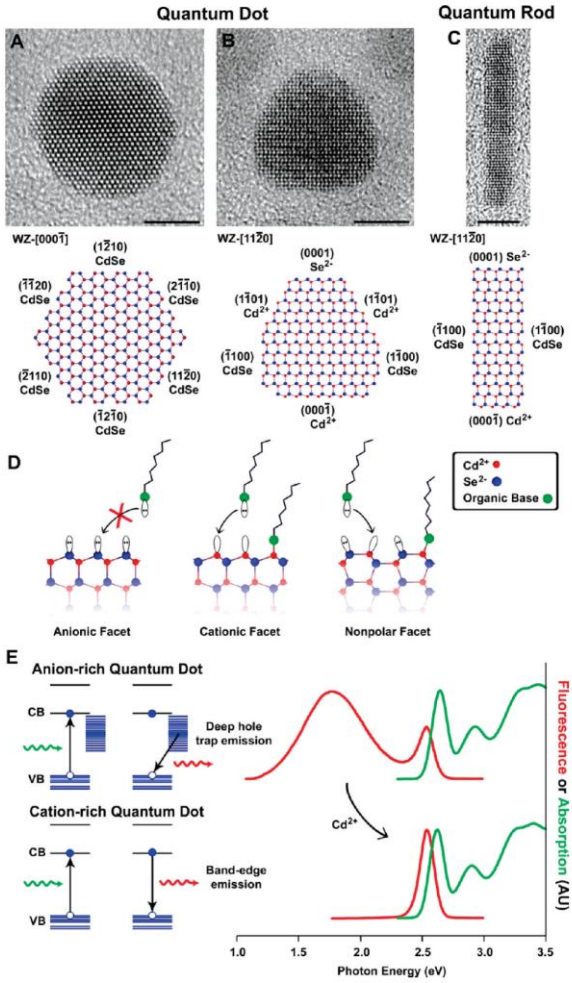

Figure 1.2. *Surface properties of CdSe QDs.* ***(a)*** *and* ***(b)*** *depict transmission electron micrographs of quasi-spherical QDs with two orientations on the substrate, and* ***(c)*** *depicts a quantum rod. All scale bars are 5 nm. In the atomic models, the crystalline orientations and lattice facets are identified by their Wurtzite Miller indices, and the polarity of each facet is noted as Cd^{2+} for cationic, Se^{2-} for anionic, and CdSe for nonpolar.* ***(d)*** *illustrates the terminal dangling orbitals on each type of facet, and* ***(e)*** *shows the effects of surface hole traps on the fluorescence of small 2.1 nm QDs. Reprinted with permission from ref [13] Copyright 2010 American Chemical Society.*

The PL of QDs can be significantly controlled by tuning their surface chemistry. For example, very small CdSe QDs display two emission bands, one due to excitonic recombination and another which is at a lower energy resulting from recombination at sub band gap defect sites

on the surface (Figure 1.2(e)).[15] This surface trap emission arises from the presence of Se^{2-}-rich facets, which have usually shown poor binding ability to most basic ligands, making these QDs especially prone to surface trapping of holes.[15] QDs with surfaces terminated by anions usually show little or no fluorescence emission due to the very high number of surface trap states for nonradiative recombination. The addition of excess Cd^{2+} ions to the surface of QDs can passivate these selenium sites. These cationic rich surface sites are known to strongly bind to basic ligands. This results in passivation of hole trap states. The resultant PL efficiency gets enhanced as shown in Figure 1.2(e).

The number of surface atoms and the types of facets are also dictated by the QD shape. Figure 1.2(b) shows the fraction of surface atoms on a CdSe QDs for different shapes and sizes. Spherical QDs have the smallest number of surface atoms and are thermodynamically most stable. This makes them potential candidates for applications where emission play a major role, e.g. in light emitting applications. On the other hand, the nano structures such as rods and wires contains a very high number of their atoms on their surface. This is useful in utilizing them for applications such as for redox chemistry, energy transfer, photocatalysis, water splitting and sensing as the QD photo-generated charge carriers can stay mostly on the surface. Several other interesting materials properties are closely related with the fraction of atoms on the QD surface.

However, it is not possible to passivate all kinds of trap states using the ligands as it depends upon various factors such as nature of passivating ligands[17-19] and the bulkiness of the ligands.[20] This results in reducing the PL QY. This problem can be overcome by passivating with a shell of another semiconductor material which leads to formation of heterostructure QDs.

1.1.3. Tunability from heterostructure QDs:

The two well established strategies to improve QDs' surface passivation drastically which was not achieved with simple ligand passivation is by overcoating with a shell of a second semiconductor, resulting in core/shell QDs, or by mixing with a second semiconductor material homogeneously, results in forming alloy QDs.

Depending on the bandgaps and the relative band edge positions of the involved semiconductors, these core/shell materials are mainly classified into type I, inverse type I, and type II structures.[21, 22] The classification is depicted in the scheme shown below in Figure 1.3.

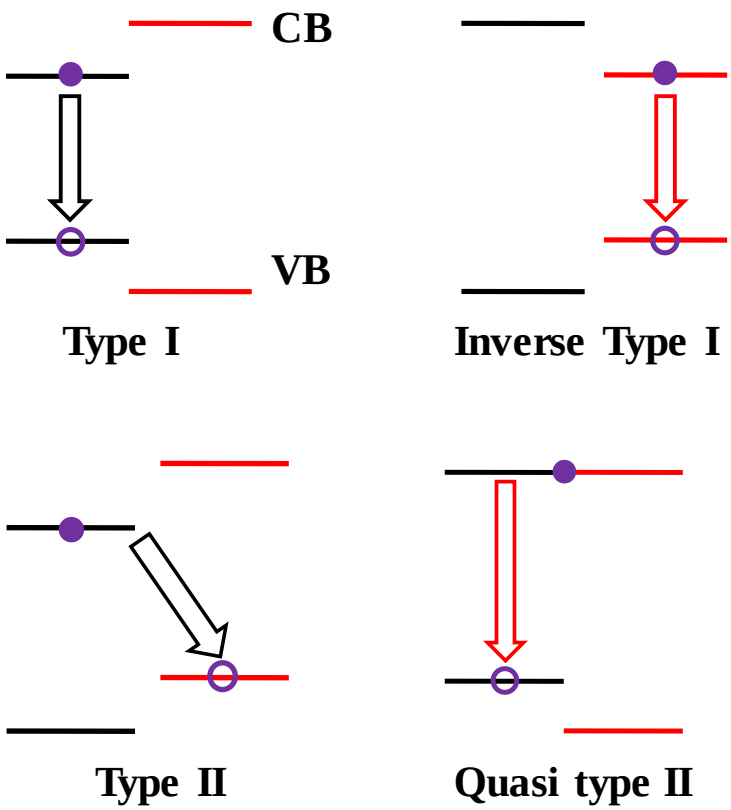

Figure 1.3. *Classification of core/shell materials depending on the relative band alignment of core and shell materials.*

In type I, the bandgap of the shell material is larger than that of the core and the band edges of the core material are buried inside that of shell material. This leads to the confinement of both electron and hole inside the core material. In inverse type I, the bandgap of the shell material is smaller than that of the core and, band edges of the core material are buried inside that of shell material. Both electron and hole are confined into the shell material. In type II, either the VB edge or the CB edge of the shell material is situated in between the band edges of the core material. When the QD is illuminated with photons, the charge carriers are separated in the core and shell regions of the material. The fourth type of alignment is one wherein one of the charge carriers is localized either inside the core or shell and the other charge carrier is delocalized over entire QD. This alignment is known as qausi type II.

In type I QDs, the shell can passivate the surface of the core by moving the surface traps energetically away from the core. This leads to enhancement of its PL efficiency. With respect to core QDs, core/shell particles show enhanced stability against photodegradation. The best example

for this system is CdSe/ZnS. The ZnS shell significantly improves the PL QY from just <5% to 50 %.[23] Shell growth leads to a small red shift in both absorption wavelength maximum and the PL wavelength. This small red-shift can be attributed to the partial leakage of charge carriers into the shell material.

In reverse type-I systems, a material with smaller bandgap is overgrown onto the core with wider bandgap. Charge carriers are localized into the shell material and both the absorption and emission wavelengths can be red-shifted. The most extensively analyzed systems of this type are CdS/HgS,[24] CdS/CdSe,[25] and ZnSe/CdSe.[26] These materials are shown to be potential candidates for photovoltaic devices.[2] Growing third material of a higher band gap material on top of these core/shell material leads to resistance against photobleaching and the enhancement of PL QY.[25]

In type II systems, with increase in shell growth, both absorption and emission wavelengths of the QDs gets red-shifted. The band gap of these materials is much smaller than either one of the constituting materials. The advantage with these materials is the possibility to play with the shell thickness which allows us to attain the wide-range tunability of both absorption and PL, that is not that easily achieved with other materials. For example, type II CdSe/CdTe,[27] CdTe/CdS,[28] CdTe/CdSe[29] and CdSe/ZnTe[30] QDs have been designed to show NIR emission which are very useful for bio applications. The PL decay times are highly prolonged in these materials contrary to type I materials due to the weaker overlap of the electron and hole wave functions as a result of separation of the charge carriers into core and shell regions.

Inverse type I systems like CdSe/CdS shows that the electron is delocalized into shell material while the hole is confined to CdSe core.[31] [32, 33] This system has very interesting applications as active material for light emitting applications due to very high PL efficiency.[31]

As already discussed, size dependent band gap variation of semiconductor QDs have been widely studied. However, in many applications, very small QDs are necessary to achieve the desired energy for the band gap. So, it is challenging to tune the properties of QDs keeping their size constant. Another means of tuning the semiconductor band gap is by changing the particle composition by means of varying the stoichiometry of constituent materials. This can be achieved by mixing two or more semiconductor materials with different band gaps called alloy materials.[34] Usually, an increase (decrease) in band gap energy is observed with increasing composition of the

wider (smaller) band gap semiconductor in the alloy QDs. These alloyed QDs have properties that are composition-dependent along with the effects arising due to quantum confinement. For example, CdSe QDs were widely studied which was shown to be continuously tunable over entire visible range, however, the NIR region is outside its spectral range. $CdSe_xTe_{1-x}$ QDs, an alloy of CdSe and CdTe, can efficiently emit in the NIR spectral window.[34, 35] These NIR-emitting QDs are potentially useful in several biomedical applications. Highly stable QDs of $Zn_x Cd_{1-x}Se$ are formed by alloying CdSe with ZnSe which emit blue light with excellent PL efficiency.[36] So, these materials can be used for short range light emitting applications.[37]

These core/shell and alloy systems are two ideal and extreme cases. The combinations such as alloy core with shell, core with alloy shell, core shell with alloy interface and etc. do exist.[38]

1.2. Doping in bulk semiconductors:

In semiconductors, doping intentionally introduces impurities into an extremely pure intrinsic semiconductor for the purpose of modulating its properties.

Doping into semiconductors affect magnetic, electrical and optical properties of the host material. Doping with transition metal ions into ZnO leads to appearance of magnetism in these materials. Mn doped ZnO which was prepared by solid state reaction show ferromagnetism.[39] Other transition metal ions of Fe and Co also induce magnetism in ZnO.[40] One of the ways of achieving room-temperature ferromagnetism in bulk $Zn_{1-x}Fe_xO$ was found to be adding a little Cu. A transition temperature of 550 K was observed in this system. This doping also strongly enhances the conductivity of the host material. ZnO is one of the most studied systems due to its optical transparency like tin oxide and can be made n-type conducting by doping with Al.[41] However, achieving p-type conductivity in ZnO thin films would be useful for making better devices out of this material and efforts were made in that direction. The p-type conductivity in ZnO (at room temperature) was achieved first by chemical vapor deposition, through N doping using NH_3.[42] But that study showed poor reproducibility, high resistance and low carrier concentration which cannot be useful for practical purposes. The p-type conductivity of ZnO thin films was improved by co-doping with Ga and N.[43] Doping not only affects magnetic and electrical properties but also affects the optical properties of the host material. Doping with lanthanide ions make silica or silica-based glass visible or NIR optically active material which can be used for photonic

applications.[44, 45] The luminescence in these lanthanide materials is due to f-f transitions of lanthanide ions. Silica colloids with a diameter of 240–360 nm which were doped with Er ions show a clear room-temperature PL at 1.53 mm, with lifetimes as high as 17 ms. They show a high PL QY of about 80%. [46] Doping transition metal ions gives interesting optical properties in II-VI semiconductor materials. Luminescent Cu semiconductors play a central role in the emergence of lighting and display technologies. Cu incorporated ZnS and related Cu-containing semiconductors have been employed as integral components of many black-and-white and color display technologies, including, in televisions, and electroluminescent devices. The Cu doping in bulk semiconductors was known as luminescent phosphors where the Cu related emission was observed. The green Cu luminescence in ZnS was widely used as glow in dark materials.[47] Several types of luminescence are observed in bulk Cu incorporated ZnS and related semiconductors. Different colored Cu emissions were also observed.

Doping in semiconductors will be much more interesting if the size of the material is reduced to quantum confined regime. That leads to the emergence and development of doped QDs.

1.3. Doping in semiconductor QDs:

1.3.1. Synthesis of doped QDs:

QDs are synthesized by mixing the molecular precursors that contain the constituent elements. Thermal decomposition of the precursors leads to nucleation and growth. The separation of nucleation and growth during QD synthesis lead to development of high quality QDs.[48] The most uniform particles have been obtained by using colloidal chemistry either in organic or aqueous phase. The most successful method involves the fast injection of anion precursor to the cation precursor at very high temperatures in presence of surfactants to obtain high quality QDs.[12] Surfactants in the solution are used to control growth and passivate dangling bonds.[49]

Doping into semiconductor QDs is not an easy or a simple process as it depends upon the nature of dopant, temperature at which dopants are incorporated, crystal structure and size of host material, surfactants and so on which makes the process complicated. A lot of efforts were made during past many years on doping transition metals into semiconductor QDs[50-53] but the exact mechanism of doping is not completely understood. For example, Mn was shown to be doped into CdS[54] and ZnSe[52] QDs but not into CdSe.[55] It was assumed that this is only due to intrinsic

mechanism which is called self-purification[56] where the dopant atoms are expelled out of the QD material specially when the QD size is very small. More dopants can be incorporated into the larger QDs which were grown in anion-rich limit. Erwin et al.[57] have shown the underlying mechanism that controls doping is the initial adsorption of impurities on the QD surface during growth. They found that the doping efficiency is determined by three main factors namely surface morphology, QD shape, and surfactants in the growth solution. They have also explored a lot of various factors that influence the doping efficiency. Mn doping efficiency is enhanced with increasing anion to cation ratio. From the theoretical binding energy calculations, it was found that the CdSe QDs would be easier to dope if they are in zinc-blende structure. The same report shows that the surfactants themselves can also bind dopant ions, competing with surface adsorption and decreasing the doping efficiency. This plays a very important role when the dopant QD binding is just moderately strong. For example, Mn binds to (001) surface of ZnSe two times stronger than (0001) surface of wurtzite CdSe. This suggests that the previous failure attempts of Mn doping of wurtzite CdSe QDs are also due to competitive binding for Mn by surface ligands such as phosphonic acids.

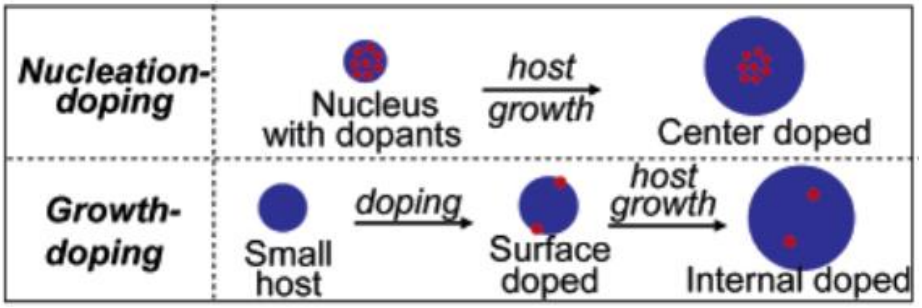

Figure 1.4. *The two important methodologies for doping in QDs. Reprinted with permission from ref [58] Copyright 2005 American Chemical Society.*

There are majorly two synthetic strategies that were proposed for doping transition metal ions into the semiconductor QDs in the literature. They are nucleation-doping and growth-doping, respectively.[58] Nucleation doping involves mixing of dopant and anionic host precursor during the nucleation step leading to the formation of dopant clusters followed by overcoating of the host material. After nucleation of QDs, the reaction conditions were varied in such a way the growth of the host material became the only dominant process. This results in diffusion of the dopants away from the QD surface. For growth-doping strategy, the formation of the small host QDs occurred under high temperature and established synthetic conditions and was quenched by lowering the

reaction temperature. At this relatively lower temperature, active dopant precursors were introduced and doping occurred without the further growth of the host. These two doping schemes are shown below in Figure 1.4.

Usually, Mn doping was achieved by nucleation doping. However, the Cu doping was mostly achieved by growth-doping strategy as the nucleation-doping involves very high temperature where the Cu dopants were shown to be expelled out of the QD. Chen et al. have found that Cu emission in ZnSe QDs is stable up to 210 ^{o}C or below and above this temperature the Cu emission intensity decreases.[59] When it is 250 ^{o}C, the Cu emission completely vanished. However, it should be noted that an optimal temperature is needed for the diffusion of Cu into QDs as the core doped QDs show higher Cu emission efficiency than surface doped QDs.[58] Along with the temperature, reaction time also determine the extent of dopant incorporation which controls the relative intensities of band edge and Cu emission. The temporal evolution of the PL spectrum of ZnSe QDs in the presence of copper oleate in octadecene at 40 °C was studied.[59] The intensity of band edge emission decreases and reaches a plateau after about 45 min, but the overall band shape is retained and the Cu emission is not observed. When the temperature is raised to 60 °C and the reaction is allowed to run for 100 min, the lower energy Cu emission appears. But, the band edge emission is still observed even after 100 minutes of annealing at 60 °C suggesting the presence of significant amount of undoped QDs. The intense and dominant Cu emission was observed only after the temperature was increased to 100 °C. The majority of QDs formed under these conditions are doped with copper atoms. The concentration of Cu dopants also affect the relative intensities of band edge and Cu emissions. Tananaev et al. have studied PL spectra of a series of Cu doped CdSe QD samples with varying the Cu concentration synthesized by a hot-injection method in which a solution of selenium in TOP was injected into a mixture of cadmium oleate and copper stearate.[60] As the amount of copper stearate increases, the band edge emission intensity decreases and the Cu emission intensity increases, suggesting increased population of Cu doped QDs.

1.3.2. Properties of doped QDs:

The introduction of impurity ions into semiconductor QDs strongly affects the properties such as magnetic, electrical and optical properties of the host QDs. For example, Cu and Mn doped ZnSe QDs were shown to be replacement to highly toxic NIR emissive CdSe QDs.[58] Doping was found

to protect against the photooxidation where materials are continuously illuminated e.g. in case of solar cells. Here, the energy absorbed can be quickly localized at dopant sites to avoid any unwanted side reactions. For magnetic dopants, confinement of the impurity within the QD can enhance its interactions with other carriers to give rise to very high magnetism. On doping ZnO QDs with Co and Ni ions, the magnetic and absorption properties are shown to be altered.[61] 3.6% Co doping in ZnO QDs results in paramagnetism which are otherwise non-magnetic. They show room temperature (300 K) magnetism of 2.56×10^{-3} emu/g. Similar to the case of bulk semiconductors, the doping in QDs plays an important role in tuning the transport properties of host materials. As the QD films are inherently insulating, the introduction of extra carriers is beneficial for enhancing electrical conduction. It is essential to introduce heterovalent impurities that provide the charge carriers as the isovalent dopants usually produce any additional charge carriers in the system. By introducing Cd impurities into InAs, the conductivity of these films were affected.[62] CdSe is one of the most studied QD systems in literature for this study. Several strategies were developed for introducing extra charge carriers into the QD films. They include the placement of electron donating molecules in the close vicinity of the QD surface[63, 64] and through electrochemical doping (application of external electric fields).[65, 66] When carriers were added, conductivity was dramatically increased. In principle, it should also be possible to provide extra charge carriers to CdSe QDs by adding impurity atoms. Recently, it was shown that doping Ag into CdSe QDs alter electrical properties of the host. Ag changes from a n-type to a p-type impurity with increased doping in CdSe QDs. Introducing transition metal ions such as Ni^{2+} into CdZnS QDs results in the higher conductivity or current flow in presence of light than undoped ones which is normally expected due to presence of effective charge carriers in the doped QDs.[67]

The other interesting property of these dopants is to alter the optical properties of host QDs and they are called optically active dopants. Doping with optically active ions in semiconductor QDs results in stoke's shifted emission, NIR emission, tunability of the absorption and emission over wide spectral range and so on. The photo-generated charge carriers funnel through to the dopant levels and alter the host optical spectra. For example, doping with Co^{2+} and Ni^{2+} induces changes in the absorption spectra ZnO QDs.[61] The doping results in the appearance of new bands in both the absorption and MCD corresponding to the dopant ligand field splitting and the charge transfer bands. The charge transfer bands were further characterized and found that the dopant energy levels were pinned in between the CB and VB of the host QDs.[68] These optically active

dopant ions not only affect the absorption properties of host QDs but also strongly affect their PL properties. One of the extensively studied optically active dopant ions which affects the PL properties of host material is Mn^{2+}. This introduces two energy levels in between CB and VB of the host material. The photo-generated charge carriers of host QDs funnel through to these dopant levels to give rise the Mn^{2+} dopant emission. So, both the excitation and emission involve a spin forbidden transition giving rise to a long-lived emission.[69] The energy position of this peak is constant at 580 nm irrespective of the band gap of the host material as the emission always occurs in between the two constant Mn^{2+} d-levels. Though the stoke's shift is achieved, the tunability of the emission energy is lost which is a major limitation with Mn doped QDs. Efforts were made to enhance the PL efficiency of Mn^{2+} emission despite of its lack of tunability.[52, 70, 71] Dopants like Ni also found to affect the PL properties of host QDs.[67] Ni doped QDs show a new broad PL peak which is red-shifted from the band edge emission which has a longer lifetime (~300 ns). The origin of the Ni dopant emission is not known as it is less studied or explored. There are other optically active dopants such as Cr and Ag which gives rise to the dopant emission when doped inside semiconductor QDs.[72] But, these dopants are not much explored or studied. The other optically active dopant ion which is extensively studied along with Mn is Cu and the discussion about the Cu doping and its emission mechanism is given in the next section.

1.4. Cu doping and emission mechanism:

Unlike the Mn doping, Cu doping results in band gap dependent tunable emission in quantum confined regime.[58, 73] Cu introduces a single energy level in between the CB and VB of host material.[74] The Cu emission occurs due to the radiative recombination of electron present in CB of host material with the hole present in the Cu energy level.[75] The band gap dependent tunability of this Cu emission arises due to shift in CB with the band gap variation of host QDs. As the Cu emission energy is band gap dependent, it can be tuned by varying either size of QD or the composition of material in case of alloys. For example, Pradhan and co-workers[73] have shown that when the Cu doped ZnS QDs are alloyed with the addition of Cd to form the Cu doped $Zn_{1-x}Cd_xS$ alloy QDs, the Cu emission maxima were tuned from ~ 500 nm to ~ 750 nm as shown in Figure 1.5.

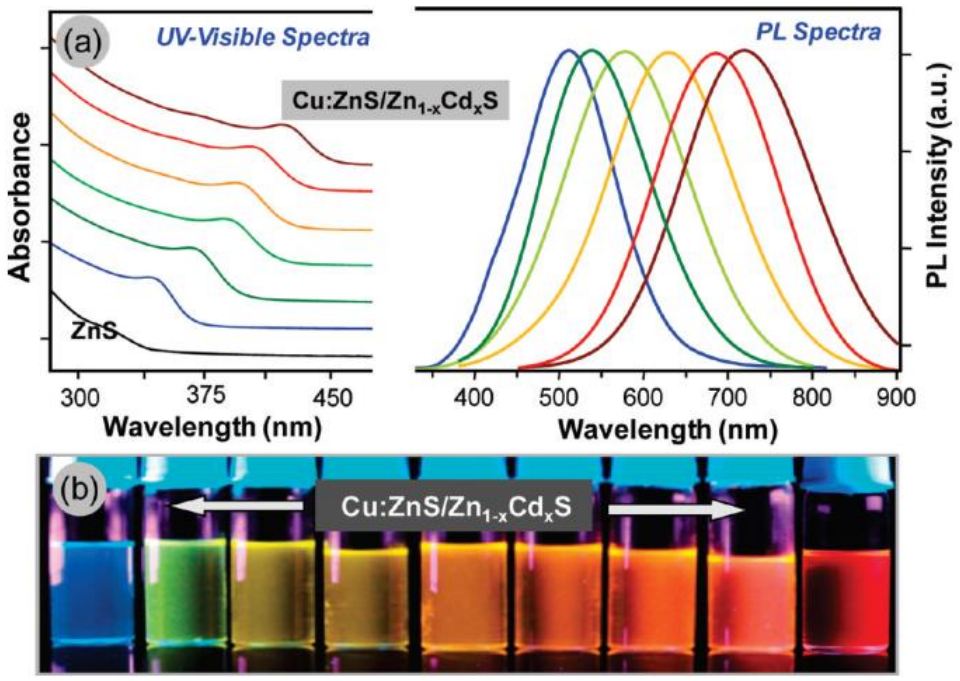

***Figure 1.5**. **(a)** The absorption and PL spectra of Cu doped $Zn_{1-x}Cd_xS$ QDs with varying Cd composition. **(b)** Digital picture of samples collected in a typical experiment from different stages of the doping process of the alloyed QDs. The samples are excited using a hand-held UV lamp at 350 nm excitation. Reprinted with permission from ref [73] Copyright 2011 American Chemical Society.*

The Cu emission shows a longer lifetime decay (~300-1000 ns) compared to band edge emission.[75] The Cu emission is found to be broad in nature whose fwhm varies from 0.2-0.6 eV.[76] This is much broader compared to fwhm of excitonic luminescence which is around ~ 0.1 eV.[77, 78] The broadness of Cu emission band cannot be completely accounted by the size distribution present in the sample. Specifically, it was shown that the broadness is not due to size distribution of the sample as the width of the Cu emission is unchanged even if the sample is excited at the lower energy side of absorption spectrum.[79] This is supported by the single particle fluorescence studies which show that the broadness is unchanged for the single particles as that of ensemble.[80] Recently, the density functional theory calculations proves that the broadness is inherent nature of Cu emission and this is due to strong vibronic coupling in the excited state causes substantial geometric distortion along totally symmetric and Jahn-Teller nuclear coordinates, with a correspondingly large excited-state nuclear reorganization energy.[81] All these measurements conclude that Cu emission is inherently broad.

For a given Cu PL spectrum, two emission bands are usually observed i.e. one due to band edge recombination and the second one is Cu related emission as shown in Figure 1.6. To

understand the origin of the band edge emission in the Cu doped samples, it is necessary to understand the mechanism of Cu emission.

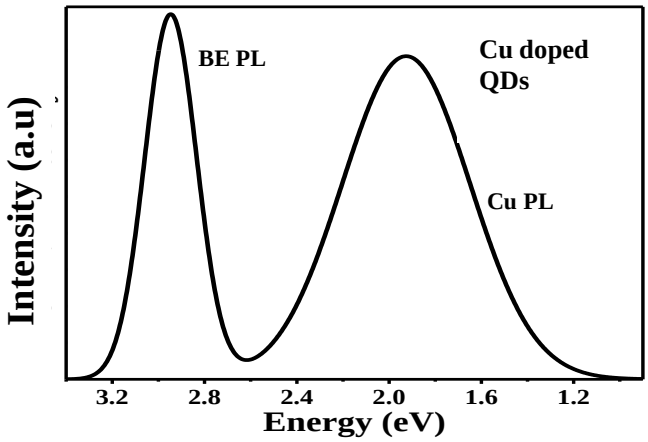

Figure 1.6. *A typical PL spectrum of Cu doped CdS QDs.*

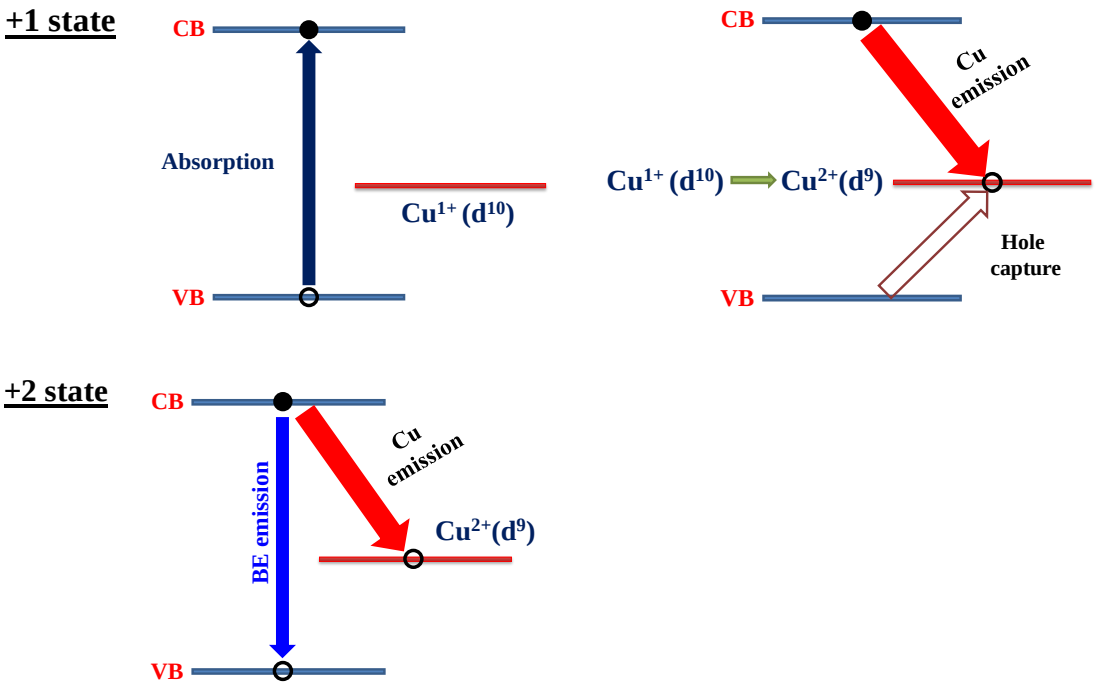

Figure 1.7. *The recombination processes that occur when Cu is in +1 (top panel) and +2 (bottom portion) oxidation state respectively.*

As already discussed the Cu emission occurs due to radiative recombination of electron present in CB of host material with the hole present in Cu level. It is well known that Cu majorly exists in two oxidations states i.e. +1(d^{10}) and +2 (d^9). If it is in +1 state, Cu level cannot take any

more electrons and so the only way the Cu emission can occur it is when it captures the photo-generated hole from the VB. In this case, the appearance of band edge emission is due to presence of undoped counter parts present in the solution. If it exists in +2 state, the electron from CB can either recombine with the hole present in VB or with Cu level to give rise to band edge and Cu emission respectively as shown in the schematic given below in Figure 1.7.

Hence, it is important to know the oxidation state of Cu in order to understand the origin of the band edge emission in the Cu doped samples. In literature, the oxidation of Cu dopants is a controversial debate as a few reports say that it exists in +1 state[73, 80, 82, 83] and a few other reports say that it exists in +2 state.[84, 85] Moreover, a few reports assumed that Cu^{+2} gets reduced to Cu^{+1} during QD synthesis or due to presence of ligands which can reduce the Cu^{+2} ions to Cu^{+1}. One of the simplest ways to determine the oxidation state of Cu is by using EPR spectroscopy. It was claimed that addition of CdS QDs to a solution of a Cu^{2+} salt causes a decrease of the EPR signal associated with Cu^{2+}, claiming the reduction of Cu^{2+} to Cu^{+} by the CdS QDs.[86] However, in semiconductor QDs; the EPR signal for Cu^{2+} is found to be very weak. Jahn-teller distortions and strong spin-orbit coupling leads to internal strains of the crystals which results in the broadening of EPR signals, too weak to be detected. So, it is not possible to determine the oxidation state of Cu dopants in semiconductor QDs. Other than spectroscopic techniques, the oxidation state of Cu dopants was probed by the X-ray absorption and X-ray photoelectron spectroscopic techniques.[83, 87] The authors of these publications claimed that Cu exists in +1 state in the ground state. For example, Meulenberg et al. have shown the comparison of the Cu L-edge X-ray absorption near-edge structure of copper-doped CdSe QDs to that of copper metal (Cu(0)), CuI (Cu+1), and CuSe (Cu^{+2}).[83] The X-ray absorption onset energy in the copper-doped CdSe QDs is found to be similar to that of CuI. This observation made the authors to claim that copper was incorporated into these QDs in the +1oxidation state. However, very high percentage (15%) of Cu was doped into these QDs for this study. This might lead to formation of Cu clusters and very high dopant concentrations are known to alter the electronic structure of host materials. Also, it is not clear where the absorption edge rises, so, it is not straight forward to conclude whether Cu exists in +1 or +2 oxidation state through this technique.

As Cu^{1+} have a filled $3d^{10}$ electronic configuration, it is expected to be nonmagnetic. In contrast, Cu^{2+} has a single unpaired spin-1/2 electron in their $3d^{9}$ shell and are therefore expected

to be magnetically active. To judge whether Cu is in +1 or +2 state, Klimov and co-workers have performed MCD studies on the Cu doped ZnSe/CdSe QDs.[75] copper-doped QDs clearly reveal a markedly enhanced Zeeman splitting (~2.5 meV at B = 6 T;) and an effective exciton g-factor of order 7 compared to undoped QDs with a small Zeeman splitting of the 1S exciton (~0.1 meV/T) and exciton g-factors of order 2. These results strongly suggest that the Cu dopants are incorporated as magnetically active Cu^{2+} ions.

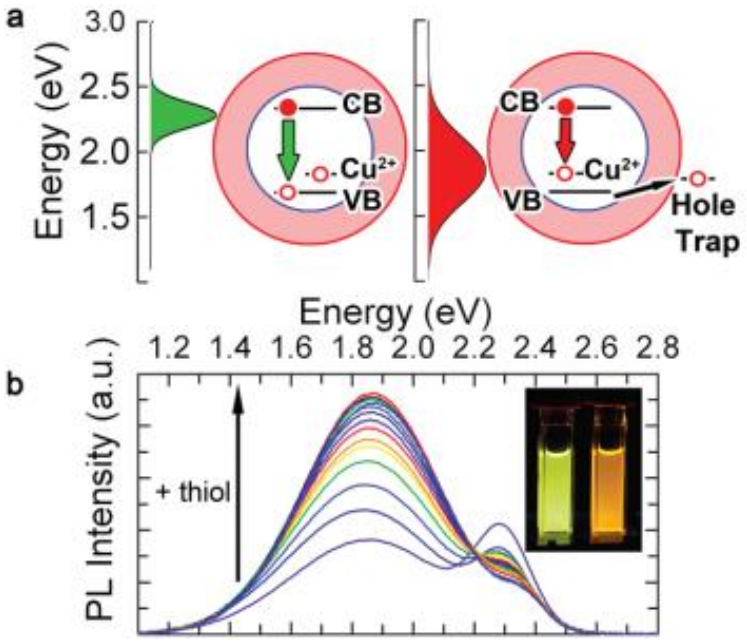

Figure 1.8. (a) *If a photo-generated hole is present in the QD for sufficiently long time, radiative recombination is primarily due to a band-to-band transition as it is much faster than the band-to-Cu transition; this results in the PL spectrum dominated by band-edge emission (left). If a photo-generated hole is instead quickly removed from the QD (using, e.g., hole-withdrawing species) emission becomes dominated by the Cu-related band (right).* ***(b)*** *Titration of Cu:ZnSe/CdSe QDs with an increasing amount of hole accepting molecules, DDT. Reprinted with permission from ref [75] Copyright 2011 American Chemical Society.*

The presence of Cu^{2+} was further supported by a simple titration experiment. As already discussed, if it is in Cu^{2+}, both the band edge and Cu emissions can occur. However, the lifetime data suggests that Cu emission decays in 500 ns while the band edge recombination occurs on the time scale of a few ns. So, in presence of the hole present in the VB the Cu emission will never occur. Hence, the only possible pathway for the Cu emission is if the hole from VB can be removed. One of the possibilities is if the hole can be trapped by the surface trap states which occurs on the time scale of fs, much faster process than the band edge recombination. Hence, it is

expected that the Cu emission intensity will be enhanced in presence of surface hole traps as shown in Figure 1.8(a). To check this, the QDs were treated with DDT which is well known to trap the photo-generated hole when attached to CdSe QD surfaces.[88] DDT molecules or ligands rapidly quench the PL emission in case of the undoped QDs. This is not the case with the Cu-doped QDs. In this particular work, the PL spectra of Cu doped ZnSe/CdSe QDs were titrated with increasing amounts of DDT. The Cu doped sample shows a band edge emission at 2.3 eV and the Cu emission at 1.85 eV. On treatment of the Cu doped QDs with the DDT, the band edge intensity was gradually quenched and the Cu emission was gradually enhanced at the same time as shown in Figure 1.8(b). A dramatic change in color from green to orange was observed during this titration experiment due to increasing contribution from Cu emission and decreasing contribution from band edge emission. These results confirm that Cu exists in +2 state but not in +1 state where the holes in Cu level and VB compete for the same CB electron and the Cu emission occurs only if hole is quickly removed from the QD. In the case of the Cu^{1+} dopants, both the band edge emission and Cu emission would be suppressed together on addition of DDT ligands. Therefore, the DDT titration experiments show that Cu dopants exists in +2 state thus strongly supporting the MCD results.

1.5. Current work:

The work in this thesis focusses on two aspects, namely, the study of bulk and surface electronic structure of II-VI semiconductor QDs and their heterostructures using Cu as an internal standard. The thesis is divided into eight chapters along with the methodology chapter where the experimental techniques employed throughout these chapters are discussed.

In **Chapter 3**, the bulk electronic structure of II-VI semiconductor QDs is studied by choosing CdSe as a model system. We determined the relative band alignment of II-VI semiconductors as a function of size in the quantum confined regime. Our experimental results are found to be in good agreement with the theoretical data and other existing experimental data.

In **Chapter 4**, the internal structure of heterostructures is studied. We have used Cu doping and its corresponding PL to differentiate an alloy from the core/shell QDs. We have studied the charge localization for a wide range of heterostructures study their internal strcture. The electron and hole localization obtained from this method concurs with the pre-existing understanding in

these well studied systems. We have also extended this method to obtain the internal structure in previously unknown heterostructures proving the usefulness of this method.

In this **Chapter 5**, we studied the variation of band gap, CB and VB edges of CdS and CdSe QDs as a function of temperature and size, utilizing Cu dopant PL as an internal probe. The band gap variation is found to be similar to that of bulk but with a higher average phonon energy. The band edge variation is characterized by a dominant CB shift for larger sizes with decreasing temperature while the smaller size QDs show the variation in both CB and VB. Further, we have also studied the binding energy of the trap states as a function of temperature using Cu PL QY and average lifetime of Cu PL.

In **Chapter 6,** we study the role of commonly used ligands such as TOP, TOPO, oleic acid, DDT, MPA, primary amines and oleylamine in passivating II-VI QDs. The role of ligands was studied during the synthesis, as well as during specific phase transfer and pyridine exchange based ligand exchange procedures. The ligand exchange with a combination of well passivating ligands results in substantial increase in the PL QY of CdSe QDs.

We discuss the role of sulfide ions in passivating CdS QDs in **Chapter 7**. The sulfide ions passivate electron traps but trap the photo-generated hole. They have shown the conductivity of ~ 10^{-4} S cm^{-1}. The conductance behavior of these QDs is correlated to their surface trap states. Cu PL is used to optimize the concentration of sulfide ligands to obtain maximum conductivity for these QDs.

In **Chapter 8,** we show the two applications based on Cu doped QDs that have not been previously studied. This is discussed in two sections.

In **section 1** of **Chapter 8,** we show that Cu doped CdS QDs can be useful as NIR phosphors due to their tunable emission varying from 1.9 eV to 1.35 eV and high PL QYs of 25 % to 35% in NIR region along with longer PL decay values of ~ 1 µs. They exhibit high thermal stability up to 100 ^{o}C in both solution and as film. The combination of all these properties makes Cu doped CdS QDs a NIR emitting phosphor material.

Doping Fe in Cu doped ZnS QDs can be used as visible Photo-detectors when doped with Fe which is discussed in **section 2** of **Chapter 8.** The doping in these QDs is shown to have a high photo-response in the visible region due to a broad absorption band in visible region unlike their undoped counterparts that is only effective in the ultra-violet region.

Bibliography:

[1] B. N. Pal, Y. Ghosh, S. Brovelli, R. Laocharoensuk, V. I. Klimov, J. A. Hollingsworth, H. Htoon, *Nano Lett.* **2011**, *12*, 331.

[2] Z. Pan, H. Zhang, K. Cheng, Y. Hou, J. Hua, X. Zhong, *ACS Nano* **2012**, *6*, 3982.

[3] P. K. Santra, P. V. Kamat, *J. Am. Chem. Soc.* **2012**, *134*, 2508.

[4] Q. Sun, Y. A. Wang, L. S. Li, D. Wang, T. Zhu, J. Xu, C. Yang, Y. Li, *Nat. Photonics* **2007**, *1*, 717.

[5] S. Liu, W. Liu, W. Ji, J. Yu, W. Zhang, L. Zhang, W. Xie, *Sci. Rep.* **2016**, *6*, 22530.

[6] I. Mora-Seró, J. Bisquert, *J. Phys. Chem. Lett.* **2010**, *1*, 3046.

[7] X. Michalet, F. F. Pinaud, L. A. Bentolila, J. M. Tsay, S. Doose, J. J. Li, G. Sundaresan, A. M. Wu, S. S. Gambhir, S. Weiss, *Science* **2005**, *307*, 538.

[8] K.-T. Yong, I. Roy, R. Hu, H. Ding, H. Cai, J. Zhu, X. Zhang, E. J. Bergey, P. N. Prasad, *Integr. Biol.*, **2010**, *2*, 121.

[9] J. McBride, J. Treadway, L. C. Feldman, S. J. Pennycook, S. J. Rosenthal, *Nano Lett.* **2006**, *6*, 1496.

[10] M. Nirmal, L. Brus, *Acc. Chem. Res.* **1999**, *32*, 407.

[11] I. Moreels, K. Lambert, D. Smeets, D. De Muynck, T. Nollet, J. C. Martins, F. Vanhaecke, A. Vantomme, C. Delerue, G. Allan, *ACS Nano* **2009**, *3*, 3023.

[12] L. S. Li, N. Pradhan, Y. Wang, X. Peng, *Nano Lett.* **2004**, *4*, 2261.

[13] A. M. Smith, S. Nie, *Acc. Chem. Res.* **2009**, *43*, 190.

[14] S. Pokrant, K. B. Whaley, *Eur. Phys. J. D* **1999**, *6*, 255.

[15] D. F. Underwood, T. Kippeny, S. J. Rosenthal, *J. Phys. Chem. B* **2001**, *105*, 436.

[16] C. Murray, D. J. Norris, M. G. Bawendi, *J. Am. Chem. Soc.* **1993**, *115*, 8706.

[17] A. M. Munro, I. Jen-La Plante, M. S. Ng, D. S. Ginger, *J. Phys. Chem. C* **2007**, *111*, 6220.

[18] G. Kalyuzhny, R. W. Murray, *J. Phys. Chem. B* **2005**, *109*, 7012.

[19] C. Bullen, P. Mulvaney, *Langmuir* **2006**, *22*, 3007.

[20] Y. Gao, X. Peng, *J. Am. Chem. Soc.* **2015**, *137*, 4230.

[21] R. Ghosh Chaudhuri, S. Paria, *Chem. Rev.* **2011**, *112*, 2373.

[22] P. Reiss, M. Protiere, L. Li, *Small* **2009**, *5*, 154.

[23] D. V. Talapin, A. L. Rogach, A. Kornowski, M. Haase, H. Weller, *Nano Lett.* **2001**, *1*, 207.

[24] A. Mews, A. Eychmueller, M. Giersig, D. Schooss, H. Weller, *J. Phys. Chem.* **1994**, *98*, 934.

[25] D. Battaglia, J. J. Li, Y. Wang, X. Peng, *Angew. Chem. Int. Ed.* **2003**, *42*, 5035.

[26] X. Zhong, R. Xie, Y. Zhang, T. Basche, W. Knoll, *Chem. Mater.* **2005**, *17*, 4038.

[27] N. McElroy, R. C. Page, D. Espinbarro-Valazquez, E. Lewis, S. Haigh, P. O'Brien, D. J. Binks, *Thin Solid Films* **2014**, *560*, 65.

[28] P. Sheng, W. Li, J. Cai, X. Wang, X. Tong, Q. Cai, C. A. Grimes, *J. Mater. Chem. A* **2013**, *1*, 7806.

[29] J. Wang, I. Mora-Seró, Z. Pan, K. Zhao, H. Zhang, Y. Feng, G. Yang, X. Zhong, J. Bisquert, *J. Am. Chem. Soc.* **2013**, *135*, 15913.

[30] S. Kim, B. Fisher, H.-J. Eisler, M. Bawendi, *J. Am. Chem. Soc.* **2003**, *125*, 11466.

[31] A. Saha, K. V. Chellappan, K. S. Narayan, J. Ghatak, R. Datta, R. Viswanatha, *J. Phys. Chem. Lett.* **2013**, *4*, 3544.

[32] J. J. Li, Y. A. Wang, W. Guo, J. C. Keay, T. D. Mishima, M. B. Johnson, X. Peng, *J. Am. Chem. Soc.* **2003**, *125*, 12567.

[33] J. Li, L.-W. Wang, *Appl. Phys. Lett* **2004**, *84*, 3648.

[34] R. E. Bailey, S. Nie, *J. Am. Chem. Soc.* **2003**, *125*, 7100.

[35] N. P. Gurusinghe, N. N. Hewa-Kasakarage, M. Zamkov, *J. Phys. Chem. C* **2008**, *112*, 12795.

[36] X. Zhong, M. Han, Z. Dong, T. J. White, W. Knoll, *J. Am. Chem. Soc.* **2003**, *125*, 8589.

[37] P. O. Anikeeva, J. E. Halpert, M. G. Bawendi, V. Bulovic, *Nano Lett.* **2009**, *9*, 2532.

[38] P. K. Santra, R. Viswanatha, S. M. Daniels, N. L. Pickett, J. M. Smith, P. O'Brien, D. D. Sarma, *J. Am. Chem. Soc.* **2008**, *131*, 470.

[39] S. J. Han, T. H. Jang, Y. H. Jeong, J. H. Park, B. G. Park, Y. B. Kim, *Appl. Phys. Lett.* **2003**, *83*, 920.

[40] S. W. Yoon, S. B. Cho, S. C. We, S. Yoon, B. J. Suh, H. K. Song, Y. J. Shin, *J. Appl. Phys.* **2003**, *93*, 7879.

[41] Z. Y. Ning, S. H. Cheng, S. B. Ge, Y. Chao, Z. Q. Gang, Y. X. Zhang, Z. G. Liu, *Thin Solid Films* **1997**, *307*, 50.

[42] K. Minegishi, Y. Koiwai, Y. Kikuchi, K. Yano, M. Kasuga, A. Shimizu, *Jpn. J. Appl. Phys.* **1997**, *36*, L1453.

[43] M. Joseph, H. Tabata, T. Kawai, *Jpn. J. Appl. Phys.* **1999**, *38*, L1205.

[44] S. Murai, K. Fujita, K. Nakanishi, K. Hirao, *J. Phys. Chem. B* **2004**, *108*, 16670.

[45] M. Ajgaonkar, Y. Zhang, H. Grebel, M. Sosnowski, D. C. Jacobson, *Appl. Phys. Lett.* **2000**, *76*, 3876.

[46] L. H. Slooff, M. J. A. de Dood, A. Van Blaaderen, A. Polman, *Appl. Phys. Lett.* **2000**, *76*, 3682.

[47] S. Shionoya, T. Koda, K. Era, H. Fujiwara, *J. Phys. Soc. Jpn.* **1964**, *19*, 1157.

[48] X. Peng, J. Wickham, A. P. Alivisatos, *J. Am. Chem. Soc.* **1998**, *120*, 5343.

[49] W. W. Yu, X. Peng, *Angew. Chem. Int. Ed.* **2002**, *41*, 2368.

[50] R. N. Bhargava, D. Gallagher, X. Hong, A. Nurmikko, *Phys. Rev. Lett.* **1994**, *72*, 416.

[51] L. Levy, J. F. Hochepied, M. P. Pileni, *J. Phys. Chem.* **1996**, *100*, 18322.

[52] D. J. Norris, N. Yao, F. T. Charnock, T. A. Kennedy, *Nano Lett.* **2001**, *1*, 3.

[53] J. F. Suyver, S. F. Wuister, J. J. Kelly, A. Meijerink, *Phys. Chem. Chem. Phys.* **2000**, *2*, 5445.

[54] M. A. Malik, P. O'Brien, N. Revaprasadu, *J. Mater. Chem.* **2001**, *11*, 2382.

[55] F. V. Mikulec, M. Kuno, M. Bennati, D. A. Hall, R. G. Griffin, M. G. Bawendi, *J. Am. Chem. Soc.* **2000**, *122*, 2532.

[56] G. M. Dalpian, J. R. Chelikowsky, *Phys. Rev. Lett.* **2006**, *96*, 226802.

[57] S. C. Erwin, L. Zu, M. I. Haftel, A. L. Efros, T. A. Kennedy, D. J. Norris, *Nature* **2005**, *436*, 91.

[58] N. Pradhan, D. Goorskey, J. Thessing, X. Peng, *J. Am. Chem. Soc.* **2005**, *127*, 17586.

[59] D. Chen, R. Viswanatha, G. L. Ong, R. Xie, M. Balasubramaninan, X. Peng, *J. Am. Chem. Soc.* **2009**, *131*, 9333.

[60] P. N. Tananaev, S. G. Dorofeev, R. B. Vasil'ev, T. A. Kuznetsova, *Inorg. Mater.* **2009**, *45*, 347.

[61] D. A. Schwartz, N. S. Norberg, Q. P. Nguyen, J. M. Parker, D. R. Gamelin, *J. Am. Chem. Soc.* **2003**, *125*, 13205.

[62] S. M. Geyer, P. M. Allen, L.-Y. Chang, C. R. Wong, T. P. Osedach, N. Zhao, V. Bulovic, M. G. Bawendi, *ACS Nano* **2010**, *4*, 7373.

[63] M. Shim, P. Guyot-Sionnest, *Nature* **2000**, *407*, 981.

[64] D. V. Talapin, C. B. Murray, *Science* **2005**, *310*, 86.

[65] C. Wang, M. Shim, P. Guyot-Sionnest, *Science* **2001**, *291*, 2390.

[66] A. L. Roest, J. J. Kelly, D. Vanmaekelbergh, E. A. Meulenkamp, *Phys. Rev. Lett.* **2002**, *89*, 036801.

[67] S. Jana, B. B. Srivastava, S. Jana, R. Bose, N. Pradhan, *J. Phys. Chem. Lett.* **2012**, *3*, 2535.

[68] N. S. Norberg, G. M. Dalpian, J. R. Chelikowsky, D. R. Gamelin, *Nano Lett.* **2006**, *6*, 2887.

[69] R. Beaulac, P. I. Archer, S. T. Ochsenbein, D. R. Gamelin, *Adv. Funct. Mater.* **2008**, *18*, 3873.

[70] B. B. Srivastava, S. Jana, N. S. Karan, S. Paria, N. R. Jana, D. D. Sarma, N. Pradhan, *J. Phys. Chem. Lett.* **2010**, *1*, 1454.

[71] P. T. K. Chin, J. W. Stouwdam, R. A. J. Janssen, *Nano Lett.* **2009**, *9*, 745.

[72] S. Jana, G. Manna, B. B. Srivastava, N. Pradhan, *Small* **2013**, *9*, 3753.

[73] B. B. Srivastava, S. Jana, N. Pradhan, *J. Am. Chem. Soc.* **2011**, *133*, 1007.

[74] I. E. Türe, M. Claybourn, A. W. Brinkman, J. Woods, *J. Appl. Phys.* **1986**, *60*, 1670.

[75] R. Viswanatha, S. Brovelli, A. Pandey, S. A. Crooker, V. I. Klimov, *Nano Lett.* **2011**, *11*, 4753.

[76] K. E. Knowles, K. H. Hartstein, T. B. Kilburn, A. Marchioro, H. D. Nelson, P. J. Whitham, D. R. Gamelin, *Chem. Rev.* **2016**, *116*, 10820.

[77] G. Schlegel, J. Bohnenberger, I. Potapova, A. Mews, *Phys. Rev. Lett.* **2002**, *88*, 137401.

[78] L. Qu, X. Peng, *J. Am. Chem. Soc.* **2002**, *124*, 2049.

[79] S. Brovelli, C. Galland, R. Viswanatha, V. I. Klimov, *Nano Lett.* **2012**, *12*, 4372.

[80] P. J. Whitham, K. E. Knowles, P. J. Reid, D. R. Gamelin, *Nano Lett.* **2015**, *15*, 4045.

[81] H. D. Nelson, X. Li, D. R. Gamelin, *J. Phys. Chem. C* **2016**, *120*, 5714.

[82] C. Corrado, Y. Jiang, F. Oba, M. Kozina, F. Bridges, J. Z. Zhang, *J. Phys. Chem. A* **2009**, *113*, 3830.

[83] R. W. Meulenberg, T. van Buuren, K. M. Hanif, T. M. Willey, G. F. Strouse, L. J. Terminello, *Nano Lett.* **2004**, *4*, 2277.

[84] S. Jana, B. B. Srivastava, S. Acharya, P. K. Santra, N. R. Jana, D. D. Sarma, N. Pradhan, *Chem. Commun.* **2010**, *46*, 2853.

[85] J. F. Suyver, T. Van der Beek, S. F. Wuister, J. J. Kelly, A. Meijerink, *Appl. Phys. Lett* **2001**, *79*, 4222.

[86] A. V. Isarov, J. Chrysochoos, *Langmuir* **1997**, *13*, 3142.

[87] A. M. Jawaid, S. Chattopadhyay, D. J. Wink, L. E. Page, P. T. Snee, *ACS Nano* **2013**, *7*, 3190.

[88] S. F. Wuister, C. de Mello Donega, A. Meijerink, *J. Phys. Chem. B* **2004**, *108*, 17393.

Chapter 2

Methodology

In this chapter, the details of the experimental techniques that were used in this thesis are discussed in detail. The techniques are UV-visible absorption spectroscopy, photoluminescence (PL) spectroscopy, X-ray diffraction (XRD), transmission electron microscopy (TEM), nuclear magnetic resonance (NMR) spectroscopy, inductively coupled plasma-optical emission spectroscopy (ICP-OES) and zeta (ζ) potential.

2.1. UV-visible absorption spectroscopy:

This technique was used to monitor the formation of QD samples. We have also used this technique to find the band gap of the QD samples. When light falls the QD sample, it goes to the exited state from the ground state. The energy required for the process to occur is the energy difference between CB and VB and hence the band gap of the material can be determined from the absorption spectrum.

Practically, when a beam of light hits a substance, the spectrometer measures the intensity before it strikes the substance (I_0), and then again after it goes through the substance (I_T). The incident light may undergo absorption, reflection, interference, and scattering before it is transmitted to the detector. Thus, the intensity of light through the substance (I_T) will be reduced by a certain amount.

The change in intensity of light can therefore be equated as:

$$\Delta I = I_0 - I_T$$

The ratio of the light passing through a substance is measured as transmittance. The % transmittance is therefore given as:

$$\%T = 100\ (I_T/I_O)$$

Absorbance is defined as the amount of light which is absorbed by the substance and is calculated as the negative logarithm of transmittance.

$$A=\log_{10}(I_O/I_T) = \log_{10}(1/T) = -\log_{10}(T) = 2-\log_{10}(\%T)$$

Beer-Lambert's law allows UV-visible spectroscopy to be useful as not just a qualitative but also a quantitative tool.

Using this law, we have determined the concentration of the samples as the absorbance is given by

$$A = \varepsilon.c.l$$

where A = absorbance, ε = absorption cross-section, c = concentration of sample and l = sample thickness.

UV-visible absorption spectra of various samples in this thesis were dissolved in solvents such as hexane, toluene, chloroform and formamide were obtained using Agilent 8453 UV-visible spectrometer.

2.2. Photoluminescence (PL) spectroscopy:

PL spectroscopy is one of the most commonly used experimental techniques in studying photochemistry and photophysics of semiconductor QDs. We have used this technique extensively in the thesis to study the electronic structure of QDs.

2.2.1. Steady state PL spectroscopy:

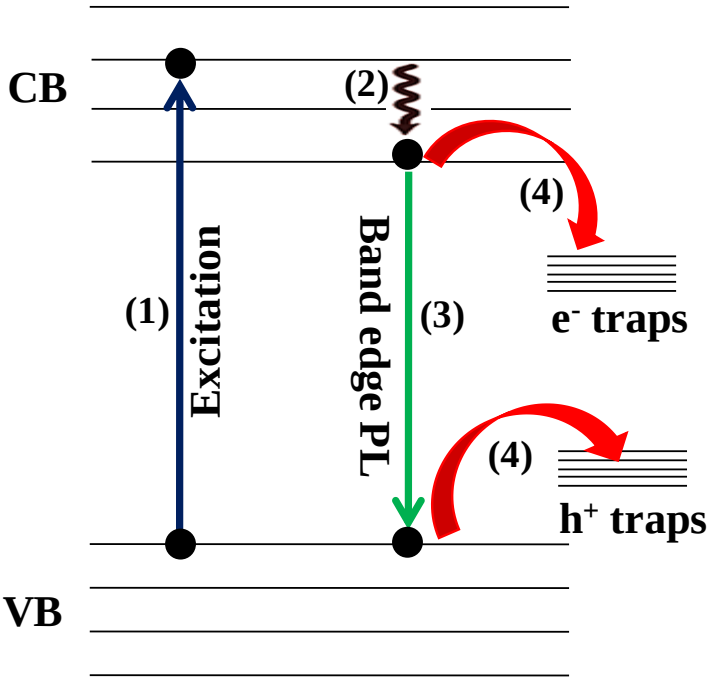

Figure 2.1. *Schematic of the processes that can occur when a QD is photo-excited.*

PL is the subsequent process to the absorption wherein the excited molecule or material comes to ground state by releasing the energy in the form of photons. The excited QD can come back to ground state through various decay channels as shown in Figure 2.1.

When the QD absorbs photons, the photo-generated electron goes to the CB leaving the photo-generated hole in the VB (process 1). The excited electron usually comes back to the lower excited state of CB through a non-radiative decay as shown as a process 2 in the Figure 2.1. This process occurs in the time scale of 10^{-13}s. If the electron from the lowest CB state recombines back with the hole present in VB, it gives rise to the band edge PL which occurs on the time scale of a few ns (process 3). However, the QDs have high surface to volume ratio which gives rise a lot of unpassivated atoms (dangling bonds) on their surface which all together form surface trap states. The trap states can be of electron trapping or hole trapping nature depending upon whether the surface is rich of unpassivated cations or anions respectively. The electron traps usually energetically lie below the CB whereas the hole traps energetically lie above the VB of QD and trap the charge carriers on the time scale of a few ps which is much faster process than the band edge recombination. This can be either radiative or non-radiative recombination (process 4). The surface trap emission in QDs is due to radiative recombination of the charge carriers with the trap states.

2.2.1.1. Correction of PL spectrum with grating efficiency:

Spectral correction is necessary to obtain the true emission spectra of the sample which is free from any instrumental artifacts. Most of the detectors have very less efficiencies in the 600-800 nm regime. For example, the Cu related emission in the Cu doped QD sample looks very weak in intensity when compared to the band edge emission as shown in Figure 2.2(a). Basically, the PL spectrum of the Cu doped sample looks almost similar to the undoped sample which is shown in the same figure. However, a visual inspection of the doped and undoped sample (Figures 2.2(b) and 2.2(c)) clearly showed that the Cu doped samples emit in a different wavelength regime. It suggests that the as obtained spectrum of the Cu doped samples needs to be corrected with the grating efficiency curve which is given in Figure 2.2(a). On correcting the PL spectrum of the Cu doped sample, the less intense higher wavelength Cu emission band dominates the PL spectrum as shown in Figure 2.2(d). This shows the importance of the grating correction in obtaining the true emission spectrum especially in the 600-800 nm regime. We have applied this grating correction for the PL spectra that are shown throughout this thesis.

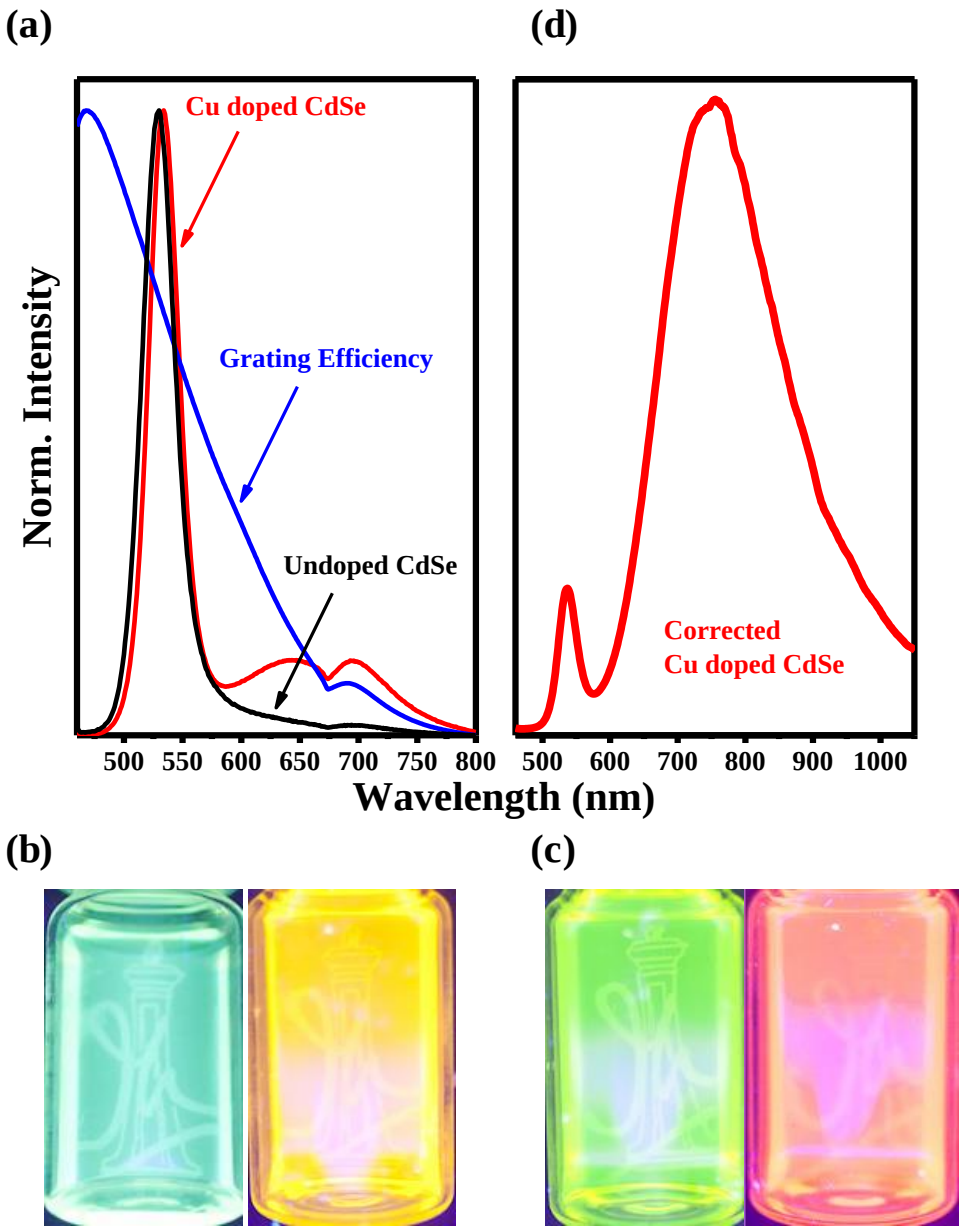

Figure 2.2. (a) *Uncorrected emission spectra of Cu doped and undoped CdSe QDs along with the grating efficiency curve. Digital image of the emission of different sizes of* ***(b)*** *undoped CdSe QDs and* ***(c)*** *Cu doped CdSe QDs.* ***(d)*** *Spectrally corrected emission spectra of Cu doped CdSe QDs.*

2.2.1.2. Conversion of signal data from Wavelength to Energy units:

Conventionally, PL spectra are plotted with respect to wavelength. But, it is always preferred to plot with respect to energy in material science. Directly changing the x-axis from wavelength to energy scale will result in improper data. For example, consider a constant unit signal over the range of 400-800 nm. The area over this wavelength range is 400 units. The wavelength

scale can be converted to energy scale by using the familiar equation, E=hc/λ. After this conversion, the x-axis changes from 400 nm-800 nm to 3.1 eV-1.55 eV. Now, the area will be 1.55 units which is not equal to that of wavelength scale. To correct this, the signal in the wavelength will be scaled by hc/E^2 as the function of signal in the energy scale can be written as

$$f(E)\,dE = f(\lambda)\,d\lambda$$

$$f(E) = f(\lambda)\,d\lambda/dE = f(\lambda)\,(d/dE\,(hc/E)) = -f(\lambda)\,(hc/E^2)$$

The factor, hc/E^2 is called Jacobian transformation.[1]

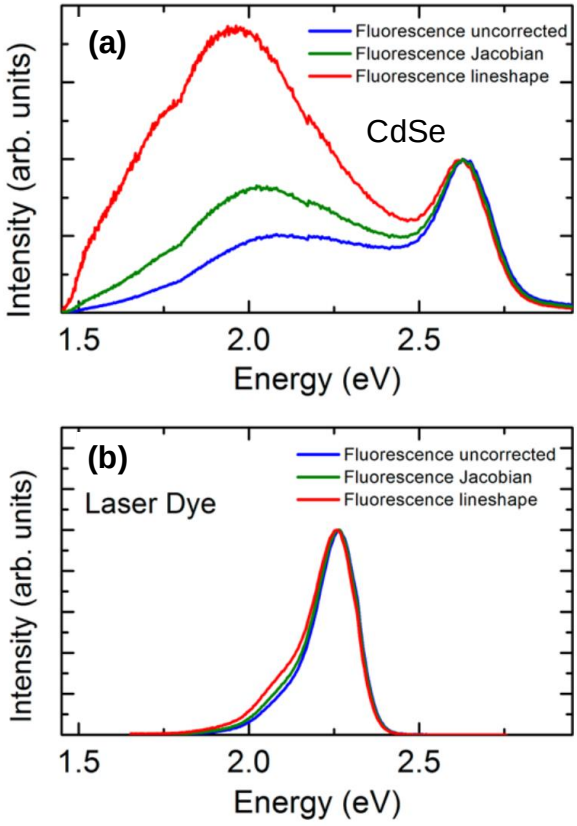

Figure 2.3. *Corrected and uncorrected fluorescence spectra for CdSe* ***(a)*** *and fluorescence from a laser dye* ***(b)****. Adapted from ref [1] Copyright 2013 American Chemical Society.*

This conversion is important when the spectra are broad enough to cover a wide range of energies compared to the ones which are having narrow fwhm. The importance of this correction is explained in Figure 2.3. for two different spectra. In case of a QD with broad surface trap emission band along with the band edge PL (Figure 2.3(a)), the transformation

significantly alters the spectrum. It leads to slight red shift in the PL energy maximum in case of surface trap emission and also affects the intensity of the overall spectrum. In contrast, a laser dye (Figure 2.3(b)) or the band edge PL of a QD is mostly unaffected by the Jacobian transformation.

We have applied this correction to all the PL spectra shown in the thesis as the Cu emission band is usually very broad in nature.

2.2.2. PL quantum yield (QY):

The PL QY is defined as the ratio of the number of photons emitted to the number of photons absorbed. It gives the information how the excited QD be deactivated either through radiative or non-radiative processes. PL QY will be 100% if all the excited photons decay radiatively to the ground state.

$$\text{PL QY} = \frac{\text{Number of photons emitted}}{\text{Number of photons absorbed}}$$

Experimentally, PL QY can be used measured by comparative method or absolute method.[2]

"Comparative method" involves the use of well characterized standard samples with known QY values. This method is widely used and suitable for weakly absorbing samples in dilute solutions. The solutions of the reference and test samples with identical absorbance at the same excitation wavelength can be assumed to be absorbing the same number of photons. Hence, the ratio of the integrated PL intensities of the two solutions (recorded under same slit width, dwell time and other conditions) will yield the ratio of the QY values. Since QY for the reference sample is already known, it is straight forward to calculate the QY for the sample under measurement from the equation given below.

$$\mathbf{QY_{sample}} = \frac{I_{sample}\ A_{ref}\ \eta_{sample}}{I_{ref}\ A_{sample}\ \eta_{ref}}\ \mathbf{QY_{ref}}$$

where I= integrated PL Intensity

A=absorbance at excitation wavelength

η= refractive index of the solvent

This method strongly relies on the reference sample and there are only few reference samples that are available in longer wavelengths which limits this method for measuring PL QY as the method requires similar optical properties for the standard as that of the sample.

These limitations can be overcome by use of integrating sphere which collects all the emission from the sample and this method is known as "Absolute method". We have used this method to calculate the PL QY of the QD samples in this thesis. The method involves measuring the scattering spectra of solvent and samples along with the emission spectrum of sample. The intensity of the scattering spectrum of the sample is less than that of solvent as the QDs present in the sample absorbs the incident light. The intensity difference in the scattering spectra of solvent and sample gives the number of photons absorbed by the sample. Then with the help of emission spectrum which gives the number of photons emitted and the intensity difference in the scattering spectra, the measurement of PL QY of the sample is trivial.

2.2.3. Time-resolved PL spectroscopy (TrPL):

Here, the PL of QDs is monitored as a function of time after excitation by a flash of light. The time resolution can be obtained in a number of ways which depends on the required sensitivity and time resolution. TCSPC (Time-Correlated Single Photon Counting) is one of them and it is a digital counting technique which counts photons that are time-correlated in relation to a short excitation light pulse. This technique is used in finding the radiative and non-radiative lifetimes that occur during the relaxation of QD to the ground state as shown in Figure 2.1. In this thesis, we have extensively used this technique to obtain average lifetimes of Cu PL and band edge PL. Average lifetime is the time taken for the population of excited state molecules to become 37% of its original intensity after the excitation of QDs at time, t=0. Also, the lifetime and the percentage contributions of non-radiative decay processes in the PL decay curves are obtained by analyzing the fast components present in decay curve.

2.2.4. Temperature dependent PL spectroscopy:

Here, the PL spectra (both steady state and time resolved) are measured as a function of temperature. Low temperature PL studies are of great interest in semiconductor materials.[3] The electron-phonon interaction usually decreases at low temperature leads to increase in the band gap of material. Also, the PL intensity and the average lifetime of the sample is usually

high at low temperature compared to room temperature as the traps are relatively ineffective at low temperature. This will be discussed in detail in **Chapter 5.**

Steady state PL spectra of the QD samples which are dissolved in hexane or Formamide were collected using the 450 W xenon lamp as the source on the FLSP920 spectrometer, Edinburgh Instruments, while the lifetime measurements were carried out using a pulsed diode laser, EPL-405 (λ_{ex}=405 nm) and pulsed LEDs, EPLED-380 (λ_{ex}=380 nm) and EPLED-270 (λ_{ex}=270 nm) as excitation sources. Absolute PL QY was determined using an integrating sphere for both doped and undoped samples. For low temperature measurements, the samples which are dissolved in hexane were drop casted on a glass substrate and the solvent was allowed to evaporate leaving behind the QDs on the substrate and the measurements were performed using an Oxford DN2 liquid nitrogen cryostat with the same spectrometer.

2.3. X-ray Diffraction (XRD):

This is very common and useful technique for material chemists in day to day life for determining the crystal structure of materials.

X-ray diffraction technique mainly works based on the constructive interference of the x-rays that were diffracted from the different crystal planes of the QD. It obeys Bragg's law. Suppose, an x-ray beam incident on a pair of parallel planes P1 and P2 which have an interplanar distance of d. The two parallel incident rays 1 and 2 make an angle, θ with these planes. A reflected beam will have a maximum intensity if the waves represented by 1' and 2' are in phase. The difference in path length between 1 to 1' and 2 to 2' must then be an integral number of wavelength of incident ray, λ. We can express this relationship mathematically as Bragg's law.

$$n\lambda=2d\sin\theta \text{ where } n=1,2,3,\ldots..$$

where d is the interplanar distance and θ is the angle of incident X-rays.

The XRD peaks become broader with decreasing the size of the particles due to the finite size of the QDs. There is a relation between the peak broadening and the size of the QDs and it is given by Scherrer's equation,

$$D_{hkl=}\ (0.89\,\lambda/\ \beta_{hkl}\cos\Theta)$$

where D_{hkl}= thickness of the crystal

λ= X-ray wavelength

β= line broadening at fwhm

Θ=Bragg angle.

Crystal structure identification of the QDs was carried out using X-ray diffraction, recorded on Bruker D8 Advance diffractometer using Cu K_α radiation. Since the diffracted intensities from these QDs are generally weak, all patterns were recorded at a slow scan rate (0.75^o per minute) in order to get a high signal-to noise ratio. The bulk XRD patterns were obtained from the inorganic crystal structure database and broadened using the Scherrer formula to simulate the corresponding QD XRD.

2.4. Transmission electron microscopy (TEM):

TEM is a very powerful tool for material science. The interaction between the electrons and the material can be used to observe the crystal structure and other features in the structure by illuminating a high-energy beam of electrons through a thin QD sample. TEM can be used to study the quality, shape, size, growth of layers in core/shell materials and defects in semiconductors QDs.

The TEM works on the same basic principle as the light microscope but uses electrons not light. Because the wavelength of electrons is much smaller than that of light, the optimal resolution attainable for TEM images is many orders of magnitude better than that from a light microscope. The beam of electrons from the electron gun is focused into a small, thin, coherent beam by the use of the condenser lens. The beam then strikes the sample and parts of it are transmitted depending upon the thickness and electron transparency of the sample. This transmitted portion is focused by the objective lens into an image on charge coupled device camera, to obtain the image of sample.

We have used this technique to determine the formation, size and shape of the QDs. The monodispersity of the formed QDs was examined by calculating the size distribution of large number of QDs present on TEM grid.

Samples for TEM were prepared by adding a solution of the QDs dissolved in hexane dropwise on carbon coated Cu grid. The solution was allowed to evaporate leaving behind the QDs. TEM images were recorded using Technai F30 UHR version electron microscope, using a field emission gun at an accelerating voltage of 300 kV.

2.5. Inductively coupled plasma-optical emission spectroscopy (ICP-OES):

This technique is widely used for quantitative detection of the elements present in the given unknown sample or to determine the composition of constituents in a given sample. The instrument consists of a light source unit, plasma generator, spectrometer, detector and a data processing unit. The component elements of the material are excited into higher energy levels by applying plasma energy which has very high electron density and temperature (10000 K). A very high electromagnetic field is used for ionizing the argon gas so that the plasma is generated. Solution samples are introduced into the plasma environment through a narrow tube. When the excited atoms return back to lower energy states by emitting photons. The element type is determined based on the energy of the emitted photons, and the content of each element is determined based on the signal intensity.

We have used ICP-OES mainly for detecting the percentage of Cu in the Cu doped samples and the composition of constituent elements in the alloy QDs. First, the standards of constituent elements of different concentrations were prepared and measured to obtain a plot of concentration vs intensity within the linear regime. The concentration of the elements in the unknown sample is then obtained from this calibration plot by measuring the intensity and obtaining the corresponding concentration. Sample preparation was done by washing the QDs several times to remove excess precursors and then digested in concentrated HNO_3 and diluted with Millipore water. ICP-OES measurements were carried out using a Perkin-Elmer Optima 7000 DV instrument.

2.6. Nuclear Magnetic Resonance (NMR) spectroscopy:

It has become the important method of analysis for organic compounds, because in many cases it provides a way to determine an entire structure using one set of analytical tests. It is also increasingly used in inorganic chemistry and biochemistry in the recent years.

Nuclear Magnetic Resonance is a property of the nucleus of an atom and it depends on nuclear spin (I). When a nucleus with I = 1/2 is placed in a magnetic field, it can either align itself with the field (lower energy) or against it (higher energy), two energy levels will be formed. When radio waves are applied, nuclei in the lower energy state can absorb the energy and jump to the higher energy state. We can observe either the absorption of energy or the subsequent release of energy as the nucleus "relaxes" back to the lower energy state. Traditionally this was done by scanning slowly through a range of radio wave frequencies (continuous wave). However this has largely been replaced by the faster Fourier Transform method where one big and broad pulse of radio waves is used to excite all nuclei and then the results are analyzed by computer. Most commonly used NMR nuclei are proton (^{1}H), ^{13}C, ^{15}N and ^{31}P.

NMR is also used in studying the ligand bonding and dynamics on the QD surface.[4, 5] The advantage of this technique comes from the broadening of the NMR peaks of the ligands when they are bound on the QD surface compared to the free ligands. The slow motion of the ligands causes the broadening of the NMR peaks of the ligand molecules when they are bound to the QD surface because of quasi solid-nature of QDs. In other words, the broadening is due to inhomogeneity of the chemical environment of the ligands when they are bound to the QD surface. In this thesis, we have monitored the ligand exchange on the QD surface by studying the peak broadening of the ^{1}H NMR and ^{31P} NMR spectra.

^{1}H and ^{31}P NMR spectra were measured using a Bruker AV-400 spectrometer with chemical shifts reported as parts per million (ppm). $CDCl_3$ was used as solvent for all the compounds except pyridine and pyridine capped QDs which were collected in DMSO-d_6 solvent. TMS was the internal standard for ^{1}H NMR, and TPP with δ = -6 was the internal standard for ^{31}P NMR spectra.

2.7. Zeta (ζ) potential:

This is very important tool in determining the colloidal stability of charged species in the given dispersion medium. ζ-potential is the potential difference between the dispersion medium and the stationary layer of fluid attached to the dispersed particle. The magnitude of the ζ- potential indicates the extent of electrostatic repulsion among the charged particles present in a

dispersion. When the potential is small, attractive forces may exceed this repulsion and the dispersion may break and flocculate. So, colloids with high ζ-potential are electrically stabilized and the colloids with low ζ-potentials tend to agglomerate. The sign of the ζ-potential indicates whether they are negatively charged (negative ζ-potential) or positively charges particles (positive ζ-potential). We have used this measurement to characterize the formation of sulfide rich CdS QDs in **Chapter 7.** The presence of negative ζ-potential indicates the presence of sulfide ligands on the CdS QD surface.

ζ-potential measurements were done in both water and formamide. ζ- Potential measurements were carried out using a Nano ZS (Malvern, UK) employing a 532-nm laser at a back-scattering angle of 173° .

Bibliography:

[1] J. Mooney, P. Kambhampati, *J. Phys. Chem. Lett.* **2013**, *4*, 3316.

[2] L. Porres, A. Holland, L.-O. Pålsson, A. P. Monkman, C. Kemp, A. Beeby, *J. Fluoresc.* **2006**, *16*, 267.

[3] H. Temkin, G. J. Dolan, M. B. Panish, S. N. G. Chu, *Appl. Phys. Lett.* **1987**, *50*, 413.

[4] X. Ji, D. Copenhaver, C. Sichmeller, X. Peng, *J. Am. Chem. Soc.* **2008**, *130*, 5726.

[5] Z. Hens, J. C. Martins, *Chem. Mater.* **2013**, *25*, 1211.

Part I

Study of Bulk Electronic Structure Using Cu Emission

Chapter 3

II-VI Semiconductor Quantum Dots

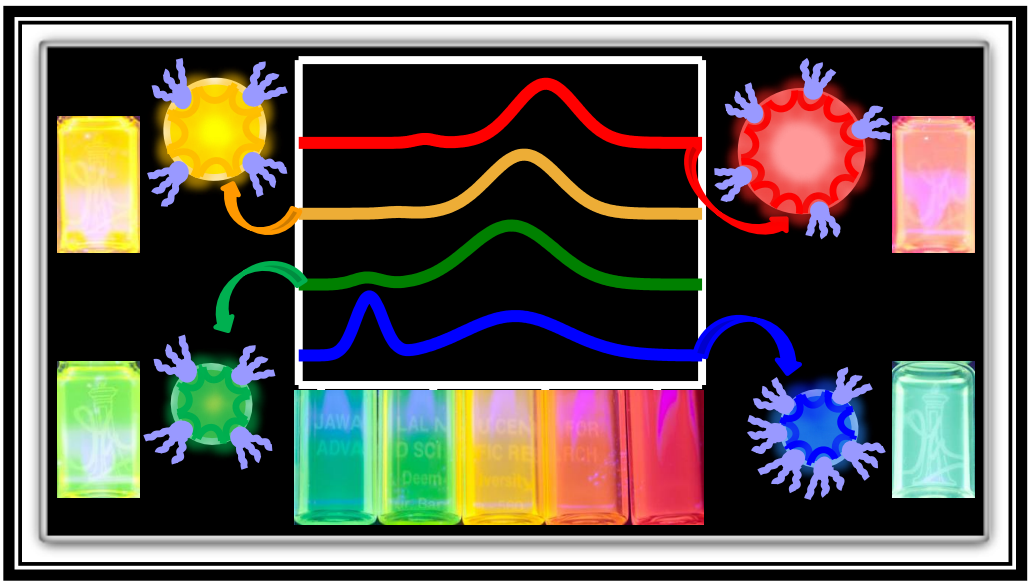

The following papers have been published based on work presented here: G Krishnamurthy Grandhi, Renu Tomar and R. Viswanatha. Study of Surface and Bulk Electronic Structure of II-VI Semiconductor Nanocrystals Using Cu as a Nanosensor. *ACS Nano* **2012,** *6,* 9751.

3.1. Abstract:

Efficiency of the QD based solar cells relies on charge transfer at the interface and hence on the relative alignment of the energy levels between materials. In spite of high demand to obtain size specific band offsets, very few studies exist and are studied using meticulous methods like photoelectron spectroscopy. However, semiconductor charging during measurements could result in indirect and possibly inaccurate measurements due to shift in VB and CB position. Here, in this report, we devise a novel method to study the band offsets by associating an atomic like state with the CB and hence obtaining an internal standard. This is achieved by doping copper in semiconductor QDs, leading to the development of a characteristic intra-gap Cu-related emission feature assigned to the transition from the CB to the atomic like Cu *d* state. Using this transition, we determine the relative band alignment of II-VI semiconductor QDs as a function of size in the below 10 nm size regime. The results are in excellent agreement with the available photoelectron spectroscopy data as well as the theoretical data.

3.2. Introduction:

The study of electronic structure of QDs plays an important role in tailoring the band offsets to maximize the degree of overlap between the wave functions[1] as well as in various applications like the excitonic solar cells [2] along with obtaining of high quality QDs.[3] One of the key factor governing the efficiency of the solar cells is the interfacial electronic energy alignment and hence is important to accurately determine the electronic energy offsets in QDs.[4, 5] An in-depth understanding of the bulk electronic structure in QDs greatly enhances our capability of obtaining high quality QDs and using them more effectively in potential applications.

It is well known for a long time that the band gap of the QD varies as a function of size and several techniques, particularly absorption spectroscopy, have been used extensively to study the evolution of bandgap of these materials.[6] Cyclic voltammetry, that is more compatible with organic ligands, has been useful in finding out the absolute positions of band edges in bulk with respect to vacuum using ionization potential and electron affinity.[7-9] However, along with specific concerns about solvent, electrode and electrolyte, it is not quite straight forward to obtain the shift in CB and VB of the QDs from the ionization potential since

optically observed band gap is not related to the ionization potential and electron affinity in a direct manner.[10] More recently, a rapid technique known as the photoelectron spectroscopy in air has been introduced to determine the ionization potential on films and powder. While this technique has been used to determine the VB and CB variation as a function of size in QD samples,[10] it is evident that it involves substantial number of assumptions to derive the CB and VB shift including the effective mass approximation and an arbitrary assumption of the dielectric constant of the matrix. Clearly, although extensive research has been devoted for the study of size dependent evolution of CB and VB via experiment, deconvolution of the shift in CB and VB in QDs has mainly been dominated by theoretical results.[11-14] Nevertheless a few examples exist wherein the position of the band edges have been determined using photoemission spectroscopy,[15-19] x-ray absorption spectroscopy[18] or scanning tunnelling spectroscopy.[20] These methods, while providing the basis for the experimental realization of the isolated study of evolution of CB and VB has major limitations in terms of experiment. Both photoemission and x-ray absorption spectroscopy and most often scanning tunnelling spectroscopy have to be carried out in ultra-high vacuum that makes these measurements very expensive and time consuming.[17] Additionally inaccuracies in the energy positions set in due to the problems of charging of semiconductor QDs.[16, 17, 21] Due to the presence of surface organic ligands, the samples may also be damaged in the beam or may degas extensively.[21] Hence development of a simple alternate method that is organic ligand friendly, less time consuming and straight forward to measure is necessary to accurately map the CB and VB positions in the QDs. The presence of such a method has an additional important consequence in study of hetero-nanostructures. Currently, due to the absence of extensive data for the band offsets as a function of size, it has been generally assumed that the band alignment in QDs follow the same trend as that of bulk materials. Consequently, it would not be possible to determine the presence of band crossings, if any, although it would drastically affect the properties of the hetero-structure in question. The measurement of band offsets for a large number of sizes in various QDs opens up a new arena of study in the field of QD heterostructures.

In this chapter, we introduce a novel way of measuring band offsets by doping small amounts of Cu into the QD and studying the emission from the CB to the atomic-like Cu *d* level. This method, along with being a more direct probe that can be performed at atmospheric

conditions with a simple optical measurement also has an additional advantage of being an internal standard present permanently in the QD. This technique allows us to study the band offsets in large scale assemblies thus acting as an excellent internal standard to study the bulk electronic structure of the QDs. In this chapter, we have first used CdSe as a model system to study the variation of band offsets as a function of size. Further we not only prove the generality of the proposed method by extending this technique to other II-VI semiconductors but also use this technique to determine the relative band alignment in II-VI semiconductor QDs. Interestingly, we show for the first time that while band alignment in bulk can be extended to QDs in the study of VB, it is not true in the case of CB. Consequences of these band crossings have also been explored in this chapter.

3.3. Experimental section:

3.3.1. Materials: CdO, stearic acid and copper(II) acetate monohydrate were purchased from S D Fine chemicals. oleic acid (90%), ODE (90%), and TOP (90%) and Se pellets were obtained from Sigma Aldrich. TMAH (98%) was obtained from Spectrochem. All purchased chemicals were used without further purification.

Copper stearate was synthesized and purified similar to the literature reports [22] published previously. Briefly, copper acetate was dissolved in methanol and added dropwise to a flask containing TMAH and oleic acid to obtain precipitates of copper stearate that was thoroughly washed with methanol and acetone.

Cadmium oleate was synthesized using modified literature methods. Briefly, CdO, oleic acid and ODE (4.5 mL) were degassed in vacuum and backfilled with Ar and heated to high temperature in argon atmosphere till the solution turns colorless. Cadmium oleate with different molarities were prepared by varying the weight ratios of CdO to oleic acid (1:2.5 – 1:5). 2 M TOPSe solution was prepared by dissolving appropriate amount of Se in TOP in a glove box. It was then further diluted with TOP to obtain different molarities (1.2 M – 0.33 M) of the solution.

3.3.2. Synthesis of Cu doped CdSe QDs: Appropriate solution of cadmium oleate and ODE were degassed in a three-necked flask and heated to 180˚C. TOPSe (0.47 mmol – 1.68

mmol TOP/ 0.0197 g Se) was injected at 180 ˚C in Ar atmosphere and annealed for a minute to form CdSe QDs. The reaction was cooled down to 140 ˚C and copper stearate solution of different molarities was added drop wise and annealed for 20 mins. Samples were washed with hexane methanol mixture and precipitated using ethanol. To obtain the bigger sizes, reaction mixture was heated to higher temperature after 20 minutes with additional injection of cadmium oleate precursor. In the undoped case, instead of the copper stearate solution of ODE, only ODE was added as blank and was annealed for similar length of time. Samples were washed with hexane methanol mixture and precipitated using ethanol.

3.3.3. Synthesis of other Cu doped II-VI semiconductor QDs: Cu doped CdS QDs were synthesized by first preparing the different sizes of CdS QDs using already reported method in literature.[23] Following the formation of CdS QDs, 10 µmoles of copper stearate solution in 1 mL of ODE was added at 150 ^{o}C and maintained for two hours at that temperature to obtain Cu doped CdS QDs of different sizes. Cu doped CdTe QDs were synthesized by preparing CdTe QDs of different sizes as reported in literature[24] followed by cooling the reaction mixture to 160 ^{o}C. At this temperature, 50 µmoles of copper acetate in 0.5 mL of oleylamine was added as the copper precursor[25] to the reaction mixture in order to obtain Cu doped CdTe QDs of various sizes. Samples thus obtained were washed with a mixture of hexane and methanol and then precipitated using acetone. Cu doped ZnS and Cu doped ZnSe QDs were synthesized using the methods reported in literature.[22, 26]

3.4. Results and discussion:

Cu doping of semiconducting QDs has been extensively explored in several recent reports.[22, 25, 27-30] One common trend emerging from these studies is the presence of the characteristic long-lived intra-gap Cu-related PL band accompanied by suppression of the intrinsic BE emission. It is well known in the community that the impurities like Cu,[22, 25, 27, 30, 31] Eu,[31-34] Co[35, 36] or Mn[31, 37-39] introduce atomic-like states within the forbidden gap of the host semiconductor that can exchange charges with the VB and CB via radiative and non-radiative transitions. While the mechanism of this intra-gap luminescence in Cu has been extensively debated in several recent reports,[25, 28, 30] the origin of this wide band has been universally accepted and has been attributed to the optical transition from the CB of the host semiconductor

to the atomic-like Cu *d* level. It has been extensively proven in literature that energies of atomic levels with respect to vacuum is independent of the host semiconductor (for example, Mn *d-d* transition at 2.15 eV,[31, 37, 38] or Eu $^5D_0$ - $^7F_2$ transition at ~ 2eV [31-34]) and size. [36, 39] However in most of these cases optical transition has been observed from an atomic level to an atomic level and hence cannot be used to determine the electronic structure of the host. The presence of a single Cu *d* level in the mid band gap region presents us with a unique opportunity to measure the association of an atomic state with the CB of the host semiconductor providing an important internal standard[40] to study the shift in the CB as a function of size and as a function of various host materials.

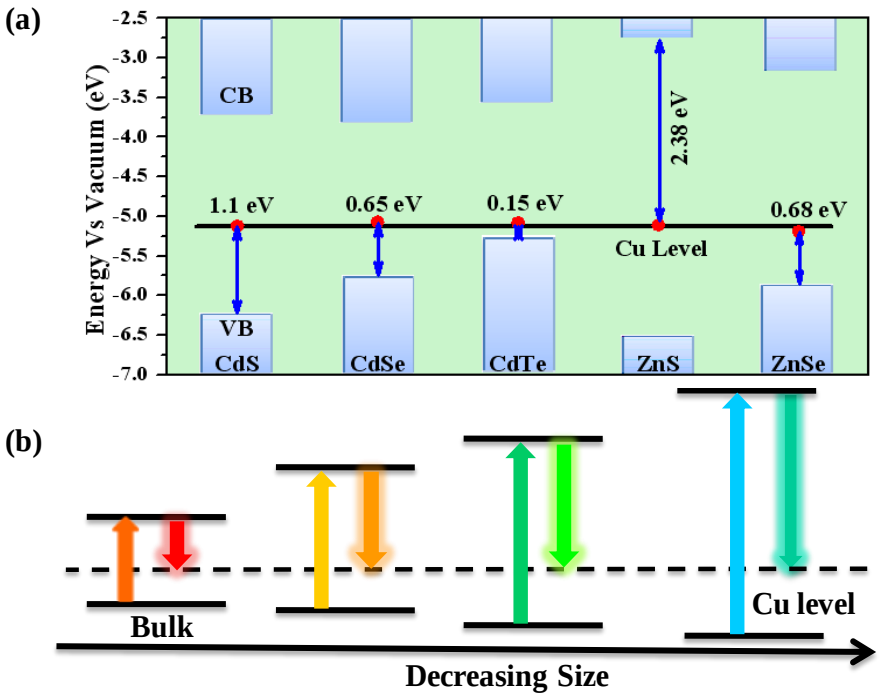

Figure 3.1. ***(a)*** *Bulk band gap and position of the Cu state in CdS, CdSe, CdTe, ZnS and ZnSe. The relative bulk band alignment[41, 42] and the Cu state positions[43-47] are collected from various literature references.* ***(b)*** *Schematic of the energy level diagram showing the variation of the CB, VB and the Cu d level with decreasing size.*

A compilation of available literature[41-47] on the band alignment as well as Cu levels in bulk semiconductors is shown in the Figure 3.1(a). Analogous to the other transition metal and lanthanide energy levels arising from atomic states, it is evident that the Cu level also remains constant from one semiconductor to another in the bulk regime. Similarly, as shown

by earlier theoretical results for Mn[39] and experimental and theoretical results for Co and other impurity levels,[36] one would expect that same would be true as a function of size for the Cu *d* levels. The schematic representing the transitions from the CB to the Cu *d* level in addition to the band gap transition under this assumption is shown in Figure 3.1(b). If this assumption was indeed true, it would be possible to independently investigate the shift in the CB of the host QDs as a function of size by determining the position of the Cu related PL peak.

3.4.1. Characterization of Cu doped CdSe QDs:

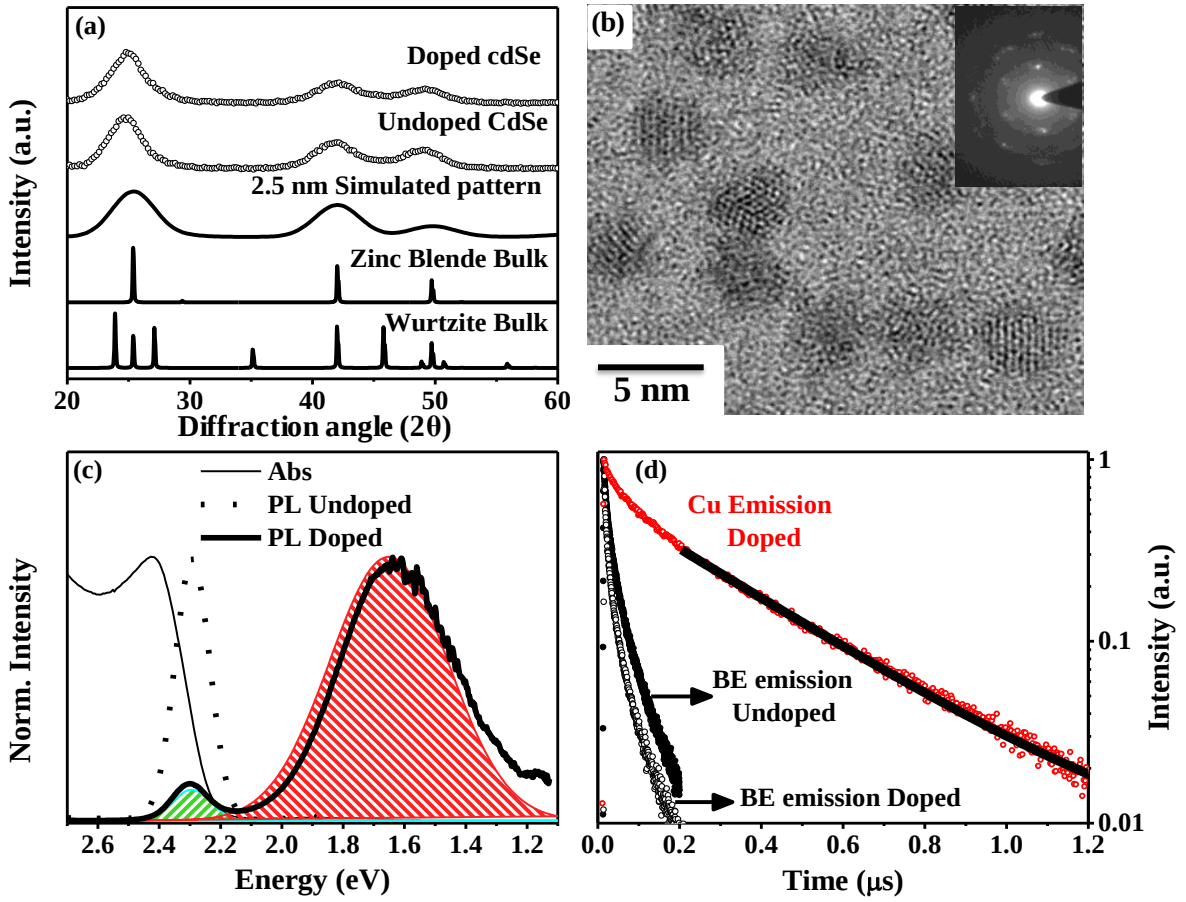

Figure 3.2. (a) *XRD patterns of a typical Cu doped and undoped CdSe QDs along with the simulated pattern for 2.5 nm particle and the bulk wurtzite and zinc blende crystal structures.* ***(b)*** *Typical high resolution TEM of Cu doped CdSe QDs. Shown in the inset is the SAED pattern of the QDs.* ***(c)*** *Absorption (thin solid line) and PL spectra of doped (thick solid line) and undoped sample (dotted line) along with a typical area under the PL peaks.* ***(d)*** *Time resolved PL data of the undoped (closed circles) and doped (open circles) sample at the BE emission (black circles) and the doped sample at Cu related emission (red circles) along with a single exponential fit (black line).*

We have used CdSe QDs as a model system to study the bulk electronic structure since it has been one of the most widely synthesized QDs in literature with narrow size distributions and excellent optical stability. However, doping CdSe with various dopants including Cu have been tried by different groups and has been classified as undopable[48] based on the absence of Cu emission peak in the optical spectrum, with reasons being attributed to intrinsic self-purification to fundamental thermodynamic or kinetically controlled processes such as the crystal structure.[22, 48, 49] In this chapter, we demonstrate that presence or absence of PL emission attributed to Cu states does not determine the efficacy of doping in QDs. For example, in this specific case of CdSe, we illustrate in **Chapter 6** that it is possible to obtain the emission from the CB to the copper *d* state by systematically varying the ligands to alter the surface of the QD. A logical route to the synthesis and characterization of Cu doped CdSe with a prominent emission from CB to the Cu *d* level has been established by systematically varying the surface ligands.

Cu doped CdSe QDs were synthesized using cadmium oleate as the Cd source and TOP complex of Se (TOPSe) as the Se source. The details of the synthesis are given in the experimental section. Copper stearate in ODE solution was injected into the solution after the formation of CdSe, the amount of Cu being determined such that the solution did not precipitate when heated at high temperatures. The formation of QDs was characterized using XRD measurements. Typical XRD patterns of doped and undoped CdSe are shown in Figure 3.2(a). Comparing the XRD patterns with that of the bulk CdSe, crystallizing in zinc blende and wurtzite structures, we observe that both doped and undoped QDs crystallize in the same cubic zinc blende phase with similar lattice parameters. Similar to earlier literature reports, [50] the pattern was simulated (also shown in Figure 3.2(a)) by broadening the bulk XRD pattern using the Scherrer formula and quantitative information on the size of the QDs was obtained. The size of the QDs obtained by this procedure for both doped and undoped samples was found to be 2.5 nm implying that the size and crystal structure have not changed after doping Cu. In the earlier literature, there has been a debate[49] on the viability of doping based on the crystal structure of the QD and has been concluded that the QD can only be doped if it is formed in the cubic phase. Thus, our QDs should be ideal candidates to dope with Cu. QD sizes were also confirmed using TEM and a typical TEM image is shown in Figure 3.2(b) that shows an abundance of spherical particles with sizes in agreement with XRD results. SAED shown in

the inset to Figure 3.2(b) as well as lattice fringes seen in these particles confirms a high degree of crystallinity of the sample as is also evident from the XRD patterns. The amount of Cu present in the sample was measured using ICP-OES and found to be 0.25%.

Typical PL and absorption spectra of doped and undoped QDs are shown in Figure 3.2(c). It is important to note here that "as obtained" spectrum of doped QDs do not result in the spectrum shown in Figure 3.2(c). Since the Cu related emission is broad and occurs in the 600-800 nm regime where most detectors are known to have decaying efficiencies we obtain a Cu peak that is weak as a consequence of the artifact of decaying detector efficiency. We have corrected the as obtained PL spectrum using the grating efficiency curve as explained in the **Chapter 2**. Additionally, since we are interested in studying absolute energy of the host QD, we have also applied the necessary energy correction[51] as explained in **Chapter 2** to arrive at the final spectrum that will be referred to as PL spectra for future references. In Figure 3.2(c), on comparison of the PL spectra with the undoped CdSe, we observe the presence of an intense PL at ~1.63 eV (shaded red) and a weak residual BE emission peaked at about 2.25 eV (shaded green) in case of Cu doped CdSe QDs. ICP-OES analysis of the extensively washed sample shows the presence of substantial Cu within the QD. Upon incorporation of copper, the ratio of the red-shifted PL peak relative to the BE absorption feature has traditionally been used to determine the extent of success in integrating the Cu atom into the lattice of the QD.[28] However, PL lifetime studies shown in Figure 3.2(d), collected at both the spectral features shows that the Cu related emission is several orders of magnitude slower than the BE emission similar to the earlier reports,[30] and hence intensity ratio of the Cu related PL emission cannot be used as a direct measure of the capability to dope Cu into the lattice of the QD. The BE emission lifetime is found to be about ~20 ns while the Cu^{2+} PL lifetime is mostly single exponential with a much larger lifetime (~500 ns), confirming that the peak is not due to the surface states and is due to the weak spatial overlap between the CB electron wave function and the localized copper state. The QY of the Cu emission at ~1.63 eV was found to be quite high (~ 15%).

3.4.2. Size dependent bulk electronic structure of the CdSe QDs:

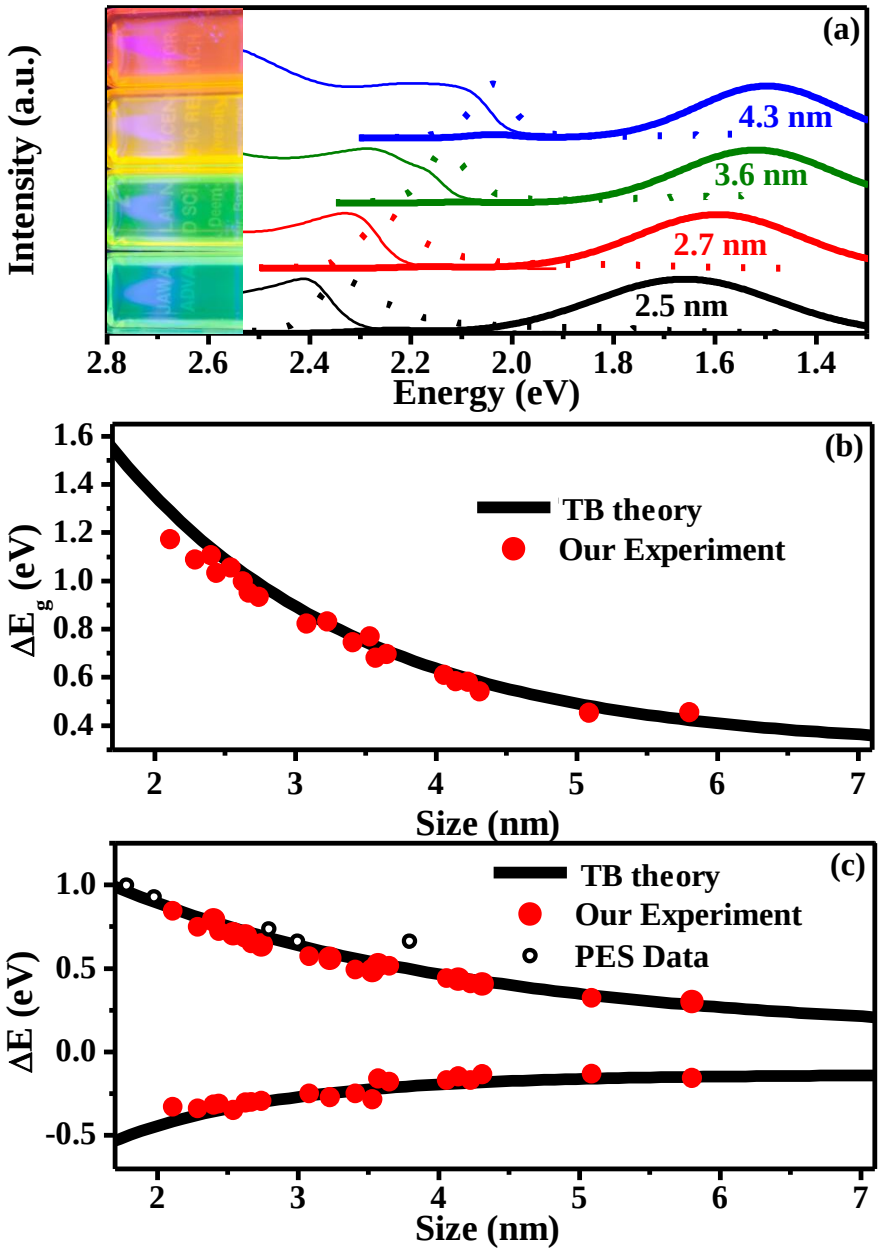

Figure 3.3. (a) *Typical absorption and PL spectra of the doped and undoped CdSe QDs for varying sizes showing a shift in the Cu related emission position. Inset shows a digital picture of Cu doped samples of various sizes. These are excited using a hand-held UV lamp at 350 nm excitation.* ***(b)*** *Variation of bandgap as a function of size along with the TB prediction (solid line)* ***(c)*** *Variation of VB and CB shift in bandgap obtained from analyzing the Cu related emission shown as red circles overlapped with the TB theoretical technique (solid line) (Ref [11]) and from photoemission spectroscopy, PES data (open circles) (Ref [19]).*

It has been explored by systematically studying the position of the Cu related emission in doped systems. The position of the Cu emission has been extensively studied prompted by the constant 2.15 eV emission of Mn *d-d* transition irrespective of the size or the host material, and is observed to be red shifted with respect to the BE emission and is tunable by tuning the size of the QD.[27, 29] Similar to other systems studied till date, typical absorption and emission spectra of doped and undoped CdSe QDs obtained for varying sizes is observed to have an intense tunable Cu related emission (Figure 3.3(a)) that is red shifted with respect to the BE emission.

This tunability of the Cu related emission is expected since the emission occurs from the CB of the QD to the atomic like Cu *d* level and the CB is known to shift as a function of size. However, it is important to note that since the Cu *d* level is not expected to shift as a function of size, the shift in the position of the Cu related emission is entirely due to the shift in the CB of the QD and hence allows us to have a novel method to separately probe the CB and VB of the QD. Hence taking extensive care to correct the wide Cu related PL emission spectra with the necessary grating efficiency and energy correction to determine the exact PL maxima of the Cu related emission, we have used the Cu related emission maxima to determine the shift in the CB.

Typical variation of the bandgap of the QD as a function of size is shown in Figure 3.3(b) while the variation of CB and VB as obtained from the Cu emission position is shown as filled circles in Figure 3.3(c). The solid line shows the values obtained from semi empirical TB model[11] for the theoretical prediction of bandgap and the VB and CB variation of CdSe QDs. In the case of CB and VB variation, the theoretical prediction is calculated by subtracting the entire coulomb correction term from the CB and shifting the experimental value of the VB position of the largest QD to match the theoretical value. With this one arbitrary shift, it is found that the experimental data obtained from Cu related emission position shows an excellent agreement with the theoretical values as shown in Figure 3.3(c). The open symbols were obtained from literature where the position of CB was obtained using time consuming photo emission spectroscopy and x-ray absorption measurements.[19] The excellent agreement with these experimental data as well as theoretically predicted values proves that the Cu level is

independent of size and that this technique can indeed be used to measure the shift in the CB of the QD.

3.4.3. The determination of relative band alignment of various semiconductors:

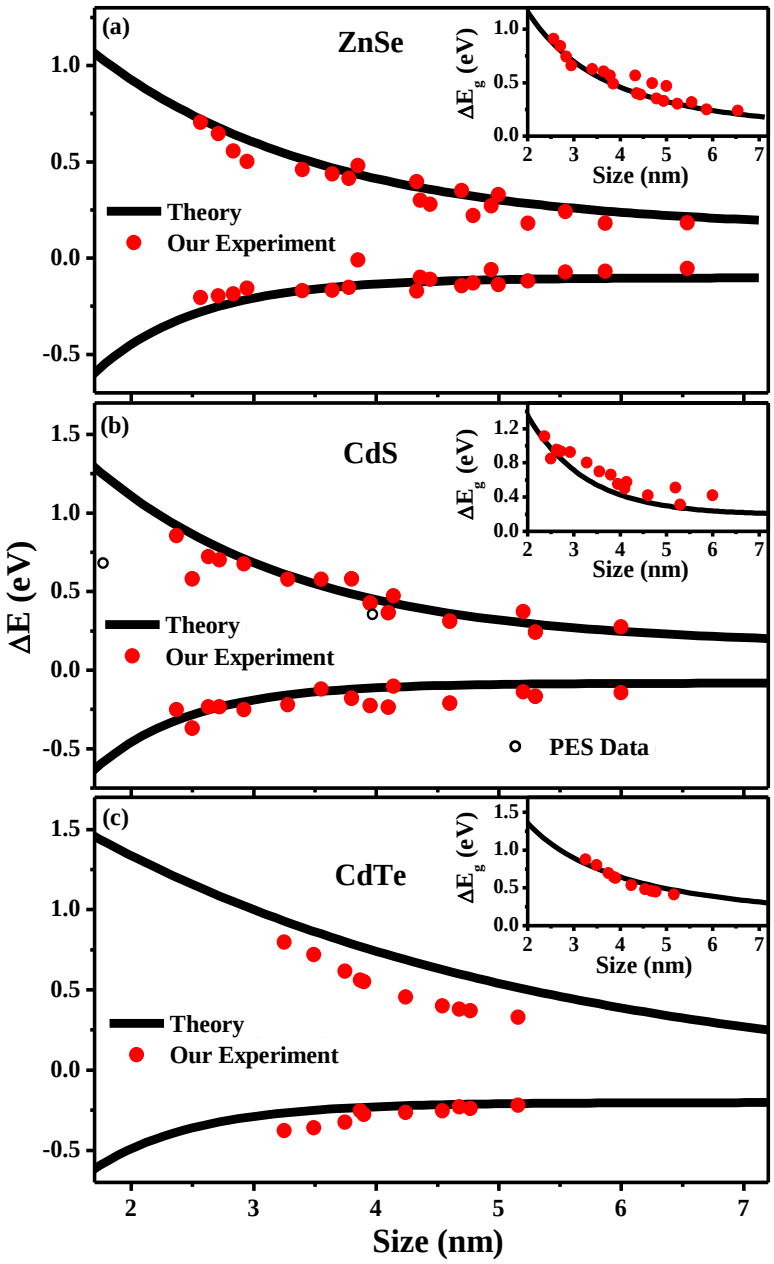

Figure 3.4. *The main panels show the CB and VB variation as a function of size as obtained from the analysis of Cu doped QDs (Red solid dots) along with TB theoretical curve (Solid lines) (Ref [11]) and data obtained from PES data from literature (Black open circles) for* ***(a)*** *ZnSe QDs,* ***(b)*** *CdS QDs and* ***(c)*** *CdTe QDs. The insets show the corresponding band gap variation as a function of size.*

It is a natural consequence of the simplicity and the ease of this technique. This allows us to acquire large number of data points by obtaining varying sizes of the doped QDs with different host materials. Hence, we first went about this by synthesizing various Cu doped semiconductor QDs. The synthesis techniques are described in the experimental section and the samples were characterized using TEM, XRD, ICP-OES and absorption and PL techniques. PL data showed the presence of a strong Cu related emission in every case. In order to prove the validity of the approach mentioned above, we quantified the shift in the Cu related emission and obtained the CB and VB variation for various semiconductors and plotted them as a function of size along with the theoretical curves and other experimental data, when available, in literature as shown in Figure 3.4. While the extremely good agreement with the theoretical data as well as photoemission data from earlier literature[15, 52, 53] in all cases proves the generality of this approach it would be more instructive to obtain the relative band alignment of the host semiconductors in the nano size regime.

Figure 3.5(a) shows the absorption and PL data for the 3.8 nm doped and undoped semiconductor QDs. From the figure, it is evident that the shift in the Cu position for the same size QD is indeed dependent on the host QD and varies from 0.2 eV to 1.3 eV. However, it is important to quantify the CB and VB variation to find out if the bulk alignment is valid in the QD regime. Towards this end, we subtracted the theoretically obtained energy of the band offset at 9 nm in every case and plot the CB variation and the VB variation in Figures 3.5(b) and 3.5(c) for the various semiconductors. It is interesting to note that while the VB follows a universal curve and can hence be translated from the bulk, the CB alignment changes drastically from that of the bulk semiconductors. Hence, we plot the actual band offsets of the CB (Figure 3.6(a)) and VB (Figure 3.6(b)) as a function of size keeping the vacuum level as a single reference. Figure 3.6 clearly shows that the band alignment changes as a function of size in QDs leading to interesting band crossings. For example, it can be seen that while 3 nm CdTe and ZnSe have the CB at the same energy, the CB of 6 nm ZnSe lies 270 meV higher than similar sized CdTe as compared to 400 meV in bulk semiconductors. These relative alignments as a function of size are important in understanding the optical properties of core/shell heterostructures that subsequently determines the efficiencies of various absorption and emission based devices.

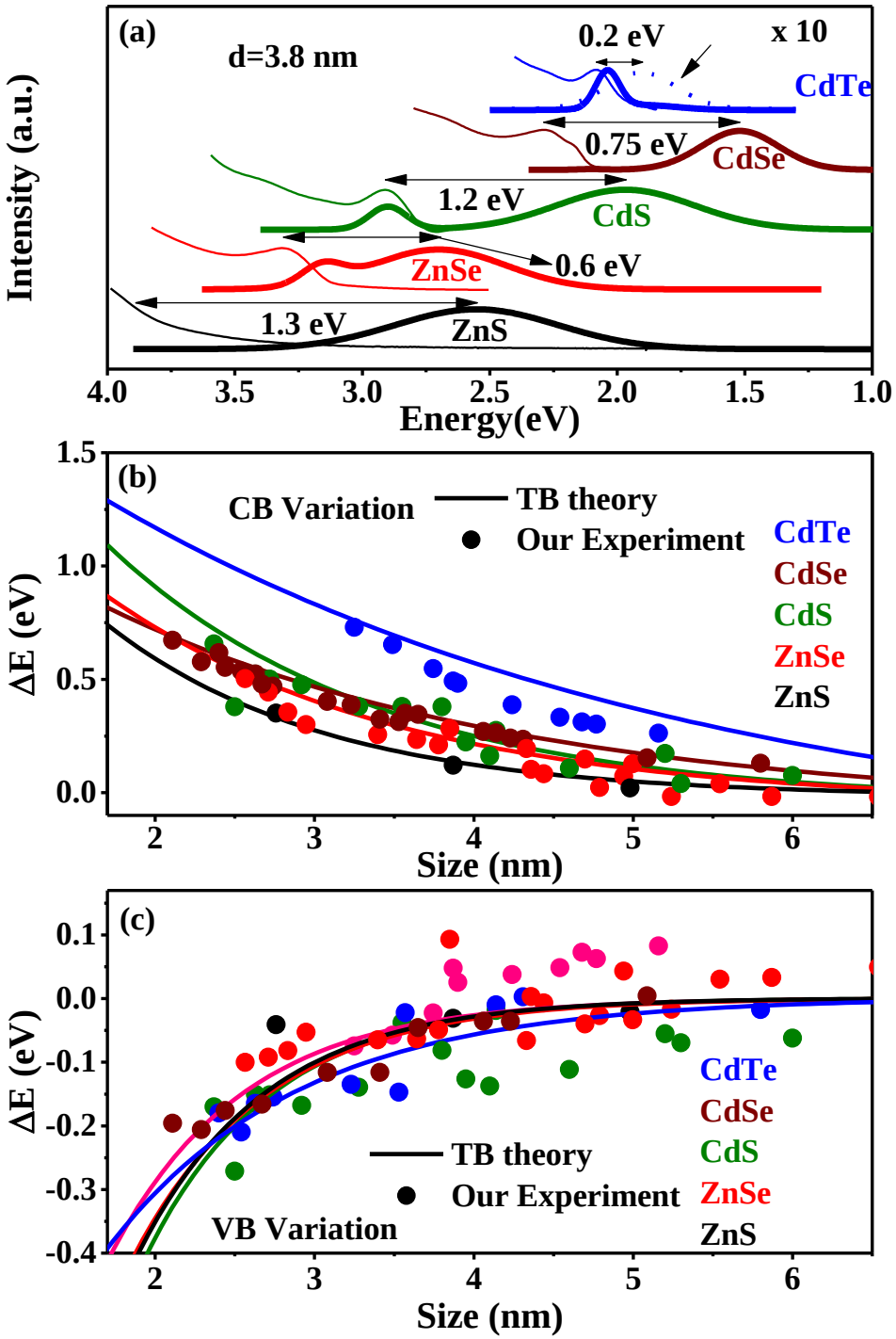

Figure 3.5. (a) *Typical absorption and PL spectra of the 3.8 nm Cu doped II-VI semiconductor QDs showing a shift in the Cu related emission position. Universal curve to study the relative alignment of band offsets as a function of size in various semiconductors for the CB* ***(b)*** *and the VB* ***(c)****. The solid line represents the TB theoretical data (Ref [11]).*

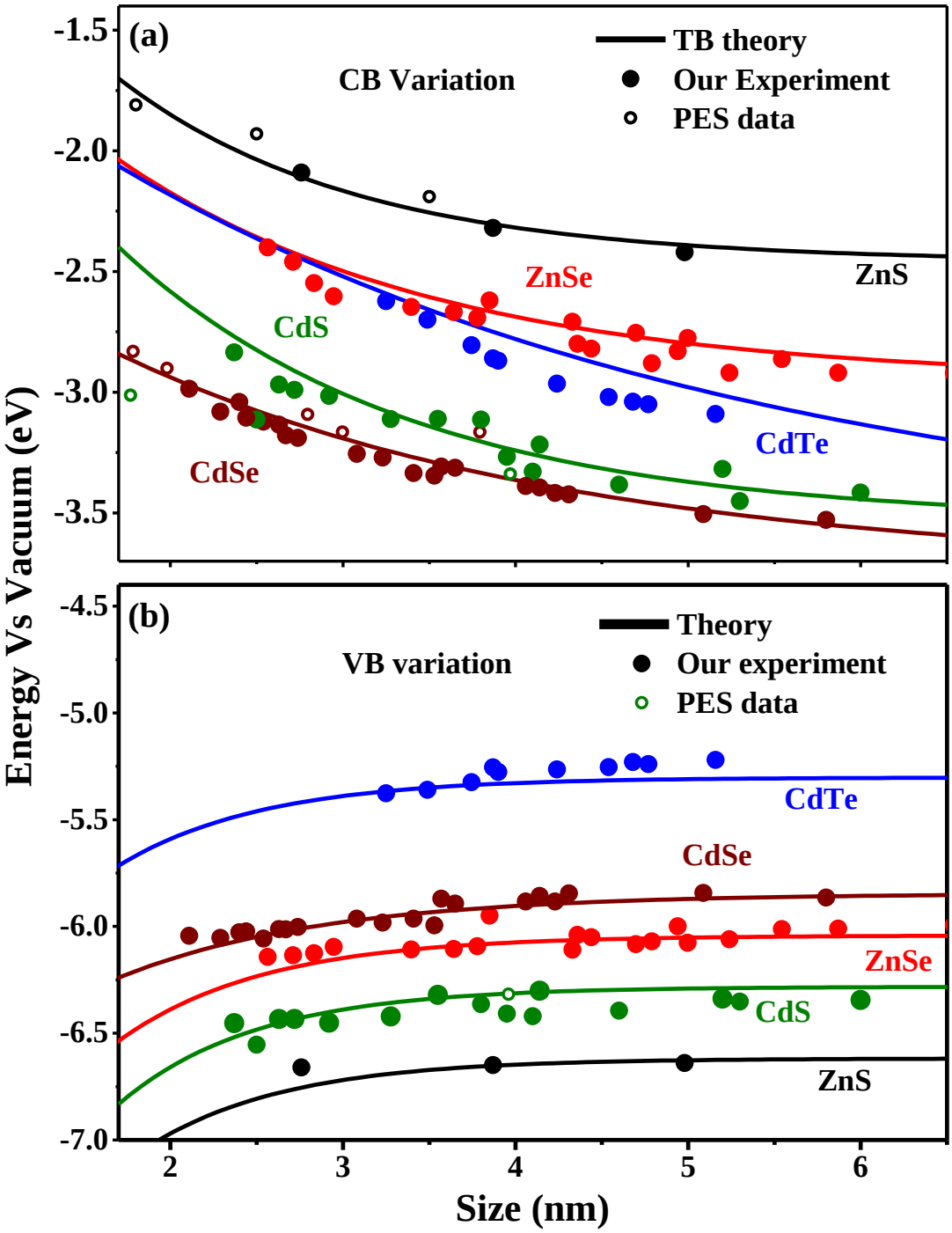

Figure 3.6. ***(a)*** *and* ***(b)*** *Relative band alignment of various II-VI semiconductors as a function of size for the CB and VB respectively. The solid line represents the TB theoretical data (Ref [11]) while the open circles represent the photoemission spectroscopy, PES data obtained from literature.*[15, 19, 52, 53]

3.5. Conclusions:

We have shown that it is indeed possible to dope CdSe QDs with Cu and obtain the Cu related emission. We have used Cu doping to study the variation of CB and VB as a function of size in the QDs using CdSe as a model system. This study has been further extended to different sizes of other semiconductors leading to the relative band alignment in QDs for the first time. Thus, we show that by appropriately studying the mechanism of the Cu related emission it is possible to dope Cu in any QD and study the bulk electronic structure of the QD using Cu *d* level as an internal standard.

Bibliography:

[1] R. J. Ellingson, M. C. Beard, J. C. Johnson, P. Yu, O. I. Micic, A. J. Nozik, A. Shabaev, A. L. Efros, *Nano Lett.* **2005**, *5*, 865.

[2] B. Carlson, K. Leschkies, E. S. Aydil, X. Y. Zhu, *J. Phys. Chem. C* **2008**, *112*, 8419.

[3] L. Sun, J. J. Choi, D. Stachnik, A. C. Bartnik, B. R. Hyun, G. G. Malliaras, T. Hanrath, F. W. Wise, *Nat. Nanotechol.* **2011**, *7*, 369.

[4] A. Kongkanand, K. Tvrdy, K. Takechi, M. Kuno, P. V. Kamat, *J. Am. Chem. Soc.* **2008**, *130*, 4007.

[5] P. V. Kamat, *J. Phys. Chem. C* **2008**, *112*, 18737.

[6] W. W. Yu, L. Qu, W. Guo, X. Peng, *Chem. Mater.* **2003**, *15*, 2854.

[7] E. Kucur, J. Riegler, G. A. Urban, T. Nann, *J. Chem. Phys.* **2003**, *119*, 2333.

[8] S. K. Haram, A. Kshirsagar, Y. D. Gujarathi, P. P. Ingole, O. A. Nene, G. B. Markad, S. P. Nanavati, *J. Phys. Chem. C* **2011**, *115*, 6243.

[9] S. K. Poznyak, N. P. Osipovich, A. Shavel, D. V. Talapin, M. Gao, A. Eychmueller, N. Gaponik, *J. Phys. Chem. B* **2005**, *109*, 1094.

[10] J. Jasieniak, M. Califano, S. Watkins, *ACS Nano* **2011**, *5*, 5888.

[11] R. Viswanatha, D. D. Sarma, *Chem. Asian J.* **2009**, *4*, 904.

[12] R. Viswanatha, S. Sapra, T. Saha-Dasgupta, D. D. Sarma, *Phys. Rev. B* **2005**, *72*, 045333.

[13] J. Hu, L. Wang, L. Li, W. Yang, A. P. Alivisatos, *J. Phys. Chem. B* **2002**, *106*, 2447.

[14] J. E. Bernard, A. Zunger, *Phys. Rev. B* **1987**, *36*, 3199.

[15] V. L. Colvin, A. P. Alivisatos, J. G. Tobin, *Phys. Rev. Lett.* **1991**, *66*, 2786.

[16] P. K. Santra, R. Viswanatha, S. M. Daniels, N. L. Pickett, J. M. Smith, P. O' Brien, D. D. Sarma, *J. Am. Chem. Soc.* **2008**, *131*, 470.

[17] J. Nanda, B. A. Kuruvilla, D. D. Sarma, *Phys. Rev. B* **1999**, *59*, 7473.

[18] T. Van Buuren, L. N. Dinh, L. L. Chase, W. J. Siekhaus, L. J. Terminello, *Phys. Rev. Lett.* **1998**, *80*, 3803.

[19] J. R. I. Lee, R. W. Meulenberg, K. M. Hanif, H. Mattoussi, J. E. Klepeis, L. J. Terminello, T. van Buuren, *Phys. Rev. Lett.* **2007**, *98*, 146803.

[20] B. Alperson, I. Rubinstein, G. Hodes, D. Porath, O. Millo, *Appl. Phys. Lett.* **1999**, *75*, 1751.

[21] H. J. Choi, J. K. Yang, H. H. Park, *Thin Solid Films* **2006**, *494*, 207.

[22] D. Chen, R. Viswanatha, G. L. Ong, R. Xie, M. Balasubramaninan, X. Peng, *J. Am. Chem. Soc.* **2009**, *131*, 9333.

[23] W. W. Yu, X. Peng, *Angew. Chem. Int. Ed.* **2002**, *41*, 2368.

[24] V. Kloper, R. Osovsky, J. Kolny-Olesiak, A. Sashchiuk, E. Lifshitz, *J. Phys. Chem. C* **2007**, *111*, 10336.

[25] N. S. Karan, D. D. Sarma, R. M. Kadam, N. Pradhan, *J. Phys. Chem. Lett.* **2010**, *1*, 2863.

[26] B. B. Srivastava, S. Jana, N. S. Karan, S. Paria, N. R. Jana, D. D. Sarma, N. Pradhan, *J. Phys. Chem. Lett.* **2010**, *1*, 1454.

[27] N. Pradhan, D. Goorskey, J. Thessing, X. Peng, *J. Am. Chem. Soc.* **2005**, *127*, 17586.

[28] B. B. Srivastava, S. Jana, N. Pradhan, *J. Am. Chem. Soc.* **2011**, *133*, 1007.

[29] R. Xie, X. Peng, *J. Am. Chem. Soc.* **2009**, *131*, 10645.

[30] R. Viswanatha, S. Brovelli, A. Pandey, S. A. Crooker, V. I. Klimov, *Nano Lett.* **2011**, *11*, 4753.

[31] F. H. Su, Z. L. Fang, B. S. Ma, K. Ding, G. H. Li, S. J. Xu, *J. Appl. Phys.* **2004**, *95*, 3344

[32] Y. P. Du, Y. W. Zhang, L. D. Sun, C. H. Yan, *J. Phys. Chem. C* **2008**, *112*, 12234.

[33] A. Ishizumi, Y. Kanemitsu, *Appl. Phys. Lett.* **2005**, *86*, 253106.

[34] L. Wang, Y. Li, *Chem. Mater.* **2007**, *19*, 727.

[35] D. A. Schwartz, N. S. Norberg, Q. P. Nguyen, J. M. Parker, D. R. Gamelin, *J. Am. Chem. Soc.* **2003**, *125*, 13205.

[36] N. S. Norberg, G. M. Dalpian, J. R. Chelikowsky, D. R. Gamelin, *Nano Lett.* **2006**, *6*, 2887.

[37] D. J. Norris, N. Yao, F. T. Charnock, T. A. Kennedy, *Nano Lett.* **2001**, *1*, 3.

[38] A. Nag, S. Chakraborty, D. D. Sarma, *J. Am. Chem. Soc.* **2008**, *130*, 10605.

[39] S. Sapra, D. D. Sarma, S. Sanvito, N. A. Hill, *Nano Lett.* **2002**, *2*, 605.

[40] I. E. Ture, F. Poulin, A. W. Brinkman, J. Woods, *Phys. Stat. Sol. A* **1983**, *77*, 535.

[41] D. J. Norris, A. L. Efros, S. C. Erwin, *Science* **2008**, *319*, 1776.

[42] C. G. Van de Walle, J. Neugebauer, *Nature* **2003**, *423*, 626.

[43] H. G. Grimmeiss, N. Kullendorff, R. Broser, *J. Appl. Phys.* **1981**, *52*, 3405.

[44] H. G. Grimmeiss, C. Ovren, W. Ludwig, R. Mach, *J. Appl. Phys.* **1977**, *48*, 5122.

[45] J. P. Laurenti, G. Bastide, M. Rouzeyre, R. Triboulet, *Solid State Commun.* **1988**, *67*, 1127.

[46] S. Shionoya, T. Koda, K. Era, H. Fujiwara, *J. Phys. Soc. Jpn.* **1964**, *19*, 1157.

[47] I. E. Ture, M. Claybourn, A. W. Brinkman, J. Woods, *J. Appl. Phys.* **1986**, *60*, 1670.

[48] S. C. Erwin, L. Zu, M. I. Haftel, A. L. Efros, T. A. Kennedy, D. J. Norris, *Nature* **2005**, *436*, 91.

[49] A. Nag, A. Hazarika, K. V. Shanavas, S. M. Sharma, I. Dasgupta, D. D. Sarma, *J. Phys. Chem. Lett.* **2011**, *2*, 706.

[50] R. Viswanatha, S. Sapra, S. S. Gupta, B. Satpati, P. V. Satyam, B. N. Dev, D. D. Sarma, *J. Phys. Chem. B* **2004**, *108*, 6303.

[51] J. R. Lakowicz, *Principles of Fluorescence Spectroscopy*, 3rd ed., Springer Publications, New York, **2006**.

[52] S. Sapra, Indian Institute of Science (Bangalore), **2003**.

[53] J. Luning, J. Rockenberger, S. Eisebitt, J. E. Rubensson, A. Karl, A. Kornowski, H. Weller, W. Eberhardt, *Solid State Commun.* **1999**, *112*, 5.

Chapter 4

Demystifying Complex Quantum Dot Heterostructures Using Photo-generated Charge Carriers

4.1. Abstract:

Heterostructure QDs are extensively studied for their performance in optoelectronic and photovoltaic applications. Central to the success of these materials is the understanding of the photo-generated charge carrier localization. In spite of the theoretically expected prediction of the band edges of alloy or core/shell with a type I or type II structure, the actual location of the charges is often quite different leading to sub-optimal results. In this work, we have used Cu doping and its PL to study the internal structures ranging from alloys, core/shell and graded alloy structure. We have also studied the charge localization on inverse type I, type II and quasi type II core-shell structures. Specifically, the adeptness of this method has been assessed over a range of widely studied heterostructures like CdSe/CdS, CdS/CdSe, CdSe/CdTe, $Zn_{1-x}Cd_xSe$ and $Zn_{1-x}Cd_xS$ QDs systems by doping them with a small percentage of Cu. The electron and hole localization obtained from this method concurs with the pre-existing understanding in cases that have been explored before. We have also shown the dependence of core size for CdSe/CdTe QDs for the formation of quasi type II system. We have then extended this method to obtain the internal structure in previously unknown heterostructures proving the usefulness of this method.

4.2. Introduction:

QD heterostructures has been an integral part of the development of nano devices for use in optoelectronic applications. High PL efficiencies suitable for light emitting diodes,[1] and photo-voltaic materials suitable for solar cell applications[2, 3] have been attained not only by appropriate alignment of band edges but also due to a multitude of other factors like smooth alloying to reduce Auger recombination,[4] appropriate surface passivation[5] and so on. Additionally, due to high temperature annealing during synthesis and the strains involved in the formation of these heterostructures the theoretically planned structure is rarely formed. The challenges involved in realizing a high-quality material to maximize the efficiency of either the charge separation or recombination processes can be two-fold. Firstly, the band offset values have been obtained largely in bulk semiconductors and the actual band edges for sizes within the quantum confined regime may be different. The electronic structure prediction of these heterostructures is not straight forward when it comes to nano regime as their band offset values may not be similar to bulk values. In addition to a few theoretical reports, [6-8]

experimental techniques such as variable energy photoemission [9], scanning tunneling spectroscopy[10] and cyclic voltammetry [11, 12] were used to study the electronic structure of a few QD heterostructures. However, these measurements require ultrahigh vacuum, especially variable energy photoemission and scanning tunneling spectroscopy, rendering the measurements non-trivial and time consuming. Moreover, charging of the semiconductor QDs[11] in all these techniques poses an important shortcoming in terms of determining the shift in CB or VB positions. Ultrafast transient absorption spectroscopy was also utilized to find the type of band alignment in CdTe/CdSe[13] and $CuInS_2$/CdS[14] core-shell QDs. However, the absolute positions of these QDs were not determined using this technique. Secondly, due to the quantum confinement in these materials, several other factors like defect and strain energies also influence the localization effects on the photo-generated charge carrier. Hence an in-situ probe to study the internal structure would be very useful in obtaining high quality heterostructures suitable for the given application.

A precise in-situ probe identifying the CB and VB positions using the location of the charge carrier in various Cu doped II-VI and III-V semiconductors has been shown in **Chapter 3** to effectively predict band edge variations. This method was shown to be in good agreement with both theoretical and other experimental results. Zhang et al. have also shown that Cu PL can be used as an internal probe for determining the CB and VB positions of semiconductor QDs as a function of size. [15] The importance and novelty of this method in finding the absolute band edge positions is also highlighted in a recently published review on Cu doped QDs.[16] The advantages of using this method include the ease of operation under atmospheric conditions using simple optical measurements like absorption and PL. The presence of internal standard like the atomic-like level of Cu allows the direct determination of PGE energy from the Cu PL maximum and the PGH energy can be obtained by deducing the band gap energy from Cu PL maximum. However, the major bottleneck for the use of this method arises from a synthesis perspective. Although Cu doping in II-VI and III-V semiconductors has been extensively studied, there are not many reports on Cu doping in QD heterostructures. This could be due to the need to maintain lower temperatures to retain Cu within the QD[17] while high temperature annealing for extended period of time is necessary for the formation of high quality heterostructures.[18] In this chapter, we have shown that by appropriate use of ligands as well as suitable variation of temperatures, it is possible to attain both high quality

heterostructures along with Cu doping for a range of heterostructures. We have used these Cu doped heterostructures to understand the charge localization in a range of heterostructure QDs including type I, type II, inverse type I, quasi type II QDs along with alloys and alloy shell heterostructures using Cu emission and absorption spectra. The validity of this measurement over a wide range of materials proves the generality of this approach.

4.3. Experimental section:

4.3.1. Materials:

CdO, Se shots, Te shots, S powder, oleic acid (90 %), oleylamine (70 %), ODE (90 %) and TOP (90%) were purchased from sigma-Aldrich. Hexane, methanol, chloroform and acetone were purchased from Merck. Copper (II) acetate monohydrate and stearic acid were purchased from SD Fine chemicals. TMAH (98%) was purchased from Spectrochem. All the purchased chemicals were used without any further purification.

0.2 M Cadmium Oleate was prepared by degassing a mixture of (0.32 g of CdO), oleic acid (6.18 g) and ODE (9 mL) at 80 ^{o}C for one hour prior to heating it to above 250 °C to obtain a colourless solution. 0.09 M cadmium oleate (for synthesis of CdSe QDs) was prepared by reducing the amount of oleic acid to 2.68 g in the above procedure**.**

1 M TOPSe, 0.1 M TOP/Te and 0.2 M S/ODE were prepared by dissolving 0.79 Se in 10 mL of TOP, 0.13 g of Te in 10 mL of TOP and 32 mg of S in 5 mL of ODE in Ar. Copper stearate was synthesized and purified similar to literature reported procedure.[17]

4.3.2. Synthesis of Cu doped CdSe/CdS QDs:

These QDs were synthesized by first synthesizing Cu doped CdSe QDs using similar to method followed in **Chapter 3**. The Cu doped CdSe QDs were purified by washing once with hexane-methanol mixture and then precipitated by adding excess of acetone. The over coating of CdS shell was achieved by SILAR technique.[18, 19] The purified QDs were mixed with 5 mL of ODE and 5 mL of oleylamine and degassed for 10 minutes at room temperature. The reaction mixture was then heated to 200 ^{o}C-230 ^{o}C under Ar flow. At this temperature, Cd precursors followed by S precursors were injected into the reaction mixture and the aliquots were

collected after the completion of every cycle of Cd and S additions. 0.15 mL, 0.25 mL, 0.35 mL, 0.5 ml, 0.65 mL and 0.8 mL of 0.2 M cadmium oleate and S/ODE precursor solutions were added in subsequent cycles for CdS shell growth. The sample was annealed for 10-15 minutes after every Cd addition and 5-8 minutes for every S addition. The undoped CdSe/CdS QDs were synthesized exactly in the same way excluding the Cu addition step.

4.3.3. Synthesis of Cu doped CdS/CdSe QDs:

These QDs were synthesized by first synthesizing Cu doped CdS QDs using the methods followed in **Chapter 3**. Briefly, A 4 g of ODE solution which contains 0.0128 g (0.1 mmol) of CdO and 0.22g of oleic acid was degassed for one hour at 80 ^{o}C and then backfilled with Ar. The temperature of the reaction mixture was raised to 290 ^{o}C-300 ^{o}C and the S precursor (1.6 mg S/0.5 mL ODE) was injected into it to form CdS QDs. The temperature was immediately reduced to 150 ^{o}C and the Cu precursor solution (4-5 mg of copper stearate /1 mL of ODE) was added drop-wise and annealed for 2 hours. After this, CdSe over coating was achieved by SILAR technique.[20] The reaction mixture was heated to 200 ^{o}C under Ar flow just after the addition of 0.2 mL of oleylamine. At this temperature, Cd precursors followed by Se precursors were injected into the reaction mixture and the aliquots were collected after the completion of every cycle of Cd and S additions. 0.09 mL, 0.14 mL, 0.20 mL, 0.25 mL, 0.33 mL, 0.42 mL and 0.50 mL of 0.2 M cadmium oleate and TOP/Se solutions were added subsequently for CdSe overcoating. The sample was annealed for 10 minutes after every Cd addition and 6 minutes after every Se addition.

4.3.4. Synthesis of Cu doped CdSe/CdTe QDs with 2.5 nm and 3.4 nm CdSe cores:

First, Cu doped CdSe QDs were prepared as similar to mentioned above. 2.5 mL of cadmium oleate, 0.5 mL of TOPSe, 5 mL of ODE and 8-9 mg of copper stearate were used in the synthesis of Cu doped CdSe QDs. The synthesis of 2.5 nm and 3.4 nm CdSe QDs was carried out at 180 ^{o}C and 250 ^{o}C respectively. SILAR technique was used for overcoating of CdTe shell.[3] The purified QDs were mixed with 6 mL of ODE and 4 mL of oleylamine and degassed for 10 minutes at room temperature. The reaction mixture was then heated to 190 ^{o}C under Ar flow. At this temperature, the reaction mixture was annealed for 6-7 minutes after the first Cd addition. Later, TOP/Te precursor was added and the reaction temperature was immediately

raised to 230 ^{o}C and then annealed for 5 minutes followed by second addition of Cd precursor. The subsequent additions of Cd and Te precursors continue till the desired size is obtained. 0.2 mL, 0.35 mL, 0.4 mL, 0.6 mL, 0.8 mL and 1 mL of 0.1 M cadmium oleate and TOP/Te solutions were added subsequently for the growth of CdTe.

4.3.5. Synthesis of Cu doped $Zn_{1-x}Cd_xSe$ alloy QDs:

These QDs were synthesized similar to literature reported methods.[21] 0.063 g (0.1 mmol) of zinc stearate, 0.5 g of octadecylamine and 10 mL of ODE were taken in a 50 mL three necked flask and degassed at 40 °C for 1 hour and then backfilled with Ar. 1 mL of 2.4 M TBP/Se was injected into Zn^{2+} solution and the temperature was raised to 180 °C-190 ^{o}C. The formation of ZnSe QDs was confirmed by recording their absorbance and PLspectra. This was followed by the dropwise addition of 6 mg copper stearate/1 mL ODE. The doping of Cu into ZnSe QDs was monitored by the PL spectroscopy. After the Cu-PL was stabilized, 0.12 g Zinc undecylenate/2 mL ODE was injected in a drop wise manner and the temperature was raised to 200 °C and annealed for 4 hours, leading to further growth in the QD size. The undoped QDs were also synthesized in a similar way except the amount of octadecylamine was 0.2 g without introducing Cu^{2+} ions into the reaction flask.

After that, 1 mL of 0.2 M cadmium oleate was added drop-wise over a period of one hour. Aliquots were collected at regular intervals and the PL and absorbance spectra were monitored.

4.3.6. Synthesis of Cu doped $Zn_{1-x}Cd_xS$ QDs:

0.063 g (0.1 mmol) of zinc stearate and 0.012 g of S powder were mixed with 10 mL of ODE and the reaction mixture was degassed for one hour followed by back filling with Ar gas. The reaction mixture was then heated to 270 ^{o}C and annealed for 5 minutes. The temperature was reduced to 220 ^{o}C where Cu precursor solution (1 mg of copper stearate in 1 mL ODE) was added drop-wise to the reaction mixture and annealed for 30 minutes. Once the Cu PL was stabilized, 0.12 g of Zinc undecylenate in 1.5 mL ODE was added drop-wise to the reaction mixture and annealed for two hours, leading to further growth in QD size. After that, 1.5 mL of 0.2 M cadmium oleate was added drop-wise over a period of one hour. Aliquots were taken at regular intervals and dissolved in hexane for the absorption and PL studies.

4.4. Results and discussion:

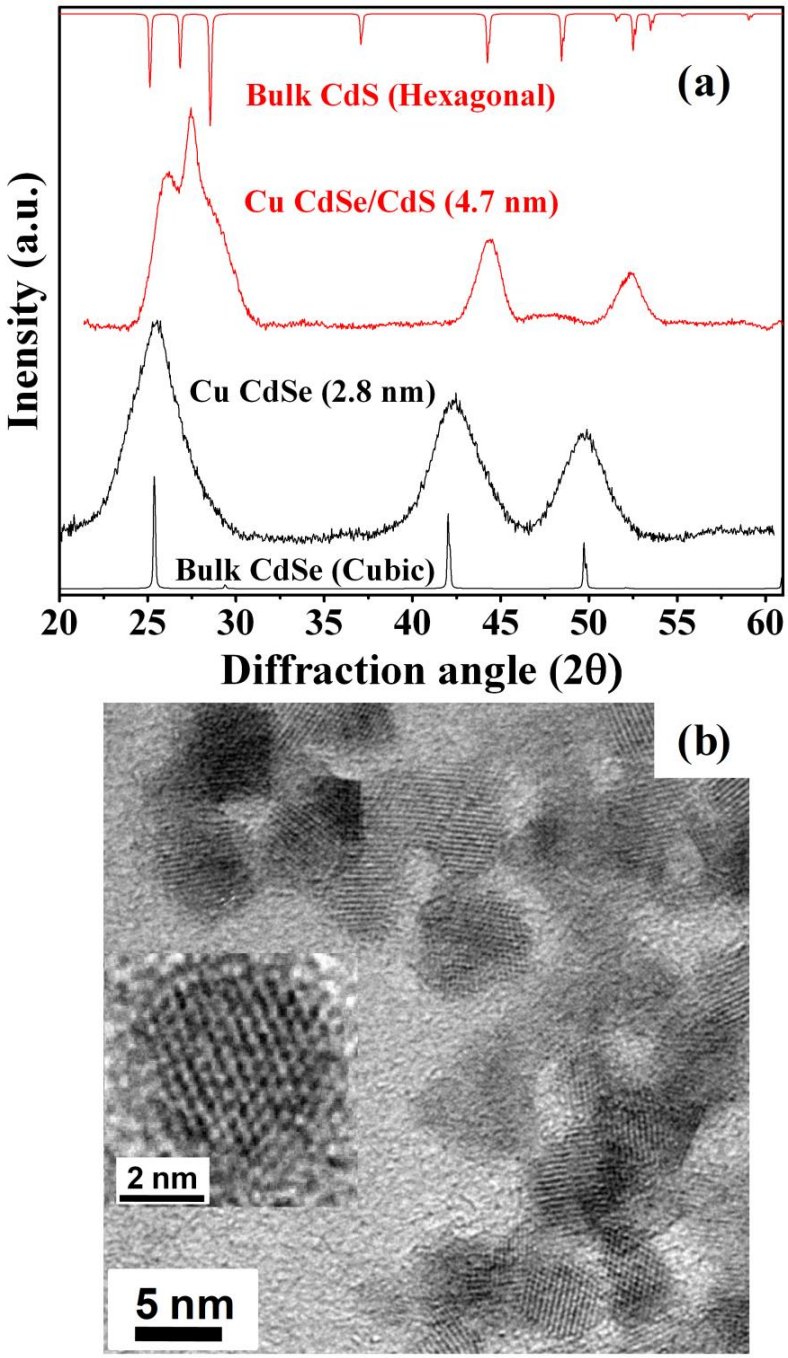

Figure 4.1. (a) *The XRD patterns of Cu doped core CdSe QDs and the corresponding Cu doped core/shell CdSe/CdS QDs along with the bulk XRD patterns of CdSe and CdS and* ***(b)*** *the TEM image of Cu doped CdSe/CdS QDs with 4.7 nm size. The inset of* ***(b)*** *shows the corresponding high resolution TEM image.*

One of the most widely studied heterostructures in literature is the CdSe/CdS core/shell QDs with a thin as well as thick shell.[1, 18, 19] Theoretically, the structure of CdSe/CdS is expected to be type I structure from the bulk band edges wherein both the charge carriers are localized in CdSe core. However, since the earliest reports of the formation of these QD heterostructures,[19] along with an increase in PL QY, we also observe a decrease in the band gap as a function of shell thickness which is unexpected in ideal type I heterostructures. Charge carrier delocalization beyond the traditional boundaries of the core and/or shell is well known in literature due to change in material composition as well as energetics. In the current case, this red shift was observed in many literature reports[18, 19] and first principles calculations[6] show the quasi type II nature of CdSe/CdS QDs where the electron is delocalized into CdS shell as a result of small CB offset. However, this quasi type II character does not completely explain the observed optical behavior. In order to predict the optical behavior in heterostructures, it is crucial to understand the internal structure of these QDs. To study the internal structure, we prepared Cu doped CdSe/CdS heterostructure QDs. The formation of CdS shell over CdSe core is confirmed from XRD as well as the growth observed from TEM images as shown in Figure 4.1. It is well known that it is not possible to differentiate the presence of a core and shell material even from high resolution TEM images. Hence, we studied the optical properties of both undoped and Cu doped QDs and typical absorption and PL spectra for the undoped and doped QDs for varying shell thicknesses are shown in Figure 4.2(a) and Figure 4.2(b) respectively. The red shifted emission and the long lifetime of this emission (shown in Figure 4.3) confirms the origin of the emission peak in Cu doped QDs as due to radiative recombination of CB electron with Cu *d* level.[21]

This Cu PL energy is indicative of the energy of the PGE while the difference between band gap and the Cu PL energy is indicative of the PGH energy. In order to avoid confusion, in the entire chapter we discuss the energy of PGE and PGH rather than the CB and VB. The variation of energy of the PGE (red open circles) and the PGH (black open circles) of CdSe/CdS with increasing CdS shell thickness are compiled in Figure 4.2(c). The dotted lines in this figure show the variation of CB (red dashed line) and VB (black dashed line) of CdSe QDs within the same size regime.

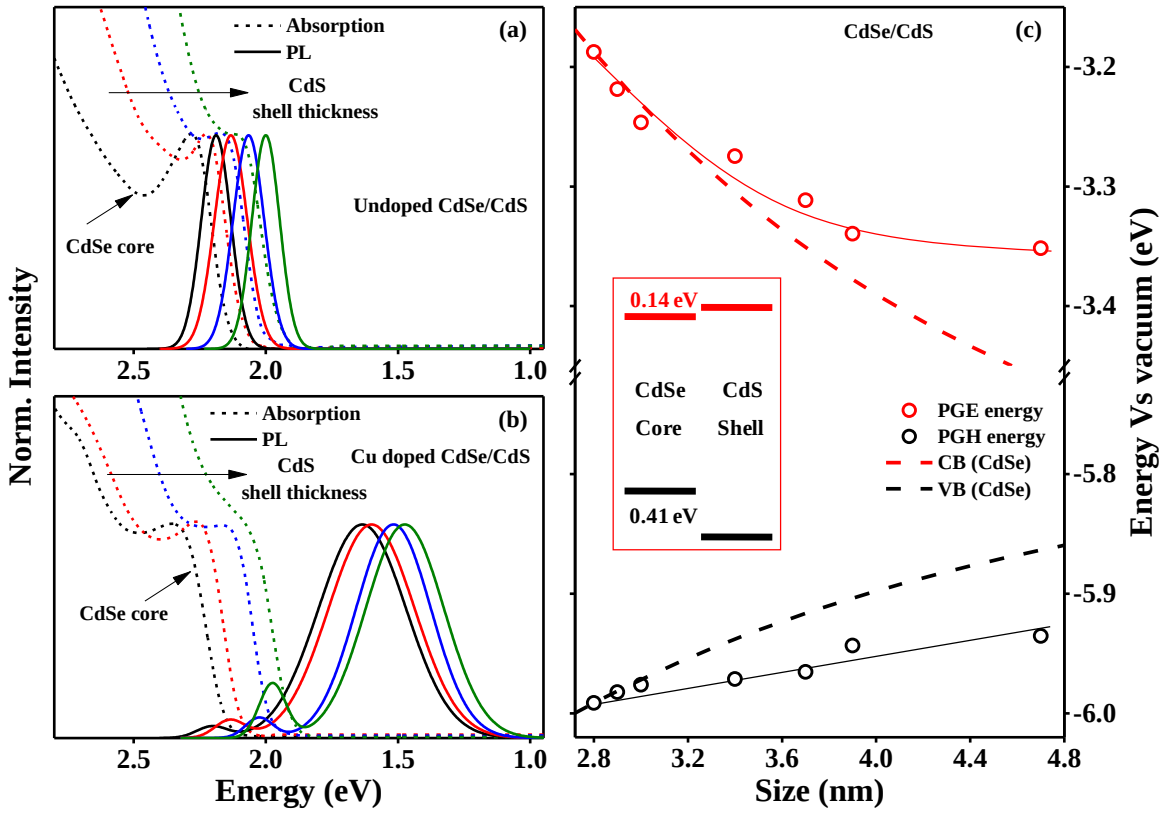

Figure 4.2. (a) *and* ***(b)*** *show the absorption and PL spectra of undoped and Cu doped CdSe/CdS QDs respectively.* λ_{ex}*=405 nm.* ***(c)*** *The variation of energies of PGE (red open circles) and PGH (black open circles) of CdSe/CdS QDs with increasing the CdS shell thickness. The dashed lines indicate the variation of energies of PGE (red) and PGH (black) of CdSe QDs. The insets of* ***(c)*** *shows the bulk band alignment of CdSe/CdS.*

The decrease in energy of the PGE is very similar to the variation of the CB of CdSe for thinner shells of CdS suggesting that the electron experiences an increase in overall size of QD with almost similar potential to that of CdSe with increasing CdS shell thickness. This, in turn, implies a delocalization of the PGE into the CdS shell due to small CB offset in CdSe and CdS QDs supporting the quasi type II nature of CdSe/CdS predicted in literature.[6, 19] However, surprisingly, two aspects that cannot be explained using the quasi type II nature is the relative flattening of the PGE energy at thicker shells of CdS as well as small increase in the energy of the PGH for thinner shells. In this context, it is interesting to note that extended annealing in this CdSe/CdS structure can give rise to a graded alloy at the interface. The thickness of this alloy at the interface from these studies can be found to be about one monolayer thick. Similar alloy interface was also predicted due to indirect evidence of decrease in Auger-recombination rates in CdSe/CdS QDs[22]. The presence of a graded alloy at the interface would gradually

blend the band edges of CdSe and CdS. Due to smaller energy difference between the CB edges of CdSe and CdS, the PGE would delocalize into the entire region while the PGH delocalizes into a much smaller shell region, possibly only into the alloy region at the interface. Hence, we observe a small increase in the energy levels of PGH and larger decrease in the PGE energies. This is also in accordance with literature[4] wherein the presence of a deliberately manicured sharp interface between CdSe/CdS shows a smaller red shift in the PL (~ 0.27 eV) compared to a graded alloy interface (up to ~ 0.34 eV) of same total size, proving the power of this technique.

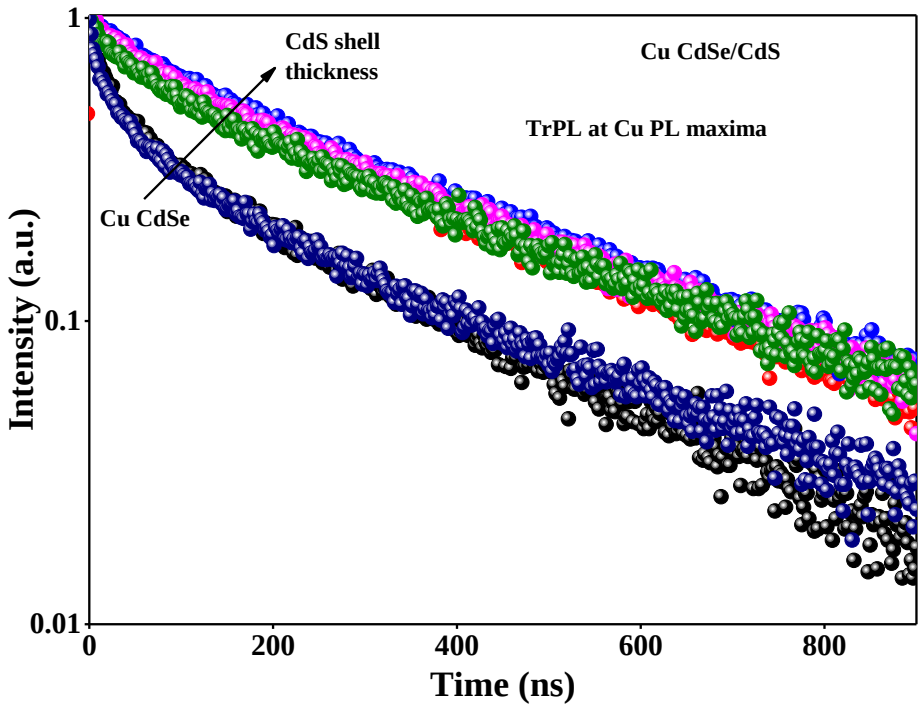

Figure 4.3. *TrPL spectra of Cu doped CdSe and Cu doped CdSe/CdS QDs with increasing CdS shell thickness.* λ_{ex}*=405 nm.*

We have then extended this technique to study the internal structure of the inverse type I CdS/CdSe structure. The overcoating of CdSe on Cu doped CdS QDs leads to red shift in both band gap and Cu PL as shown in Figure 4.4(a) and Figure 4.4(b) respectively. The variations of PGE and PGH energies are plotted in Figure 4.4(c) while the bulk band offset is shown in the corresponding inset. The PGE energy is shifted by 210 meV when a 0.25 nm thick CdSe shell is overcoated on 3.0 nm CdS QDs, while the PGH energy is shifted by 670 meV. These shifts are comparable to the corresponding bulk CB offset of 140 meV and VB offset of 410 meV. Additionally, the PGH energy becomes constant at higher shell thickness

suggesting the localization of both PGH and PGE within CdSe shell with increasing shell thickness. The efficiency of the hole transfer to the shell is slightly higher than that of the electron due to the large VB offset of the component materials. Thus, CdS/CdSe QDs form inverse type I structure even in quantum confined regime similar to bulk alignment.

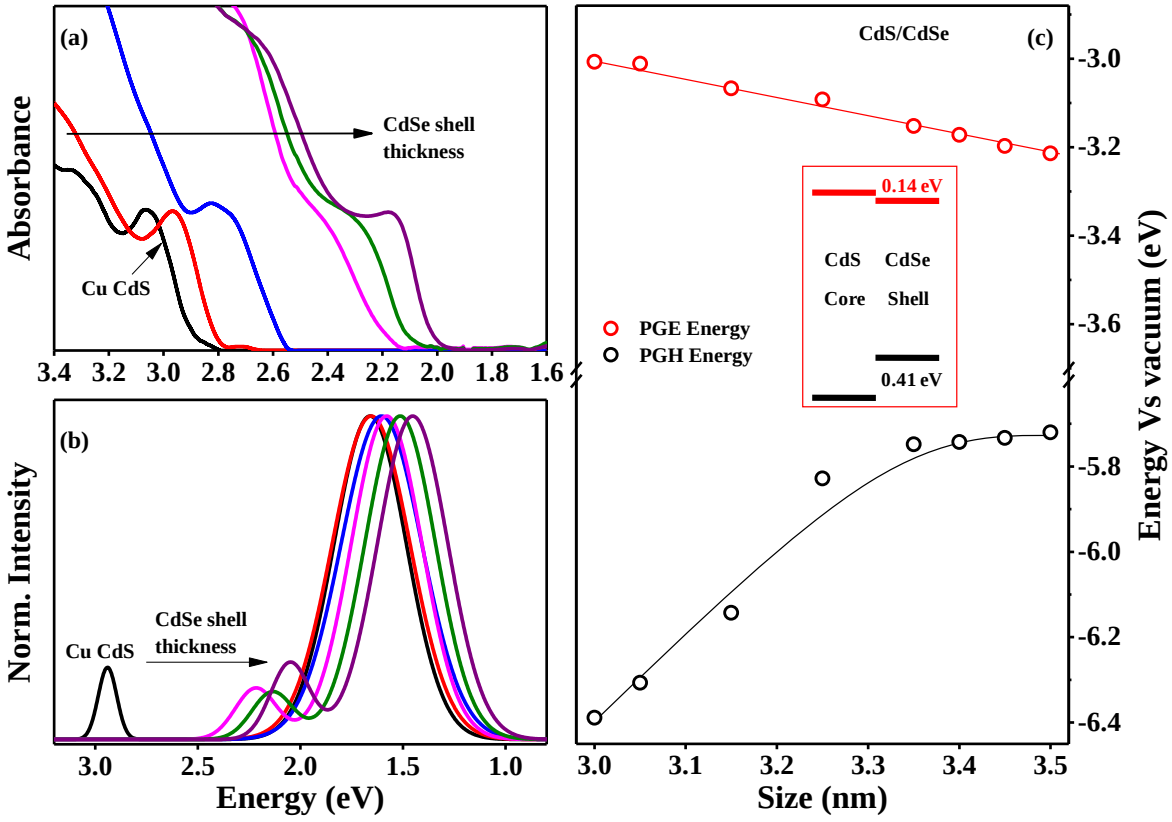

Figure 4.4. ***(a)*** *and* ***(b)*** *are the absorption and PL spectra of Cu doped CdS/CdSe QDs.* λ_{ex}*=405 nm.* ***(c)*** *The variation of energies of PGE (red open circles) and PGH (black open circles) of CdS/CdSe QDs with increasing the CdS shell thickness. The inset of* ***(c)*** *shows the bulk band alignment of CdS/CdSe.*

The versatility of this technique was explored by extending our study to type II CdSe/CdTe QDs semiconductor. We have first studied Cu doped CdSe/CdTe QDs with 3.4 nm CdSe core. The absorption spectra of these QDs gets red-shifted with increasing shell thickness as shown in Figure 4.5(a) whereas the PL spectral position is unchanged with increasing shell thickness as shown in Figure 4.5(b). The longer lifetime of this emission (shown in Figure 4.5(c)) confirms the origin of the emission peak in Cu doped QDs as due to radiative recombination of CB electron with Cu *d* level.

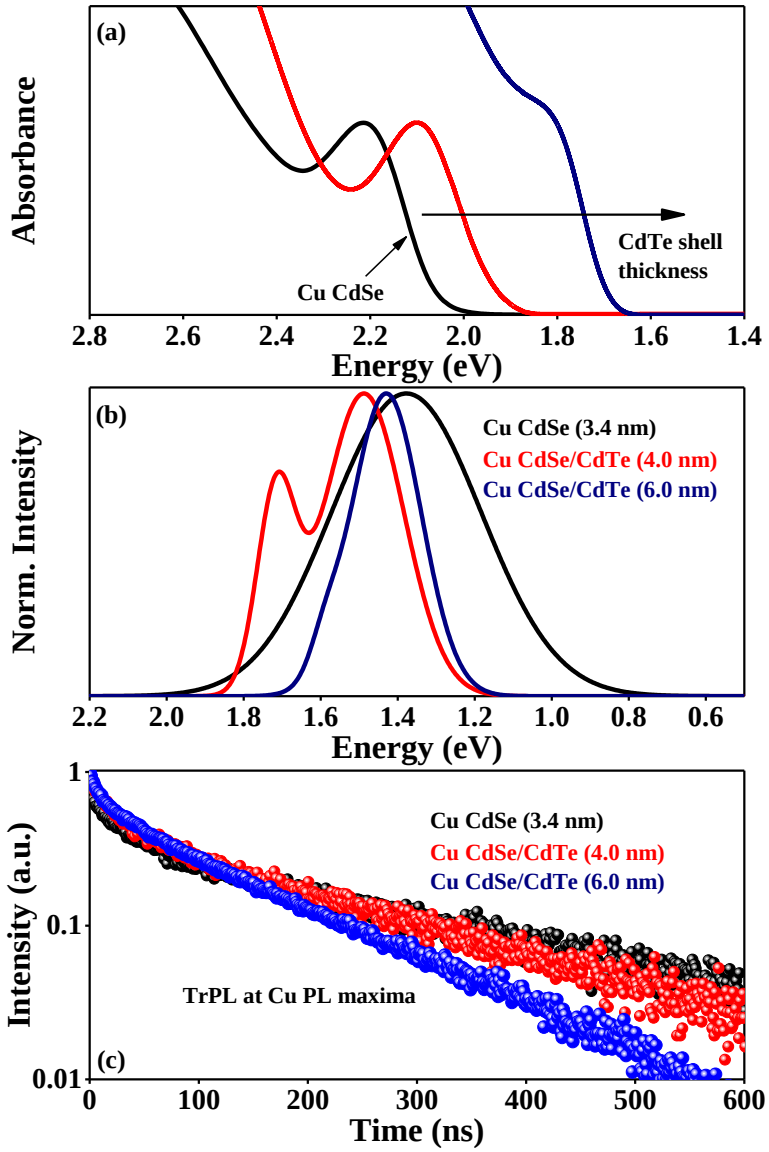

Figure 4.5. *Characterization of Cu doped CdSe/CdTe QDs with 3.5 nm CdSe core.* ***(a)*** *The absorption spectra,* ***(b)*** *the PL spectra and* ***(c)*** *the TrPL spectra of Cu doped CdSe and CdSe/CdTe QDs. All the PL and TrPL spectra were obtained by exciting the samples at 405 nm (λ_{ex}=405 nm).*

Figure 4.6 shows the variation of PGE and PGH as a function of shell thickness. From the figure, it is evident that the PGE energy is almost constant with increasing CdTe shell thickness while the PGH energy increases with increasing shell thickness consistent with the expected type II nature of the interface. Specifically, we observe the localization of electron within core while the hole is getting localized into the shell with increasing shell thickness.

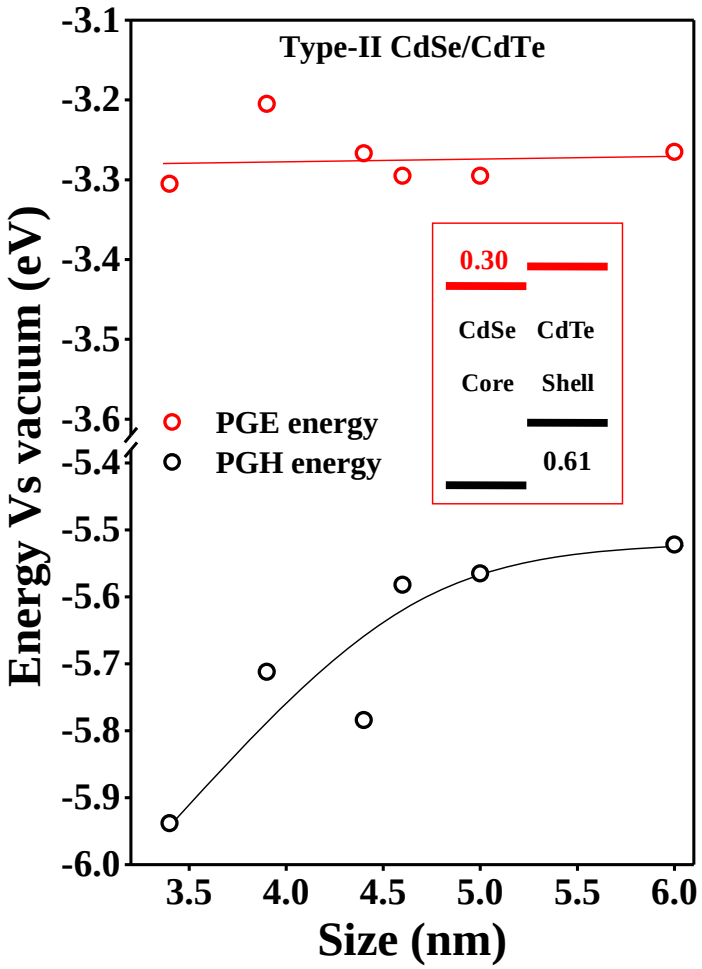

Figure 4.6. *The variation of energies of PGE (red open circles) and PGH (black open circles) of CdSe/CdTe QDs with 3.4 nm CdSe core with increasing shell thickness. The inset shows the bulk band alignment of CdSe/CdTe.*

Theoretically, it was shown that these type II QDs show quasi type II nature for a thin shell on top of a small core (< 4 nm).[8] However, it is well known though these effective mass based theoretical calculations are known to be qualitatively correct, quantitative values may not be experimentally correct. Hence though the recommended core size is lower than 4 nm, we observe type II alignment even for CdSe/CdTe QDs with a 3.4 nm CdSe core. However, we have studied the effect of core size on the electronic structure of type II QDs by synthesizing CdSe/CdTe QDs with a smaller (2.5 nm) CdSe core. The optical spectra of the CdSe/CdTe QDs (with 2.5 nm core) with increasing shell thickness are shown in Figure 4.7.

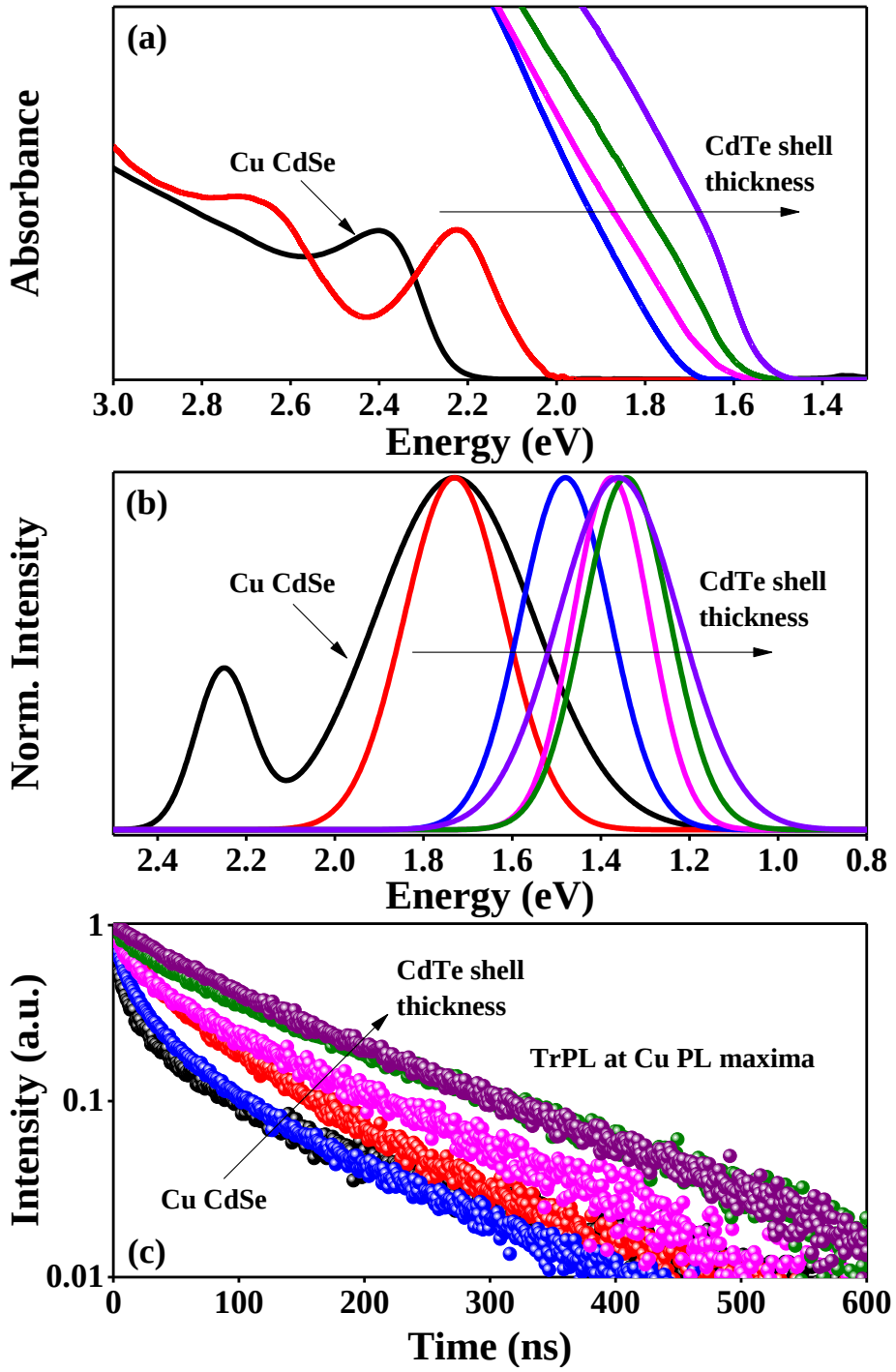

Figure 4.7. *Characterization of Cu doped CdSe/CdTe QDs with 2.5 nm CdSe core.* ***(a)*** *The absorption spectra,* ***(b)*** *the PL spectra and* ***(c)*** *the TrPL spectra of Cu doped CdSe and CdSe/CdTe QDs with increasing shell thickness. All the PL and TrPL spectra were obtained by exciting the samples at 405 nm (λ_{ex}=405 nm).*

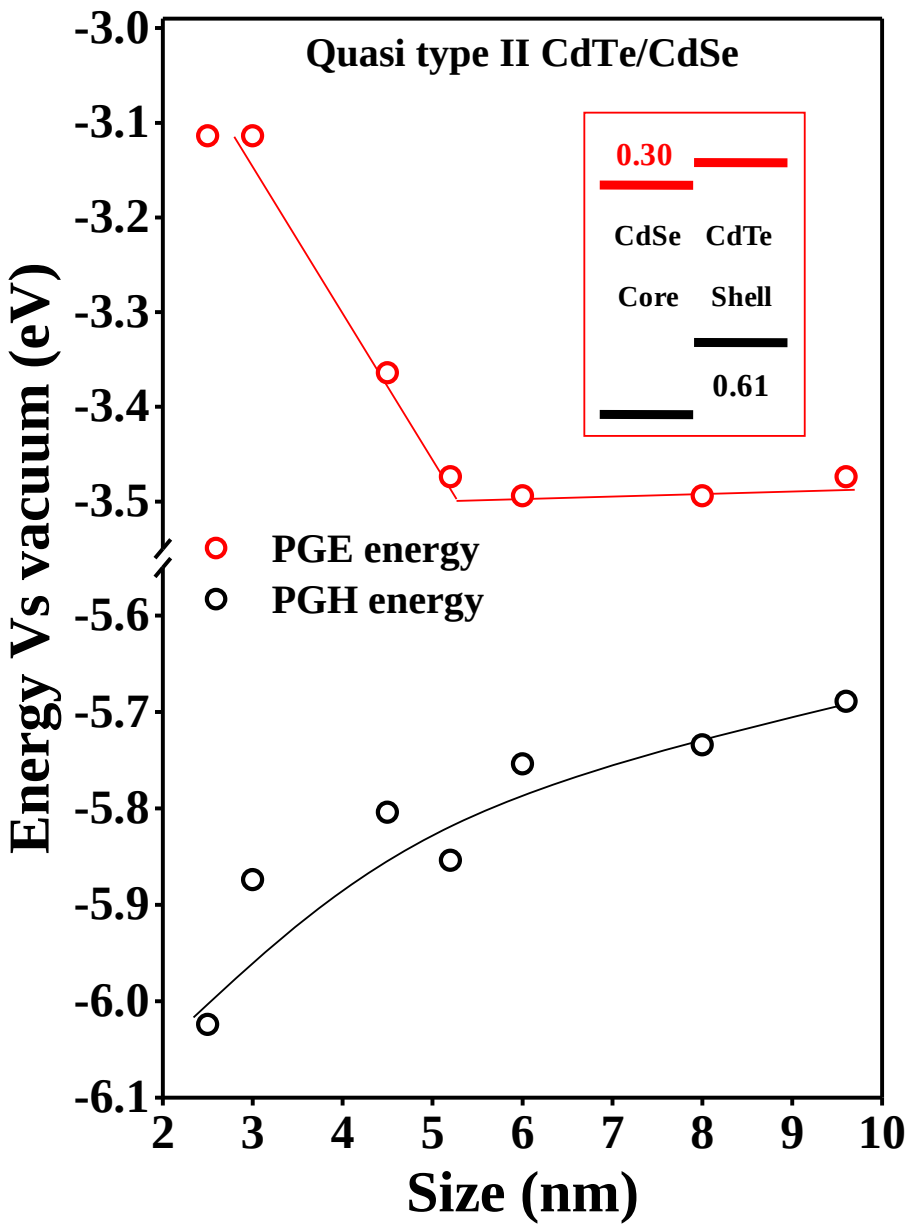

Figure 4.8. *The variation of energies of PGE (red open circles) and PGH (black open circles) of CdSe/CdTe QDs with 2.5 nm CdSe core with increasing shell thickness. The inset shows the bulk band alignment of CdSe/CdTe.*

Figure 4.8 shows the variation of PGE and PGH energies as a function of shell thickness. Interestingly, the PGE energy decreases with increasing CdTe thickness until the overall size of core-shell QDs reaches approximately 5 nm and thereafter remains constant. The variation of PGH energy is similar to the earlier case and is monotonously increasing with

increasing shell thickness. The continuous increase in PGH energy with increasing CdTe shell thickness is a consequence of hole localization into CdTe shell. The initial decrease in electron energy indicates the electron delocalization into CdTe shell which suggests that smaller cores with thinner shells are consistent with a quasi type II structure. Further increase in shell thickness leads to a regular type II structure.

To further explore the widespread applicability of this technique, we have studied the internal structure of alloy QDs. $Zn_{1-x}Cd_xSe$ characterized from TEM shows no change in size while the XRD shows a shift in the peaks from bulk ZnSe to bulk CdSe like structure with the incorporation of Cd confirming the formation of alloys as shown in Figure 4.9.

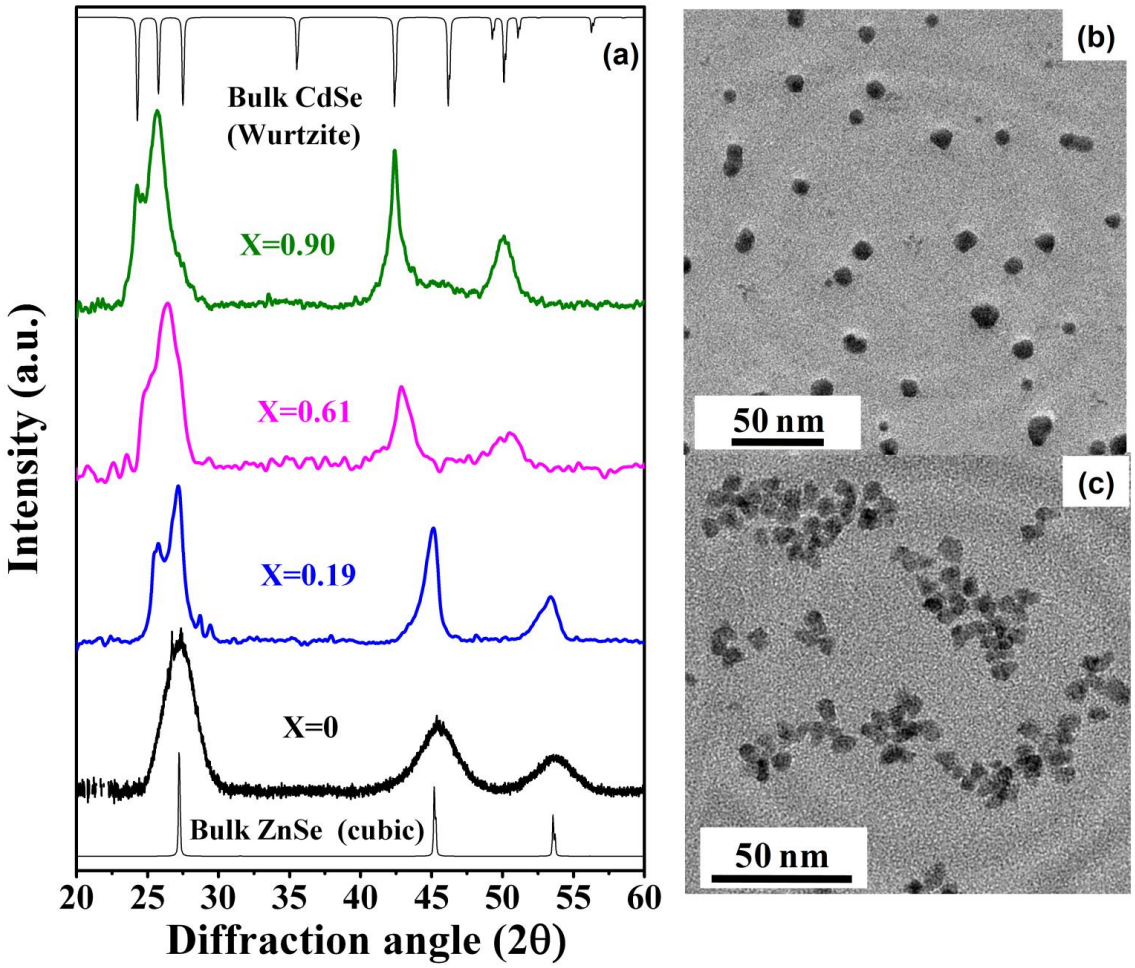

Figure 4.9. *Characterization of Cu doped $Zn_{1-x}Cd_xSe$ alloy QDs.* ***(a)*** *The XRD patterns of alloy QDs with increasing Cd composition.* ***(b)*** *The TEM image of core Cu doped ZnSe QDs and* ***(c)*** *that of alloy QDs with 90% Cd incorporation.*

Both the band gap and PL energy of undoped QDs decreases with increase in Cd composition in the alloy QDs (Figure 4.10(a)). The corresponding Cu doped counter parts show the dominant Cu emission in the PL spectra as shown in Figure 4.10(b).

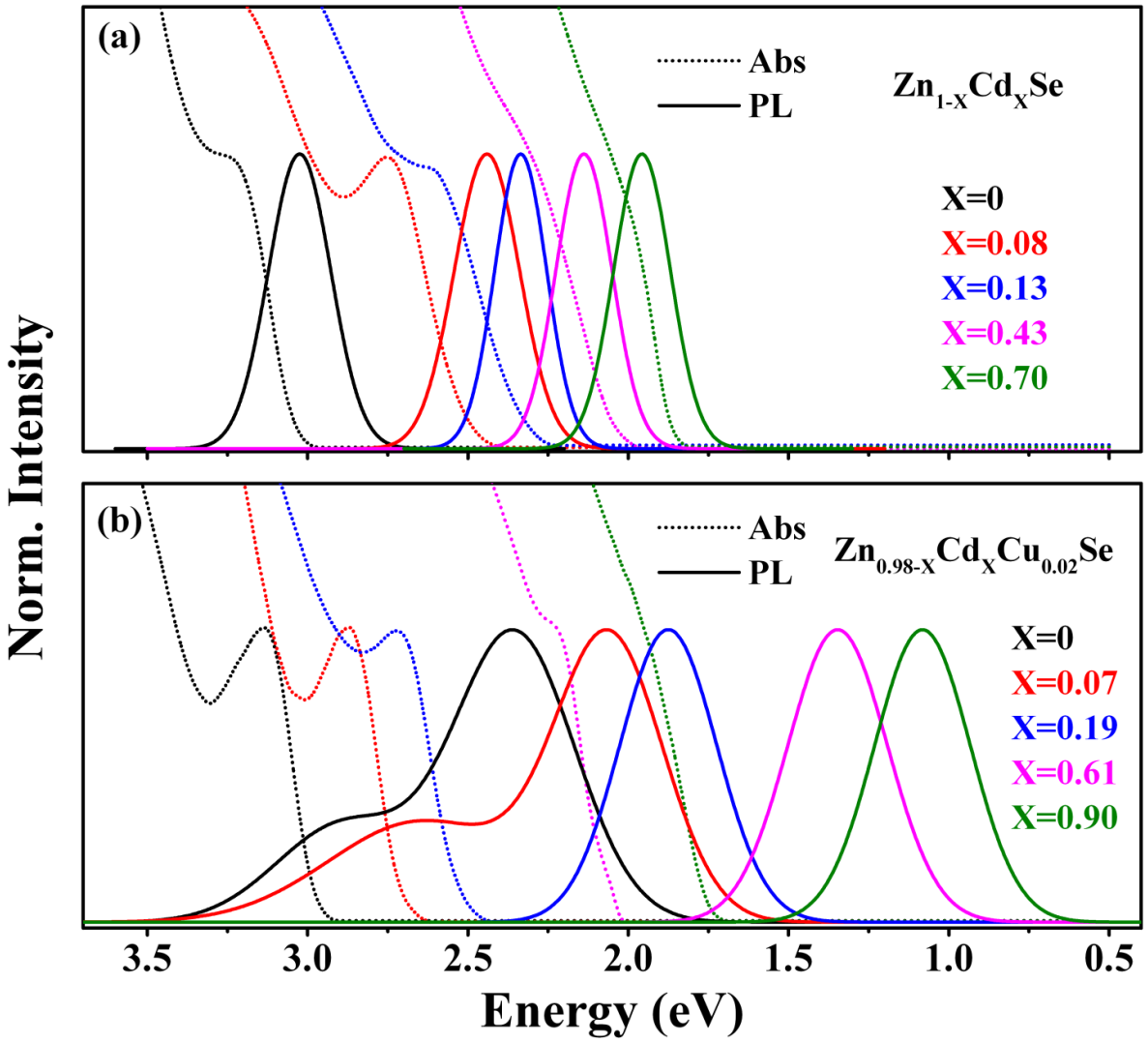

Figure 4.10. *The absorption and PL spectra of* ***(a)*** *undoped and* ***(b)*** *Cu doped* $Zn_{1-x}Cd_xSe$ *alloy QDs with increasing Cd composition.*

Figure 4.11(a) shows the variation in PGE and PGH energies with increase in Cd composition in the QDs. The band gap variation is dominated by decrease in the PGE energy with increase in Cd composition whereas PGH energy is largely constant. This can be understood as a result of higher CB offset than VB offset in ZnSe/CdSe system in bulk as shown in the inset of Figure 4.11(a).

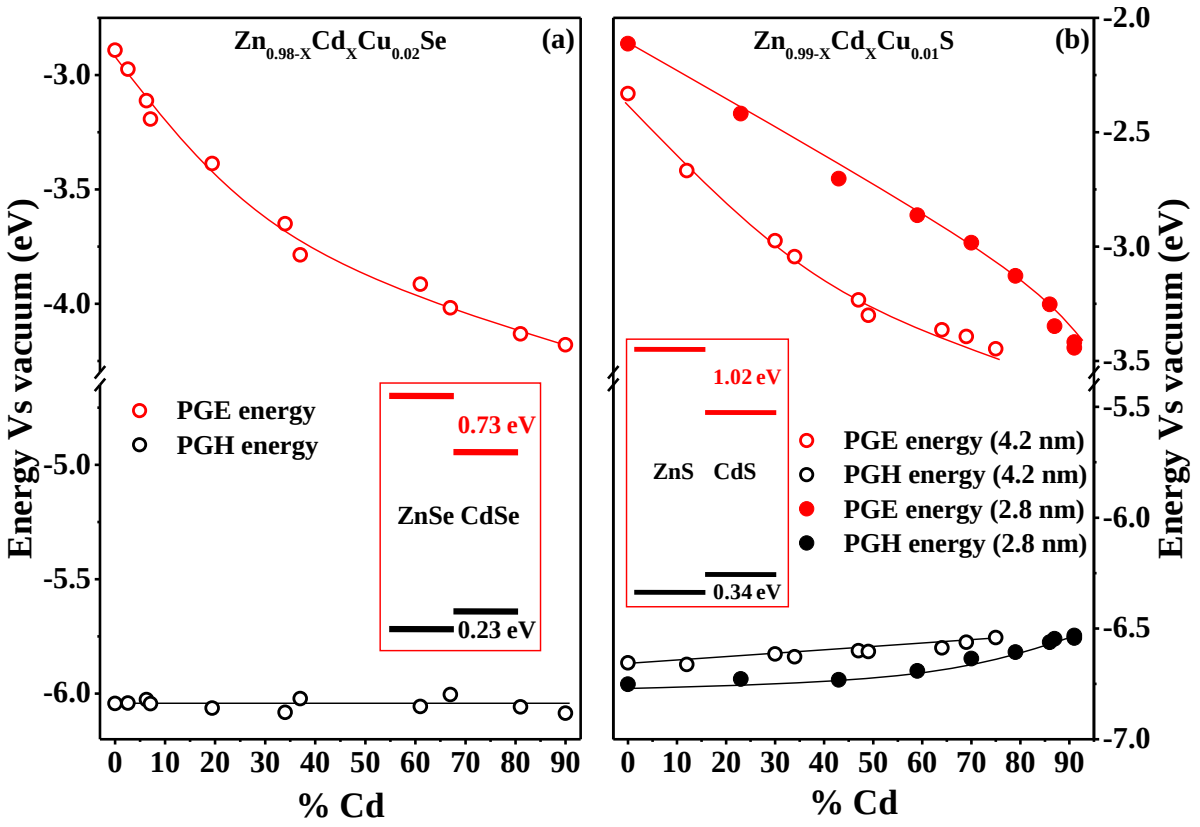

Figure 4.11. ***(a)*** *The variations of energies of PGE (red open circles) and PGH (black open circles) of* $Zn_{0.98-x}Cd_xCu_{0.02}Se$ *QDs with increasing Cd composition.* ***(b)*** *The variations of energies of PGE (red circles) and PGH (black circles) of* $Zn_{0.98-x}Cd_xCu_{0.01}S$ *QDs of 2.8 nm (closed circles) and 4.2 nm (open circles) ZnS core QDs with increasing Cd composition. The insets of* ***(a)*** *and* ***(b)*** *show the bulk band alignments of ZnSe/CdSe and ZnS/CdS respectively.*

Similar studies on the internal structure of $Zn_{1-x}Cd_xS$ alloy QDs for two different sizes are shown in Figure 4.11(b). The absorption and PL spectra of undoped and Cu doped $Zn_{1-x}Cd_xS$ alloy QDs are shown in Figure 4.12. Similar to the case of $Zn_{1-x}Cd_xSe$ alloy QDs, the PGE energy deceases with increase in Cd composition of $Zn_{1-x}Cd_xS$ alloy QDs whereas the PGH energy remains constant. This variation is a consequence of bulk band alignment of ZnS/CdS (inset of Figure 4.11(b)). Further with a decrease in size of ZnS core, we observe a smaller shift in the PGH energy compared to the PGE energy consistent with the variation of band edges as a function of size in ZnS QDs.

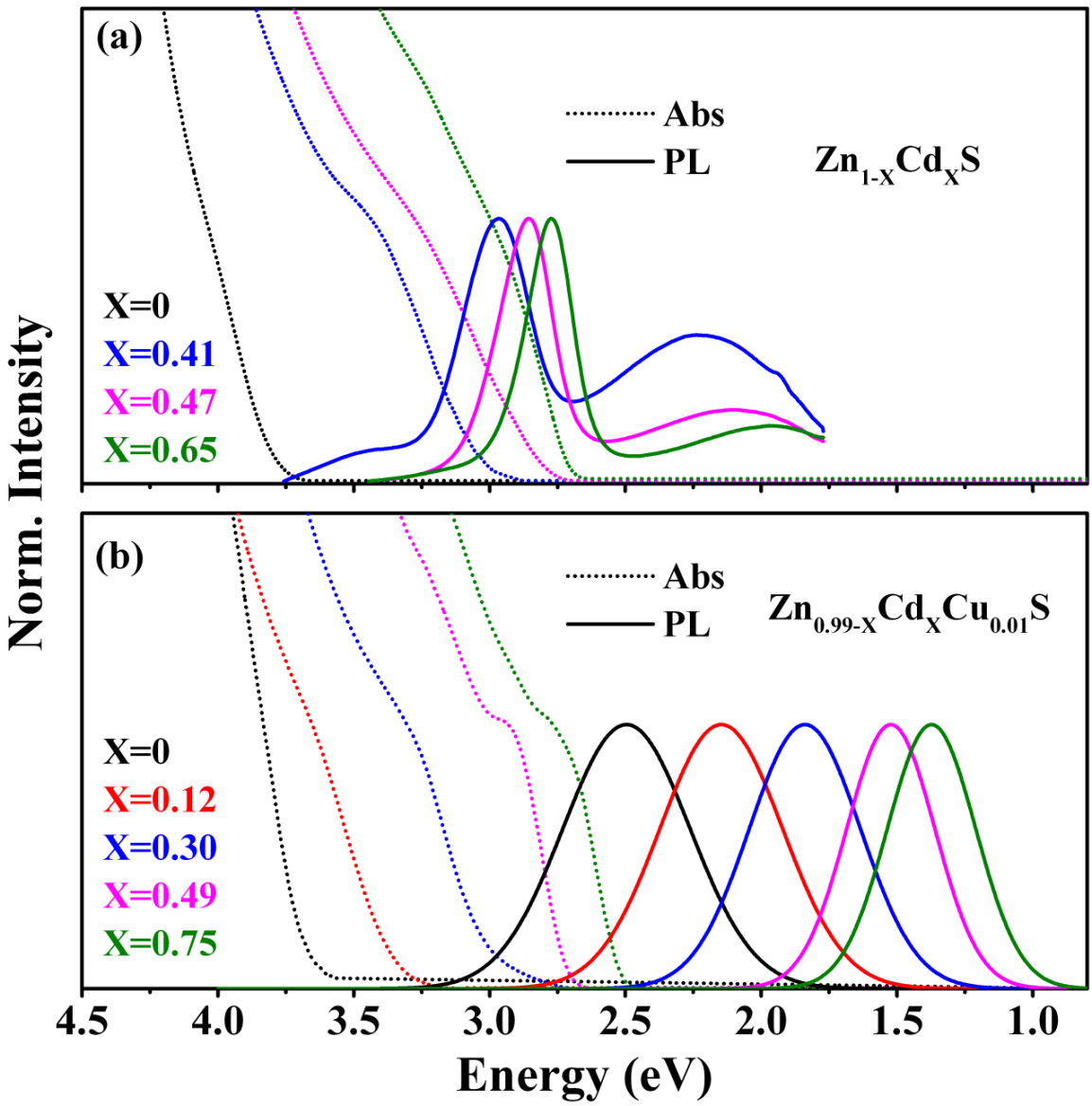

Figure 4.12. *The absorption and PL spectra of* ***(a)*** *undoped and* ***(b)*** *Cu doped* $Zn_{1-x}Cd_xS$ *alloy QDs with increasing Cd composition.*

However, surprisingly, we observe a sudden increase in PGH energy at higher Cd composition of $Zn_{1-x}Cd_xS$ alloy QDs as shown in Figure 4.11(b). This could be due to formation of a thin shell during the addition of Cd precursor resulting in an increased size of the QDs and hence a decreased quantum confinement. However, the size of QDs as obtained from TEM was found to increase from 4.2 nm to 4.6 nm only as seen from Figure 4.13(b) and Figure 4.13(c), which is within the error limit of the measurement.

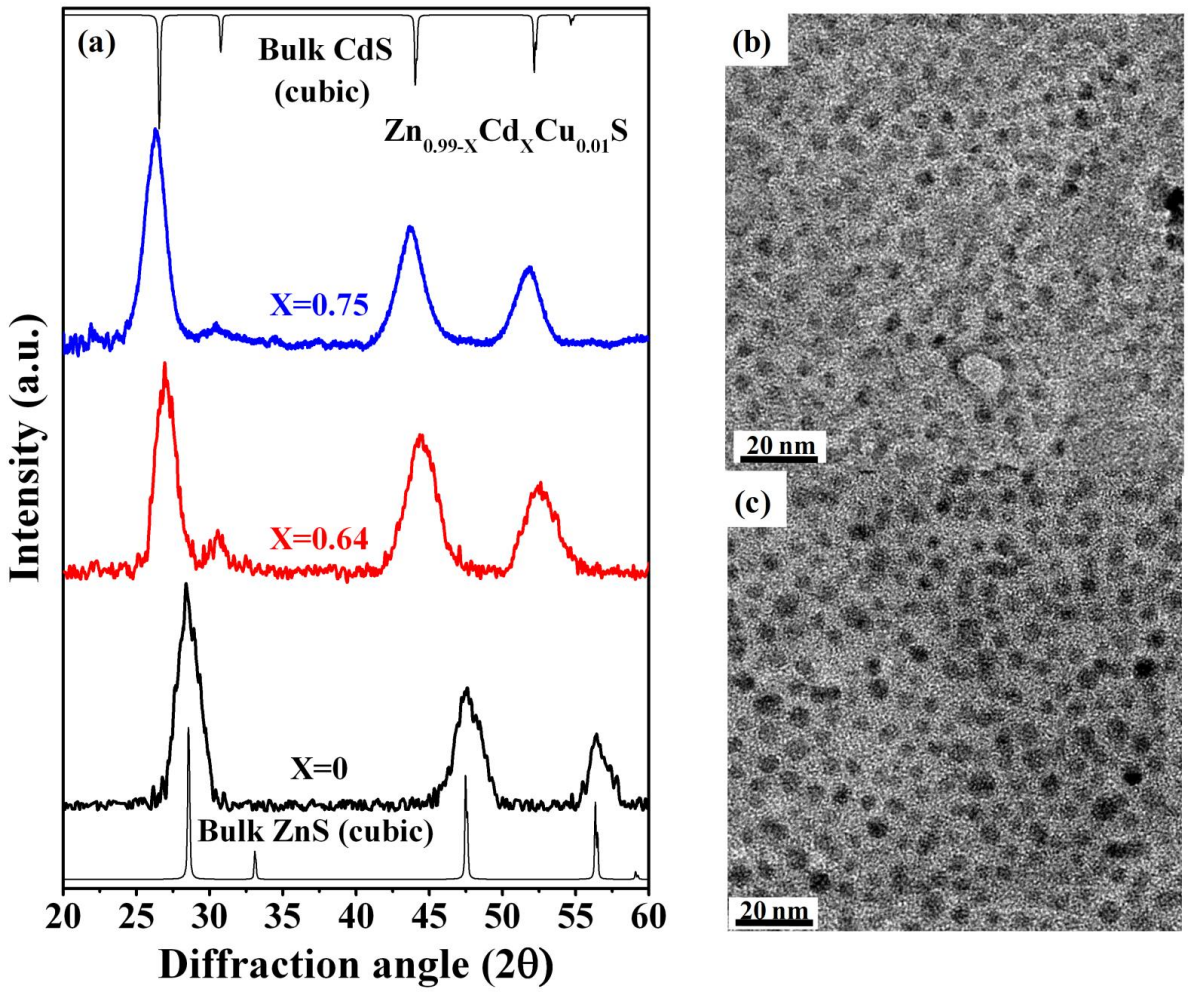

Figure 4.13. *Characterization of Cu doped $Zn_{1-x}Cd_xS$ alloy QDs.* ***(a)*** *The XRD patterns of alloy QDs with increasing Cd composition.* ***(b)*** *The TEM image of core Cu doped ZnS QDs and* ***(c)*** *that of alloy QDs with 75% Cd incorporation.*

So, we have modified the synthetic conditions by swiftly adding all Cd^{2+} precursor and annealing the reaction mixture for similar period of time as in previous case to observe a thicker shell formation. TEM images before and after this addition of Cd are shown in Figure 4.14(a) and 4.14(b) respectively clearly showing an increase from 4.2 nm to 5.7 nm in the size of QDs. These QDs also show enhanced Cu PL compared to the alloy QDs of similar band gap as shown in Figure 4.14(c) suggesting the formation of ZnS shell rather than CdS shell (type I alignment). The etching experiments on Cu doped $Zn_xCd_{1-x}S$ QDs (Figure 4.15) shows the decrease in their Zn composition from 33% to 15% after etching the surface of QDs further reinforcing the ZnS rich shell formation.

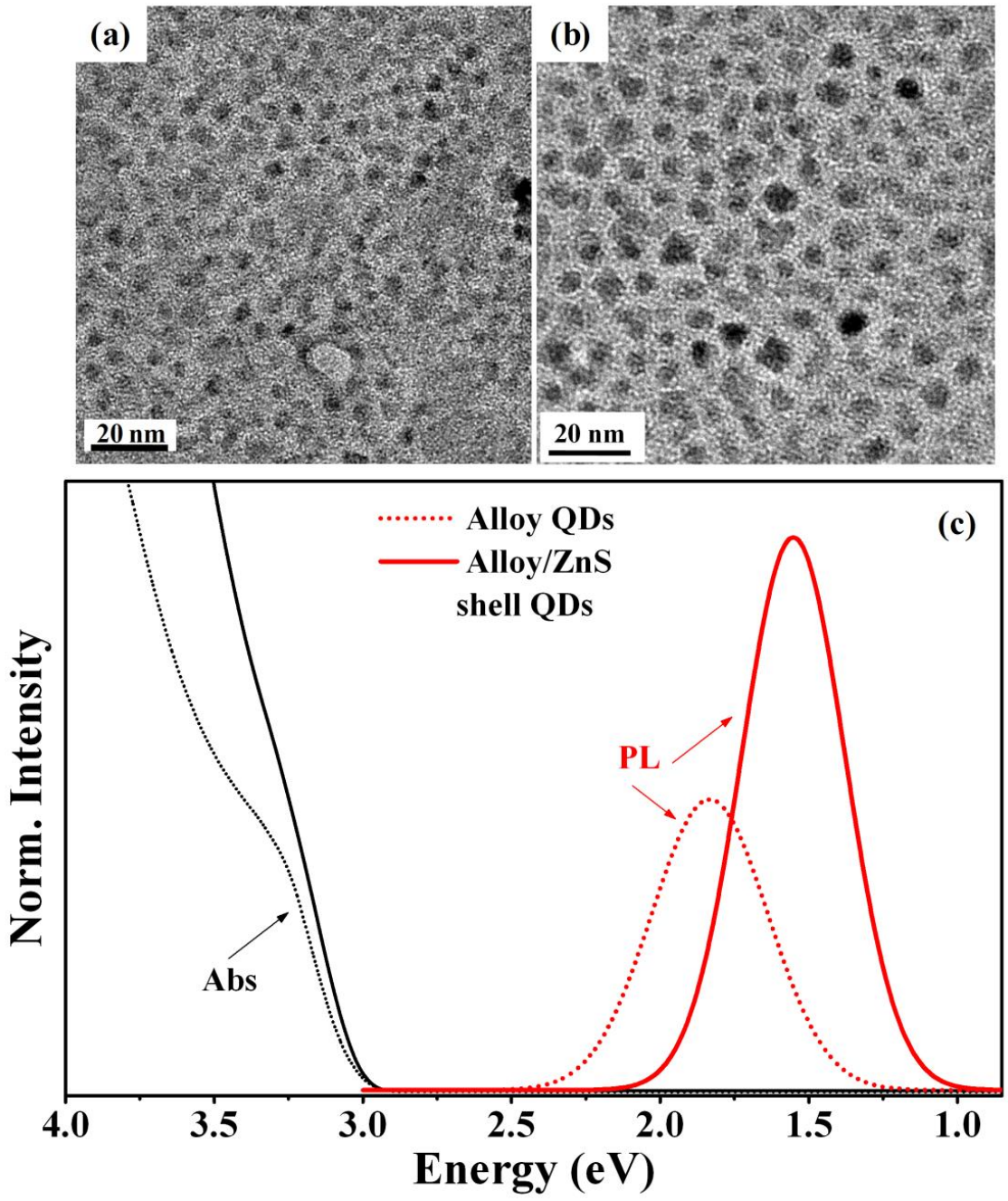

Figure 4.14. ***(a)*** *and* ***(b)*** *show the TEM images of 4.2 nm core Cu doped ZnS QDs and the corresponding final QDs obtained by swift addition of* Cd^{2+} *precursor.* ***(c)*** *The absorption and PL spectra of Cu doped alloy QDs which were obtained by slow and swift addition of* Cd^{2+}.

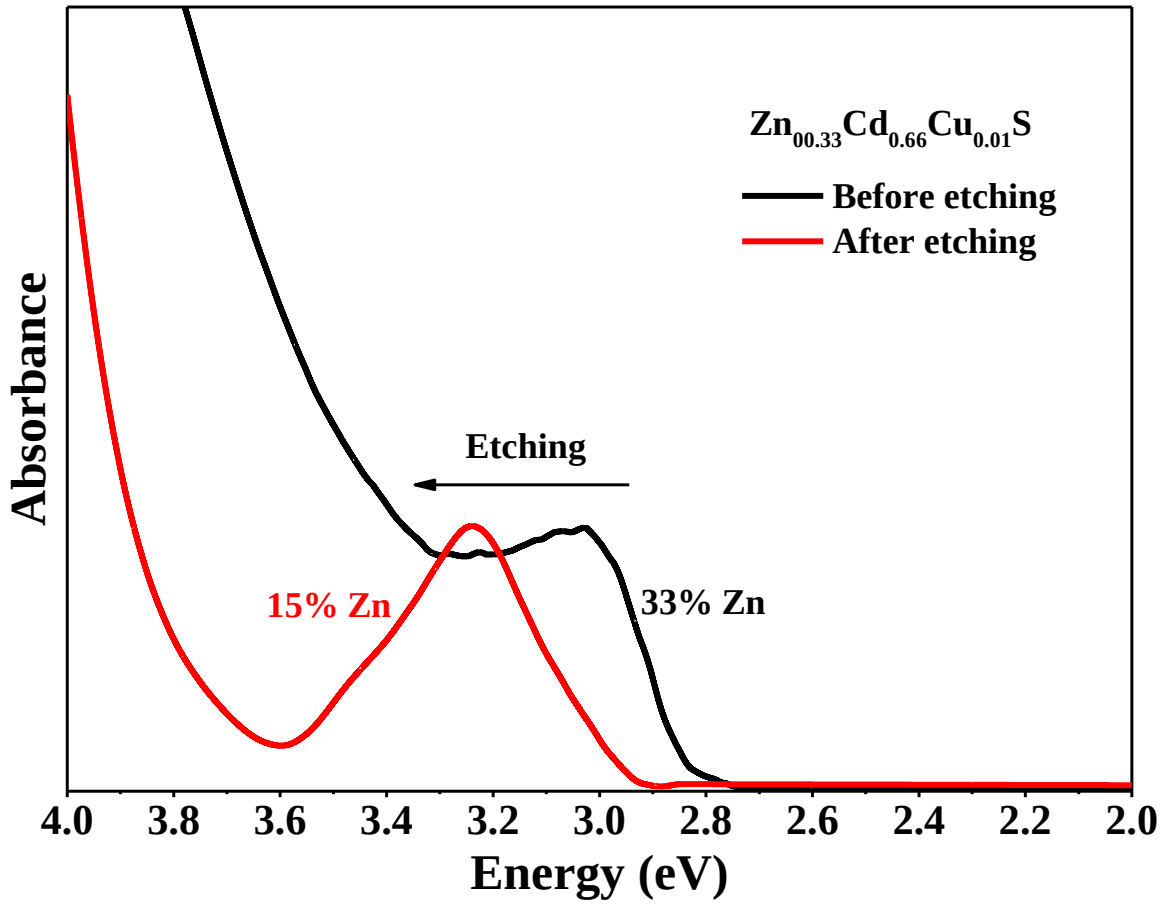

Figure 4.15. *The absorption spectra of $Zn_{0.33}Cd_{0.66}Cu_{0.01}S$ QDs before and after etching of their surface with hydrogen peroxide.*

These alloy/ZnS core-shell QDs (closed circles) show higher band gap than the $Zn_{1-x}Cd_xS$ alloy QDs (open circles) for a given Cd composition as shown in Figure 4.16(a). To understand the origin of this increase in band gap, we have compared the variation of PGE and PGH energies of both alloy QDs and alloy/ZnS core-shell QDs as a function of Cd composition as shown in Figure 4.16(b). The PGE energy variation remains similar in both cases while the PGH energy decreases faster in alloy-shell QDs compared to the alloy only QDs. This proposes the localization of the PGE within the alloy core while the PGH is delocalized in the entire alloy core and ZnS shell due to smaller VB offset between the alloy and ZnS.

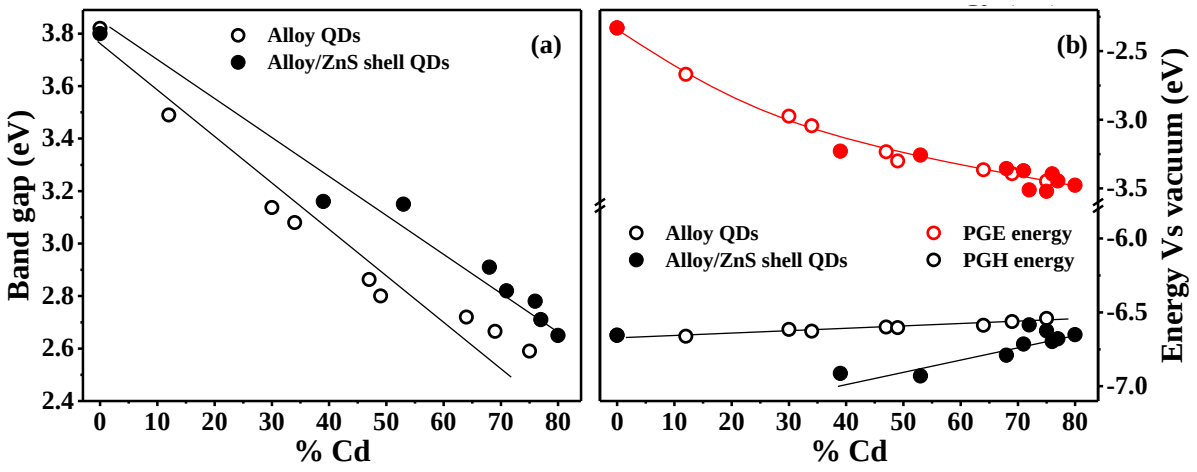

***Figure 4.16**. **(a)** The band gap variations of alloy QDs and alloy/ZnS core-shell QDs with varying Cd composition. **(b)** The variation of energies of PGE (red circles) and PGH (black circles) of $Zn_{0.98-x}Cd_xCu_{0.01}S$ alloy (open circles) and alloy/ZnS core-shell (closed circles) QDs as a function of Cd composition.*

4.5. Conclusions:

We have studied the internal structure of CdSe/CdS, CdS/CdSe, CdSe/CdTe, $Zn_{1-x}Cd_xSe$ and $Zn_{1-x}Cd_xS$ QDs by doping Cu. In case of CdSe/CdS QDs, the PGE delocalizes over the entire QD while the PGH delocalization is restricted to the alloy interface. The CdTe overcoating on CdSe core QDs of larger size results in formation of type II CdSe/CdTe QDs whereas it leads to the formation of quasi type II structure for smaller core sizes qualitatively consistent with the theoretical predictions. We have also shown that this method can be useful in studying the internal structure of previously unknown heterostructures like $Zn_{1-x}Cd_xS$/ZnS alloy-shell QDs. Thus, having successfully predicted the internal structure of a wide range of heterostructures, this method can be widely applied to study heterostructure interfaces and hence correlate their properties to the corresponding structures.

Bibliography:

[1] B. N. Pal, Y. Ghosh, S. Brovelli, R. Laocharoensuk, V. I. Klimov, J. A. Hollingsworth, H. Htoon, *Nano Lett.* **2012**, *12*, 331.

[2] Z. Pan, H. Zhang, K. Cheng, Y. Hou, J. Hua, X. Zhong, *ACS Nano* **2012**, *6*, 3982.

[3] N. McElroy, R. C. Page, D. Espinbarro-Valazquez, E. Lewis, S. Haigh, P. O'Brien, D. J. Binks, *Thin Solid Films* **2014**, *560*, 65.

[4] W. K. Bae, L. A. Padilha, Y.-S. Park, H. McDaniel, I. Robel, J. M. Pietryga, V. I. Klimov, *ACS Nano* **2013**, *7*, 3411.

[5] D. V. Talapin, A. L. Rogach, A. Kornowski, M. Haase, H. Weller, *Nano Lett.* **2001**, *1*, 207.

[6] J. Li, L.-W. Wang, *Appl. Phys. Lett.* **2004**, *84*, 3648.

[7] S. Pokrant, K. B. Whaley, *Eur. Phys. J. D* **1999**, *6*, 255.

[8] A. Piryatinski, S. A. Ivanov, S. Tretiak, V. I. Klimov, *Nano Lett.* **2007**, *7*, 108.

[9] P. K. Santra, R. Viswanatha, S. M. Daniels, N. L. Pickett, J. M. Smith, P. O'Brien, D. D. Sarma, *J. Am. Chem. Soc.* **2008**, *131*, 470.

[10] D. Steiner, D. Dorfs, U. Banin, F. Della Sala, L. Manna, O. Millo, *Nano Lett.* **2008**, *8*, 2954.

[11] Y. C. Li, H. Z. Zhong, R. Li, Y. Zhou, C. H. Yang, Y. F. Li, *Adv. Funct. Mater.* **2006**, *16*, 1705.

[12] B. Hou, D. Parker, G. P. Kissling, J. A. Jones, D. Cherns, D. J. Fermín, *J. Phys. Chem. C* **2013**, *117*, 6814.

[13] C.-H. Chuang, S. S. Lo, G. D. Scholes, C. Burda, *J. Phys. Chem. Lett.* **2010**, *1*, 2530.

[14] K. Wu, G. Liang, D. Kong, J. Chen, Z. Chen, X. Shan, J. R. McBride, T. Lian, *Chem. Sci.* **2016**, *7*, 1238.

[15] Z. Zhang, D. Li, R. Xie, W. Yang, *Angew. Chem. Int. Ed.* **2013**, *52*, 5052.

[16] K. E. Knowles, K. H. Hartstein, T. B. Kilburn, A. Marchioro, H. D. Nelson, P. J. Whitham, D. R. Gamelin, *Chem. Rev.*, **DOI 10.1021/acs.chemrev.6b00048**.

[17] D. Chen, R. Viswanatha, G. L. Ong, R. Xie, M. Balasubramaninan, X. Peng, *J. Am. Chem. Soc.* **2009**, *131*, 9333.

[18] A. Saha, K. V. Chellappan, K. S. Narayan, J. Ghatak, R. Datta, R. Viswanatha, *J. Phys. Chem. Lett.* **2013**, *4*, 3544.

[19] J. J. Li, Y. A. Wang, W. Guo, J. C. Keay, T. D. Mishima, M. B. Johnson, X. Peng, *J. Am. Chem. Soc.* **2003**, *125*, 12567.

[20] D. Battaglia, J. J. Li, Y. Wang, X. Peng, *Angew. Chem. Int. Ed.* **2003**, *42*, 5035.

[21] R. Viswanatha, S. Brovelli, A. Pandey, S. A. Crooker, V. I. Klimov, *Nano. Lett.* **2011**, *11*, 4753.

[22] F. García-Santamaría, S. Brovelli, R. Viswanatha, J. A. Hollingsworth, H. Htoon, S. A. Crooker, V. I. Klimov, *Nano Lett.* **2011**, *11*, 687.

Chapter 5

Low Temperature Dynamics of Surface and Bulk Electronic Structure of Quantum Dots

5.1. Abstract:

Temperature dependence of band gap is well known in bulk semiconductor literature. However, there are only a few studies on variation of band gap in QDs and none of them characterize the variation of band edges. Here, in this chapter, we report the variation of band gap, CB and VB edges of CdS and CdSe QDs as a function of temperature and size, utilizing Cu dopant emission as an internal probe. We found that band gap variation is similar to that of bulk but with a higher average phonon energy. The band edge variation is characterized by a dominant CB shift for larger sizes with decreasing temperature while the smaller size QDs show the variation in both CB and VB. Further, we have also utilized this method to study the binding energy of the trap states as a function of temperature using Cu PL QY and average lifetime of Cu PL.

5.2. Introduction:

Semiconductor QDs, due to their size dependent optical properties and electronic structure, have a crucial role in today's science. One of the many manifestations of this size dependent properties is the variation of band gap as a function of size due to quantum confinement.[1] The corresponding variation of CB and VB has been extensively theoretically[2] studied in literature and experimentally[3, 4] discussed in the earlier chapters of this thesis as well as in literature, even though the literature experimental techniques suffer with a few limitations. The second extensively studied effect of quantum confinement is the surface passivation and the ligand-host chemistry. This extensive attention is reasonable due to the possibility of a wide range of optoelectronics and non-linear optical device applications, in addition to its fundamental importance to physical chemistry. However, one of the most fundamental physical chemistry problem that has not received considerable attention is the temperature dependence of the band gap, the corresponding band edges which is a basic material specific property. In bulk semiconductors, the temperature dependence has been attributed primarily to the electron phonon interactions and to a smaller extent to the thermal expansion of the lattice. The temperature dependence study is important not only from a fundamental perspective of understanding the role of electron-phonon interaction and phonon dispersion in band gap tuning but is also of practical importance given that semiconductor devices are intended to operate within a large temperature range. With the advent of nanotechnology, fundamental

understanding of optical and transport properties arising out the enhanced electron-phonon interactions has received further attention. The band gap of QDs was shown to decrease with increasing temperature which can be directly measured using absorption techniques.[5]

Another factor that plays an important role in the efficiency of any QD application is the efficiency of the surface ligands. Most of the properties of QDs are due to the kinetically stabilized states, driven largely by the surface ligands and the thermodynamics of electron and hole passivation at different temperature and is crucial for the adeptness of their corresponding devices. There are extensive temperature dependent studies on semiconductor QDs such as the temperature dependent exciton lifetimes[6] which gives information regarding the dark and bright excited states, the mechanism for PL enhancement in core-shell QDs with decreasing temperature[7] and so on. To the best of our knowledge, however, there are no experimental or theoretical studies of variation of CB and VB. Theoretically, even though extensive calculations on electronic structure properties have been studied, most ab-initio calculations are carried out at T = 0 K and finite temperature effects are neglected as they are quite cumbersome.[8] Experimentally, only recently techniques such cyclic voltammetry,[9, 10] photoemission spectroscopy,[4, 11] X-ray absorption spectroscopy[12] and scanning tunneling spectroscopy[13] have been introduced to study the variation of band edges and variation of temperature in these methodologies is non-trivial. Hence so far, there is no reported literature, to the best of our knowledge, on temperature dependence of CB and VB.

One of the simple and efficient ways reported for determining the band edge positions was by using Cu dopant emission as an internal probe as discussed in the earlier chapters. Cu dopants introduce an atomic like state in between CB and VB of host QDs and the Cu emission occurs due to the recombination of electron present in CB with the hole present in Cu *d* level. Hence, the CB position can be directly obtained from Cu emission maxima. The VB position can be obtained by subtracting the Cu emission maximum value from the band gap. This method is shown to be efficient in determining the variation of CB and VB of II-VI semiconductor QDs and other heterostructure QDs as a function of size. In this chapter, we have performed a temperature dependence study of band gap and band edges using Cu emission as an internal probe for varying sizes of CdS and CdSe. Further, in this chapter, we have explored the activation energy of the electron and hole trap passivation using temperature

dependent studies of Cu PL QY variation and the average lifetime of Cu emission for both CdS and CdSe QDs.

5.3. Experimental section:

5.3.1. Materials:

CdO, stearic acid and copper (II) acetate monohydrate were purchased from S D Fine chemicals. Oleic acid (90%), ODE (90%) and TOP (90%), S powder and Se pellets were obtained from Sigma Aldrich. TMAH (98%) was obtained from Spectrochem. All purchased chemicals were used without further purification. HPLC hexane, acetone and methanol were purchased from Merck.

Copper stearate was synthesized and purified similar to the literature reports published previously.[14] Briefly, copper acetate was dissolved in methanol and added dropwise to a flask containing TMAH and oleic acid to obtain precipitates of copper stearate that was thoroughly washed with methanol and acetone. Cadmium oleate was prepared by heating a mixture of 0.32 g of CdO, 2.68 g of oleic acid and 9 mL of ODE to a higher temperature (~200 °C) in the Ar atmosphere until the reaction mixture becomes colorless. 1M TOPSe solution was prepared by dissolving 0.79 g of Se in 10 mL of TOP in glove box.

5.3.2. Synthesis of Cu doped CdS QDs: Various sizes of Cu doped CdS QDs were synthesized by following methods reported in **Chapter 6**. Briefly, the synthesis of CdS QDs was carried out by degassing a mixture of CdO (0.2 mmol), oleic acid (0.6-2.0 mmol) and ODE in a three necked flask in vacuum and backfilling with Ar. To this solution, 0.1 mL of TOP was injected at 80 ^{o}C in argon atmosphere followed by the injection of 0.5 mL of 0.2 M S in ODE solution at 300 ^{o} C. This solution was immediately cooled down to 150 ^{o}C to avoid the further growth of CdS QDs. To this solution, 8 µmoles of copper stearate solution of ODE (1 mL) was added and the reaction mixture was annealed for several hours to obtain the Cu doped CdS QDs. Samples were washed with hexane methanol mixture and precipitated using acetone.

5.3.3. Synthesis of undoped and Cu doped CdSe QDs: Various sizes of Cu doped CdS QDs were synthesized by following reported methods.[15] Briefly, 1.25 mL of 0.1 M cadmium oleate and 5 mL of ODE were degassed in a three necked flask and heated to 180˚C. 0.25 mL

of 1M TOPSe was injected at 180 ˚C in argon atmosphere and annealed for a minute to form CdSe QDs. The reaction was cooled down to 140 ˚C and copper stearate solution (20 mmol of copper stearate in 2 mL of ODE) was added drop wise and annealed for 20 mins. In the undoped case, instead of the copper stearate solution of ODE, only ODE was added as blank and was annealed for similar periods of time. Samples were washed with hexane methanol mixture and precipitated using ethanol. To obtain the bigger sizes, reaction mixture was heated to higher temperature after 20 minutes with additional injection of Cadmium oleate. The undoped QDs were synthesized in the similar way just by excluding the Cu precursor addition step. Samples were washed with hexane methanol mixture and precipitated using acetone.

5.4. Results and discussion:

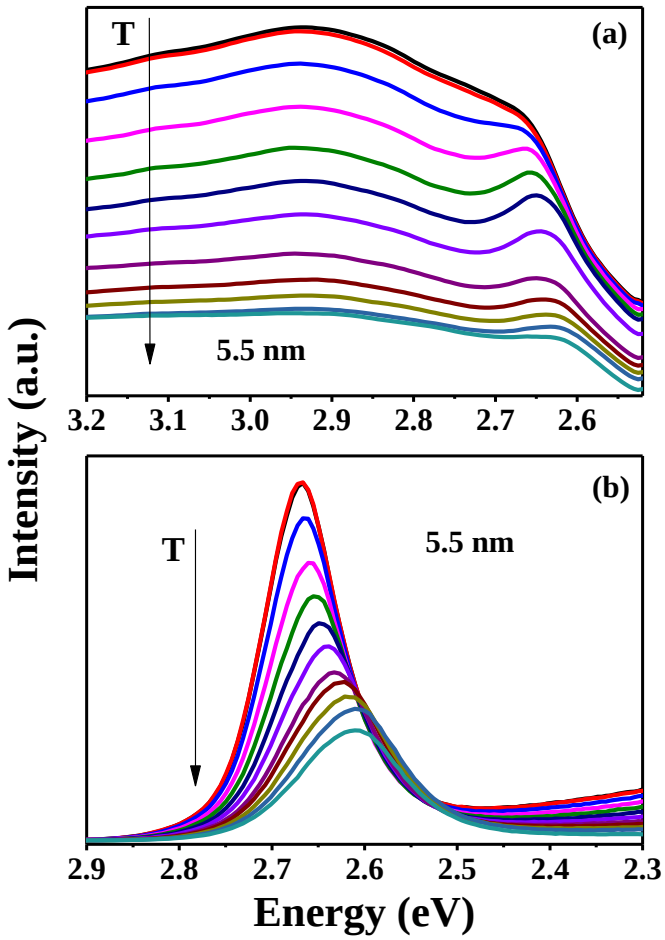

Figure 5.1. *The variation of* ***(a)*** *PLE spectra,* ***(b)*** *PL spectra of 5.5 nm undoped CdS QDs as a function of increasing temperature. The spectra correspond to the temperature varying from 80 K (black color) to 300 K (cyan color) with intervals of 20 K.*

Figure 5.1(a) shows the variation of PLE spectra of 5.5 nm CdS QDS as a function of temperature along with the absorption spectra at room temperature while the PL spectra are shown in Figure 5.1(b). The PLE spectra and the PL spectra show red-shift of the absorption edge as well as band edge emission with increase in temperature similar to that observed in the literature. This can be largely explained by the stronger exciton-phonon coupling at higher temperatures.[16, 17] The intensity of PL spectra decreases with increase in temperature due to the activation of trap states at higher temperatures.[18, 19] The normalized integrated intensity of the band edge emission for different sizes of CdS and CdSe QDs[15] is shown in Figure 5.2 as a function of 1/T.

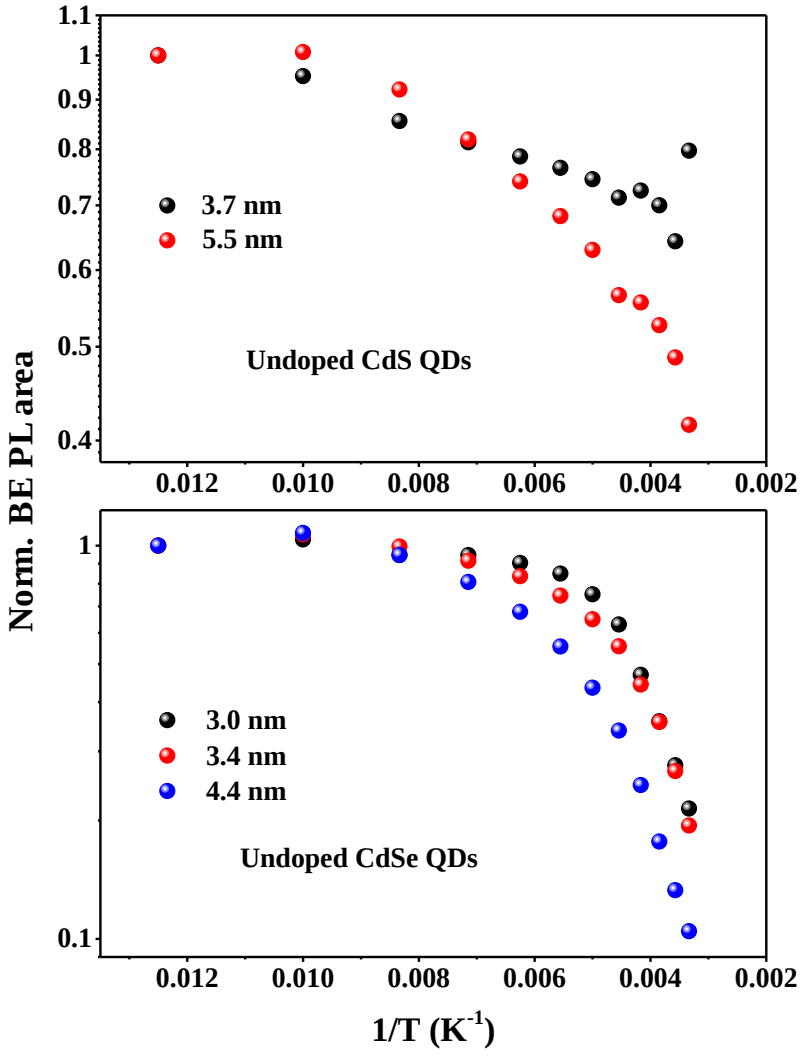

Figure 5.2. *The variation of normalized BE PL area as a function of 1/T (where T=temperature) for* ***(a)*** *undoped CdS QDs and* ***(b)*** *undoped CdSe QDs for different sizes.*

From the figure, it is evident that the trap state passivation cannot be explained by a simple Arrhenius type behavior. This is not surprising as the trap state passivation is related to the bonding efficiency of various passivating agents as well as the dynamics of both the electron and hole traps. Hence it is evident that one needs to separately probe the variation of electron trap passivation and hole trap passivation.

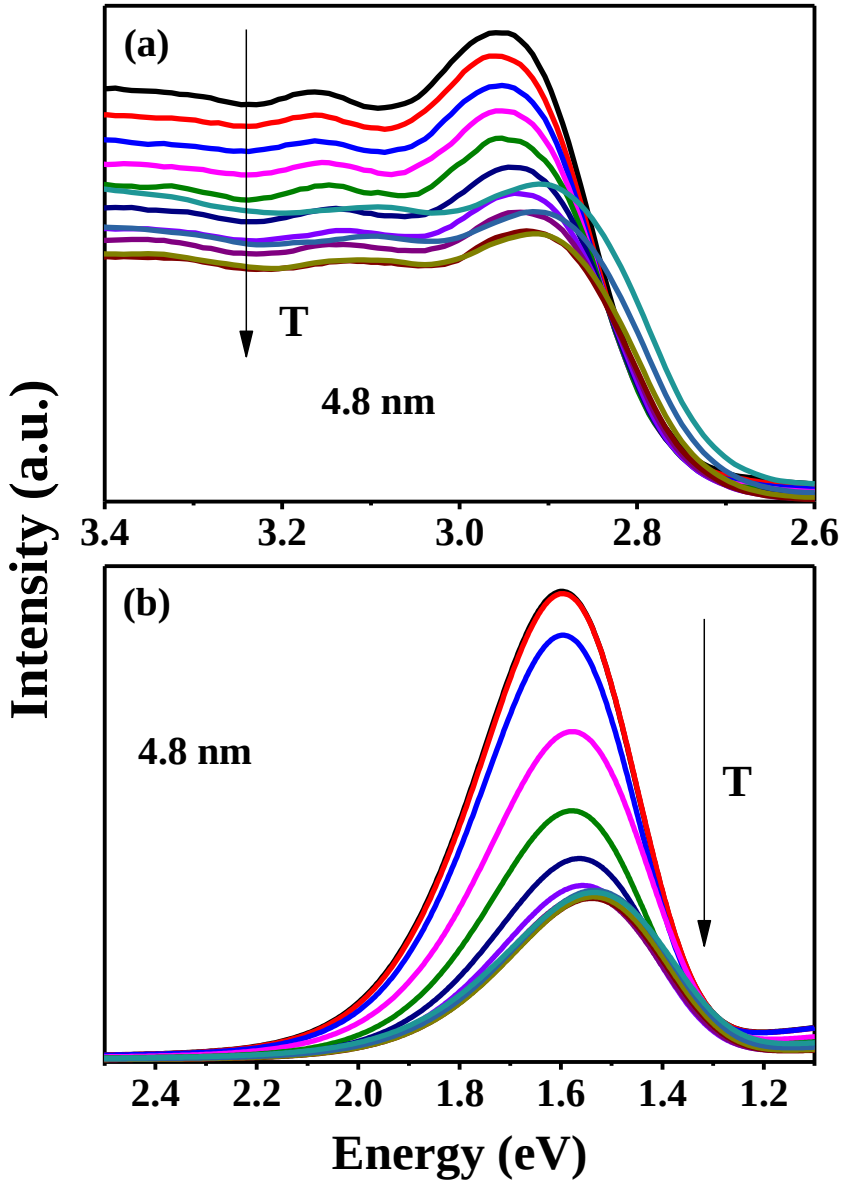

Figure 5.3. *The variation of* ***(a)*** *PLE spectra,* ***(b)*** *PL spectra of 4.8 nm Cu doped CdS QDs as a function of increasing temperature. The spectra correspond to the temperature varying from 80 K (black color) to 300 K (cyan color) with intervals of 20 K.*

One of the efficient ways of separately probing electron and hole trap states is the use of small amount of Cu doping as studied in **Chapter 6**. The temperature dependent PLE and

PL spectra for the 4.8 nm Cu doped CdS are shown in Figures 5.3(a) and 5.3(b) respectively. PL features a dominant red-shifted emission peak and the longer lifetime of this emission (Figure 5.4) confirms that its origin is due to radiative recombination of electron in CB with the Cu *d* level and not due to trap states as explained in **Chapter 3**. Similar to the undoped case, both the PLE and PL show a red shift in the peak position with increase in temperature. The variation of the PLE in doped and undoped cases are found to be similar. However, the variation of the Cu emission peak position differs quite dramatically compared to the variation of band edge emission. This is not surprising given that the Cu emission only reflects the variation of CB of the host QD while the band edge emission arises out of both the CB and VB variation. Further, the PL spectra not only red-shifts in energy but also loses intensity with increasing temperature similar to undoped case as the high temperatures activate the trap states. This decrease in the overall intensity of the Cu emission with temperature reflects the strength of hole trap passivation as a function of temperature. The trap state activation is also supported by decrease in average lifetime of Cu emission with increasing temperature. In order to obtain more quantitative information regarding these variations, we have plotted these parameters for various sizes of CdS and CdSe in the subsequent figures.

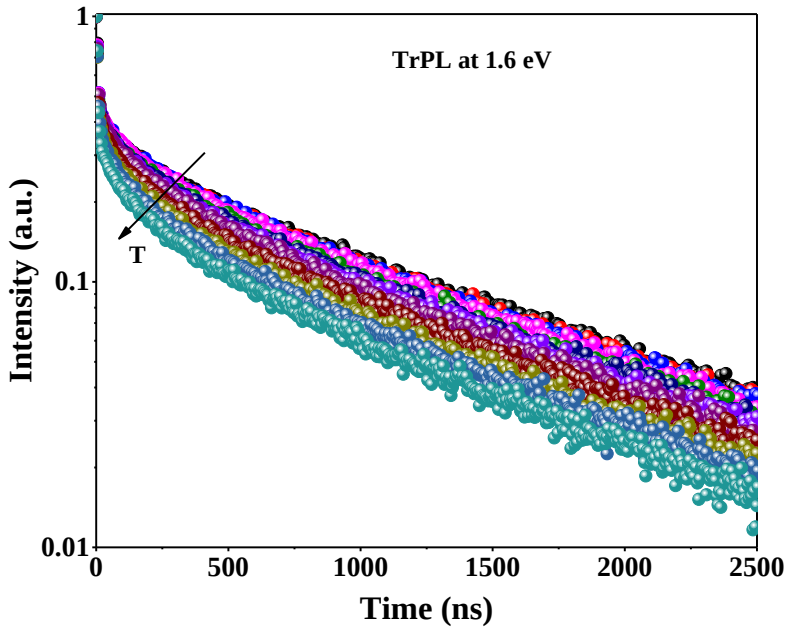

Figure 5.4. *TrPL spectra of 4.8 nm Cu doped CdS QDs as a function of temperature. The spectra correspond to the temperature varying from 80 K (black color) to 300 K (cyan color) with intervals of 20 K.*

The band gap variation of four sizes of Cu doped CdS QDs are plotted in Figure 5.5(a). Similar temperature dependent band gap variations for different sizes of Cu doped CdSe QDs[15] are shown in Figure 5.5(b). It is clearly observed that the shift in band gap is similar in both the cases. The temperature dependent bandgap variation of semiconductors can be fit to Bose-Einstein model[5] which is given by

$$E_g(T) = E_g(0) - \frac{2a_B}{\exp\left(\frac{\theta}{T}\right) - 1} \quad \text{.....(1)}$$

where a_B is electron-phonon interaction and θ is the temperature corresponding to the average energy of the phonons involved in the process.

All the band gap variations are fit well to equation (1) as shown in Figures 5.5(a) and 5.5(b). We have extracted the value of θ from these fits for different sizes of QDs and plotted these values in Figure 5.5(c) for CdS QDs as well as CdSe QDs[15]. From the plot, it is evident that the average energy of the phonons increases with decrease in size, possibly due to confinement effects in CdS QDs. In the case of CdSe, variation is rather small within the given size range. However, it should be noted that the θ value for bulk CdSe is 179 K[20] which is much lesser than the values observed for QDs. This suggests that even though the variation of the phonon energy with size is much more gradual in the case of CdSe QDs, the trends are similar to the CdS QDs.

However, the power of this technique is not only to study the variation of band gap but also to study the variation of CB and VB as a function of temperature. Using PLE and PL spectra, we first analysed the variation of band gap and band edges as a function of size at various temperatures for the case of CdS and have plotted the variation of band gap as well as the CB and VB variation as a function of size in Figure 5.6 for different temperatures for CdS QDs.

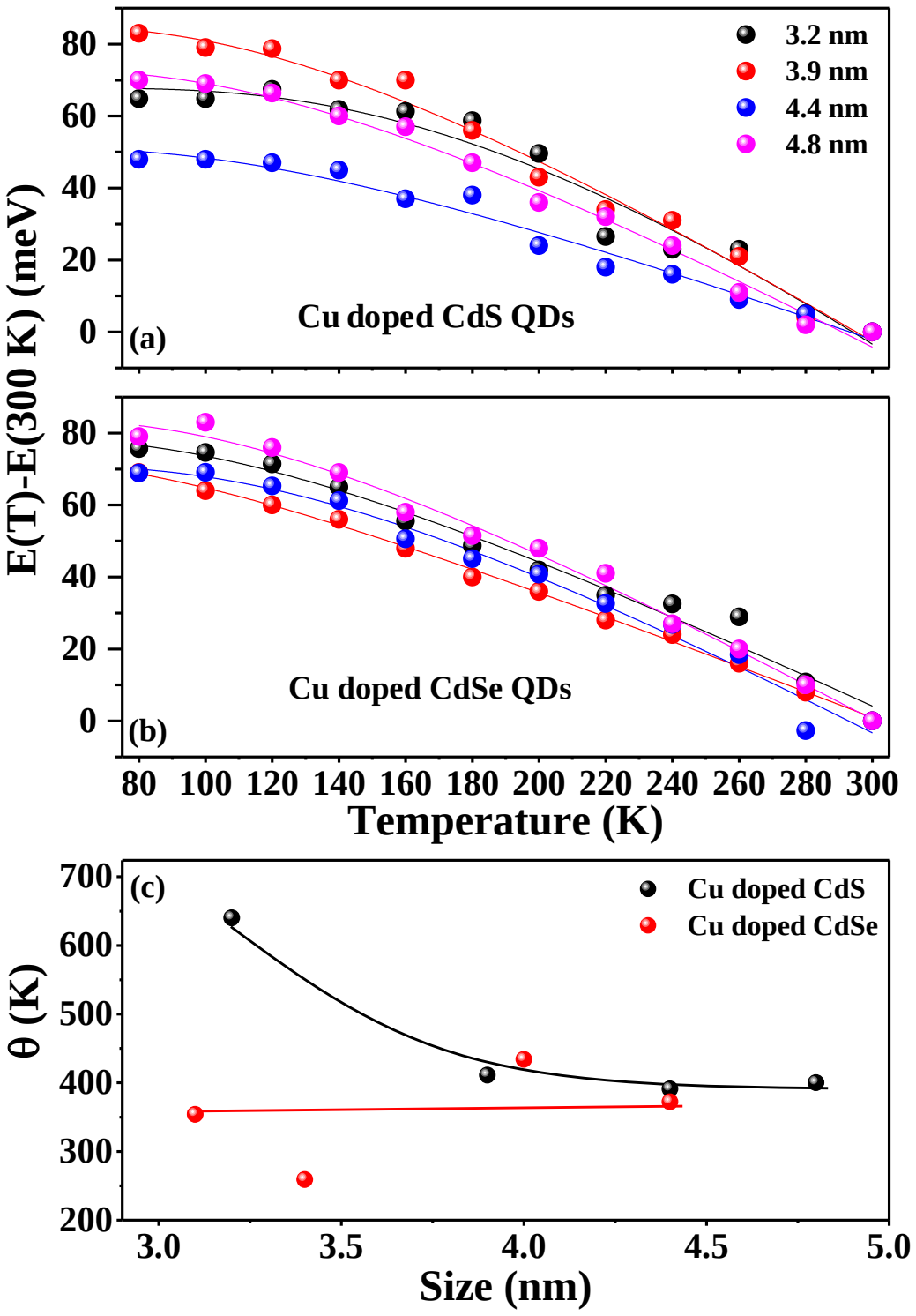

Figure 5.5. *The variation of shift in band gap of* ***(a)*** *Cu doped CdS QDs and* ***(b)*** *Cu doped CdSe QDs of different sizes. The solid lines in* ***(a)*** *and* ***(b)*** *are the Bose-Einstein equation fits to the band gap variation.* ***(c)*** *The variation of θ for Cu doped CdS and Cu doped CdSe QDs as a function of size.*

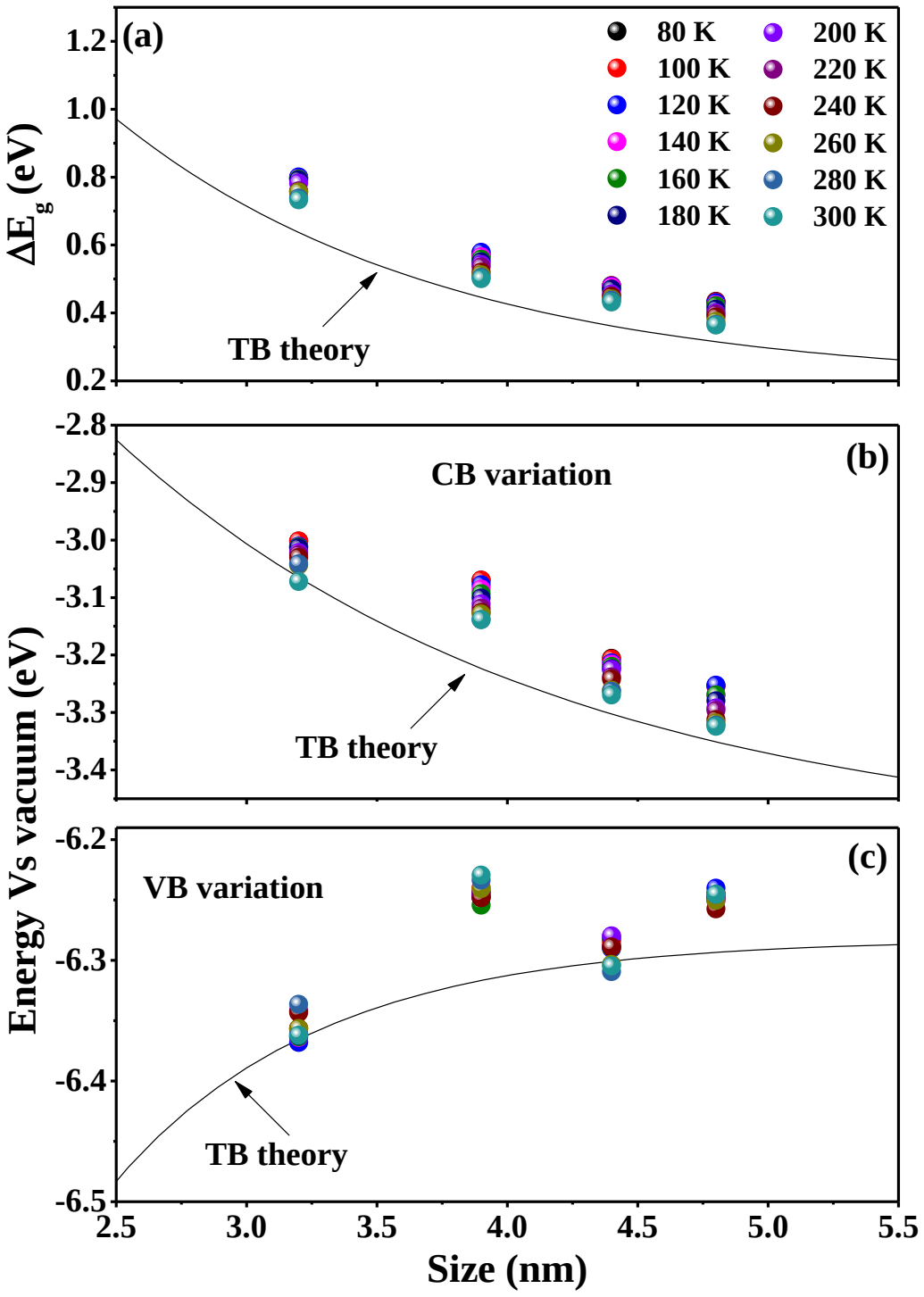

Figure 5.6. *The variation of* ***(a)*** *band gap of CdS QDs as a function of size at different temperatures.* ***(b)*** *The variation of CB and* ***(c)*** *VB as a function of size at different temperatures. The solid lines indicate the TB*[2] *theoretical variations.*

Figure 5.6(a) shows the variation of band gap of CdS QDs as a function of size at different temperatures in comparison with the TB theory which is shown as a solid line. Figure 5.6(b) and Figure 5.6(c) shows the variation of CB and VB as a function of size at various temperatures and the variations are compared with that of theory. It is found that the size dependent variations of band gap and band edges are largely consistent with the theoretical curve and that the variation of band gap and CB and VB as a function of size is much more dominant compared to that of the temperature variation. However, this is consistent with the electron-phonon origin of the band gap variation as a function of temperature which is known to be a second order correction term and is expected to be much smaller. In order to obtain an in depth understanding of the band gap variation as a function of temperature for different sizes, we have plotted the energy values obtained from absorption and Cu emission peaks for low temperature as a difference of that obtained for room temperature in Figure 5.7.

In Figure 5.7(a), the closed and open circles indicate the variations of shift in CB and VB with respect to the 300 K value respectively for CdS QDs. The band gap variation is mainly dominated by shift in CB and the shift in VB is within the range of 20 meV for all the sizes compared to about 70 meV in the case of CB variation. The CB shift dominates the VB shift is more evidently manifested in the case of bigger particles.

To prove the applicability of this technique, we have compared our study with the variation of CB and VB of CdSe QDs performed earlier[15] as a function of temperature. Figure 5.7(b) shows the variation of band edges of different sizes of CdSe QDs as a function of temperature. Smaller, 3.1 and 3.4 nm QDs show the variation in both CB and VB while the bigger, 4.0 and 4.4 nm QDs show the dominant variation in CB than VB as shown in Figure 5.7(b). 3.1 and 3.4 nm particles show a shift of ~ 40 meV for both CB and VB. But bigger particles show more CB shift than VB shift. Hence, the value of CB shift to VB shift increases with increasing the size of QDs. In other words, the temperature dependent band gap variation is dominated by CB shift with increasing the CdSe QD size.

The exact explanation for these variations is unknown at this moment and requires theoretical understanding. However, this is the first experimental evidence wherein the variation of absolute positions of CB and VB as a function of temperature for CdSe and CdS QDs is determined.

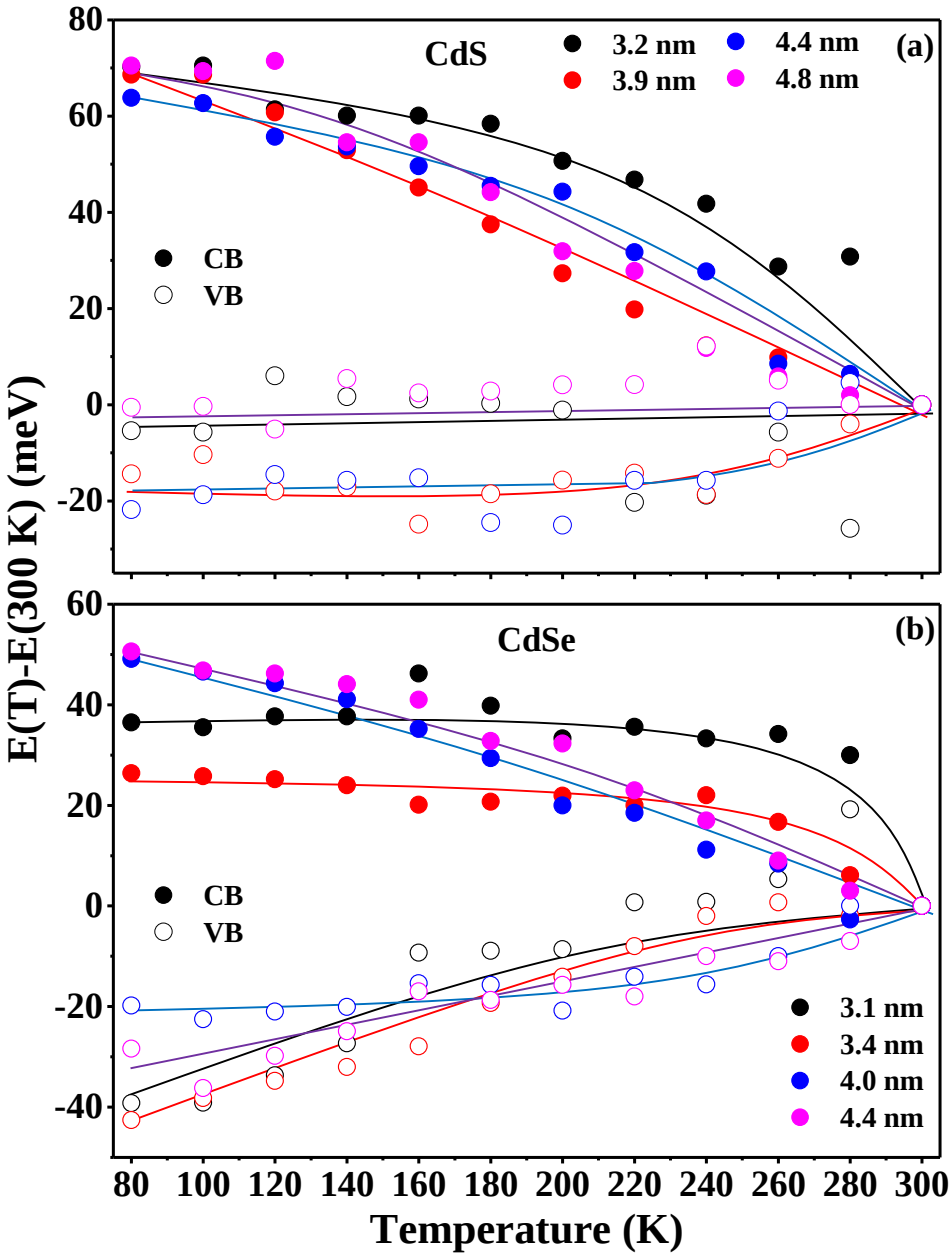

Figure 5.7. *The variation of CB and VB of* ***(a)*** *CdS QDs and* ***(b)*** *CdSe QDs of different sizes as a function of temperature. Panel* ***(b)*** *is adapted from ref*[15]

Secondly, to monitor the activation energy of the hole and electron trap passivation, we have studied the normalized intensity variation of Cu emission band with respect to temperature and size as well as the variation of the average lifetime of the Cu emission peak respectively. These results for both CdS and CdSe QDs are compiled in Figure 5.8. It was observed that log E vs 1/T does not show a straight line ruling out a complete Arrhenius type behavior.

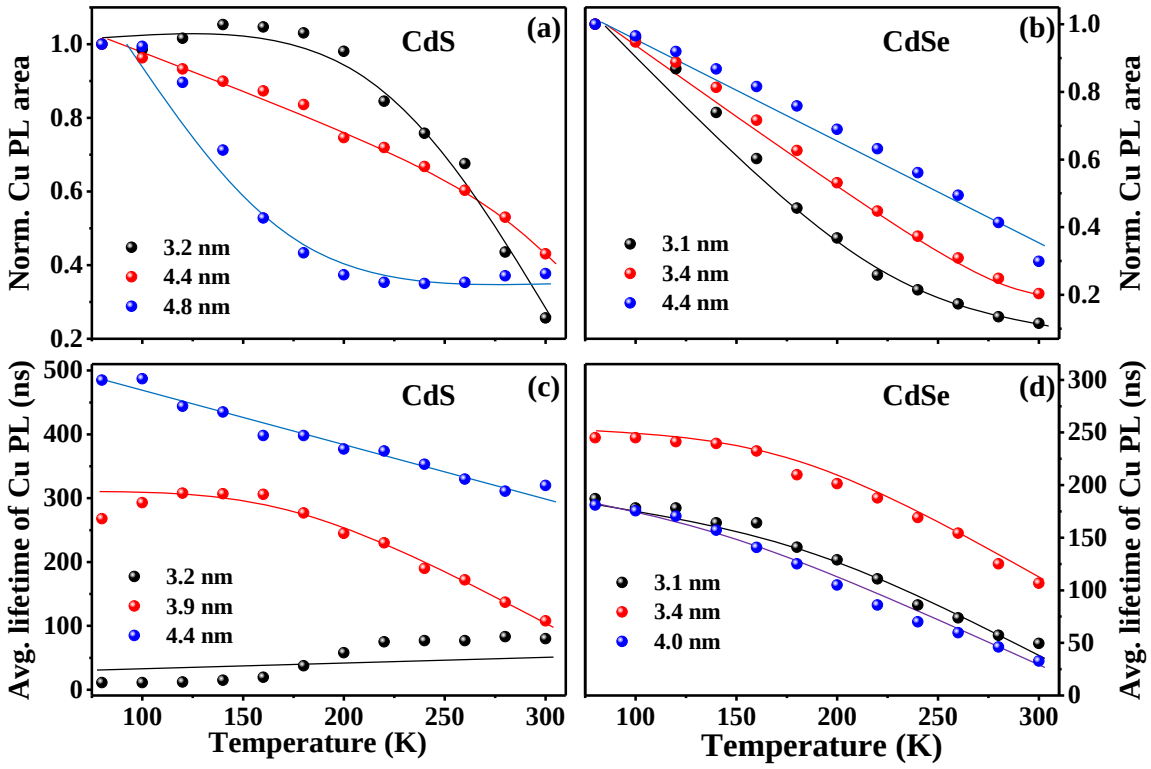

Figure 5.8. *The variation of normalized Cu PL area as a function of temperature for* ***(a)*** *Cu doped CdS QDs and* ***(b)*** *Cu doped CdSe QDs for different sizes. The variation of average lifetime of Cu PL as a function of temperature for* ***(c)*** *Cu doped CdS QDs and* ***(d)*** *Cu doped CdSe QDs for different sizes.*

Figure 5.8(a) shows the variation of normalized Cu PL area of CdS QDs of different sizes as a function of temperature. The Cu PL area decreases with increase in temperature suggesting a decrease in hole traps, i.e., a more efficient passivation of holes with increasing the temperature. While this is surprising, the reason for the non-Arrhenius behavior is evident. It is clear that more number of hole traps are not being passivated at lower temperature suggesting that the passivating ligands are only efficiently adsorbed at higher temperature and the changes are not driven by thermal variation. It is also evident that the passivation is more efficient for smaller clusters showing a smaller change compared to the larger QDs for both CdS and CdSe QDs. In case of smaller particles (3.2 nm), the decrease happens at around 220 K while the same happens at a much lower temperature (~ 100 K) in case of 4.8 nm CdS QDs. We have studied the similar variation in case of CdSe QDs also as shown in Figure 5.8(b). However, we found an opposite trend in case of CdSe QDs wherein the passivation efficiency is higher for bigger particles. However, this is not surprising given the different bonding and adsorbing efficiencies of the ligand molecules with the host QDs. In fact, an analysis of the

synthesis techniques provides answers to these discrepancies. We have used more ligands for synthesizing the bigger particles than the smaller ones in case of CdS while higher number of ligands were used for synthesizing the smaller particles than bigger ones in case of CdSe QDs. We have also probed the electron trap passivation or creation using time dependent Cu PL decay studies. Figure 5.8(c) shows the average lifetime variation of Cu PL as a function of temperature for different sizes of CdS QDs. Though the temperature dependence is similar across the sizes, the average lifetime is higher for bigger sizes indicating that less number of electron traps in case of bigger CdS QDs. This is clear from the fact that more oleic acid ligands are present during the synthesis of bigger CdS QDs and oleic acid was shown to passivate the electron traps on CdS QD surface (**Chapter 6**). Similar variation is observed in case of CdSe QDs as shown in Figure 5.8(d).

5.5. Conclusions:

We have synthesized different sizes of Cu doped CdS and CdSe QDs. We have probed the variation of CB and VB for different sizes of CdS and CdSe QDs as a function of temperature using Cu emission. The CB shift completely dominates the VB shift in case of CdS QDs especially in bigger size particles. The observation of CB and VB shifts suggests that most of the variation in bandgap as function of temperature is dominated by shift in CB with increase in size of CdSe QDs. θ varies inversely proportional with the size of CdSe and CdS QDs. The activation energy of hole trap passivation is higher when more hole traps present on the QD surface.

Bibliography:

[1] W. W. Yu, L. Qu, W. Guo, X. Peng, *Chem. Mater.* **2003**, *15*, 2854.

[2] R. Viswanatha, D. D. Sarma, *Chem. Asian J* **2009**, *4*, 904.

[3] J. Jasieniak, M. Califano, S. E. Watkins, *ACS Nano* **2011**, *5*, 5888.

[4] J. R. I. Lee, R. W. Meulenberg, K. M. Hanif, H. Mattoussi, J. E. Klepeis, L. J. Terminello, T. van Buuren, *Phys. Rev. Lett.* **2007**, *98*, 146803.

[5] G. Perna, M. Lastella, M. Ambrico, V. Capozzi, *Appl. Phys. A* **2006**, *83*, 127.

[6] C. de Mello Donegá, M. Bode, A. Meijerink, *Phys. Rev. B* **2006**, *74*, 085320.

[7] P. Jing, J. Zheng, M. Ikezawa, X. Liu, S. Lv, X. Kong, J. Zhao, Y. Masumoto, *J. Phys. Chem. C* **2009**, *113*, 13545.

[8] J. Bhosale, A. K. Ramdas, A. Burger, A. Muñoz, A. H. Romero, M. Cardona, R. Lauck, R. K. Kremer, *Phys. Rev. B* **2012**, *86*, 195208.

[9] E. Kucur, J. Riegler, G. A. Urban, T. Nann, *J. Chem. Phys.* **2003**, *119*, 2333.

[10] S. K. Haram, A. Kshirsagar, Y. D. Gujarathi, P. P. Ingole, O. A. Nene, G. B. Markad, S. P. Nanavati, *J. Phys. Chem. C* **2011**, *115*, 6243.

[11] V. L. Colvin, A. P. Alivisatos, J. G. Tobin, *Phys. Rev. Lett.* **1991**, *66*, 2786.

[12] T. Van Buuren, L. N. Dinh, L. L. Chase, W. J. Siekhaus, L. J. Terminello, *Phys. Rev. Lett.* **1998**, *80*, 3803.

[13] B. Alperson, I. Rubinstein, G. Hodes, D. Porath, O. Millo, *Appl. Phys. Lett.* **1999**, *75*, 1751.

[14] D. Chen, R. Viswanatha, G. L. Ong, R. Xie, M. Balasubramaninan, X. Peng, *J. Am. Chem. Soc.* **2009**, *131*, 9333.

[15] R. Tomar, Jawaharlal Nehru Centre for Advanced Scientific Research (Bangalore), **2014**.

[16] P. Ramvall, S. Tanaka, S. Nomura, P. Riblet, Y. Aoyagi, *Appl. Phys. Lett.* **1999**, *75*, 1935.

[17] J. Z. Wan, J. L. Brebner, R. Leonelli, G. Zhao, J. T. Graham, *Phys. Rev. B* **1993**, *48*, 5197.

[18] D. Valerini, A. Creti, M. Lomascolo, L. Manna, R. Cingolani, M. Anni, *Phys. Rev. B* **2005**, *71*, 235409.

[19] G. Morello, M. De Giorgi, S. Kudera, L. Manna, R. Cingolani, M. Anni, *J. Phys. Chem. C* **2007**, *111*, 5846.

[20] S. Logothetidis, M. Cardona, P. Lautenschlager, M. Garriga, *Phys. Rev. B* **1986**, *34*, 2458.

Part II

Study of Surface Electronic Structure Using Cu Emission

Chapter 6

Understanding the Role of Commonly Used Organic Ligands in Passivating II-VI Semiconductor Quantum Dots

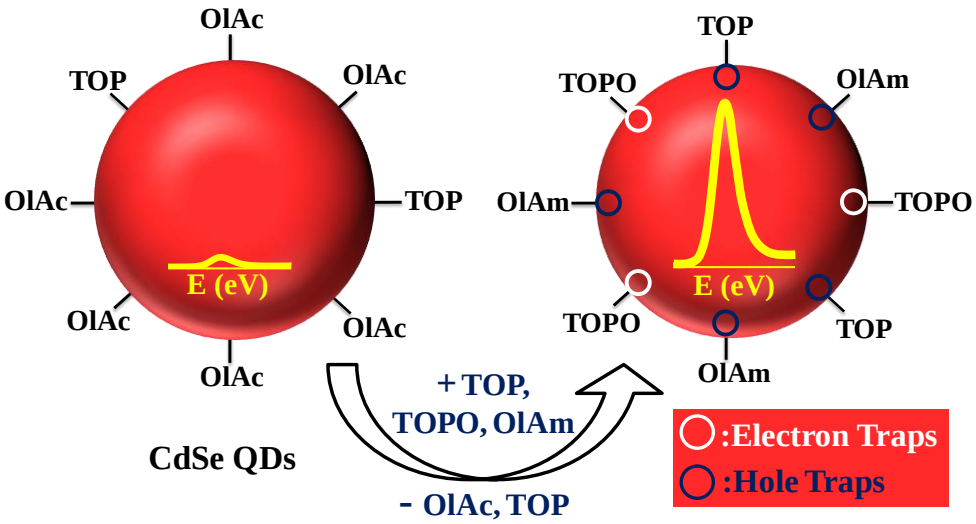

The following papers have been published based on work presented here:
G Krishnamurthy Grandhi, R. Tomar and R. Viswanatha. Study of Surface and Bulk Electronic Structure of II-VI Semiconductor Nanocrystals Using Cu as a Nanosensor. *ACS Nano* **2012,** *6*, 9751.

G Krishnamurthy Grandhi and R. Viswanatha. Tunable Infrared Phosphors Using Cu Doping in Semiconductor Nanocrystals: Surface Electronic Structure Evaluation. *J. Phys. Chem. Lett.* **2013**, *4*, 409.

G Krishnamurthy Grandhi, Arunkumar M. and R. Viswanatha. Understanding the Role of Surface Capping Ligands in Passivating the Quantum Dots Using Copper Dopants as Internal Sensor. *J. Phys. Chem. C* **2016**, *120*, 19785.

6.1. Abstract:

Surface electronic structure of II-VI semiconductor QDs have been studied using quantitative measurements of PL QY and PL decay studies of the Cu related emission and the excitonic emission. We study the role of commonly used ligands such as TOP, TOP, oleic acid, DDT, MPA, primary amines in passivating II-VI semiconductor QDs. The role of ligands was studied during the synthesis, as well as during specific phase transfer and pyridine exchange based ligand exchange procedures. This study was utilized to plan a synthesis of highly emitting CdSe QDs leading to a substantial increase in the PL QY.

6.2. Introduction:

Colloidal QDs are well known for their applications in diverse fields.[1-5] One of the key factors responsible for colloidal stability of the QDs is the presence of surface capping agents. Surface ligands are known to play a pivotal role in the synthesis of QDs and in altering their properties like growth rate, shape, size, electron transfer reactions and crystal structure.[6-11] More importantly, surface ligands are known to effect QD properties like PL as well as electrical conductivity. For example, Talapin *et al.* have shown that PL efficiencies can be varied from 15% to 40% in CdSe QDs by modifying surface passivation with alkylamine, TOP, TOPO ligands attached to the QDs.[12] Similarly, in recent times, it was shown that the presence of all inorganic ligands increased the electrical conductivity of QD solutions.[13] Hence the appropriate choice of the ligand has a crucial role to play for the efficiency of the particular application using QDs. However, in spite of its importance, the mechanism of passivation for various ligands is largely in the realm of trial and error. Though the final effect of different ligands on the PL properties of QDs have been extensively studied in literature[14], the molecular processes involved have not been understood. Ligand exchange with original ligands have been carried out[15, 16] in spite of incomplete or limited exchange or by the synthesis of QDs with and without ligands. For example, it has been observed that the primary amines like hexadecylamine,[12] decylamine, hexylamine and butylamine[17] enhance the PL efficiency in smaller CdSe QDs (size ~ 3 nm) in most cases but at the same time butylamine is shown to quench the PL efficiency in CdSe QDs (size ~ 3 nm) in a few reports.[18, 19] On the other hand, thiol is universally known to be a PL quencher both in organic and aqueous phases. It has also been recognized as being responsible for creating hole traps in CdSe QDs.[20, 21]

Mulvaney *et al.* have studied the effect of a series of ligands on the PL of CdSe QDs wherein the ligands like alkylamine, TOP, TPP and TOPO affect the PL efficiency.[17] Recently, it has also been shown that TOPO increases both the PL intensity and average lifetime when bound to CdSe QD surface.[22] Munro *et al.*[15] have shown that the nature of the ligand passivation can also vary with the concentration wherein butylamine increases PL intensity at lower concentration while quenches the same at higher concentration of ligands. Surprisingly, excess reagents were also shown to passivate the surface of ZnO QDs. Viswanatha *et al.*[23] have shown that Na^+ ions being attracted by the hydroxyl ions on the surface of ZnO QDs form the virtual capping layer. In summary, various papers have studied the effect of different ligands on properties such as PL efficiency, radiative lifetime, size of the QD and the like. However, much effort has not been invested in understanding the mechanism of these properties from fundamental view point. For instance, it is not evident from these studies if a particular ligand creates electron traps and/or passivates hole traps. Unless this systematic study has been carried out, the synthesis of efficient QDs becomes an art of chemical intuition.

While the position of the Cu related emission can be used to determine the shift in the CB as shown in **Chapter 3**, it is fascinating to note that the QY and the lifetime dynamics of the Cu related emission can be effectively used as a direct probe to study the surface electronic structure of the QDs. Consequently, with an intention of accomplishing this, we initially try to understand the mechanism of PL decay of the Cu related emission in doped QDs. In order to elucidate the actual mechanism of emission from CB to the Cu *d* level, it is important to determine the oxidation state of Cu. While some early papers attribute the intra-gap luminescence to the Cu^{1+} state [24] and the reminiscent BE emission to the fraction of undoped dots, recent results have proved otherwise.[25] Using magnetic circular dichroism, Klimov *et al.*[25] have shown that Cu is indeed in the 2+ oxidation state and hence acts as a permanent optical hole. This implies that Cu emission can be activated in the absence of photo-generated hole (Figure 6.1). Nevertheless, since this emission is known to be several orders of magnitude slower than the BE transition, the emission would be dominated by the BE transition[25] (Figure 6.1), if the photo-generated holes are not lost by some mechanism like for example, the surface hole traps. Therefore, intensity ratio of emission and the lifetime decay studies of Cu emission give important information regarding the presence of surface electron and hole traps and can

be used to study the surface electronic structure of the QD, thus contributing to our understanding of the role of various ligands in passivating the QD surface.

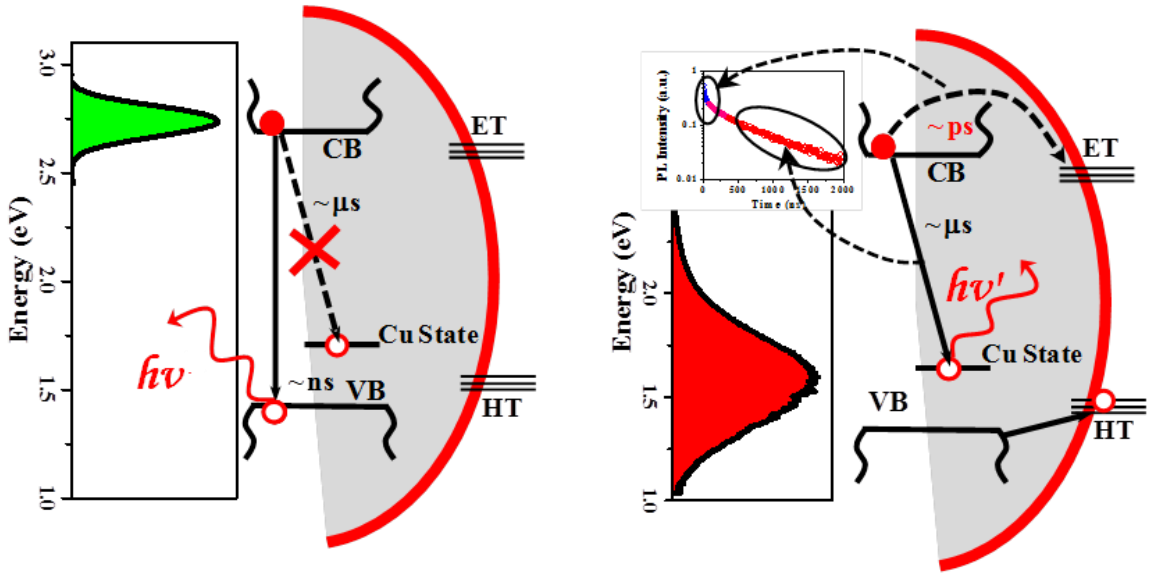

Figure 6.1. *Schematic showing the various pathways of radiative and non-radiative recombination.*

In this chapter, we have used CdSe QDs as a model system to study the electronic structure since it has been one of the most widely synthesized QDs in literature with narrow size distributions and excellent optical stability. However, doping CdSe with various dopants including Cu have been tried by different groups and has been classified as undopable[26] based on the absence of Cu emission peak in the optical spectrum, with reasons being attributed to intrinsic self-purification to fundamental thermodynamic or kinetically controlled processes such as the crystal structure.[26-28] In this chapter, we demonstrate that presence or absence of PL emission attributed to Cu states does not determine the efficacy of doping in QDs. For example, in this specific case of CdSe, we illustrate that it is possible to obtain the emission from the CB to the copper *d* state by systematically varying the ligands to alter the surface of the QDs. A logical route to the synthesis and characterization of Cu doped CdSe with a prominent emission from CB to the Cu *d* level has been established by systematically varying the surface ligands. We first studied the role of TOP and oleic acid ligands which are added during the QD synthesis. We have extended this study to other II-VI semiconductor QDs such as CdS and CdTe QDs. In the later section, we studied the complete role of various ligands

such as thiols, TOPO, primary amines through the phase transfer and ligand exchange processes.

6.3. Experimental section:

6.3.1. Materials:

CdO, oleic acid (90%), ODE (90%), DDT (98 %), MPA (99%), TOP (90%), TOPO, 99%, butylamine (99.5 %), hexylamine (99 %), octylamine, oleylamine (70 %), and Se pellets were obtained from Sigma-Aldrich. Pyridine (AR) was obtained from Rankem. $CDCl_3$ and DMSO (DMSO-*d*6, 0.03 % TMS) were purchased from Euriso-top. Chloroform (AR), hexane (AR), methanol (AR) and acetone (AR) were obtained from Merck. TPP was purchased from SD Fine chemicals. Stearic acid, copper (II) acetate monohydrate and TMAH (98%) were obtained from Spectrochem. All purchased chemicals were used without further purification.

Cadmium oleate was prepared by heating a mixture of 0.32 g CdO, 2.68 g oleic acid and 9 mL of ODE to a higher temperature (~ 200 ^{o}C) in the Ar atmosphere till the solution becomes clear. 1 M TOPSe was prepared by overnight stirring of 0.79 g Se pellets in 10 mL TOP in Ar atmosphere. Copper stearate was synthesized and purified similar to the literature reports published previously.[29]

CdSe QDs were synthesized using two different techniques to study the effect of surface passivation. For both these methods, cadmium oleate was synthesized using modified literature methods. Briefly, CdO, oleic acid and ODE (4.5 mL) were degassed in vacuum and backfilled with Ar and heated to a high temperature in argon atmosphere till the solution turns colourless. To study the surface effects, cadmium oleate with different molarities were prepared by varying the weight ratios of CdO to oleic acid (1: 2.5 – 1: 5). 2 M TOPSe solution was prepared by dissolving appropriate amount of Se in TOP in a glove box. It was then further diluted with TOP to obtain different molarities (1.2 M – 0.33 M) of the solution

6.3.2. Standard synthesis of CdSe QDs:

It was carried out by degassing ODE (5 mL), octadecylamine (1.5 g) and TOPO (650 mg) in a three-necked flask in vacuum and backfilling with Ar. To this solution, 1mL of 0.1 M cadmium

oleate was injected at 100 ˚C in argon atmosphere followed by addition of 1.5 mL TOPSe (1M) at 210 ˚C. This solution was heated at 210˚C for a minute and then cooled to 140 ˚C in order to avoid the further growth of QDs. To this solution, 50 μmol copper stearate solution in 2 mL of ODE was added to the reaction mixture and annealed for 20 minutes to obtain Cu doped QDs. In the undoped case, instead of the copper stearate solution of ODE, only ODE was added as blank and was annealed for similar length of time. Samples were washed with hexane methanol mixture and precipitated using ethanol.

6.3.3. Low ligand method:

Appropriate solution of cadmium oleate and ODE were degassed in a three-necked flask and heated to 180˚C. TOPSe (0.47 mmol – 1.68 mmol TOP/ 0.0197 g Se) was injected at 180 ˚C in Ar atmosphere and annealed for a minute to form CdSe QDs. The reaction was cooled down to 140 ˚C and copper stearate solution of different molarities was added drop wise and annealed for 20 minutes. Samples were washed with hexane methanol mixture and precipitated using ethanol. To obtain the bigger sizes, reaction mixture was heated to higher temperature after 20 minutes with additional injection of cadmium oleate precursor.

6.3.4. Synthesis of CdS and Cu doped CdS QDs:

CdS and Cu doped CdS QDs were synthesized by degassing a mixture of CdO (0.2 mmol), oleic acid (0.6-2.0 mmol) and ODE in a three-necked flask in vacuum and back-filling with Ar. To this solution, 0.1 mL of TOP was injected at 80 °C in an Ar atmosphere followed by the injection of 0.5 mL of 0.2 M S in ODE solution at 300 °C. This solution was immediately cooled down to 150 °C to avoid the further growth of CdS QDs. To this solution, 8 μmoles of copper stearate solution of ODE (1 mL) was added, and the reaction mixture was annealed for several hours to obtain the Cu doped CdS QDs. Samples were washed with a hexane/methanol mixture and precipitated using acetone.

6.3.5. Ligand exchange in organic media:

This is a modified procedure to that of reported by Ji *et al.*[30] For the pyridine exchange, the purified original CdSe QDs were first sonicated with 5-6 mL of pyridine for 10 min and then

precipitated by adding excess of ODE. Here, ODE acts as non-solvent which helps in precipitating the QDs. This leads to partial exchange of the original ligands with pyridine ligands. Further for the exchange into ligands of interest, these QDs were again sonicated with 3 mL of pyridine for 5 min and then precipitated with the addition of excess of hexane to give pyridine capped CdSe QDs. For the exchange of new ligands (amines, TOP and thiols), these pyridine capped CdSe QDs were treated with the 5-6 mL of new ligands and sonicated for 10 minutes and then precipitated with the excess of acetone. This procedure was repeated twice to ensure ligand exchange. The exchange of ligands in each step was monitored by NMR spectroscopy. It is important to note that methanol/acetone mixture wasused only during the washing of original QDs. It is possible that use of these solvents can strip off the existing ligands leading to lower coverage of ligands and hence increasing the trap states. In order to avoid such errors, we have only used acetone (polar aprotic solvent) for washing the QDs after ligand exchange to avoid formation of any additional dangling bonds.[31, 32]

6.3.6. Ligand exchange from organic to aqueous phase:

The purified original CdSe QDs were taken in 3 mL of chloroform (organic phase) and excess MPA ligands (pK_a = 10.8) were taken in buffer solution (aqueous phase) of pH = 11.0 to form two immiscible phases. These two phases are stirred rapidly for ~ 5 min till CdSe QDs will transfer from organic phase to the aqueous phase.

6.4. Results and discussion:

6.4.1. Role of ligands added during the QD synthesis:

Cu doped CdSe QDs synthesized using standard technique using TOP, TOPO, oleic acid and octadecylamine as ligands, synthesis being discussed as the “standard technique” in the experimental section, showed no incorporation of Cu in CdSe as determined by the absence of the red shifted PL peak as well as ICP-OES data. The XRD data (Figure 6.2) shows that the QD crystallizes at least partially in the wurtzite structure. Further studies into these QDs indicated that the BE QY of these samples were found to be quite high (~ 6-10%) and should have been well passivated. In the light of earlier investigations in the case of Cu doped in ZnSe/CdSe system,[25] it has been shown that the CB to Cu *d* level emission is several orders

of magnitude slower compared to the BE emission and hence requires a surface hole trap to remove the photo-generated hole thus creating a pathway for the Cu related emission. Consequently, in order to observe the red-shifted PL emission, it is necessary to increase the hole traps during the synthesis of the QDs. This can be achieved by studying the chemistry of the ligand molecules.

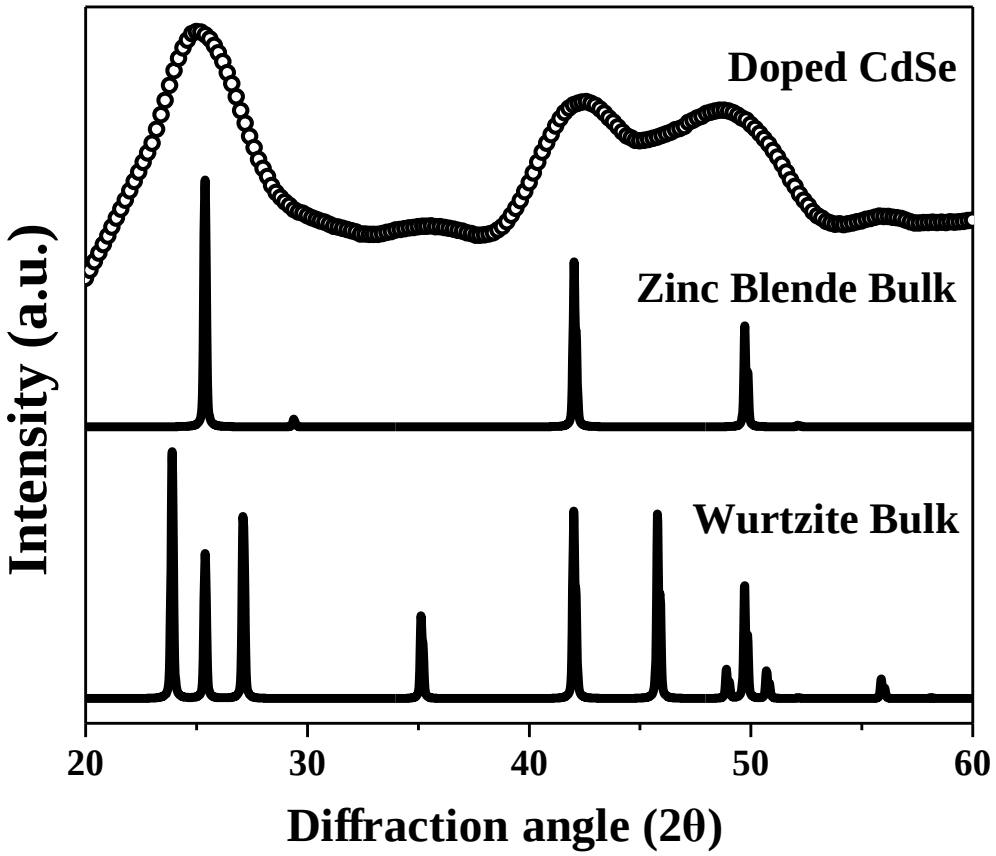

Figure 6.2. *XRD of Cu doped CdSe synthesized using TOPO and octadecylamine along with TOP and oleic acid. Also, shown in the figure are the bulk XRD patterns of zinc blende and wurtzite CdSe.*

In order to isolate functions of the various ligands, we have restricted the ligands to only TOP and oleic acid though it is known to give a low PL QY and the synthesis method is discussed under the heading of 'low ligand method' in the Experimental section. In this case, the Cu emission is observed and the characterization of these samples was already discussed in **Chapter 3**. TOP has P atom with a lone pair of electrons giving rise to some extra electron

density on the P atom. This electron density, in principle should be capable of passivating the hole in the VB of the QD if its absolute energy level is above the VB of the QD.

In order to obtain more insight into the nature of the surface of the QD for any given size of the QD and hence the function of ligand molecules in passivating the surface, we varied each of the ligands systematically and studied the QY of the BE emission and the Cu related emission as well as the lifetime dynamics of these two spectral features as shown in Figure 6.3. Traditional wisdom suggests that the presence of larger amount of Cu within the QD increases the QY of the Cu related emission. With the intention of verifying this we measured the QY of the Cu related emission for varying amounts of Cu added stoichiometrically and is shown in the main panel of Figure 6.3(a). The maximum amount of 0.25% of Cu to Cd ratio was a direct result of the onset of precipitation. Surprisingly, contrary to the expectations, the QY of the Cu related emission decreases drastically with increasing stoichiometric percentage of Cu. However, it is also known in literature that the entire amount of Cu injected is rarely incorporated into the lattice. Hence, we performed ICP-OES measurements to determine the actual amount of Cu incorporated within the QD after washing the samples several times to remove the Cu ions that are not intercalated within the lattice of the QD and are shown in the inset to Figure 6.3(a). These data show that, though the amount of Cu intercalated into the system is much lower than the stoichiometric concentration, not surprisingly the actual concentration increases with increasing stoichiometric concentration. This suggests that the QY of the Cu related emission is not solely determined by the amount of Cu present within the QD but also based on surface electronic structure of the host QD. In order to have better understanding of the role of surface on the Cu related emission, for the rest of the studies described in this chapter, we have used a constant Cu to Cd ratio of 0.25%. Figure 6.3(b) shows the area normalized PL spectra obtained using the same Cu concentration with changing TOP amounts during the formation of CdSe. From the figure, it is clear that the ratio of band edge to Cu related emission peak varies drastically as a function of TOP concentration. The amount of Cu present in these samples giving rise to such widely varying intensities of the Cu related emission as obtained using ICP-OES was found to be similar within the experimental error. In order to get a more accurate quantitative estimate of the PL emission, we calculated the absolute QY of the BE emission and the Cu related emission that is plotted for two different concentrations of oleic acid in Figure 6.3(c) along with QY of the undoped species obtained

using similar reaction conditions. By studying the variation of QY of the BE emission in the doped and undoped sample as seen in the Figure 6.3(c), it is evident that the QY of the BE emission in the doped sample is similar to that of the undoped sample. However, in the case of doped sample synthesized using 3 mmol of oleic acid, in addition to the ~3% QY of the BE emission, there exists another brighter peak related to Cu emission with QY decreasing monotonically from ~30% to ~10% with increasing TOP concentration. This is a clear indication of decrease in the number of surface hole traps with increasing TOP concentration and hence suggesting that TOP mainly acts as a hole passivating agent. It is important to note that the Cu related emission does not arise at the cost of the BE emission but rather happens independently. This further corroborates the theory that the Cu emission can only be seen in presence of surface hole traps whereas BE emission would be absent in presence of either surface hole or electron traps. However, in the case of 4.5 mmol of oleic acid, we observe that the QY of the Cu related emission is non- monotonic suggesting the interaction of oleic acid with the TOP molecules in creating surface electron and hole traps. In presence of large amount of oleic acid and a small amount of TOP, TOP also acts as an electron trap creator and hence the QY of both the Cu related emission and the BE emission decreases in presence of low TOP and high oleic acid concentration.

While the study of QY of the Cu related emission provides us with information on the surface hole traps, study of the fast component of the PL lifetime of the Cu related emission should be an ideal tool to study the surface electron traps since Cu related emission occurs without the involvement of the photo-generated hole. Typical decay plots of Cu related emission for varying concentrations of TOP are shown in Figure 6.4(a). The percentage of the fast multi-exponential component while analyzing PL decay kinetics of the Cu related emission approximated as a biexponential fitting function is shown in the inset to Figure 6.3(c) and illustrates a monotonic increase with increasing TOP concentration for high oleic acid concentration while it is almost constant for low oleic acid concentration. The increase in the fast component implies an increase in the surface electron traps while proving that TOP not only acts as a hole passivating agent but is also a mild creator of electron traps, especially in presence of other hole passivating agents like oleic acid. However, when low oleic acid concentration is used, the effect on the electron traps is minimal in agreement with the QY data.

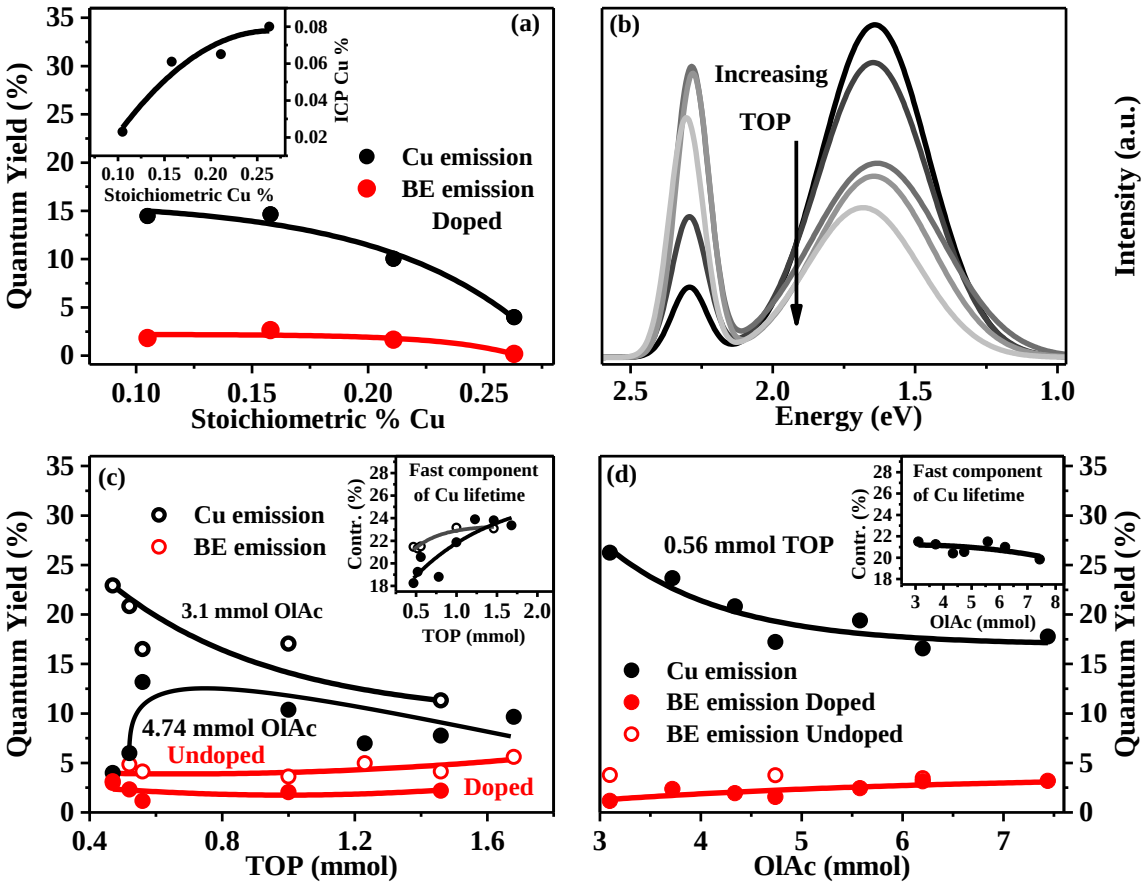

***Figure 6.3**. **(a)** Variation of QY with increasing Cu content in the QDs. The inset shows the actual Cu/Cd ratio as a function of stoichiometric Cu added during the synthesis. **(b)** Typical PL spectra of Cu doped CdSe QDs with similar Cu content but synthesized with different TOP concentrations. Variation of the QY of the Cu related emission and BE emission for both doped and undoped species as a function of **(c)** TOP concentration for two different concentrations of oleic acid and **(d)** oleic acid concentration for a given TOP concentration. The insets show the variation of the percentage of the fast components of the lifetime of the Cu peak with varying TOP concentration and oleic acid concentration.*

This in turn leads us to the question of the role of oleic acid in the passivation surface traps and hence a similar analysis was carried out for a given TOP concentration with varying oleic acid concentrations and the results are summarized in Figure 6.3(d). From the figure, it can be seen that the QY of the BE emission of the doped and undoped species are similar showing almost no change with changing oleic acid concentrations that indicates that either the electron and hole traps are not simultaneously being passivated by oleic acid. Study of Cu related emission however shows a strong monotonic decrease in QY suggesting that oleic acid is indeed passivating the hole traps while possibly being insensitive to electron traps. This is

further corroborated by looking at the lifetime decay data in Figure 6.4(b) and the fast component of the PL decay kinetics of the Cu related emission shown in the inset to Figure 6.3(d). Since oleic acid has no effect on the electron traps, we observe that the percentage of the fast component remains unchanged with increasing oleic acid concentration.

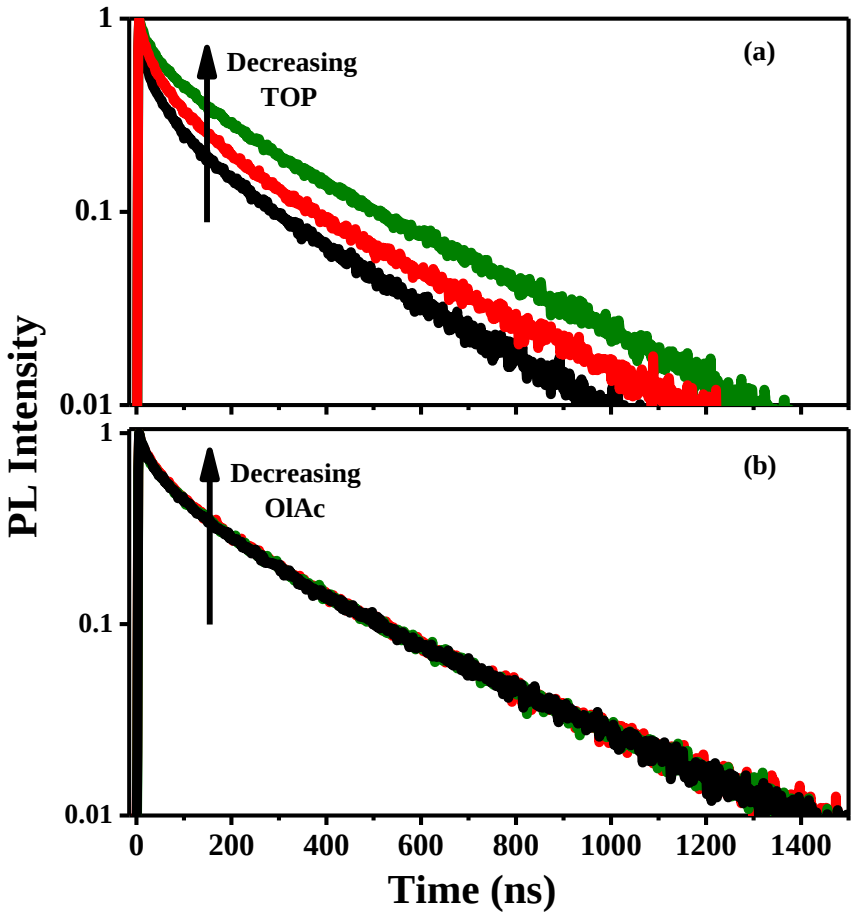

Figure 6.4. *PL decay curves for the decay of the Cu related emission with* ***(a)*** *varying TOP concentration and* ***(b)*** *varying oleic acid concentration. OlAc=oleic acid.*

In the backdrop of these studies, it is easy to understand the surprising results obtained in Figure 6.3(a). Decreasing QY of the Cu related emission with increasing Cu concentration suggests that Cu precursors are possibly acting as hole passivating agents. Given that stearic acid is used during the synthesis of copper stearate, it can be expected that in spite of multiple washings, some trace amounts of stearic acid continues to be present in copper stearate. Since increasing the concentration of Cu is achieved by increasing the amount of copper stearate injected, amount of stearic acid injected into the reaction mixture increases. As has been

observed in the case of oleic acid, increasing presence of acids act as good hole passivators for the CdSe QDs and hence the decrease in the QY of the Cu emission.

Thus, from these studies it is evident that it is possible to study the passivation of the electron and hole traps using the Cu related emission as an internal probe. Nevertheless, this technique is not limited to these ligands or the host materials and can easily be extended in presence of other ligands/hosts as well. The synthesis of all the chalcogenides was carried out in presence of both TOP and oleic acid as ligands even though high-quality CdS and CdTe QDs, unlike in the case of CdSe QDs, can be prepared in the absence of TOP as well since it is not necessary to dissolve the S/Te precursor. However, we observe that the Cu related emission in CdS is completely absent under similar synthesis conditions in the absence of TOP (Figure 6.5). This behavior is in fact similar to the case of Cu doped CdSe QDs where it was shown that small amount of TOP is indeed necessary to observe the Cu related emission in CdSe QDs. On the other hand, we also observe that the presence of high TOP concentration quenches the Cu related emission due to the passivation of the hole traps. Hence it was necessary to use optimal concentration of TOP to obtain the Cu related emission.

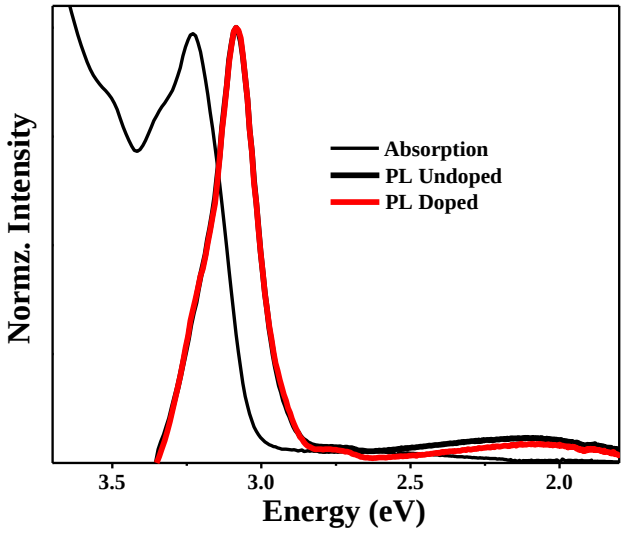

Figure 6.5. *Absorption and PL Spectra of undoped and Cu doped CdS QDs synthesized without the use of TOP.*

In case of Cu doped CdSe, the presence of oleic acid was found to purely passivate hole trap states and not the electron trap states. Since S, Se and Te belong to same group of the

periodic table one would expect similar reactivities and hence similar roles for the ligand molecules. However, the surface of the QDs is notoriously known to be quite diverse due to the numerous factors involved in determining the surface passivation using ligands like oleic acid. For example, some of the contributing factors include the redox levels of the oleic acid and/or the dissociation constant of oleic acid in different solutions and solubility of the precursors in presence of ligands. Hence, we studied the effect of oleic acid on the lifetime dynamics and the QY of the Cu related emission in various semiconductors and the results are compiled in the different panels in Figure 6.6.

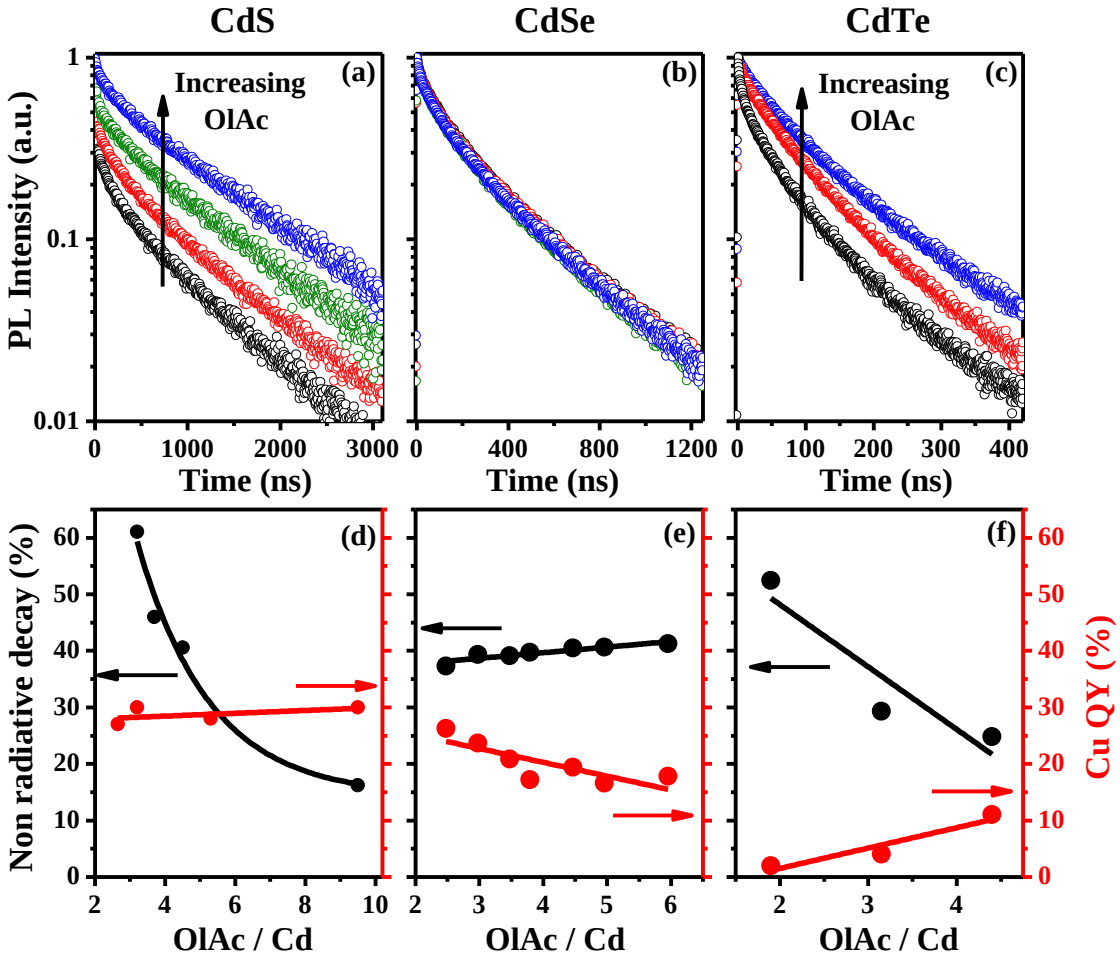

Figure 6.6. *Lifetime dynamics of Cu doped* ***(a)*** *CdS,* ***(b)*** *CdSe and* ***(c)*** *CdTe QDs collected at the Cu related emission energy shown as function of increasing oleic acid concentration. The ratio of the fast component (black) as well as the absolute quantum yield (red) of Cu related emission as a function of oleic acid concentration is shown for the case of* ***(d)*** *CdS,* ***(e)*** *CdSe and* ***(f)*** *CdTe QDs. OlAc=oleic acid.*

From Figures 6.6(a), 6.6(b) and 6.6(c), it is evident that while the fast component decreases with increasing oleic acid concentration in the case of CdS and CdTe QDs, the fast

component of CdSe QDs seems to be independent of the concentration of the oleic acid. In order to quantify this data, it is important to note that the pre-factor and exponential are correlated in a bi-exponential fit.[33] Hence we fit a limited range single exponential long lifetime component using least squared error fitting procedure. This lifetime is then fixed to obtain a bi-exponential fit to the entire data. The ratio of the fast component thus obtained is plotted in Figures 6.6(d), 6.6(e) and 6.6(f) for CdS, CdSe and CdTe respectively. From these plots in Figure 6.6, it is evident that while oleic acid does not affect the surface electron traps in CdSe QDs, it can be clearly seen to passivate these trap states in CdTe and CdS QDs.

A simple extension of these results suggests that the QY of the Cu related emission in CdS and CdTe QDs should go up with increasing oleic acid concentration due to the decrease in non-radiative component. The measurement of QY of these materials also shown in red in Figures 6.6(d)-6.6(f) show that the QY of Cu related emission in CdS QDs is unaffected with changing oleic acid while it decreases in CdSe QDs and increases in CdTe QDs. The increase in the QY in CdTe QDs, both for the band edge emission as well as Cu related emission can easily be understood from the loss of non-radiative decay as observed from the lifetime dynamics. It is also rather straight forward to understand the decay of the QY of the Cu related emission in CdSe QDs as arising due to decrease in the hole trap states on the surface of the QD and hence decreasing the yield of this emission. However, the relative constancy of the QY of the Cu related emission in CdS QDs may look quite counter-intuitive at first glance. Nevertheless, it is important to take note that Cu related emission appears not only due to decrease in the non-radiative trap states but also the presence of hole traps within the QD. In fact, the data suggests that the oleic acid assists in both decreasing the electron traps as well as decreasing the hole traps within the QD such that the QY of the Cu emission remains constant when it is perfect "balanced" as is seen in our case. However, the "balanced" passivation of electron and hole traps is only in terms of balance of Cu related PL QY and not the actual number of electron and hole traps passivated. This number depends on various parameters like area of cross-section, the density of states of the electron and hole traps and the radiative and non-radiative channels available for decay. Hence, we cannot directly correlate the increase in band edge emission to the decrease in the Cu related emission. Nevertheless, we do observe an increase in the band edge emission and hence the total QY.

6.4.2. Role of ligands during phase transfer and ligand exchange:

It is evident that a systematic study of the various ligand molecules suggest that they perform different roles in different host materials. For example, oleic acid is observed to act as an electron and hole trap passivator in CdS QDs, while it is only a hole trap passivator in CdSe QDs and an electron trap passivator in CdTe QDs. Additionally, the presence of other capping agents can also modify the role of given ligand as observed in case of CdSe QDs. Hence it is absolutely imperative to study the ligand in the presence of other ligands that is expected to be present in and around the QD. This can be achieved by separating the synthesis and ligand kinetics by first synthesizing the QDs and then followed by a ligand exchange by replacing them with ligands of interest either in the organic medium[30, 34, 35] or in the aqueous medium.[36-38] Ligand bonding onto the QD surface can be probed by infrared spectroscopy[39] and NMR spectroscopy.[40-42] However, NMR spectroscopy has been recognized as the most powerful technique for studying ligand exchange process because of its unique features of probing all the protons (or other atoms) and broadening of NMR peaks when the ligands are attached to the QD surface. In this section, we performed the ligand exchange[30] on Cu doped QDs through an intermediate pyridine exchange step as elucidated in Figure 6.7 .The combined study of NMR spectroscopy and PL spectroscopy of Cu doped QDs in each step of ligand exchange has been used to obtain a complete picture on the kind of passivation induced by the ligands. The roles of commonly used ligands like oleylamine, TOP, TOPO and thiols in passivating the CdSe QD surface are examined. The generality of this procedure was elucidated by extending it to the case of CdS QDs.

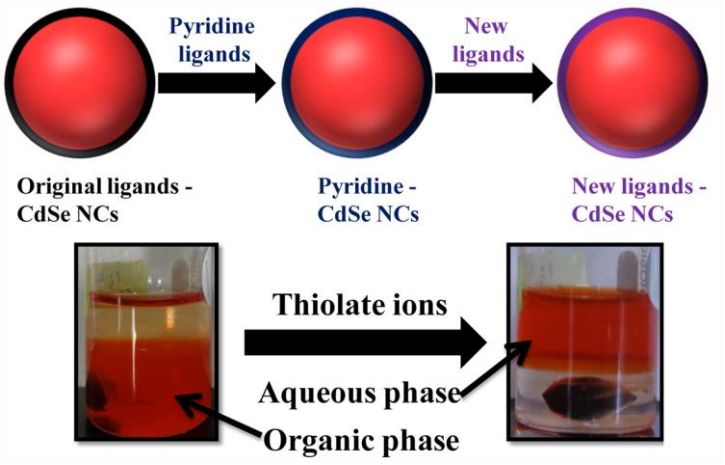

Figure 6.7. (a) *Ligand exchange within the organic medium in two steps and* ***(b)*** *phase transfer of QDs from organic medium to aqueous medium.*

6.4.2.1. Role of Thiol capping in CdSe QDs: Thiols are shown to be dominant luminescence quenchers in CdSe QDs in literature, both in organic and aqueous media. [20] However, the luminescence loss mechanism is not clearly understood. Some reports [21] predict the creation of hole traps as a probable reason for the loss of PL. Hence, an independent study of the role of DDT was carried out here in order to prove the validity of our approach.

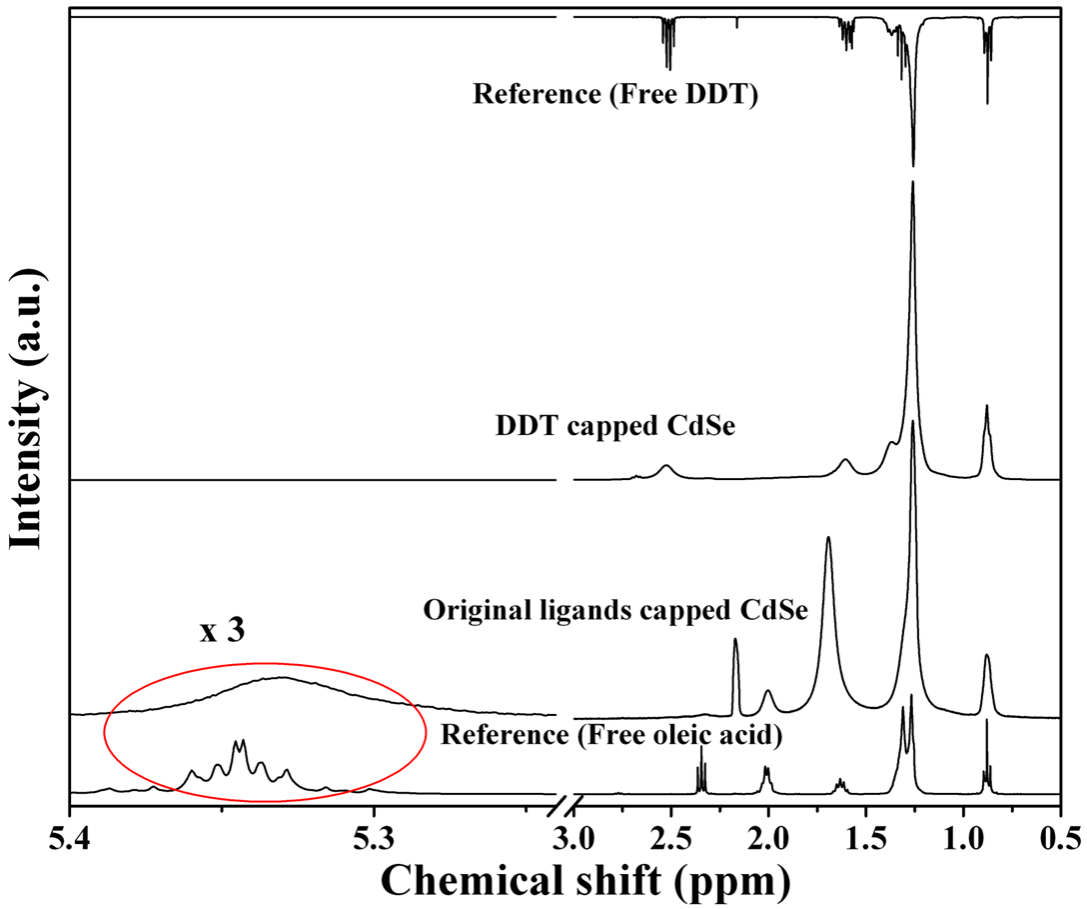

Figure 6.8. *^{1}H NMR spectra of the CdSe QDs in $CDCl_3$ before and after the ligand exchange with DDT ligands along with the free ligands as the reference.*

DDT was ligand exchanged through the pyridine intermediate while the MPA exchange was achieved by phase transfer method. NMR spectroscopy was used to probe the ligand exchange on the surface of the QDs. Figure 6.8 shows typical NMR spectra of a CdSe QDs before and after the ligand exchange where the original ligands i.e., oleic acid was replaced with the new thiol ligands. The NMR spectrum of intermediate pyridine ligands is shown in Figure 6.9. The broadening of the NMR peaks in case of ligands bound to the surface of the

QDs is a well-studied phenomena.[30, 43] The faster spin relaxation due to dipolar interaction, distribution of chemical shifts and the faster spin-spin relaxation (T2) due to slow tumbling of the particles in the solution leads to the broadening of NMR peaks in case of QD bound ligands.[44] In the present case, this broadening of the NMR peaks compared to the free ligands has been used as an indicator of surface binding. The 0.5-2.5 ppm region in the NMR spectrum of oleic acid capped CdSe QDs indicates region of $–CH_2$ and $–CH_3$ of oleic acid while the resonance at 5.35 ppm corresponds to double bond –CH protons. After exchange with DDT (with saturated carbon chain) the resonance at 5.35 ppm is absent as shown in Figure 6.8. This clearly shows the replacement of original ligands. Using these tools, we are now equipped to study the role of ligands in the passivation of the QD surface during the two-step ligand exchange using this Cu emission as an internal probe.

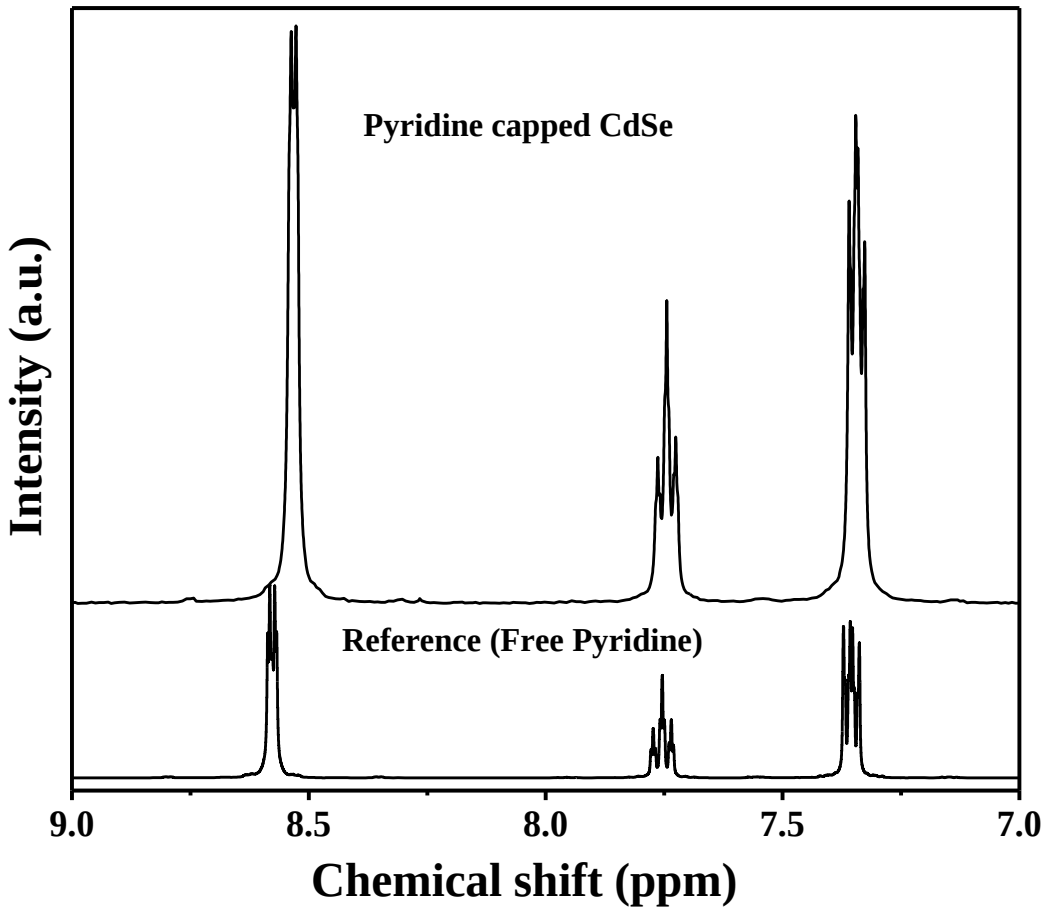

Figure 6.9. *The NMR spectra of free pyridine ligands and pyridine capped CdSe QDs in DMSO-d6.*

Figure 6.10(a) shows the PL of CdSe QDs before and after the ligand exchange to DDT ligands. As expected, the PL of CdSe QDs is quenched by the DDT ligands when compared to that of original ligands. Figure 6.10(b) shows the TRPL spectra of CdSe QDs before and after ligand exchange. The TRPL of DDT capped CdSe (CdSe-DDT) at the band edge is completely dominated by a new fast component while the component due to band edge which exists in case of original CdSe is completely absent. This can be attributed to formation of new trap states induced by DDT molecules on the QD surface. Cu doping into QDs will help in studying the nature of trap states induced by DDT ligands. Figure 6.10(c) shows the steady state PL spectra of Cu doped CdSe QDs before and after the ligand exchange with DDT. It can be observed that in the case of Cu doped CdSe-DDT QDs, the BE emission almost completely disappears as in the case of undoped CdSe QDs suggesting that the photoexcited hole is not present for radiative recombination with the photo excited electron. However, the Cu emission is quite strong, indicating a radiative recombination of the photoexcited electron with the Cu *d*-state in spite of a much longer lifetime (~ 300 ns) for this recombination as shown in Figure 6.10(d). This implies that DDT is responsible for mainly creating hole traps on the surface of CdSe QDs that is scavenging the photoexcited hole. This is consistent with the studies reported in literature[21, 42] and hence proves the reliability of this method. Additionally, it was observed that there was a slight increase in the percentage of the fast component in the TRPL after the replacement of the original ligands with DDT suggesting an increase in the number of electron trap states.

Similarly, we observed that MPA, another thiol ligand largely creates hole trap states on CdSe QD surface as observed by the steady state PL along with a slight increase in the fast component in the TRPL decay curves as observed from the insets of Figure 6.10(c) and Figure 6.10(d) respectively. This is understandable as MPA also attaches to the QD surface with its thiol group while the –COOH group is responsible for its increased aqueous solubility. From these observations, we can conclude that the thiol ligands irrespective of the other functional groups mostly create hole trap states on CdSe QD surface, similar to observations in literature.[21, 42] However, the advantage of this method is the generic nature of the method allowing one to extend it to any ligand or any QD of interest. We have now studied the effect of other ligands on CdSe QDs using similar methods, discussed in subsequent sections.

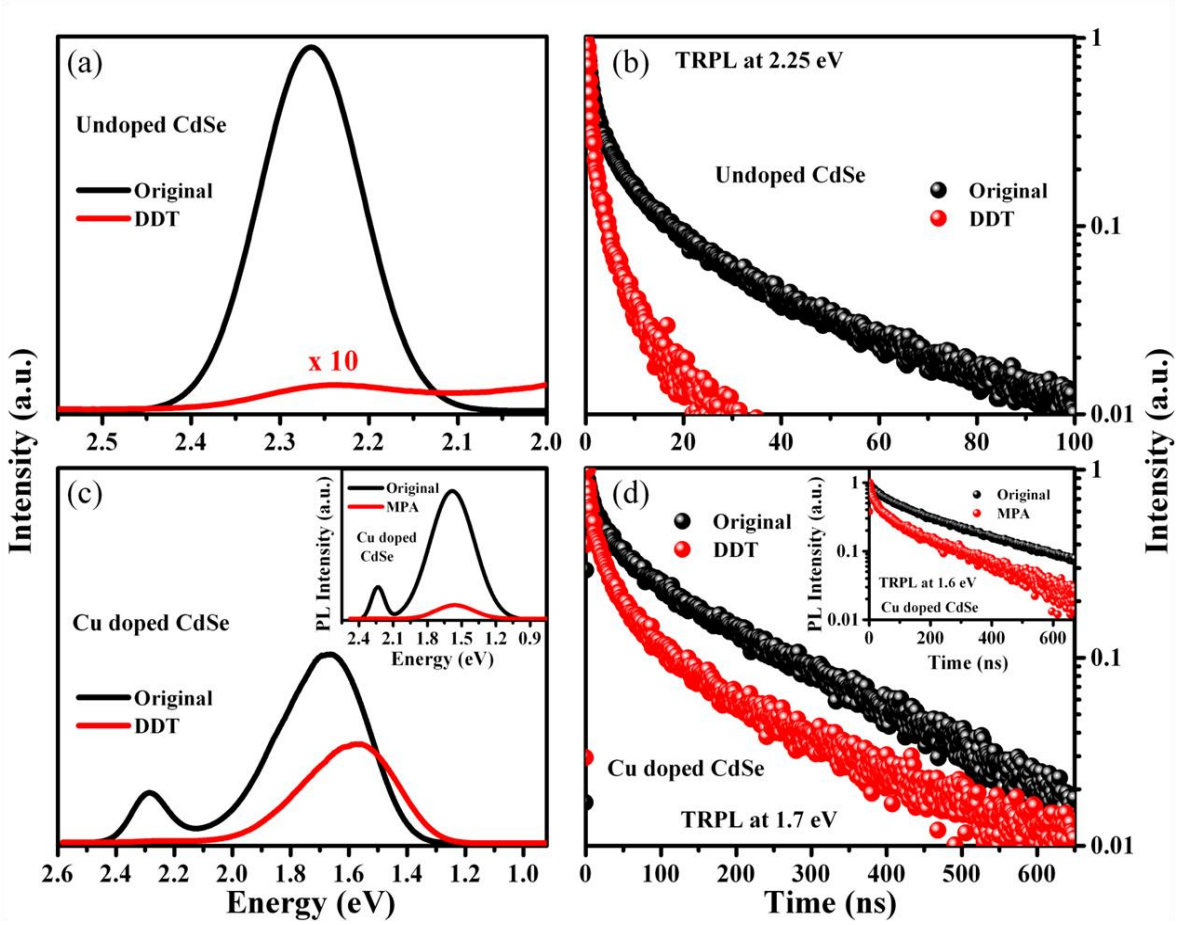

Figure 6.10. *Ligand exchange with DDT and MPA.* ***(a)*** *Steady state PL spectra of Undoped CdSe QDs before and after the ligand exchange* ***(b)*** *and the corresponding TRPL spectra with* λ_{em} *= 2.25 eV.* ***(c)*** *Steady state PL spectra of Cu doped CdSe QDs before and after the ligand exchange (d) and the corresponding TRPL spectra with* λ_{em} *= 1.7 eV. All the spectra were measured in hexane. Insets of (c) and* ***(d)*** *show the PL and TRPL spectra (*λ_{em} *= 1.6 eV) of Cu doped CdSe QDs before (*$CHCl_3$ *as solvent) and after ligand exchange (*H_2O *as solvent) with MPA respectively. Excitation wavelength,* λ_{ex} *= 405 nm (3.06 eV) for all the PL and TRPL spectra.*

6.4.2.2. Role of amine capping in CdSe QDs: Organic amines are considered as one of the most widely used capping ligands in synthesizing various QDs[45-48] and in making core-shell QDs.[49] Keeping in mind the importance of amines as capping agents in the synthesis of QDs, we elucidate below the role of primary amines of different chain lengths (C_4, C_6, C_8 and C_{18}) using Cu doping strategy in CdSe QDs.

Here, we have studied the effect of four amines, namely, butylamine, hexylamine, octylamine and oleylamine. Figure 6.11 shows the NMR spectra of CdSe QDs in $CDCl_3$ after the ligand

exchange with amine ligands. For the ease of comparison, we have also shown the typical NMR spectrum of oleylamine, octylamine and the original ligands, oleic acid. NMR data reveals that ligand exchange achieved through the ligand exchange process.

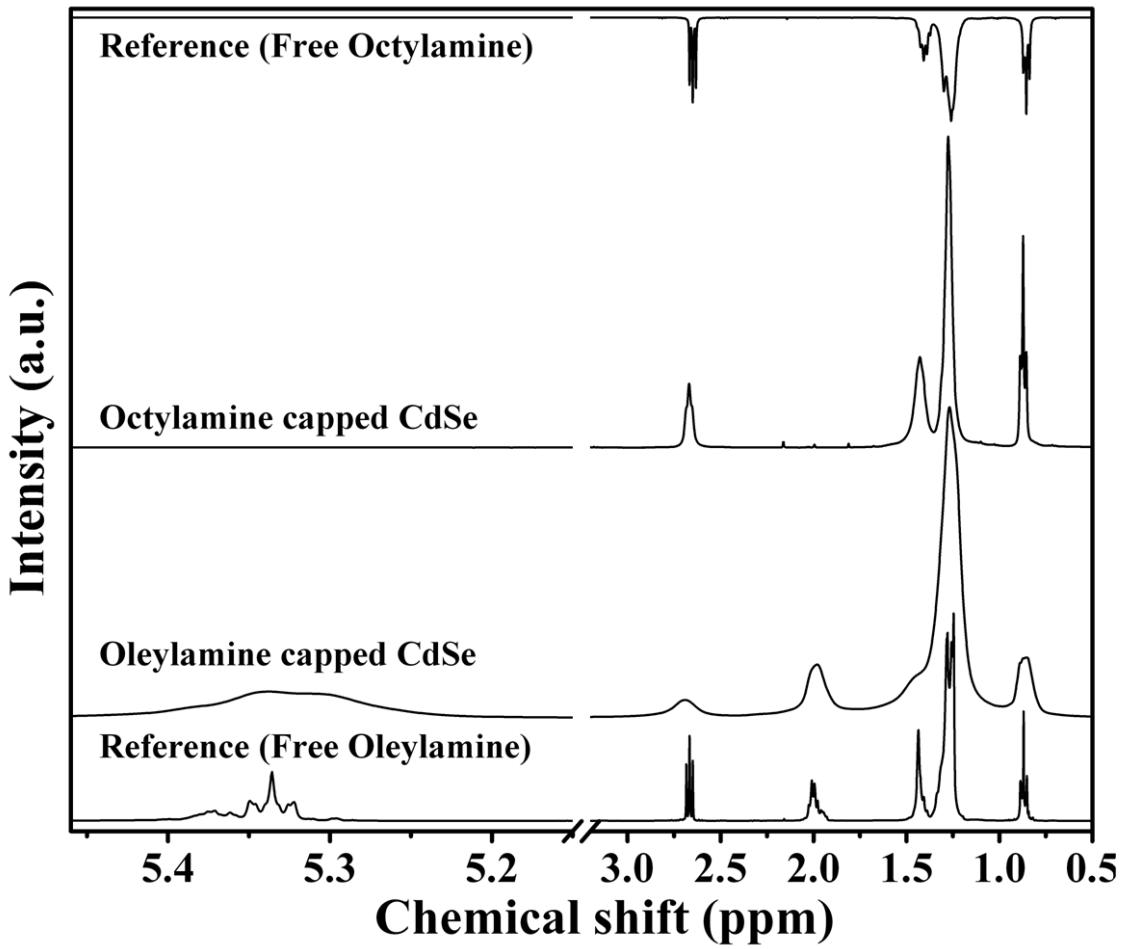

Figure 6.11. *^{1}H NMR spectra of the octylamine and oleylamine capped CdSe QDs in $CDCl_3$ after the ligand exchange along with octylamine and oleylamine ligands as the reference.*

The role of different amines in undoped QDs was probed by the PL spectroscopy and is compiled in Figure 6.12. Amines with longer carbon chains (C_8 and C_{18}) have demonstrated higher PL intensity while the shorter chain length (C_4 and C_6) amines quench PL intensity compared to the original CdSe QDs as shown in Figure 6.12(a). This indicates that while smaller chain amines are not efficient in passivating the surface of QD, the longer chain amines are capable of doing that. This is further demonstrated by decrease in average lifetime in case

of smaller chain amines compared to larger chain amines as shown in Figure 6.12(b) and its corresponding inset.

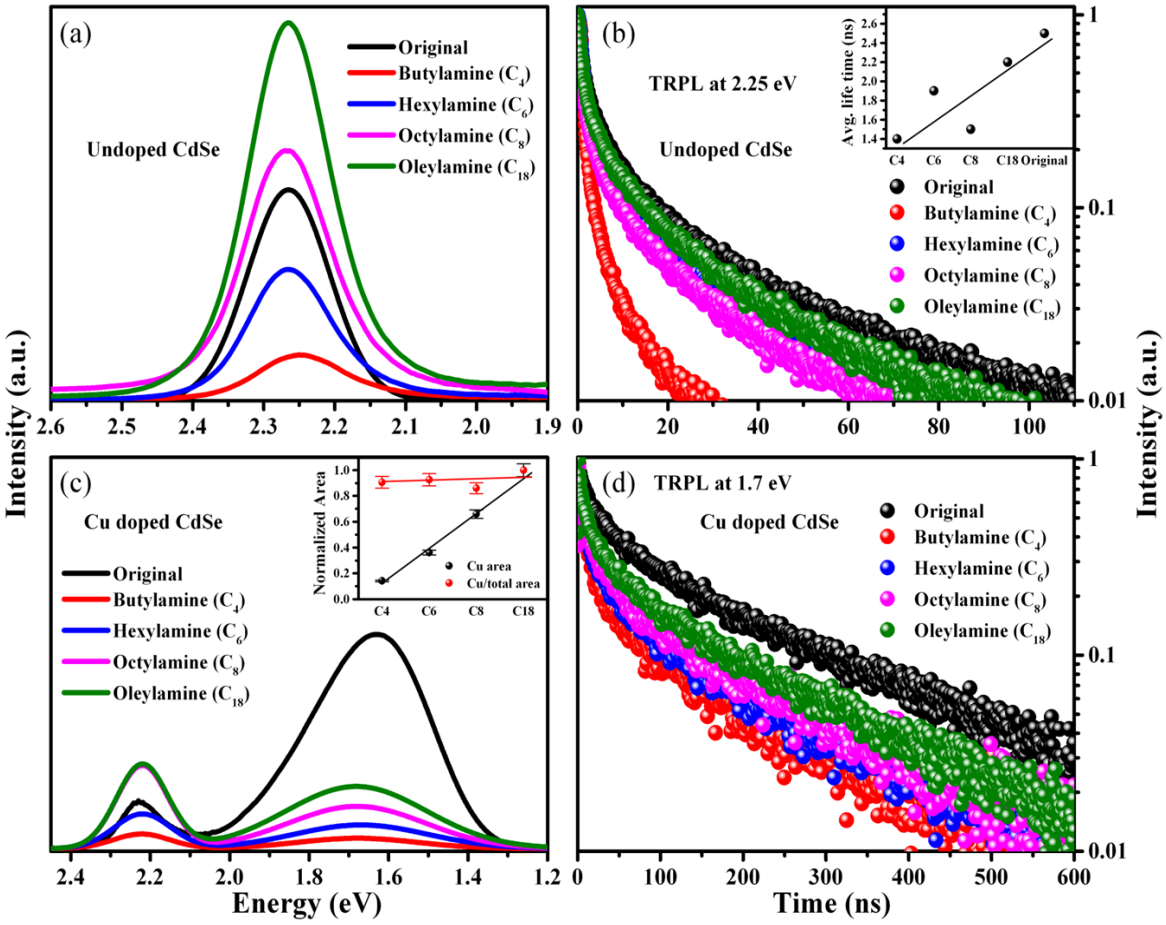

Figure 6.12. *Ligand exchange with Primary amines.* ***(a)*** *Steady state PL spectra of Undoped CdSe QDs before and after the ligand exchange with amines of different chain length* ***(b)*** *and the corresponding TRPL spectra with λ_{em} = 2.25 eV. Inset shows the average lifetime obtained from TRPL spectra.* ***(c)*** *Steady state PL spectra of Cu doped CdSe QDs before and after the ligand exchange with amines of different chain length. Inset shows the variation of absolute Cu area and Cu/total area with increasing the chain length of amine with error bars.* ***(d)*** *The corresponding TRPL spectra with λ_{em} = 1.7 eV. Excitation wavelength, λ_{ex} = 405 nm (3.06 eV) for all the PL and TRPL spectra. All the spectra were measured in hexane.*

To understand the nature of trap states in these QDs, we doped Cu into these QDs and the resultant PL spectra are shown in Figure 6.12(c). It is evident from this graph that the intensity of band edge PL is increased at the cost of Cu PL after the ligand exchange of original ligands with oleylamine and octylamine on CdSe QD surface. However, the intensities of both

band edge and Cu PL decrease in case of exchange with the butylamine and hexylamine ligands. This indicates that a similar variation of band edge intensities of Cu doped and undoped CdSe QDs before and after the ligand exchange. The lifetime studies at band edge emission shows similar trend as in the undoped case. In particular, there is a decrease in lifetime for shorter chain (C_4 and C_6) amine capped QDs compared to that of longer chain amine (C_8 and C_{18}) as well as the original QDs as shown in Figure 6.13.

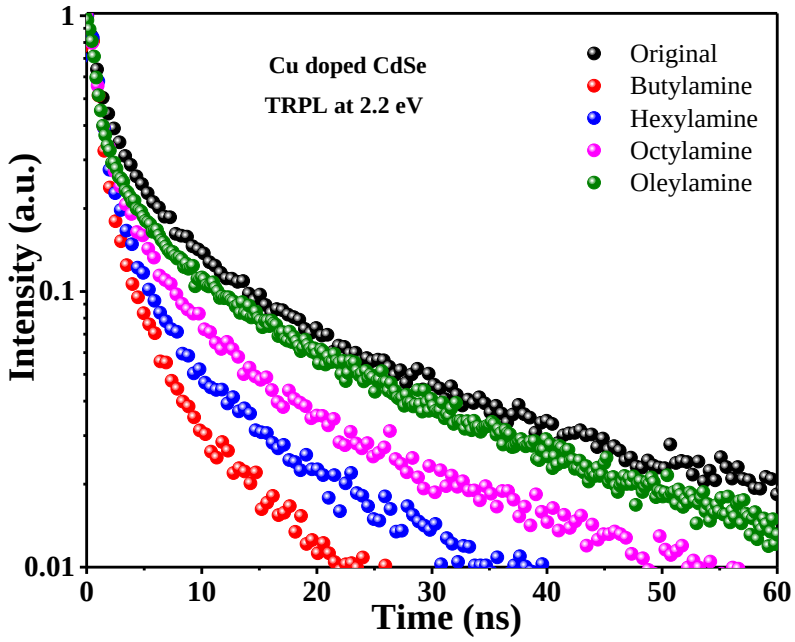

Figure 6.13. *The TRPL spectra of Cu doped CdSe QDs before and after the ligand exchange with primary amines.* λ_{ex} *= 405 nm (3.06 eV) and* λ_{em} *= 2.25 eV.*

Inset of Figure 6.12(c) shows the variation of normalized data of both Cu area and the ratio of Cu PL area to the total area with increasing the chain length of amines. Though the absolute Cu PL area increases with increase in chain length of amines the Cu/total area remains constant. This suggests that the extent of hole trap passivation is unchanged with varying the chain length of amines but the shorter chain amines create electron traps. This is further supported by the increase in the contribution of fast component (indicates electron traps) for the smaller chain amines compared to original Cu doped CdSe QDs in the decay curves of Cu PL as shown in Figure 6.12(d). Hence, we can conclude that both oleylamine and octylamine mainly passivate the hole traps in CdSe QDs along with a small percentage of electron trap creation. However, in the case of smaller chain amines, butylamine and hexylamine, hole trap

passivation is negligibly small while a large number of electron traps are created. This renders them highly inefficient for surface passivation in CdSe QDs. This effect of chain length of alkyl amines in passivating the CdSe QDs can be explained on the basis of the binding strength of the ligand on the surfaces of QDs. It has been shown earlier that as the chain length of an amine ligand increases, it binds more strongly to the surface of a QD.[50] This is due to the additional strengthening of binding on the surface of the QD obtained from the stronger ligand-ligand van der Waals interaction in the longer chain ligands compared to the shorter chain ligands. This leads to the stronger binding of longer chain amines like oleylamine to the CdSe QD surface while the shorter chain amines like butylamine binds weakly to the CdSe QD surface. A more in-depth theoretical study is necessary to obtain a systematic understanding of these trends and is not within the scope of this study.

6.4.2.3. Role of oleylamine capping in CdS QDs:

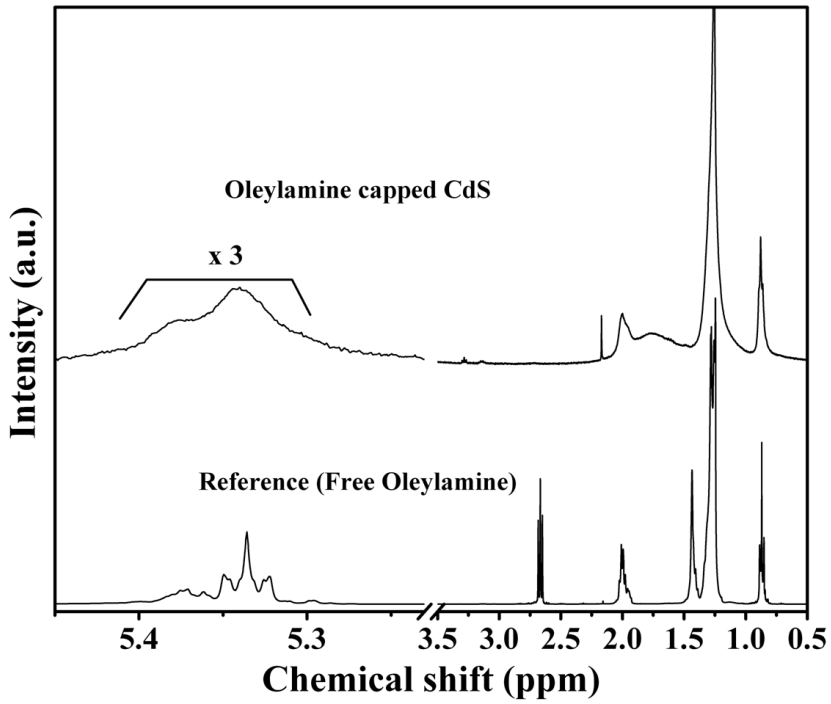

Figure 6.14. *^{1}HNMR spectra of the oleylamine capped CdS QDs in $CDCl_3$ after the ligand exchange along with the free oleylamine ligands as the reference.*

To prove the generality of our approach, we have studied the nature of passivation induced by oleylamine on the surface of CdS QDs. The NMR spectrum of CdS QDs after the ligand

exchange with oleylamine is shown in Figure 6.14. It shows that CdS QDs are covered with oleylamine on their surface after the ligand exchange.

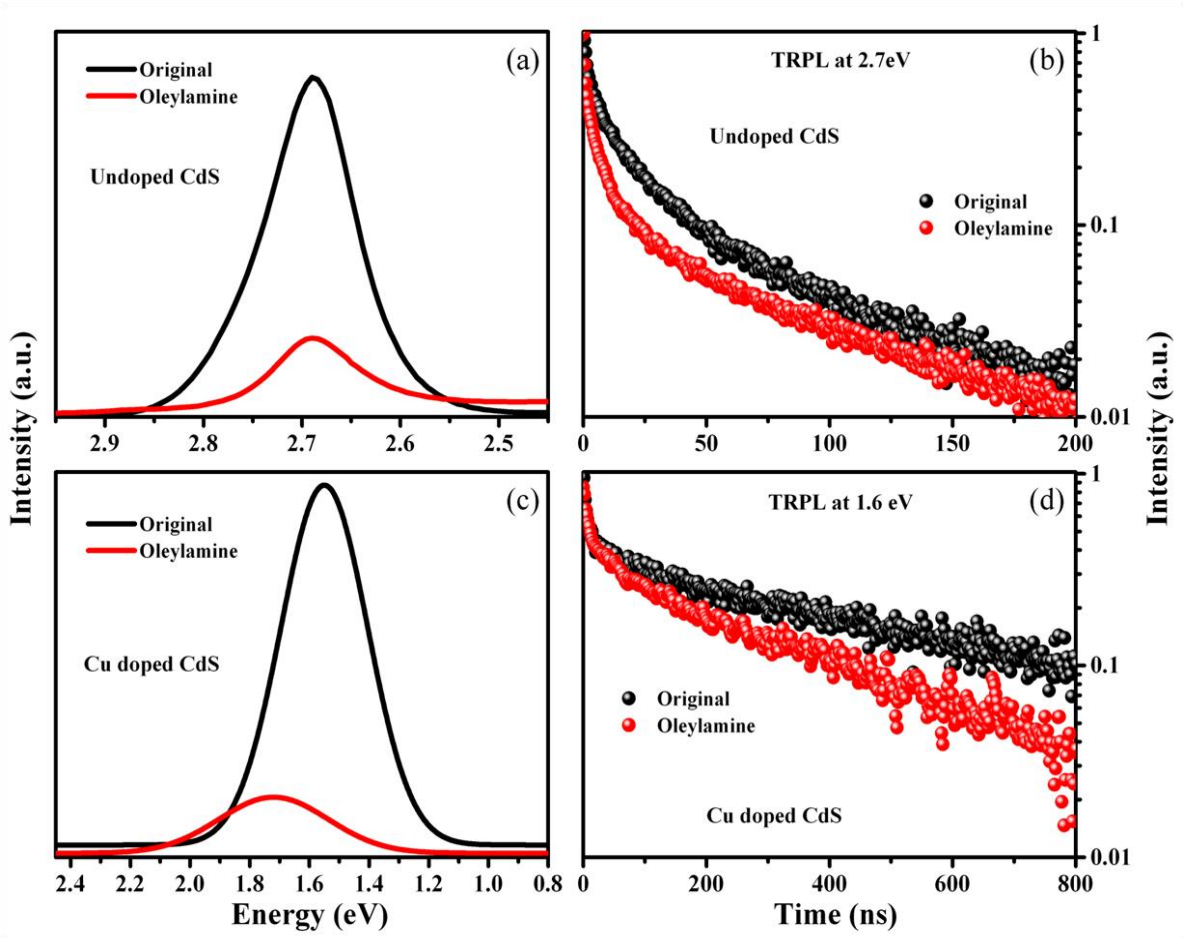

Figure 6.15. *Ligand exchange of CdS QDs with oleylamine.* ***(a)*** *Steady state PL spectra of Undoped QDs before and after the ligand exchange with oleylamine* ***(b)*** *and the corresponding TRPL spectra with* λ_{em} *= 2.2 eV.* ***(c)*** *Steady state PL spectra of Cu doped QDs before and after the ligand exchange with oleylamine* ***(d)*** *and the corresponding TRPL spectra with* λ_{em} *= 1.6 eV. Excitation wavelength,* λ_{ex} *= 405 nm (3.06 eV) for all the spectra. All the spectra were measured in hexane.*

Oleylamine mainly passivates the hole traps in case of CdSe QDs thus enhancing its PL efficiency. Contrary to this, it quenches PL intensity in CdS QDs after replacing the original ligands as shown in Figure 6.15(a). Also, there is an increase in contribution of fast component in TRPL spectrum (shown in Figure 6.15(b)) of CdS QDs after the ligand exchange with oleylamine. This indicates that oleylamine ligands induce new traps on CdS QD surface, that is consistent with the formation of the poorly emissive CdS QDs when they are synthesized in oleylamine.[51] The nature of trap states can be elucidated with the help of Cu doping. Figure

6.15(c) shows the PL spectra of CdS QDs before and after the ligand exchange with oleylamine ligands. It is clear that the absolute Cu PL was reduced after the ligand exchange. But the TRPL spectrum of oleylamine capped CdS QDs is almost unchanged or slightly changed compared to that of original capped QDs as shown in Figure 6.15(d). The combination of Figures 6.15(c) and 6.15(d) shows that oleylamine creates mainly hole traps along with a fewer electron traps. From this study, one can observe that the same ligand can behave differently in different QD materials, that is, oleylamine creates trap states in case of CdS QDs while it passivates the QD surface in the case of CdSe QDs.

6.4.2.4. Role of TOP and TOPO capping in CdSe QDs:

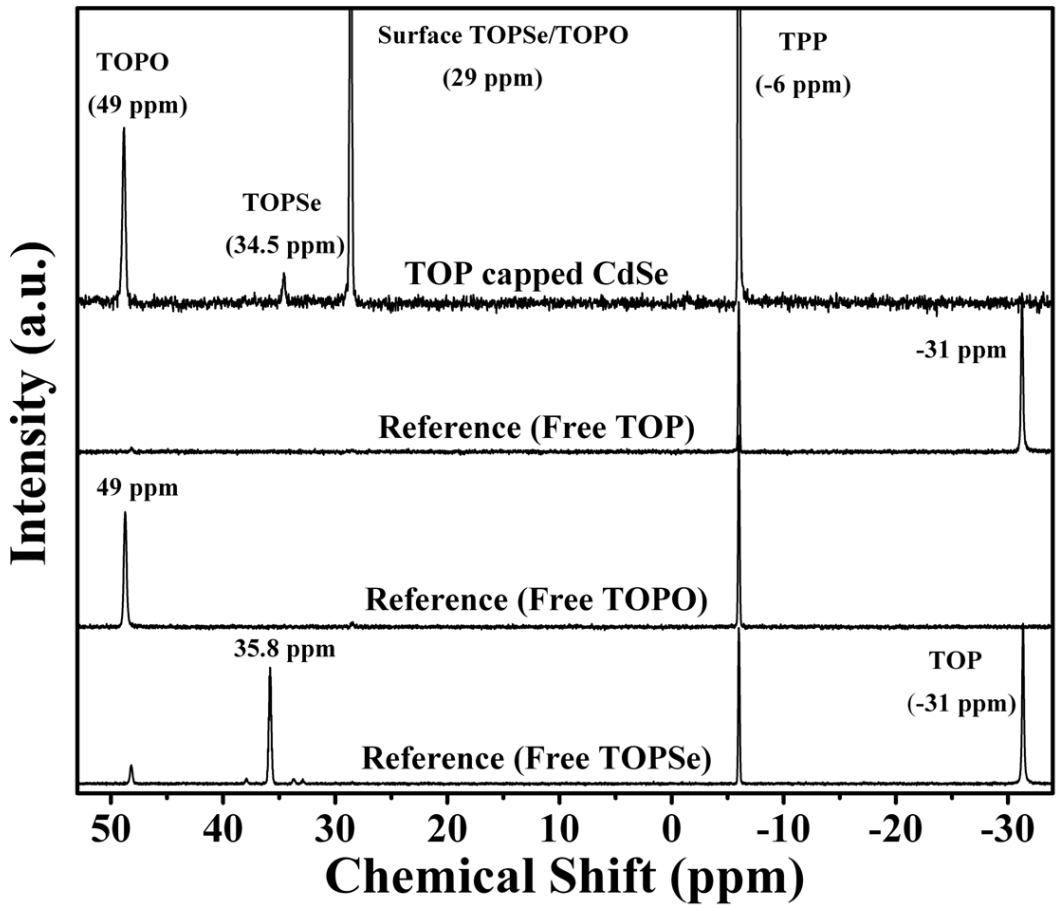

Figure 6.16. *^{31}PNMR spectra of CdSe QDs after the original ligands are replaced with TOP along with the free TOP, TOPO and TOPSe ligands as reference. TPP is added as internal reference.*

The synthesis of CdSe or any metal selenide in literature is carried out in presence of TOP as it has proven itself to be a good solvent for the Se precursor as well as in passivating the QDs. However, the exact role of TOP, beyond the capability to dissolve the Se precursors, is not completely understood. In an effort to analyze the role of TOP for ligand passivation, we first exchanged the original ligands on CdSe QD surface with the TOP ligands. The exchange of the ligands is probed by ^{31}P NMR spectroscopy as shown in Figure 6.16. Here, we have chosen TPP as an internal reference which gives a peak at -6 ppm in ^{31}P NMR. Free TOP gives a signal at -31 ppm as shown in the Figure 6.16. However, after the ligand exchange, we observe a complete absence of -31 ppm peak demonstrating the absence of free TOP molecules. This is now replaced by three new peaks. The small peak at 34.5 ppm may be assigned to TOPSe as free TOPSe shows the resonance at 35.8 ppm as shown by the NMR spectra in Figure 6.16. The upfield shift of 1.4 ppm is due to TOPSe is in close proximity to the QD surface experiencing the shielding effect. This suggests the binding of TOP molecules with the Se atoms on CdSe QD surface. However, we have not observed any noticeable broadening of ^{31}P NMR peaks of the ligands bound to CdSe QD surface unlike the traditional NMR spectra. This kind of exceptions was observed in literature but the exact reason is not clear at this moment. For example, Jones and co-workers[22] have observed no broadening in the ^{31}P NMR peaks of TOPO when it is bound to QD surface but only a small shift in the resonance peak is observed. Alivisatos and co-workers[52] have also not observed any noticeable broadening of ^{31}P NMR peaks of bound TOPSe and TOPO ligands on the as-synthesized CdSe QD surface. The small peak at around 49 ppm can be assigned to free TOPO. However, the strong peak at 29 ppm which is shifted upfield from the resonances of both TOPSe and TOPO may be attributed to the formation of surface bound TOPSe/TOPO.[53] However, due to higher concentration of TOPO than TOPSe, this peak could be predominantly due to bound TOPO. The presence of TOPO in small quantities can be explained by the reaction of TOP with free oxygen available in air during the ligand exchange process, similar to the formation of TOPO upon treating ODE-Se with TOP.[54] Importantly, the NMR spectra show clear evidence that the TOP has mostly formed surface bound TOPSe/TOPO with small percentage of TOPSe and free TOPO, upon successful ligand exchange.

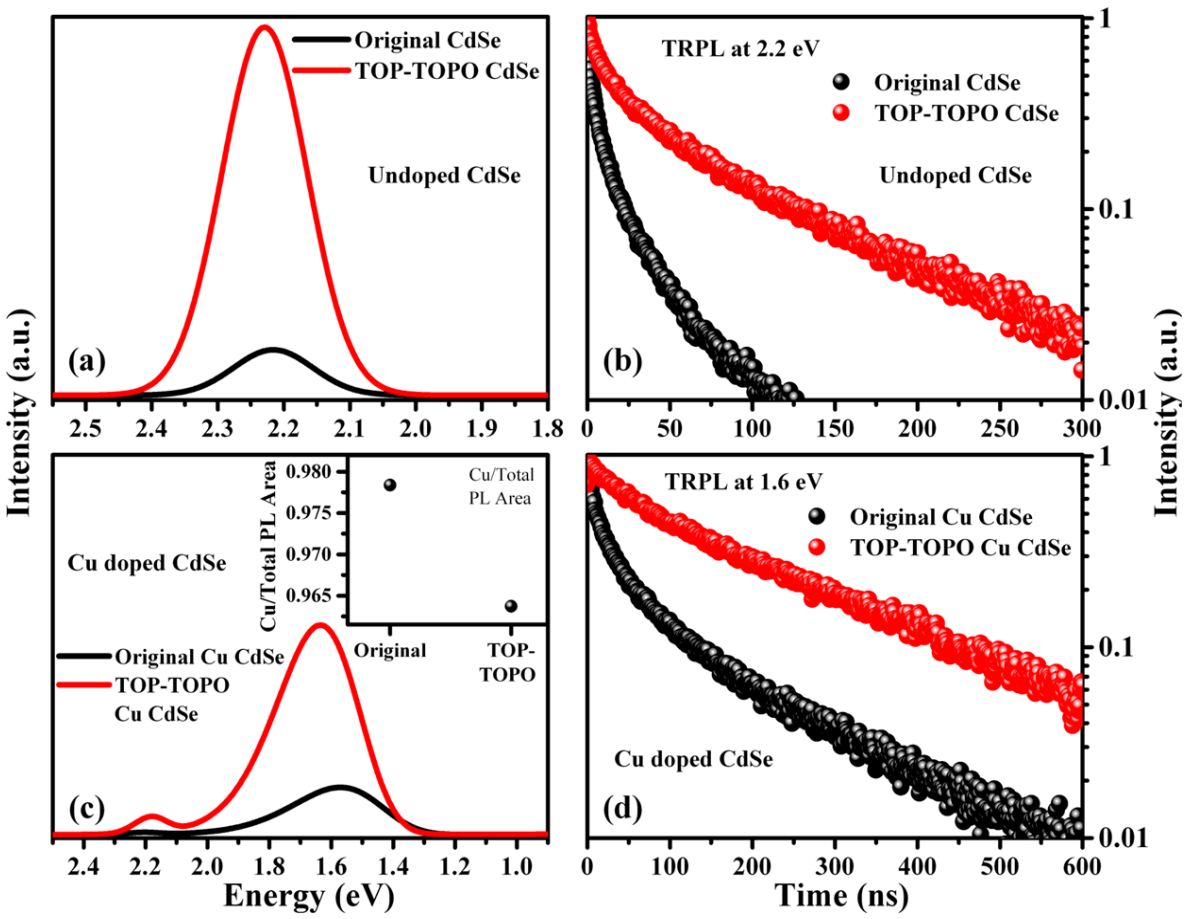

Figure 6.17. *Ligand exchange with TOP-TOPO.* ***(a)*** *Steady state PL spectra of Undoped CdSe QDs before and after the ligand exchange with TOP-TOPO* ***(b)*** *and the corresponding TRPL spectra with* λ_{em} *= 2.2 eV.* ***(c)*** *Steady state PL spectra of Cu doped CdSe QDs before and after the ligand exchange with TOP-TOPO* ***(d)*** *and the corresponding TRPL spectra with* λ_{em} *= 1.6 eV. Excitation wavelength,* λ_{ex} *= 405 nm (3.06 eV) for all the spectra. All the spectra were measured in hexane.*

The role of TOP and TOPO is probed by PL spectroscopy and is compiled in Figure 6.17. Figure 6.17(a) shows the PL spectra of undoped CdSe QDs before and after the ligand exchange with TOP-TOPO ligands. TOP-TOPO strongly improves the PL efficiency in CdSe QDs compared to the original ligands. This can be attributed to the better surface passivation of trap states of CdSe QDs by the TOP-TOPO ligands. This is also clear from the increase in the average lifetime of CdSe QDs after replacing the original ligands as shown in Figure 6.17(b). In literature, both TOPO and TOP were shown to enhance the PL efficiency of CdSe QDs by passivating their surface.[16, 54] Addition of a few Cu atoms into QDs was used to reveal the nature of passivation induced by TOP-TOPO on CdSe QD surface. Figure 6.17(c) shows

the PL intensities of both band edge and Cu emission increasing in case of Cu doped QDs after ligand exchange with the TOP-TOPO ligands to the QD surface. Figure 6.18 shows an increase in the average lifetime of the band edge emission of Cu doped CdSe QDs after the ligand exchange with TOP-TOPO ligands similar to that of undoped QDs. The ratio of Cu PL area to total area is reduced with the TOP-TOPO passivation on the QD surface as shown in the inset of Figure 6.17(c). Here, TOP passivates the hole traps on the CdSe QD surface by attaching to uncoordinated Se sites.

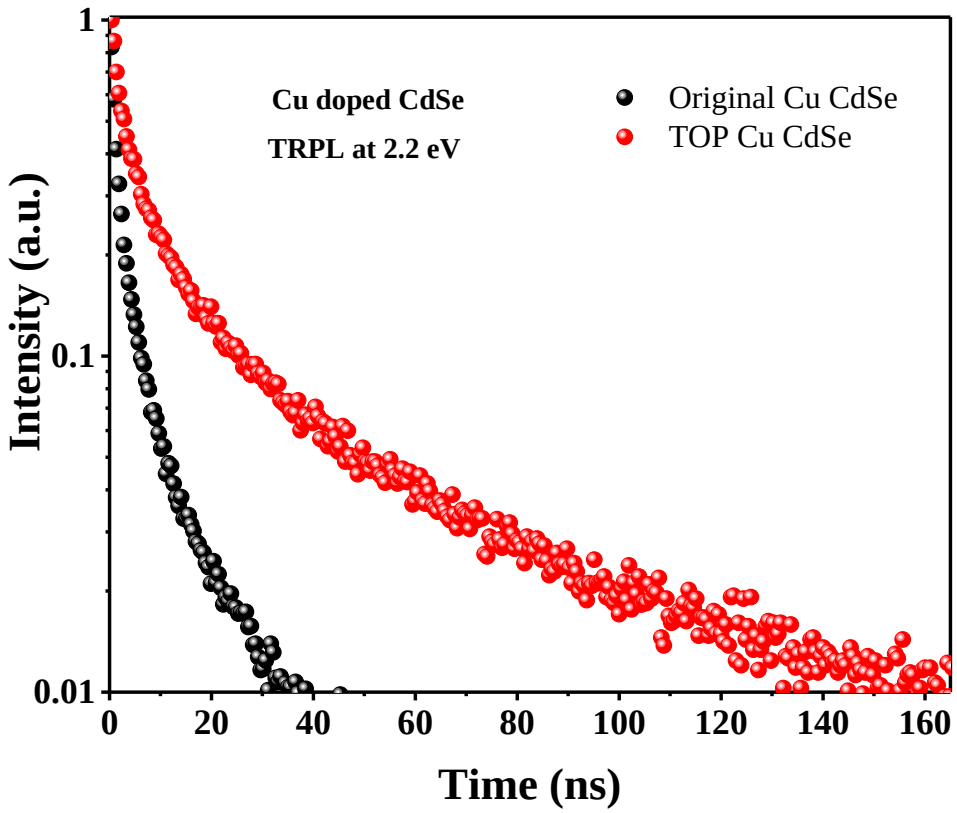

Figure 6.18. *The TRPL spectra of Cu doped CdSe QDs at band edge emission before and after the ligand exchange with TOP.* λ_{ex} *= 405 nm (3.06 eV) and* λ_{em} *= 2.2 eV.*

However, there is an increase in overall PL efficiency along with decrease in the contribution of the fast component in the TRPL spectra of Cu related emission of Cu doped CdSe QDs after the ligand exchange as shown in Figure 6.17(d). The lifetime of fast component is also increased after the ligand exchange with TOP-TOPO ligands as shown in Figure 6.19. It indicates that the new ligands also passivate electron traps on CdSe QD surface that is consistent with the huge increase in PL efficiency upon ligand exchange with TOP-

TOPO. TOP usually binds to the surface Se sites but not to the surface Cd sites and TOPO is shown to bind strongly to the surface Cd atoms only.[55] This suggests that the electron trap passivation is mainly induced by the TOPO which strongly binds to surface Cd atoms. This is further supported by the observation that TOPO enhances the PL intensity of CdSe QDs by binding to uncoordinated Cd sites on CdSe QD surface.[22] So, during the ligand exchange, TOP molecules bind to the surface Se sites while the TOPO molecules bind to surface Cd sites which lead to the passivation of hole and electron traps respectively. Here, it can be understood that choice of ligand plays an important role in passivating the QD surface of different compositions (either cation rich or anion rich).

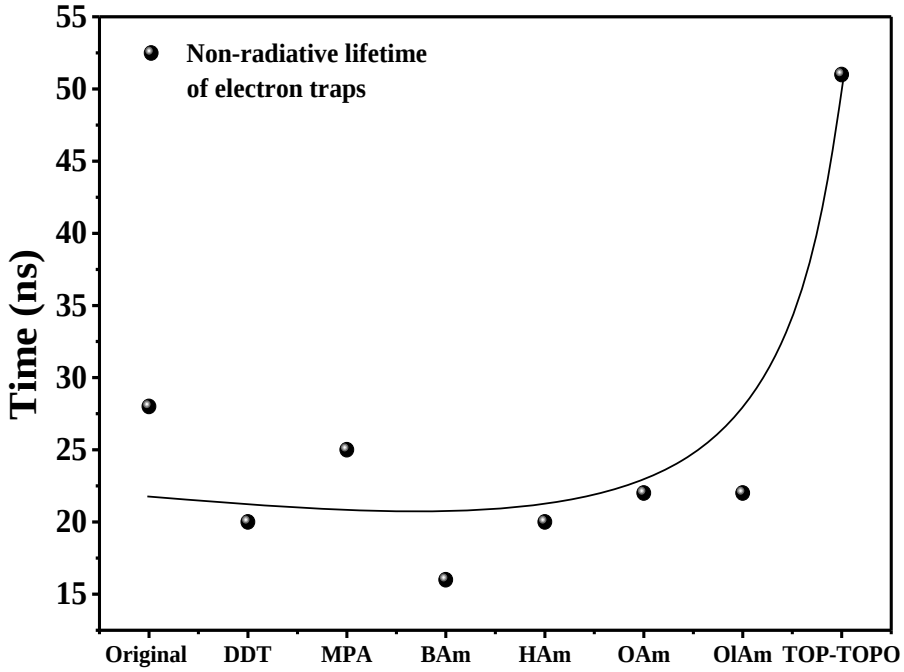

Figure 6.19. *The variation of non-radiative lifetime of electron traps on the CdSe QD surface before and after ligand exchange with different ligands.*

6.4.3. Improving the PL efficiency of CdSe QDs by performing ligand exchange with a mixture of ligands:

From this data, it is evident that not only is the ligand important but also the concentration of the ligand, the surface composition of the host QD and the crystal structure exposing different facets of the QD are important in efficient passivation of the surface. From these individual studies of amines, TOP/TOPO and thiols, we now evolve a combination of ligands and ligand concentration to obtain maximum PL efficiency in case of CdSe QDs.

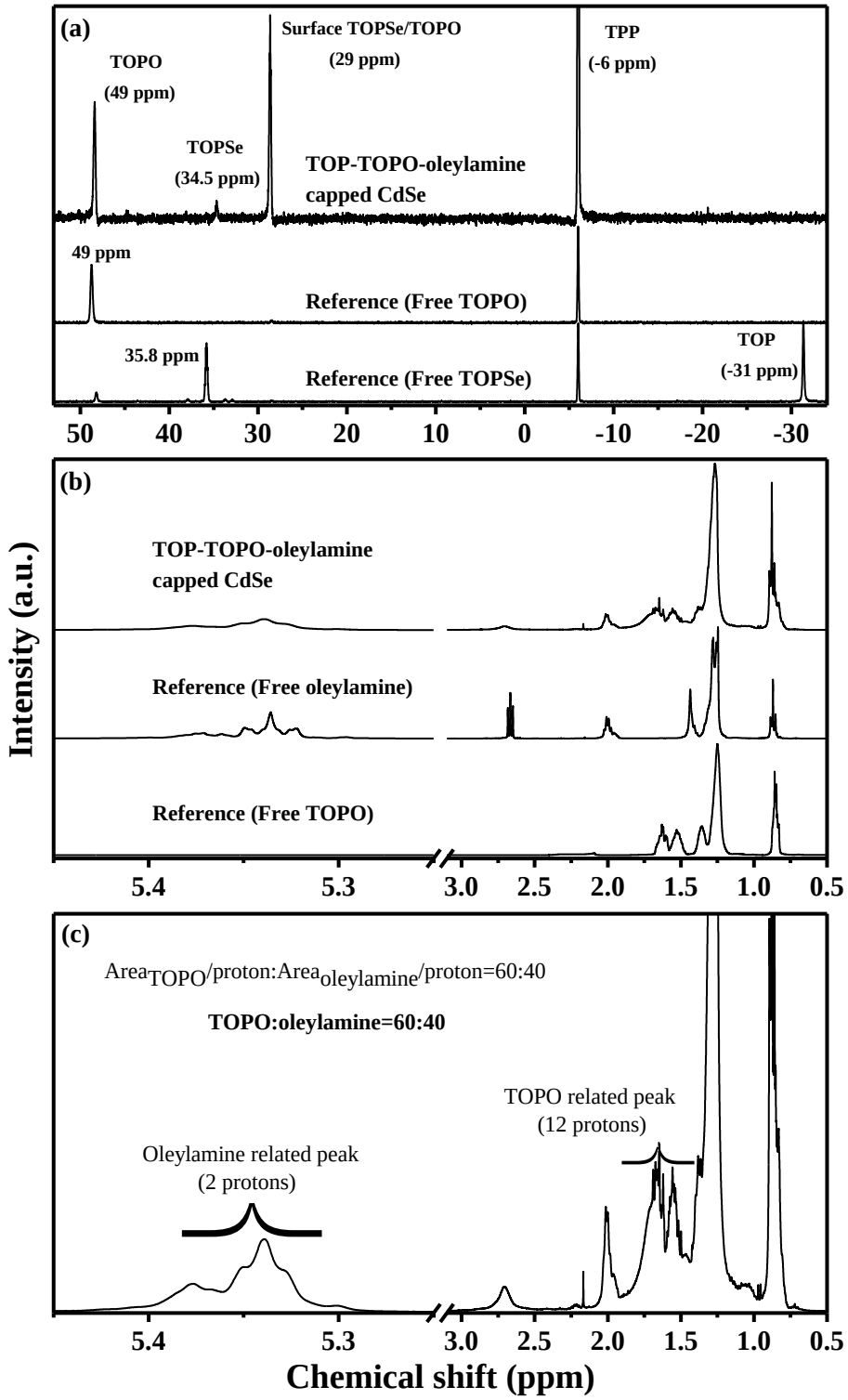

Figure 6.20. (a) *^{31}P NMR spectra and* ***(b)*** *^{1}H NMR spectra of TOP-TOPO-oleylamine capped CdSe QDs along with the reference NMR spectra of free ligands.* ***(c)*** *Calculation of approximate composition of TOPO and oleylamine from the ^{1}H NMR spectrum of TOP-TOPO-oleylamine capped CdSe QDs.*

This has been applied to ligand exchange using the optimal combination of ligands. Post synthesis, the CdSe QDs were treated with excess of a mixture of TOP and oleylamine. The surface chemistry of the mixed ligand capped CdSe QDs is probed by NMR spectroscopy as shown in Figure 6.20. ^{31}P NMR spectra (Figure 6.20(a)) shows the presence of strong resonance of TOPO at 49 ppm compared to weak resonance of TOP at 34.5 ppm on CdSe QD surface. It indicates that most of the TOP ligands are converted into TOPO during ligand exchange as observed in case of ligand exchange with TOP ligands only (Figure 6.16). ^{1}H NMR spectra (Figure 6.20(b)) also show the presence of both TOPO and oleylamine on the QD surface. Thus, the QD surface is mainly passivated by TOPO and oleylamine along with a small percentage of TOP. As shown in Figure 6.20(c), upon comparison of peaks at 1.5-1.8 ppm (TOPO) and 5.3-5.4 ppm (oleylamine), the ratio of TOPO and oleylamine is found to be 60:40 from the ^{1}H NMR spectrum after accounting for the number of protons contributing to the peaks. Figure 6.21(a) shows the enhancement in the PL intensity after the exchange of original ligands with this mixture of ligands on the CdSe QD surface showing almost ten times enhancement in PL efficiency after the ligand exchange and the relative PL intensities are shown in the inset of Figure 6.21(a). Also, the lifetime of the QDs increases after the ligand exchange as shown in Figure 6.21(b). Even though similar ligand combination has been used during the synthesis of CdSe QDs to obtain high PL QY,[12] this is the first report wherein the result has been observed during post synthesis modification using an analytical protocol. This proves the importance, validity and need of our method in understanding the role of the ligands for making efficient QDs towards various applications.

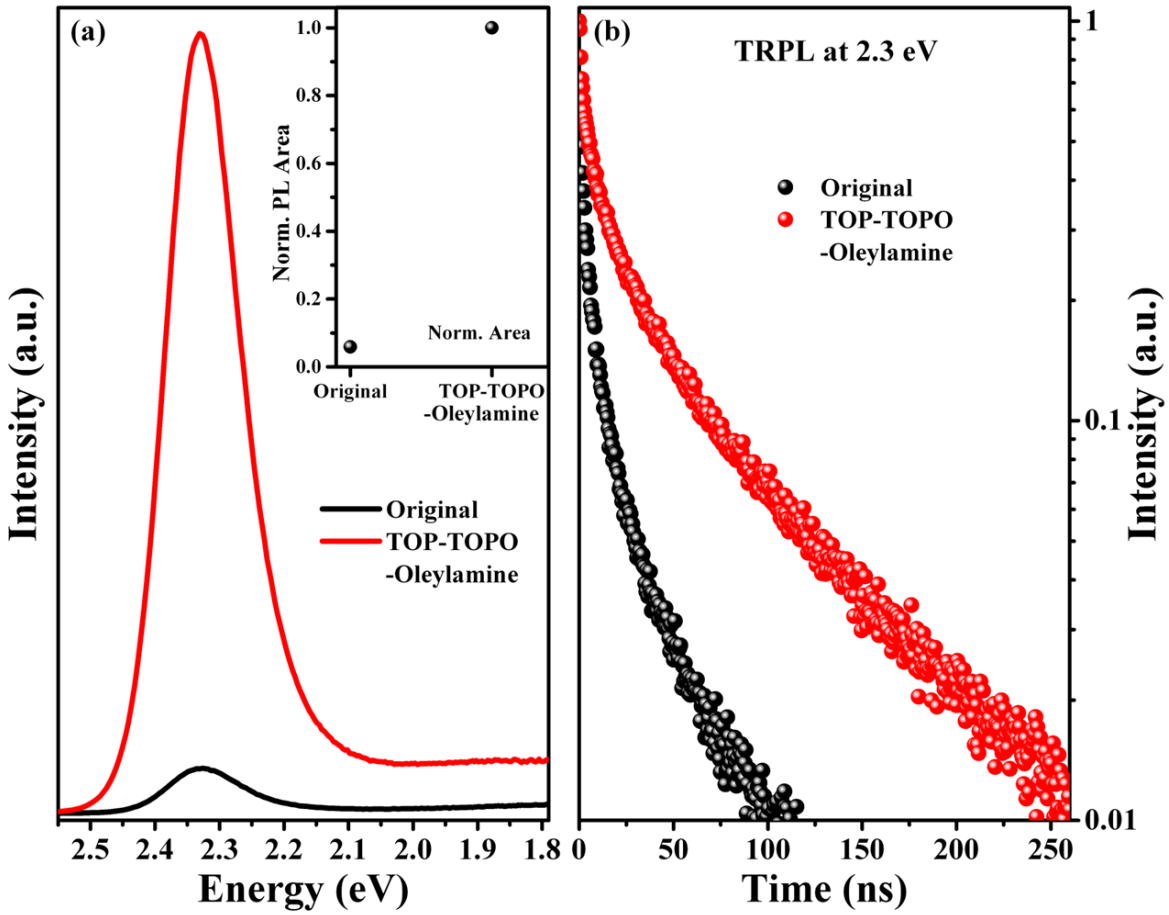

Figure 6.21. (a) *The steady state PL spectra of CdSe QDs before and after the ligand exchange with a mixture of TOP and oleylamine. The inset shows the relative PL area of CdSe QDs before and after the ligand exchange.* ***(b)*** *The corresponding TRPL spectra were collected at* λ_{em} *= 2.3 eV. All the spectra were measured in hexane with* λ_{ex} *= 405 nm (3.06 eV).*

6.4.4. Summary of the role of different ligands in passivating the QDs:

The role of thiols, primary amines, oleic acid and TOP in passivating QDs have been tabulated in Table 6.1, in order to obtain a comprehensive understanding of the QD passivation.

Table 6.1. *Role of different ligands in passivating the QDs.*

Material	Ligand	Hole traps	Electron traps
CdSe QDs	DDT	Strong creation	Mild creation
CdSe QDs	MPA	Strong creation	Mild creation
CdSe QDs	Octylamine and oleylamine	Passivation	Almost no effect
CdSe QDs	Butylamine and hexylamine	Mild passivation	Creation
CdSe QDs	TOP	Passivation	No effect
CdSe QDs	TOPO	No effect	Passivation
CdSe QDs	Oleic acid	Passivation	No effect
CdS QDs	Oleic acid	No effect	Passivation
CdS QDs	Oleylamine	Creation	Mild creation
CdTe QDs	Oleic acid	Creation	Passivation

This chapter provides a proof of concept for the study of effect of a particular ligand on passivation of the surface of the QDs. However, it is not possible to provide an exhaustive list of ligands for the various synthesis of different QDs, for example, like the presence of inorganic ligands like the halides. We also tried to study the role of inorganic ligands like halide on CdSe QDs by ligand exchange (phase transfer) experiment. Halide ligands are known to completely quench the PL of CdSe QDs as observed in case of negative ligands like S^{2-}. Due to the presence of large negative charge the emission in Cu doped QDs was very weak even in

presence of small concentration of halide ions. In **Chapter 7**, we show that S^{2-} ligands completely quench the band edge PL in CdS QDs due to photo-generated hole trapping but they were also shown to passivate electron traps on CdS QD surface. We believe that halide ligands also trap the photo-generated hole and passivate electron traps on CdSe QD surface like S^{2-} ligand does in case of CdS QDs, albeit being much more effective in forming the negative ion shield around the surface of the QD. This is further supported by the work reported by Kim et al.[56] where chloride ligands were shown to passivate electron traps on CdSe QD surface.

6.5. Conclusions:

We have shown that it is indeed possible to dope CdSe with Cu and obtain the Cu related emission by systematically increasing the hole traps within the system and the earlier reported failures were mainly due to the absence of surface hole traps. We have used the PL QY and PL decay kinetics of the Cu related emission to study the surface of the QDs. TOP passivates hole traps on CdSe QD surface. We have studied the exact role of thiols (MPA and DDT), primary amines, TOP and TOPO in passivating the CdSe QD surface can be achieved through ligand exchange or phase transfer processes. The combination of oleylamine, TOP and TOPO leads to better passivation of CdSe QDs which improves their efficiency. We have also shown that the same ligand e.g. oleic acid and oleylamine plays different role in passivating QD surface in different materials (CdSe and CdS). In the larger scheme of QD synthesis, we have developed a generic method that can be used to rationally analyze the effects of various ligands towards increasing or decreasing PL efficiency.

Bibliography:

[1] Y. Shirasaki, G. J. Supran, M. G. Bawendi, V. Bulović, *Nat. Photonics* **2013**, *7*, 13.

[2] X. Wu, H. Liu, J. Liu, K. N. Haley, J. A. Treadway, J. P. Larson, N. Ge, F. Peale, M. P. Bruchez, *Nat. biotech.* **2002**, *21*, 41.

[3] P. V. Kamat, *J. Phys. Chem. C* **2008**, *112*, 18737.

[4] F. Liu, J. Zhu, J. Wei, Y. Li, L. Hu, Y. Huang, O. Takuya, Q. Shen, T. Toyoda, B. Zhang, J. Yao, S. Dai, *J. Phys. Chem. C* **2014**, *118*, 214.

[5] Y.-S. Liu, Y. Sun, P. T. Vernier, C.-H. Liang, S. Y. C. Chong, M. A. Gundersen, *J. Phys. Chem. C* **2007**, *111*, 2872.

[6] W. Wang, S. Banerjee, S. Jia, M. L. Steigerwald, I. P. Herman, *Chem. Mater.* **2007**, *19*, 2573.

[7] Z. Li, X. Peng, *J. Am. Chem. Soc.* **2011**, *133*, 6578.

[8] Y. Gao, X. Peng, *J. Am. Chem. Soc.* **2014**, *136*, 6724.

[9] R. García-Rodríguez, H. Liu, *J. Am. Chem. Soc.* **2014**, *136*, 1968.

[10] W. W. Yu, Y. A. Wang, X. Peng, *Chem. Mater.* **2003**, *15*, 4300.

[11] D. A. Hines, P. V. Kamat, *J. Phys. Chem. C* **2013**, *117*, 14418.

[12] D. V. Talapin, A. L. Rogach, A. Kornowski, M. Haase, H. Weller, *Nano Lett.* **2001**, *1*, 207.

[13] K. P. Kadlag, M. J. Rao, A. Nag, *J. Phys. Chem. Lett.* **2013**, *4*, 1676.

[14] M. A. Boles, D. Ling, T. Hyeon, D. V. Talapin, *Nat. Mater.* **2016**, *15*, 141.

[15] A. M. Munro, I. Jen-La Plante, M. S. Ng, D. S. Ginger, *J. Phys. Chem. C* **2007**, *111*, 6220.

[16] G. Kalyuzhny, R. W. Murray, *J. Phys. Chem. B* **2005**, *109*, 7012.

[17] C. Bullen, P. Mulvaney, *Langmuir* **2006**, *22*, 3007.

[18] C. Landes, C. Burda, M. Braun, M. A. El-Sayed, *J. Phys. Chem. B* **2001**, *105*, 2981.

[19] C. F. Landes, M. Braun, M. A. El-Sayed, *J. Phys. Chem. B* **2001**, *105*, 10554.

[20] S. F. Wuister, C. de Mello Donega, A. Meijerink, *J. Phys. Chem. B* **2004**, *108*, 17393.

[21] B. Kundu, S. Chakrabarti, A. J. Pal, *Chem. Mater.* **2014**, *26*, 5506.

[22] E. S. Williams, K. J. Major, A. Tobias, D. Woodall, V. Morales, C. Lippincott, P. J. Moyer, M. Jones, *J. Phys. Chem. C* **2013**, *117*, 4227.

[23] R. Viswanatha, H. Amenitsch, D. D. Sarma, *J. Am. Chem. Soc.* **2007**, *129*, 4470.

[24] B. B. Srivastava, S. Jana, N. Pradhan, *J. Am. Chem. Soc.* **2011**, *133*, 1007.

[25] R. Viswanatha, S. Brovelli, A. Pandey, S. A. Crooker, V. I. Klimov, *Nano Lett.* **2011**, *11*, 4753.

[26] S. C. Erwin, L. Zu, M. I. Haftel, A. L. Efros, T. A. Kennedy, D. J. Norris, *Nature* **2005**, *436*, 91.

[27] D. Chen, R. Viswanatha, G. L. Ong, R. Xie, M. Balasubramaninan, X. Peng, *J. Am. Chem. Soc.* **2009**, *131*, 9333.

[28] A. Nag, A. Hazarika, K. V. Shanavas, S. M. Sharma, I. Dasgupta, D. D. Sarma, *J. Phys. Chem. Lett.* **2011**, *2*, 706.

[29] D. Chen, R. Viswanatha, G. L. Ong, R. Xie, M. Balasubramaninan, X. Peng, *J. Am. Chem. Soc.* **2009**, *131*, 9333.

[30] X. Ji, D. Copenhaver, C. Sichmeller, X. Peng, *J. Am. Chem. Soc.* **2008**, *130*, 5726.

[31] A. Hassinen, I. Moreels, K. De Nolf, P. F. Smet, J. C. Martins, Z. Hens, *J. Am. Chem. Soc.* **2012**, *134*, 20705.

[32] Y. Yang, J. Li, L. Lin, X. Peng, *Nano Res.* **2015**, *8*, 3353.

[33] J. R. Lakowicz, *Principles of Fluorescence Spectroscopy, Vol. 1*, Third ed., Springer, **2006**.

[34] A. Hassinen, I. Moreels, C. de Mello Donegá, J. C. Martins, Z. Hens, *J. Phys. Chem. Lett.* **2010**, *1*, 2577.

[35] B. Fritzinger, I. Moreels, P. Lommens, R. Koole, Z. Hens, J. C. Martins, *J. Am. Chem. Soc.* **2009**, *131*, 3024.

[36] Y. Wei, J. Yang, J. Y. Ying, *Chem. Commun.* **2010**, *46*, 3179.

[37] S. Tamang, G. g. Beaune, I. Texier, P. Reiss, *ACS Nano* **2011**, *5*, 9392.

[38] N. Gaponik, D. V. Talapin, A. L. Rogach, A. Eychmüller, H. Weller, *Nano Lett.* **2002**, *2*, 803.

[39] A. G. Young, N. Al-Salim, D. P. Green, A. J. McQuillan, *Langmuir* **2008**, *24*, 3841.

[40] Z. Hens, J. C. Martins, *Chem. Mater.* **2013**, *25*, 1211.

[41] I. Moreels, B. Fritzinger, J. C. Martins, Z. Hens, *J. Am. Chem. Soc.* **2008**, *130*, 15081.

[42] J. Aldana, Y. A. Wang, X. Peng, *J. Am. Chem. Soc.* **2001**, *123*, 8844.

[43] C. Pan, K. Pelzer, K. Philippot, B. Chaudret, F. Dassenoy, P. Lecante, M.-J. Casanove, *J. Am. Chem. Soc.* **2001**, *123*, 7584.

[44] M. J. Hostetler, J. E. Wingate, C.-J. Zhong, J. E. Harris, R. W. Vachet, M. R. Clark, J. D. Londono, S. J. Green, J. J. Stokes, G. D. Wignall, *Langmuir* **1998**, *14*, 17.

[45] L. Qu, X. Peng, *J. Am. Chem. Soc.* **2002**, *124*, 2049.

[46] M. A. Hines, P. Guyot-Sionnest, *J. Phys. Chem. B* **1998**, *102*, 3655.

[47] D. V. Talapin, S. Haubold, A. L. Rogach, A. Kornowski, M. Haase, H. Weller, *J. Phys. Chem. B* **2001**, *105*, 2260.

[48] Q. Peng, J. Gan, S. Wang, L. Kong, G. Chen, Y. Yang, G. Huang, *Ind. Eng. Chem. Res.* **2013**, *52*, 7713.

[49] X. Peng, M. C. Schlamp, A. V. Kadavanich, A. P. Alivisatos, *J. Am. Chem. Soc.* **1997**, *119*, 7019.

[50] N. Pradhan, D. Reifsnyder, R. Xie, J. Aldana, X. Peng, *J. Am. Chem. Soc.* **2007**, *129*, 9500.

[51] J. Joo, H. B. Na, T. Yu, J. H. Yu, Y. W. Kim, F. Wu, J. Z. Zhang, T. Hyeon, *J. Am. Chem. Soc.* **2003**, *125*, 11100.

[52] H. Liu, J. S. Owen, A. P. Alivisatos, *J. Am. Chem. Soc.* **2007**, *129*, 305.

[53] L. R. Becerra, C. B. Murray, R. G. Griffin, M. G. Bawendi, *J. Chem. Phys.* **1994**, *100*, 3297.

[54] J. Jasieniak, P. Mulvaney, *J. Am. Chem. Soc.* **2007**, *129*, 2841.

[55] G. Rafeletos, S. Nørager, P. O'Brien, *J. Mater. Chem.* **2001**, *11*, 2542.

[56] W. D. Kim, J.-H. Kim, S. Lee, S. Lee, J. Y. Woo, K. Lee, W.-S. Chae, S. Jeong, W. K. Bae, J. A. McGuire, *Chem. Mater.* **2016**, *28*, 962.

Chapter 7

Cu Doping in Ligand Free CdS Quantum Dots: Conductivity Study

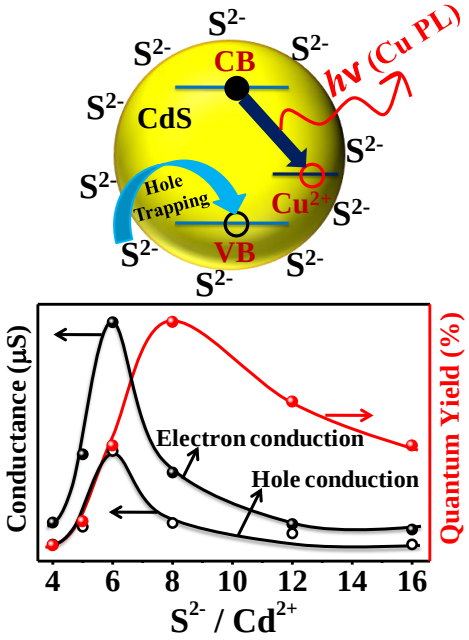

The following papers have been published based on work presented here:

G Krishnamurthy Grandhi, K. Swathi, K.S. Narayan and R. Viswanatha. Cu Doping in Ligand Free CdS Nanocrystals: Conductivity and Electronic Structure Study. *J. Phys. Chem. Lett.* **2014**, 5, 2382.

7.1. Abstract:

Ligand free Cu doped CdS QDs have been synthesized to elucidate their surface electronic structure. The Cu doped ligand free QDs unlike their undoped counterparts are shown to be luminescent. We used this Cu related emission as a probe to study the nature of the surface trap states that results in negligible luminescence in the undoped QDs. The concentration of the sulfide ligands is shown to play a crucial role in the surface passivation of the QDs. Electrical conductivity of these QDs was also studied and they were shown to exhibit significant conductivity of ~10^{-4} S cm^{-1}. Further, we have shown that the electrical conductivity is closely correlated to the surface charge and hence the trap states of the individual QDs that has far-reaching consequences in the device optimization.

7.2. Introduction:

Research on colloidal QDs has taken center stage for the past several decades mainly due to its potential as active materials in several applications.[1-4] However, in the recent past, it has been noticed that these QDs are typically poor conductors due to the presence of insulating organic capping layer surrounding the QDs.[5] This prevents electronic communication between the QDs creating a bottle-neck in improving the efficiency of several applications. Wide-range of studies are underway to resolve this problem without affecting the opto-electronic properties of the individual QDs that can be altered as a consequence of changed size, shape and/or crystal structure of these materials. One of the first studies in this direction showed that the conductivity of these QDs improved by 12 orders of magnitude by replacing the capped TOPO/TOP with small molecules like pyridine and the 1,4-phenylenediamine as linker molecules[6] or by treating the CdSe QD films with NaOH.[7] This was later followed up by several experimental[8] and theoretical[9] groups using short conducting inorganic moieties[10-18] to improve and optimize the conductivity and mobility of these inorganic QDs. These improved conductivities opens up possibilities for applications like field effect transistors with high on/off ratios,[12] photodetectors with very sensitive detectivity,[13] boost in efficiency of the solar cells[19] and improvement of the solar power conversion efficiency.[20] However, while the exchange of organic capping layer with inorganic moieties have demonstrated excellent improvements in inter-particle communication as observed through conductivity and mobility, little is known regarding the consequences of this exchange on the

properties of individual QDs. For example, only recently, it was observed that the nature of the surface of the QDs,[19, 21] specifically that of surface traps, induced decay of optical properties in presence of inorganic ligands. The knowledge of surface trap states is not only important for optimizing the optical properties, but their effect on the conductivity of QD films is also well known.[11, 22] So, a simple method to study the role of these inorganic ligands in passivating the surface and stabilizing these QDs would lead to a rational optimization of devices in a multi-dimensional space. Study of the role of passivating ligands, though recognized as highly important, is relatively sparse[23, 24] and not well understood across a broad range of ligands and host materials. This is further complicated by the fact that the same ligand performs different functions in different host materials as shown in **Chapter 6**. Fortunately, with the understanding of the mechanism of Cu emission[25] in II-VI semiconductors, it has been shown in **Chapter 6** that Cu can be used as an internal probe to understand the role of ligands in passivating the surface of the QDs. The mechanism of Cu emission is summarized in scheme 7.1. Briefly, the QY of the Cu emission is enhanced with increasing number of the hole traps and the average lifetime decreases with increasing number of electron traps. However, this technique is viable only if one observes the Cu emission in these QDs. It is well known that in these ligand free QDs, though the conductivity goes up, the optical response is negligible. This could be either due to the presence of a large number electron trap states or hole trap states or both.

In this chapter, we discuss the synthesis and characterization of Cu doped ligand-free CdS and $Cd_xZn_{1-x}S$ QDs for the first time that also shows a weak Cu related luminescence. Further we also study the role of sulfide ions and the counter ions on the surface of the QDs using ζ-potential, steady state and TrPL. While the conductivity of a few materials like PbSe (10^{-2} S cm^{-1}),[10] PbS ($8*10^{-4}$ S cm^{-1})[10] and CdSe (10^{-2} S cm^{-1})[6, 7] are well studied, CdS QDs are largely unexplored. We have studied the conductivity of Cu doped CdS QDs as a function of varying sulfide ion concentration and correlate the results with that obtained from the passivation studies. Further, with a conductivity of ~ 10^{-4} S cm^{-1} and minimal hysteresis of the I-V curves, necessary to prevent additional energy loss in FETs and integrated circuits, to the best of our knowledge, we report highest conductivity so far reported for CdS QD films and comparable to CdSe[6] and PbS[10] QD films where the conductivity reaches ~ 10^{-2} S cm^{-1} when they are capped with small molecules.

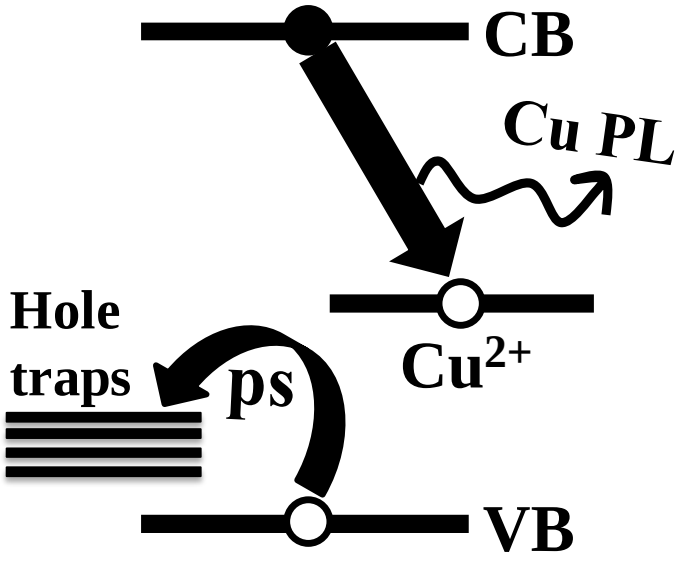

Scheme 7.1. *The mechanism of the Cu emission and the alignment of the Cu dopant level with respect to the VB and CB of the host CdS QDs.*

7.3. Experimental section:

7.3.1. Materials:

$3CdSO_4.8H_2O$, $ZnSO_4.7H_2O$, $CuCl_2.2H_2O$ and Formamide (AR grade), were purchased from SD Fine chemicals limited. Acetone (AR Grade) was purchased from Merck and $(NH_4)_2S$ was purchased from Sigma-Aldrich. All the chemicals were used without any further purification.

7.3.2. Synthesis of Cu doped ligand free CdS and $Cd_xZn_{1-x}S$ QDs:

Cu doped ligand free CdS and $Cd_xZn_{1-x}S$ QDs were prepared by modified method reported in literature.[26] $3CdSO_4.8H_2O$ and $ZnSO_4.7H_2O$ totaling to 0.2 mmol with various proportions of Cd^{2+} and Zn^{2+} and $CuCl_2.2H_2O$ (1-6 µmol) are degassed in formamide at 80 ^oC for 15 minutes. After 15 minutes, $(NH_4)_2S$ (0.8 – 1.6 mmoles) was added to this mixture and kept at 80 ^oC for 5 minutes to give Cu doped $Cd_xZn_{1-x}S$ QDs with varying sulfide concentration in the QDs. The samples were washed with the formamide/acetone mixture and then preserved in formamide or water.

7.3.3. Conductivity measurements: For the planar device fabrication, aluminum/gold (with 5 nm chromium adhesion layer) were coated as electrodes by the standard physical vapor

deposition technique at a base pressure of 10^{-6} mbar on precleaned glass substrates. The resulting thickness and width of the electrodes are 100 nm and 4 mm, respectively, separated by a channel of 70 μm length. For the sandwich structure, a 50 nm PEDOT: PSS layer was spin-coated on precleaned ITO-coated glass substrates at 4000 rpm for 1 min and annealed at 110 °C for 15 min. In both the device structures, the solution containing QDs dispersed in formamide was then drop casted and heated on a hot plate at 80 °C for 1 h to evaporate the solvent. The sample thickness was maintained at 2 μm with a variation of ±0.5 μm between samples. I(V) was obtained by studying more than five samples for each ratio of S^{2-}/Cd^{2+} QDs. I(V) measurements for all the devices were done in an inert atmosphere in dark using a 4200 semiconductor parameter analyzer. Photocurrent measurements were performed using the setup described in the literature.[27]

7.4. Results and discussion:

Ligand free CdS QDs were synthesized using $CdSO_4$ and $(NH_4)_2S$ as precursors and formamide as the solvent. The detailed synthesis procedure is discussed in the experimental section. Similar to the earlier reported literature,[26] we observe that excess sulfide is necessary to prevent the agglomeration of the QDs. The absorption and emission spectra show the presence of a band gap corresponding to the CdS QDs and the absence of band edge emission (Figure 7.1(a)), as observed in earlier literature.[26] ζ-potential measurements shown in Figure 7.1b clearly show a peak at negative voltage that is a consequence of the negatively charged surface due to the high percentage of sulfide ions. The negatively charged surface helps the QDs in repelling with each other with electrostatic force leading to colloidal stability of these QDs in highly polar solvents like water, formamide and N-methyl formamide. It is evident from earlier literature[26] and the current work that the excess sulfide ions play an important role in preventing agglomeration and stabilizing these QD surfaces. However, the exact mechanism of this stabilization has not yet been understood. In order to understand that, we synthesized (discussed in experimental section) Cu doped all-inorganic CdS by adding a small percentage of Cu salt during the synthesis. The presence of Cu in the QDs was confirmed from elemental analysis using ICP-OES. These results established that the Cu dopant concentration is about 0.5% ± 0.2% in these QDs. Detailed values for various synthesis are tabulated in Table 7.1.

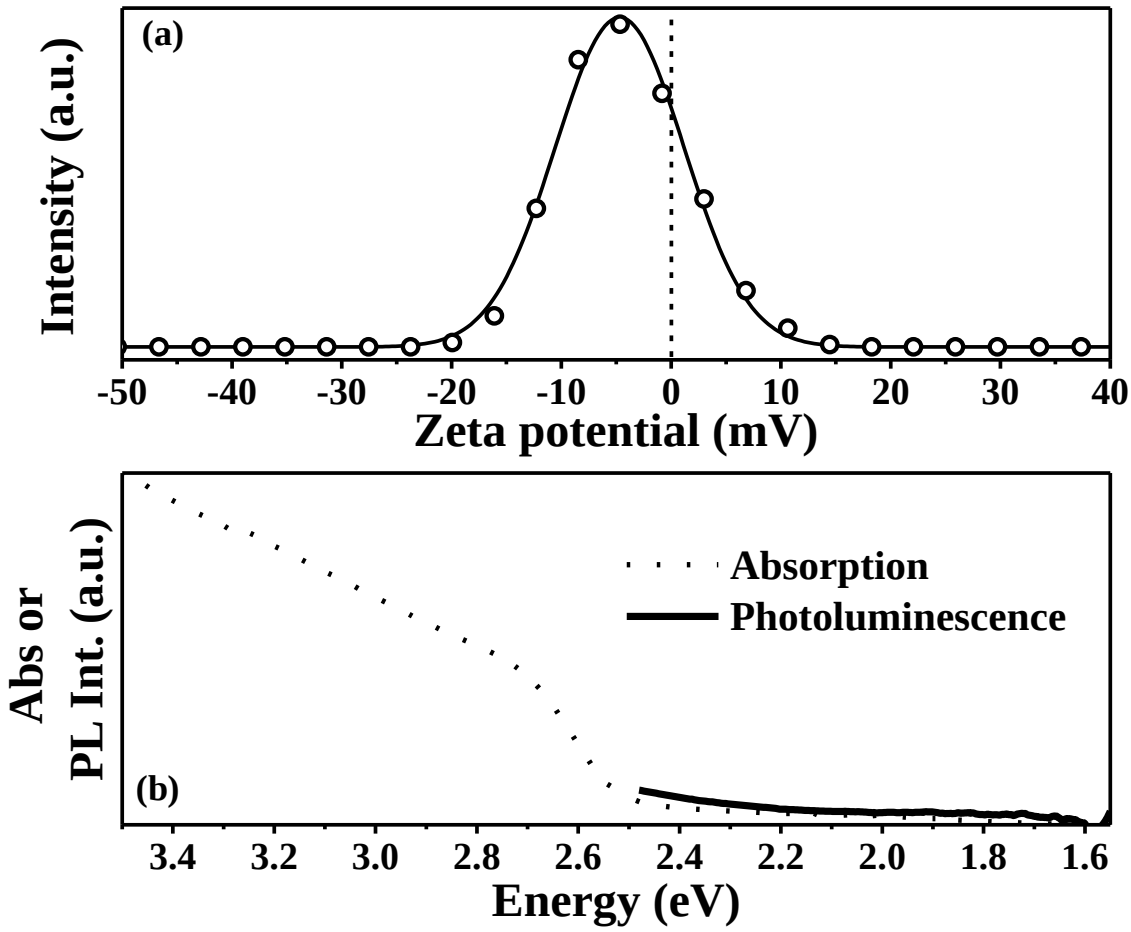

Figure 7.1. (a) *The ζ–potential curve of the undoped ligand free CdS QDs and* ***(b)*** *the corresponding absorption and PL spectra.*

Table 7.1. *The elemental analysis (ICP-OES) data for the ligand free Cu doped CdS with varying sulfide concentration.*

S^{2-}/Cd^{2+}	% Cu
4	0.4
5	0.5
6	0.7
8	0.4
12	0.4
16	0.5

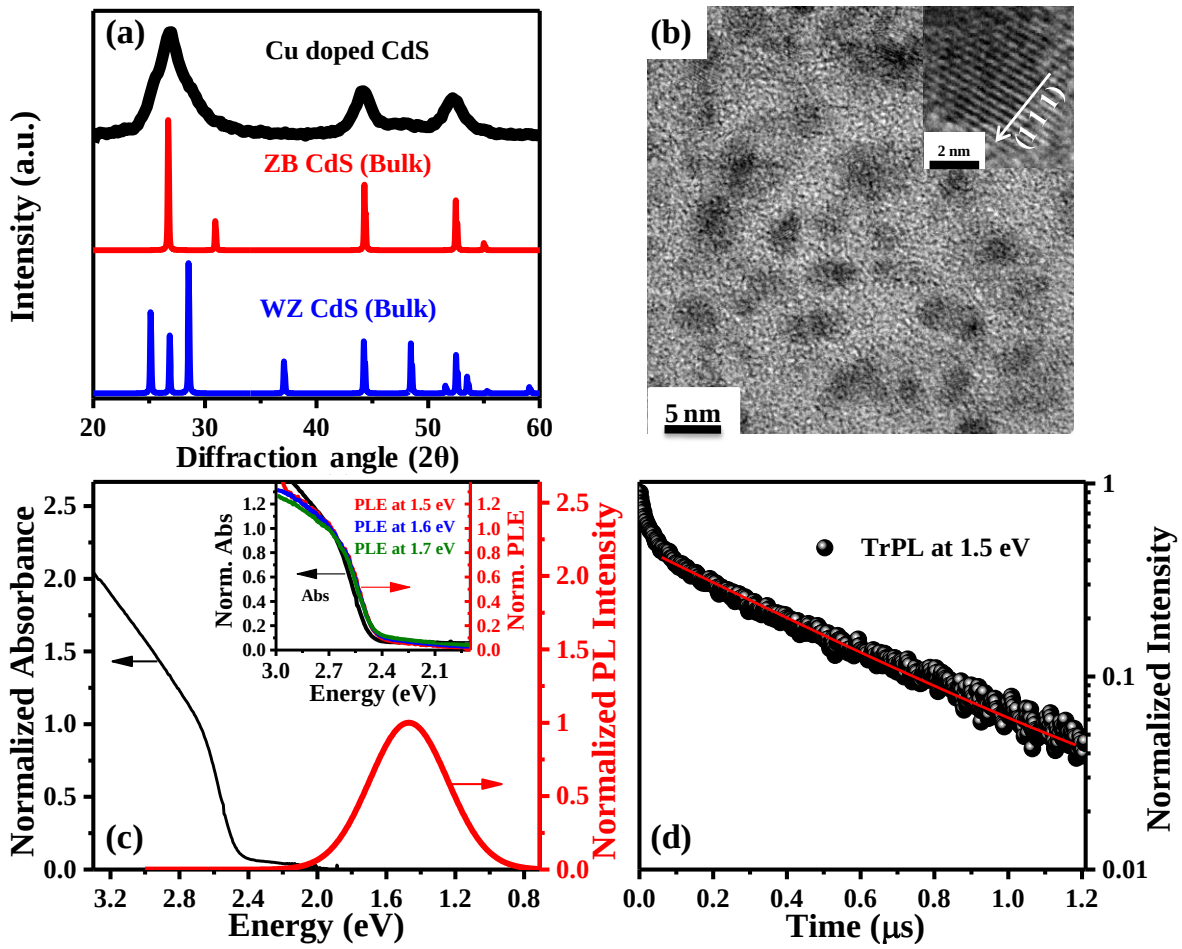

Figure 7.2. *Characterization of 0.5 % Cu doped ligand free CdS QDs.* ***(a)*** *XRD pattern of the QDs in comparison with the bulk CdS. 2θ is the diffraction angle.* ***(b)*** *TEM image of the QDs with an inset of the corresponding high resolution image in the (1 1 1) direction.* ***(c)*** *The normalized absorption and steady state PL (λ_{ex} = 405 nm (3.06 eV)) of the QDs. The inset shows the comparison of the absorption spectrum with the PLE spectra (collected at 1.5 eV, 1.6 eV and 1.7 eV).* ***(d)*** *TrPL spectrum was collected at Cu emission (1.5 eV) with the λ_{ex} of 405 nm (3.06 eV).*

Typical XRD pattern of the Cu doped CdS QDs shown in Figure 7.2(a) along with cubic and wurtzite bulk CdS patterns demonstrates the formation of zinc-blende CdS QDs. TEM image shown in Figure 7.2(b) and the high-resolution image of the same (inset of Figure 7.2(b)) indicate the formation of 4-5 nm sized particles with a broad size distribution that is not surprising in the absence of any ligands. The broad size distribution is further demonstrated by the presence of a broad absorption feature in Figure 7.2(c). The steady state PL (Figure 7.2(c)) shows that even though the undoped dots were non-luminescent, the Cu doped QDs indeed have luminescence that is very broad and highly red-shifted compared to the band edge emission. The origin of this emission band has been shown in earlier literature[25, 28-30] to arise

from the transition of the electron from the CB edge to the Cu *d* state. The long lifetime decay plots obtained from TrPL are shown in Figure 7.2(d) as well as unchanged PL excitation data taken at various points on the emission peak (inset to Figure 7.2(c)) further confirms that the PL is indeed from Cu emission and not from the surface trap states or due to the broad size distribution.

The most compelling evidence for the origin of this emission peak arises from the energy tuning of the Cu related emission. Cu related emission arises from the transition of the electron from the CB to the Cu *d* level and can be tuned by either altering the size of the host QDs or by modifying the composition of the material. Owing to ligand-free nature of the synthesis, it is non-trivial to control the size of these QDs. Hence, we synthesized Cu doped alloy of $CdxZn_{1-x}S$ QDs in a similar ligand-free synthesis by the introduction of appropriate amount of $ZnSO_4$ during the synthesis. ICP-OES measurements were performed on the purified samples and we find that the Zn/Cd ratio incorporated in these QDs was smaller than their stoichiometric amount as shown in Table 7.2. However, it is also evident that substantial percentage of Zn was incorporated into the QDs starting from 10% to 85%. The shift in the XRD peaks (shown in Figure 7.3(a)) for the various compositions also clearly demonstrate the formation of $Cd_xZn_{1-x}S$ alloy QDs. The alloy formation is further supported by the other characterizations shown in Figure 7.3. Figure 7.3(b) shows a TEM image of Cu doped $Cd_{0.6}Zn_{0.4}S$ QDs with an inset of high resolution TEM image revealing the formation of crystalline QDs with reasonable size distribution. The SAED shown in Figure 7.4 further exposes the crystalline nature of the QDs. The most important point of introducing Zn in CdS was to study the PL characteristics of these materials and obtain the nature of this emission peak.

Table 7.2. *The elemental (ICP-OES) analysis data for the Cu doped $Cd_XZn_{1-X}S$ alloy QDs.*

Sample	**% Zn (stoichiometric amount)**	**% Zn (ICP)**
CdS	0	0
$Cd_{0.9}Zn_{0.1}S$	25	10
$Cd_{0.8}Zn_{0.2}S$	50	20
$Cd_{0.6}Zn_{0.4}S$	75	40
$Cd_{0.3}Zn_{0.7}S$	90	70
$Cd_{0.15}Zn_{0.85}S$	95	85

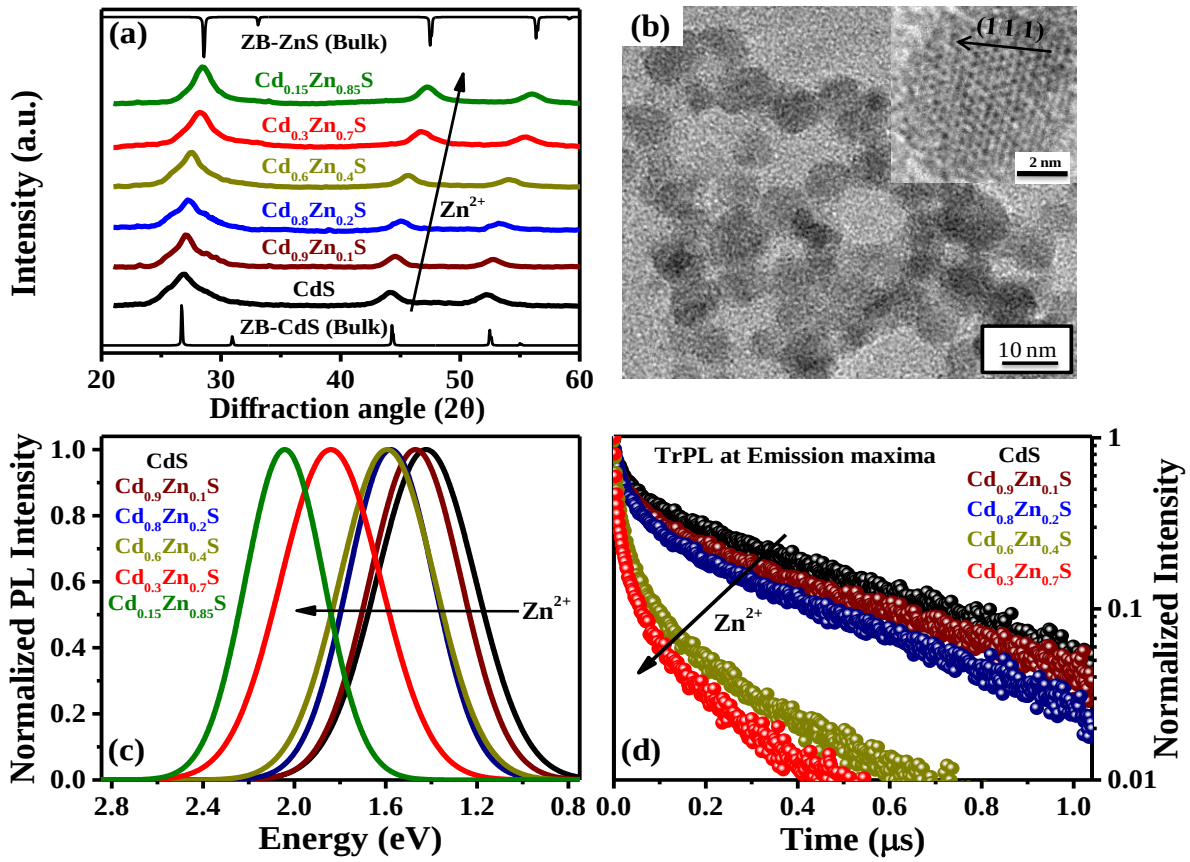

Figure 7.3. *Characterization of Cu doped ligand free alloy $Cd_xZn_{1-x}S$ QDs.* ***(a)*** *XRD pattern at different proportions of cadmium and zinc in comparison with the bulk data. 2θ is diffraction angle.* ***(b)*** *TEM image of Cu doped $Cd_{0.6}Zn_{0.4}S$ and the corresponding HRTEM image along (1,1,1) direction in the inset.* ***(c)*** *The normalized PL spectra (λ_{ex} = 405 nm (3.06 eV)) corresponding to different ratio of cadmium to zinc in the alloy and* ***(d)*** *their corresponding TrPL spectra were collected at PL emission maxima with the λ_{ex} of 405 nm (3.06 eV). Here, S^{2-} / C^{2+} = 6, C^{2+} = Cd^{2+} + Zn^{2+}.*

Figure 7.3(c) shows the PL spectra of Cu doped $Cd_xZn_{1-x}S$ QDs in formamide. The Cu related emission is gradually blue-shifted with increase in the Zn/Cd ratio in the alloy due to the increase in the bandgap of the material with increasing ZnS nature.[29] The corresponding lifetime data are also shown in the Figure 7.3(d) shows a long lifetime for this emission as expected for the Cu related emission. More importantly, it has been observed earlier that the lifetime of this Cu related emission in $Cd_xZn_{1-x}S$ alloy QDs decreases at higher zinc compositions.[29] Here we observe that as the composition approaches the ZnS end, the lifetime of Cu related emission indeed decreases further proving that this is indeed due to the Cu and not due to surface states.

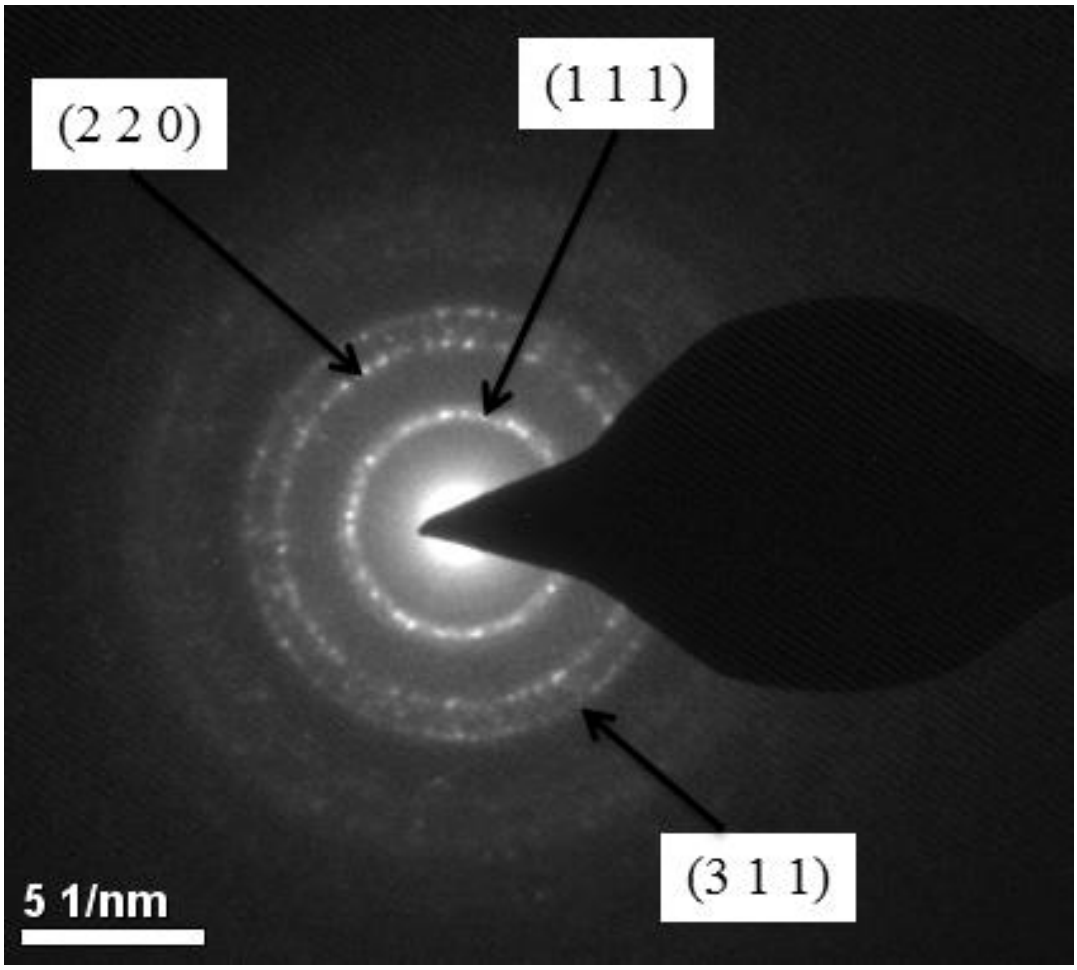

Figure 7.4. *The SAED pattern for the Cu doped ligand free $Cd_{0.6}Zn_{0.4}S$ QDs.*

However, it is interesting to note that these QDs, similar to the undoped ligand free CdS QDs[26] cannot be stabilized with stoichiometric concentrations of cadmium and sulfide ions. In fact, one requires at least four times sulfide ion concentration compared to that of cadmium to stabilize these QDs and is more stable at higher sulfide ion concentration indicating that the negative sulfide ions, most likely act as ligands stabilizing the QD. However, if this is indeed true, one would observe that the surface is negatively charged. The charge on the QD surface can be directly studied using the ζ-potential measurements and can have indirect but substantial consequences on the PL intensity of the Cu related emission. The ζ-potential measurements for varying Cd to S ion ratio are shown in Figure 7.5(a). Not surprisingly, from the figure it is evident that the ζ-potential becomes more negative with increase in sulfide ion concentration from 1:4 to 1:8 and that the charge on the surface is

sufficiently large to prevent agglomeration due to electrostatic repulsion. However, as we go to higher sulfide ion concentration of 1:12, we observe that the charge on the surface decreases. This suggests that the nature of the surface turns more negative with increasing sulfide ion concentration till about 1:8 and when the surface is sufficiently passivated, instead of increasing the charge on the individual QD, forms a shielding layer.[31] This shield could eventually block the contact to the QDs thus affecting the conductivity of the material. Hence it is important to study the exact role of the excess anions in the synthesis of ligand free QDs.

The study of role of ligands on the nature of the surface has been recently proposed by the introduction of Cu as an internal probe as shown in **Chapter 6**. This study correlates the surface properties to the extent of electron and hole traps and hence predicts their consequences on the conductivity of the QDs. Briefly, the Cu related emission originates from the recombination of the photo-excited electron with the optically active hole present on the Cu site and does not require the photo-excited hole.[25] In fact, due to the long lifetime of the Cu related emission it can only be observed in presence of hole traps and the PL QY increases with increase in hole traps. Similarly, in the current case, it is interesting to note that in spite of the fact that undoped particles do not fluoresce, the Cu doped QDs show a weak fluorescence. The presence of Cu related emission even though the band edge emission is absent indicates that the excess sulfide ions preferentially create more hole traps than the electron traps. This is reasonable given that the surface of the QDs is negatively charged and preferentially draws the photo-excited hole towards them. Figure 7.5(b) shows the variation of the Cu related emission for various sulfide ion concentrations. It is intriguing to note that PL peak is slightly redshifted with increasing anion ratio. This could arise due to three leading causes or a combination of these causes. In the ligand free synthesis, the size of the QD is not really controlled. So, it is possible that there could be some shift due to small changes in size. In addition, it is also known in literature that when a negative charge present on the QD surface, the electron or hole wave function may delocalize outside the QD surface.[32] This leads to a small red shift in both absorption and PL. The third factor relates to the number of ligands or the sulfide ions in the present case attached to the QD. Typical example in literature[33] relating to CdSe with thiol ligands have shown that both the absorption and PL gets red shifted with increasing number of ligands though the exact mechanism is not clear.

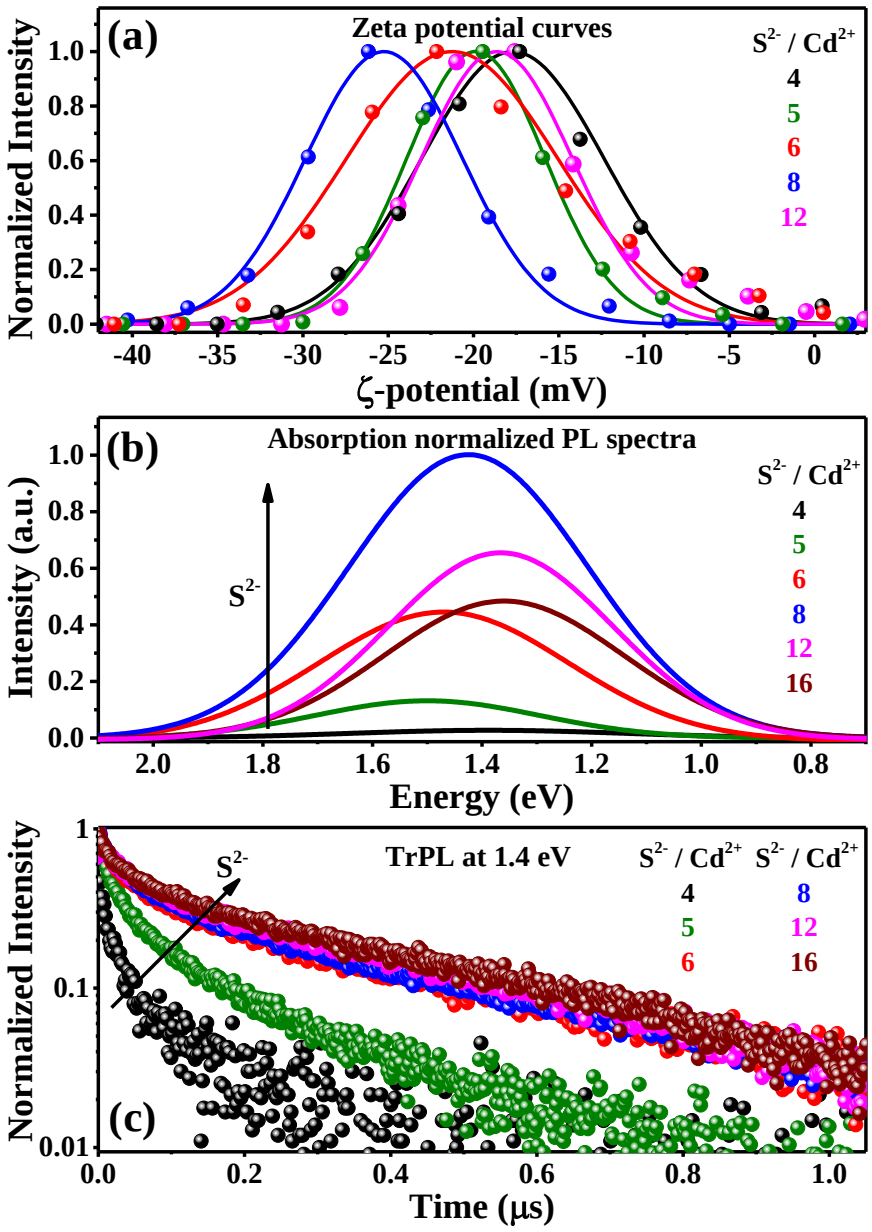

Figure 7.5. (a) *The ζ-potential curves,* ***(b)*** *absorption normalized steady state PL spectra (λ_{ex} = 405 nm (3.06 eV)) and* ***(c)*** *TrPL spectra of 0.5 % Cu doped ligand free CdS QDs with increasing sulfide concentration (1:4 to 1:16) were collected at Cu emission (1.4 eV) with the λ_{ex} of 405 nm (3.06 eV).*

However, it has to be noted that the QY of the Cu related emission is quite low (~ 6%) compared to that of oleate capped CdS QDs (~ 40%) as observed in **Chapter 6**. This points to the fact that a large number of electron traps are also formed during the synthesis of these QDs. Since Cu related emission in these doped QDs requires only a photo-generated electron, the non-radiative component of emission decay arises entirely due to the presence of electron traps

and hence the percentage of electron traps in Cu doped QDs is manifested as the fast component in the lifetime dynamics of the Cu related emission. Consequently, the average lifetime can be used as a marker to quantify of electron traps present in the QDs. A study of the lifetime decay of the Cu related emission for various sulfide ion concentrations are shown in Figure 7.5(c). From the figure, it is apparent that the average lifetime increases till about 1:6 ratio of Cd to S and remains constant thereafter suggesting that the number of electron traps do not decrease beyond the ratio of 1:6.

A comprehensive overview of the results can be obtained by analyzing the surface trap states as seen from TrPL and steady state fluorescence of the Cu emission and the surface charge as obtained from ζ–potential measurements and contrasting the same with the conductivity measurements. We observe that a minimum of 1:4 excess negative ions are needed to stabilize the surface of the QDs. Further with increase upto 1:6 ratio of Cd to S, we observe a decrease in the electron traps and an increase in hole traps suggesting that the excess sulfide ions are involved in passivating and stabilizing the surface. Additional increase in the sulfide ion concentration results in only a slight increase in the number of hole traps and then a decrease thereafter with no change in the amount of electron traps. This suggests that the excess sulfide ions are now not involved in passivating the surface and hence forming just a negative ion layer around the surface of the QDs. Even though the nature of the probe is indirect, the consequences of this study can be directly reflected in the conductivity of the QDs.

The electrical measurements performed on these samples are shown in Figure 7.6. Figure 7.6(a) shows the I-V characteristics of the QDs with varying sulfide ion concentration. I (V) measurements were done using two types of injecting contacts, gold (work function of 5.1 eV) and aluminum (work function of 4.2 eV) in the planar geometry. The conductance in Al contact devices is marginally higher than the Au contact devices. The electrode materials were chosen so as to align their work functions with the band positions of the QDs. For example, Al poses no barrier for electron transport as it is aligned close to the CB of the QDs. This can be seen from the ohmic nature of the I(V) curves for sulfide concentrations upto 1:8. This contrasts with the super linear behavior and lower values of current in Au devices where it is injection limited due to possible sources such as misalignment of the electrode work function with the QD VB energy levels.

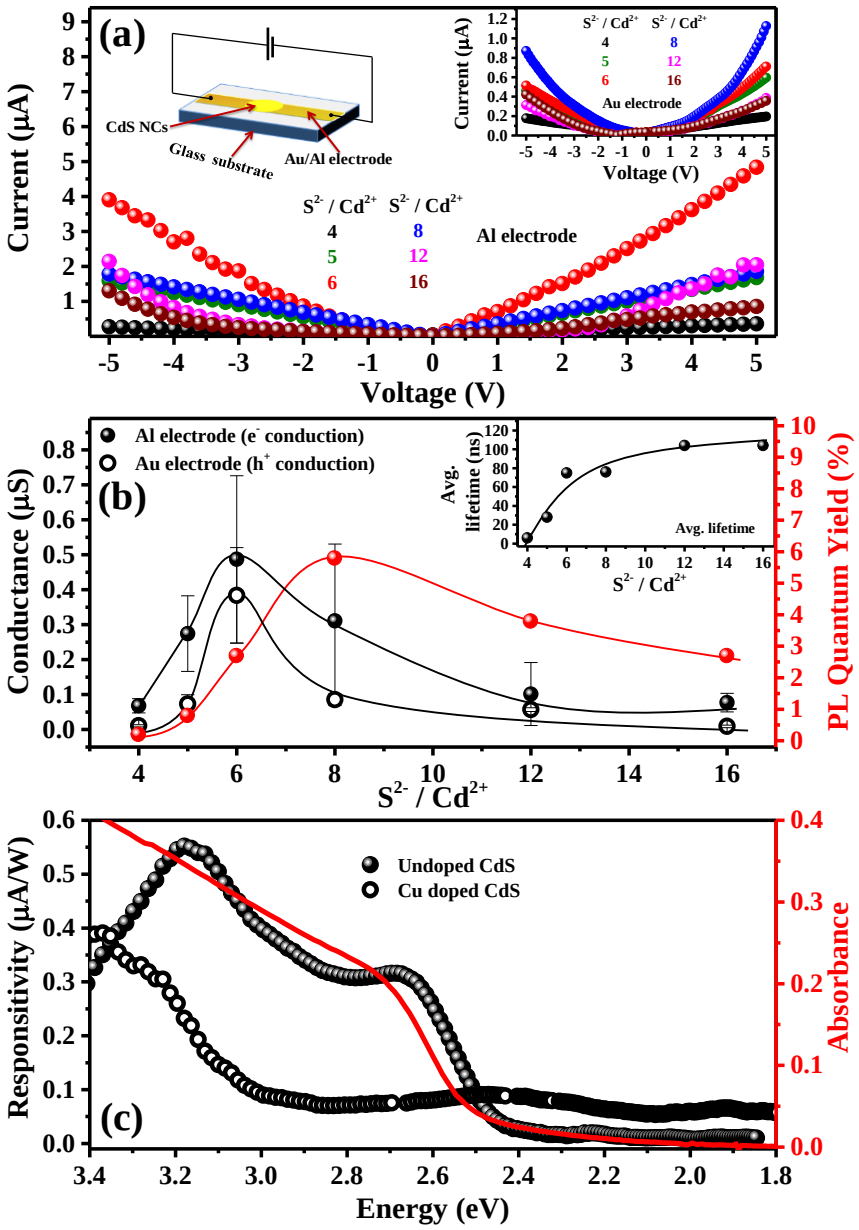

Figure 7.6. (a) *The I(V) characteristics of the 0.5 % Cu doped QDs with varying sulfide ion concentrations with respect to the Al electrode and the corresponding I-V characteristics with respect to the Au electrode (inset). The schematic of the device used for the measurement of I-V characteristics is also shown in the inset. The inter electrode distance was kept at 70 μm with the electrode width of 4 mm and the typical sample thickness of 2 μm.* ***(b)*** *The corresponding variation of conductance (black spheres and circles) and PL QY (red spheres) for varying S^{2-} to Cd^{2+} ratio. The corresponding variation of the average lifetime is shown in the inset.* ***(c)*** *shows the intensity modulated spectral photocurrent response of a sandwich device structure ITO|PEDOT:PSS|CdS|Al at two bias voltages (+10 V for Cu doped samples and +5 V for undoped samples) and modulation frequency of 70 Hz, with active layer thickness ~ 2 μm. Also shown is the absorbance of the CdS QDs. Absorption spectrum and PL QY were measured in water*

The I(V) responses directly measure the conductance of Cu doped CdS QDs and the variation in conductance for different S^{2-} to Cd^{2+} ratio for both types of carrier injection is shown in Figure 7.6(b). Here it has to be noted that the conductance with either electrodes is higher by nearly five orders of magnitude compared to the oleate capped CdS QDs (Figure 7.7). This is expected since the oleate capped QDs have long chain non-conducting molecules attached to the QD surface which reduces the electronic coupling between two QDs leading to lower conductance. In addition, though the electron and hole conductance increases with increase in S^{2-} to Cd^{2+} ratio initially, the transport mechanisms are quite different. Presence of excess anion is known to result in non-stoichiometric QDs and manifests as gap states close to the VB of the QD.[34] This results in p-doping which leads to an initial increase in hole conductance as the sulfide ion concentration is increased. Increase in electron conductance is indicative of the decrease in the number of Cd^{2+} sites (electron-traps) on the QD surface with increasing anion concentration. However, it is important to note that changing the stoichiometry of the sulfide with respect to the cadmium will lead to n-type behavior in the semiconductor. As the Fermi level is increased and the introduction of the dopant, a set of extended band-tail states and deeper localized states are created leading to a possibility of Anderson-type transition.[35-38] However, the CdS (S^{2-}) (with about 0.5% Cu doping) QDs represent a class of highly disordered solids where both the E_{fermi} position and the extent of disorder is controlled by the relative proportions of S^{2-} and Cu content. As the sulfide content is increased, a spread in the QD size distribution is observed in the TEM images. In addition, it should be noted that the Fermi level lies in the localized region in these systems and hence the transport is dominated by hopping between energy levels at room temperature. Even though the Fermi level can move closer to the mobility edge by increasing the sulfide concentration, the electrostatic repulsive forces between sulfide ions on neighboring QDs is found to dominate. This in turn localizes the electron wave function as the distance between two QDs increases, leading to lower conductivity (Figure 7.6(b)). Hence it is unlikely to be an Anderson type transition. Nevertheless, conclusive proof of the same can be obtained by performing a temperature dependent electrical transport study as a function of dopant concentration. In any case, beyond a critical ratio of 1:6 Cd:S, the conductance drops, possibly due to decreased inter-particle connectivity arising from the increased electrostatic repulsion between sulfide ions of neighboring QDs. Also, in the presence of excess anions and their counter ions and

specifically in the present case of NH_4^+, a virtual capping layer can be formed with a shield of negative ions and their positive counter ions affecting the conductance.[31, 39]

Also, shown in Figure 7.6(b) is the increase in PL QY of the Cu related emission and the average lifetime of the same, essentially reflecting the number of hole and electron traps respectively. From the figure, we can see that the average lifetime saturation occurs at the same anion concentration as that of the peak of conductance indicating the decrease in number of electron traps up to 1:6 ratio of Cd:S. This observation is in concurrence with the earlier conclusion obtained from PL and I-V data that the excess anions are involved in passivating the surface until a concentration of 1:6 and thereafter starts forming an ion shield in the presence of excess anions. The formation of ion shield is also clearly reflected in the PL QY, though at slightly higher ratio as seen from the figure. This could be reflective of the number of hole traps in the system and hence could be slightly higher. Thus, we have shown for the first time from these studies that the surface of the QDs can be studied using this novel new technique of Cu doping and that there exists a clear correlation between the surface passivation and transport properties such as conductivity.

Further in order to understand the nature of charge transport in these QDs, we have performed photoconductivity measurements that could give information on the majority carriers. Thick samples were used to ensure that the response is reflective of the photo-generated carriers in the bulk and with minimized interfacial contribution. A typical photocurrent response obtained for the device structure ITO|PEDOT-PSS|CdS|Al is shown in Figure 7.6(c). The prominent points to note in the photocurrent response are the following: A clear photocurrent with large signal to noise ratio (of the order of 20) and a spectral response similar to the absorption profile is observed in samples without Cu. The intensity dependence is clearly linear. This proposes a predominantly n-type transport in this system obtained from a simple estimate taking into account the absorption coefficient, the active layer thickness and the difference in bias polarity .[40, 41] In case of Cu-doped CdS, the photocurrent response is not as significant as the un-doped system. A spectral response of this device appears to suggest an antibatic response with a local maximum at the absorption edge. This response is suggestive of a possible dominant-hole transport in this system.[27, 40, 41] However, a careful thickness

dependence studies with appropriate buffer layers and electrodes will be necessary to ascertain this fact.

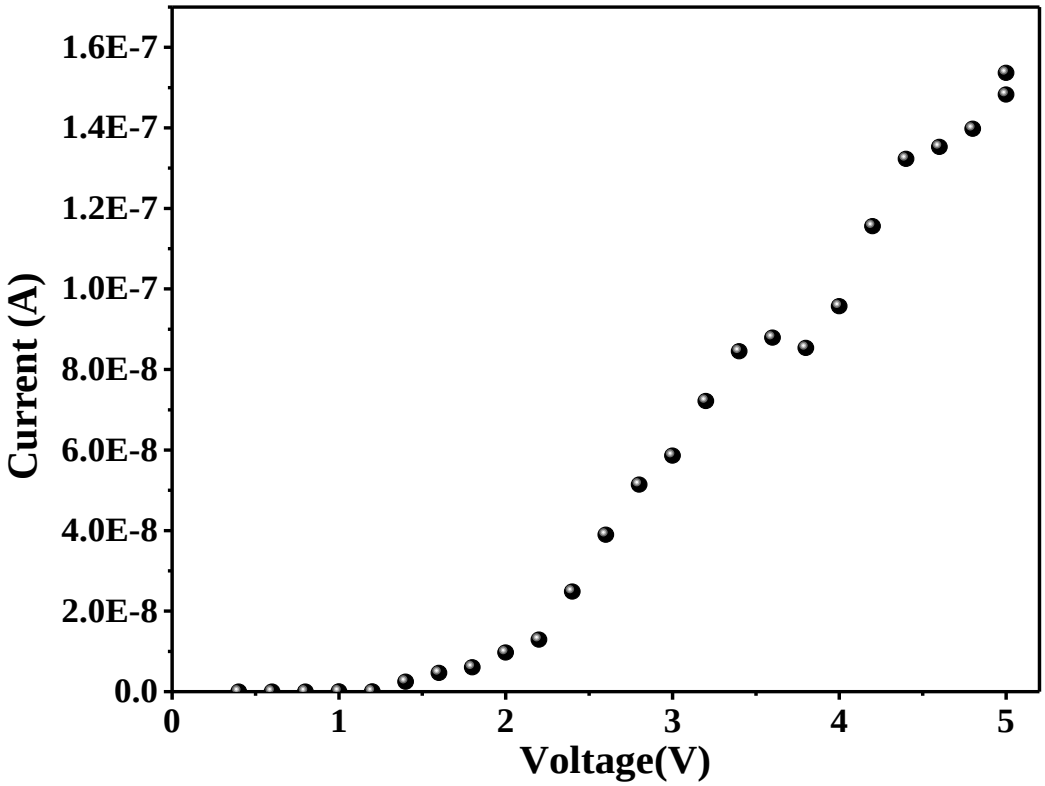

Figure 7.7*. The I-V characteristics of the oleate capped CdS QDs.*

7.5. Conclusions:

We have studied the ligand free or sulfide capped CdS as a model system to probe the role of inorganic ligands in passivation of the surface of the QDs by copper doping. Interestingly, we observed these Cu doped QDs are luminescent unlike the undoped QDs and that the sulfide ligands act as hole trapping agents on the QD surface. Further, we have shown that these QDs form good conducting films with conductivities of the order of 10^{-4} S cm^{-1}. We have studied the effect of sulfide ion concentration on the electrical properties of these QD films and found that an optimal concentration of ligands is required to get the best surface passivation that is also directly correlated with the efficiency of the electrical devices.

Bibliography:

[1] H. Zhong, Z. Bai, B. Zou, *J. Phys. Chem. Lett.* **2012**, *3*, 3167.

[2] P. V. Kamat, *J. Phys. Chem. Lett.* **2013**, *4*, 908.

[3] S. A. McDonald, G. Konstantatos, S. Zhang, P. W. Cyr, E. J. D. Klem, L. Levina, E. H. Sargent, *Nat. Mater.* **2005**, *4*, 138.

[4] Q. Sun, Y. A. Wang, L. S. Li, D. Wang, T. Zhu, J. Xu, C. Yang, Y. Li, *Nat. Photonics* **2007**, *1*, 717.

[5] N. Y. Morgan, C. A. Leatherdale, M. Drndic´, M. V. Jarosz, M. A. Kastner, M. Bawendi, *Phys. Rev. B* **2002**, *66*, 075339.

[6] D. Yu, C. Wang, P. Guyot-Sionnest, *Science* **2003**, *300*, 1277.

[7] D. Yu, B. L. Wehrenberg, P. Jha, J. Ma, P. Guyot-Sionnest, *J. Appl. Phys.* **2006**, *99*, 104315.

[8] Y. Liu, M. Gibbs, J. Puthussery, S. Gaik, R. Ihly, H. W. Hillhouse, M. Law, *Nano Lett.* **2010**, *10*, 1960.

[9] J. Lee, O. Choi, E. Sim, *J. Phys. Chem. Lett.* **2012**, *3*, 714.

[10] M. H. Zarghami, Y. Liu, M. Gibbs, E. Gebremichael, C. Webster, M. Law, *ACS Nano* **2010**, *4*, 2475.

[11] D. V. Talapin, C. B. Murray, *Science* **2005**, *310*, 86.

[12] D. S. Chung, J.-S. Lee, J. Huang, A. Nag, S. Ithurria, D. V. Talapin, *Nano Lett.* **2012**, *12*, 1813.

[13] J.-S. Lee, M. V. Kovalenko, J. Huang, D. S. Chung, D. V. Talapin, *Nat. Nanotechnol.* **2011**, *6*, 348.

[14] M. V. Kovalenko, M. Scheele, D. V. Talapin, *Science* **2009**, *324*, 1417.

[15] A. Nag, D. S. Chung, D. S. Dolzhnikov, N. M. Dimitrijevic, S. Chattopadhyay, T. Shibata, D. V. Talapin, *J. Am. Chem. Soc.* **2012**, *134*, 13604.

[16] J. S. Son, J.-S. Lee, E. V. Shevchenko, D. V. Talapin, *J. Phys. Chem. Lett.* **2013**, *4*, 1918.

[17] W. Liu, J.-S. Lee, D. V. Talapin, *J. Am. Chem. Soc.* **2013**, *135*, 1349.

[18] M. V. Kovalenko, M. I. Bodnarchuk, J. Zaumseil, J.-S. Lee, D. V. Talapin, *J. Am. Chem. Soc.* **2010**, *132*, 10085.

[19] C. E. Rowland, W. Liu, D. C. Hannah, M. K. Y. Chan, D. V. Talapin, R. D. Schaller, *ACS Nano* **2014**, *8*, 977.

[20] J. Tang, K. W. Kemp, S. Hoogland, K. S. Jeong, H. Liu, L. Levina, M. Furukawa, X. Wang, R. Debnath, D. Cha, *Nat. Mater.* **2011**, *10*, 765.

[21] A. A. Cordones, M. Scheele, A. P. Alivisatos, S. R. Leone, *J. Am. Chem. Soc.* **2012**, *134*, 18366.

[22] D. S. Ginger, N. C. Greenham, *J. Appl. Phys.* **2000**, *87*, 1361.

[23] X. Ji, D. Copenhaver, C. Sichmeller, X. Peng, *J. Am. Chem. Soc.* **2008**, *130*, 5726.

[24] N. Pradhan, D. Reifsnyder, R. Xie, J. Aldana, X. Peng, *J. Am. Chem. Soc.* **2007**, *129*, 9500.

[25] R. Viswanatha, S. Brovelli, A. Pandey, S. A. Crooker, V. I. Klimov, *Nano Lett.* **2011**, *11*, 4753.

[26] K. P. Kadlag, M. J. Rao, A. Nag, *J. Phys. Chem. Lett.* **2013**, *4*, 1676.

[27] K. S. Narayan, T. B. Singh, *Appl. Phys. Lett.* **1999**, *74*, 3456.

[28] N. S. Karan, D. D. Sarma, R. M. Kadam, N. Pradhan, *J. Phys. Chem. Lett.* **2010**, *1*, 2863.

[29] B. B. Srivastava, S. Jana, N. Pradhan, *J. Am. Chem. Soc.* **2011**, *133*, 1007.

[30] S. Brovelli, C. Galland, R. Viswanatha, V. I. Klimov, *Nano Lett.* **2012**, *12*, 4372.

[31] R. Viswanatha, H. Amenitsch, D. D. Sarma, *J. Am. Chem. Soc.* **2007**, *129*, 4470.

[32] M. T. Frederick, V. A. Amin, L. C. Cass, E. A. Weiss, *Nano Lett.* **2011**, *11*, 5455.

[33] R. Koole, B. Luigjes, M. Tachiya, R. Pool, T. J. H. Vlugt, C. de Mello Donegá, A. Meijerink, D. Vanmaekelbergh, *J. Phys. Chem. C* **2007**, *111*, 11208.

[34] D. Kim, D.-H. Kim, J.-H. Lee, J. C. Grossman, *Phys. Rev. Lett.* **2013**, *110*, 196802.

[35] D. V. Talapin, J.-S. Lee, M. V. Kovalenko, E. V. Shevchenko, *Chem. Rev.* **2009**, *110*, 389.

[36] D. l. Vanmaekelbergh, P. Liljeroth, *Chem. Soc. Rev.* **2005**, *34*, 299.

[37] A. Zabet-Khosousi, A.-A. Dhirani, *Chem. Rev.* **2008**, *108*, 4072.

[38] R. E. Chandler, A. J. Houtepen, J. Nelson, D. Vanmaekelbergh, *Phys. Rev. B* **2007**, *75*, 085325.

[39] P. K. Santra, S. Mukherjee, D. D. Sarma, *J. Phys. Chem. C* **2010**, *114*, 22113.

[40] M. G. Harrison, J. Grüner, G. C. W. Spencer, *Phys. Rev. B* **1997**, *55*, 7831.

[41] H. B. DeVore, *Phys. Rev.* **1956**, *102*, 86.

Chapter 8

Applications of Cu Doped Quantum Dots

Section I

Tunable Infrared Phosphors Using Cu Doping in Semiconductor Quantum Dots

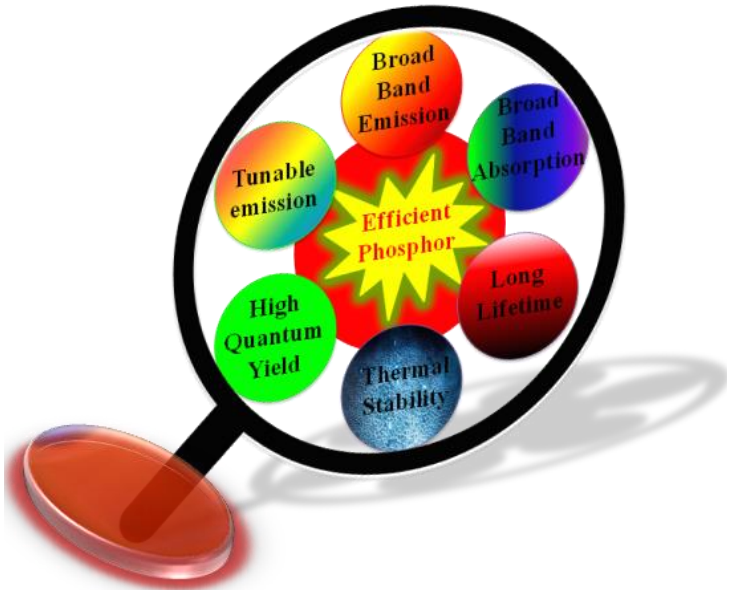

The following papers have been published based on work presented here:

G Krishnamurthy Grandhi and R. Viswanatha. Tunable Infrared Phosphors Using Cu Doping in Semiconductor Nanocrystals: Surface Electronic Structure Evaluation. *J. Phys. Chem. Lett.* **2013**, *4*, 409.

8.1. Abstract:

We show that Cu doped CdS QDs can be utilized as near infrared emitting phosphor material that have tunable, high QY (~35%) emission with a single exponential lifetime decay. Surprisingly, unlike the emission from other Cu doped II-VI QDs, emission from Cu doping in CdS QDs is found to exhibit high thermal stability, being essentially unchanged upto 100^0C, making them more viable for use in various practical applications.

8.2. Introduction:

The development of high QY NIR emitters has been highly sought-after for potential applications spanning the areas of optical amplifiers, biomarkers,[1] lasers, telecommunications, secure information display like military tagging, optoelectronics for long range transmission of remote control commands, passive heating and photovoltaic enhancement.[2] Recently, they have also been shown to improve the solar cell efficiency and have hence attracted attention for solar cell applications.[3, 4] So given the range of applications, it is not surprising that the development of high QY NIR phosphors have been extensively studied[5-10] in the recent years. Ideally, materials showing high efficiency, broadband emission with long lifetimes have been extensively investigated for tunable lasers and optical amplification as potential applications.[11] Recently IR materials consisting of lanthanide doped complexes,[8] organic donor acceptor molecules[6, 7] as well as conducting polymers[9] and inorganic semiconductor QDs[10] have been extensively investigated. However, lanthanides are known to be extremely expensive and hence phosphors based on these materials would not be cost effective. Though the luminescent QDs have a large advantage over organic polymers with regard to photostability as well as broad band absorption,[12] most of these materials including lanthanide doped QDs provide a narrow sharp emission peak and is thus non-trivial to obtain a large optical bandwidth even with a combination of dopants in the case of lanthanides or sizes in the case of semiconductor QDs. This disadvantage has been partially addressed by the use of type II core/shell semiconductors to obtain broad band Stokes' shifted emission with long lifetime.[13] However, it is well known that due to the poor spatial overlap, the QY of these QDs are quite low. Hence, the search for stable, tunable wide band emission with high QY and long lifetime, specifically in the NIR region is still a work in progress.

Recent attempts in this direction have focused on the down conversion of the emission into the NIR region and has been achieved by the introduction of atomic-like level in the mid band gap region by the use of dopant atoms.[12, 14-16] The additional intrinsic advantages of the transition metals doped QDs over the undoped QDs include insensitivity to thermal, chemical and photochemical disturbances. [12, 16] Specifically, the PL emission from Mn in doped QDs have been shown to be stable upon UV irradiation as well as on bubbling air into the solution.[16, 17] On the other hand, Cu doped QDs have revealed several advantages that cannot be achieved using Mn doped samples like tunable emission (from UV- IR region) with varying lifetimes. Nevertheless, similar photostability studies of Cu doping in ZnSe QDs have shown that even with specific overcoating of the host material on Cu doped QDs, this emission was barely stable in air at room temperature.[16] Hence it is evident that though Cu doped materials are an important class of semiconductors for application as phosphors, stability of this emission needs substantial improvement. Since then Cu doping of semiconducting QDs has been extensively explored in several recent reports[16, 18-22] including the use of ZnCdS alloy[21] or CdSe[23] as host materials to obtain upto about 750-800 nm emission. However, one of the key missing features in these reports is the tunability into the NIR region as well as a high QY and thermal stability that is desirable for various medical applications.[24] While the use of CdS as a host material due to the lower absolute energy of the conduction band edge would be a natural extension to extend the tunability into the NIR region, surface electronic studies in **Chapter 6** has shown that stabilizing and improving the QY of the Cu related emission is non-trivial. As explained in **Chapter 6**, Cu emission will be enhanced in presence of more hole traps and less electron traps. Using this information, we then use appropriate ligand concentration during the colloidal synthesis to create hole traps while passivating the electron traps on the surface of the QD leading to high QY and a nearly single exponential decay of the broad band emission arising from the transition of the electron from the conduction band of the host to that of Cu *d* level in the case of Cu doped CdS QDs to obtain high QY NIR emitting QDs with broad emission. Further, we also show that along with high QY, they also possess excellent thermal stability with stable emission upto fairly high temperatures for extended periods of time.

8.3. Experimental section:

8.3.1. Materials:

CdO, oleic Acid (90%), ODE (90%), and TOP (90%) and S powder were purchased from Sigma Aldrich. All purchased chemicals were used without further purification.

Copper stearate was synthesized and purified similar to the literature reports published previously.[18]

8.3.2. Synthesis of CdS and Cu doped CdS QDs:

CdS and Cu doped CdS QDs were synthesized by degassing a mixture of CdO (0.2 mmol), oleic acid (0.6-2.0 mmol) and ODE in a three-necked flask in vacuum and back-filling with Ar. To this solution, 0.1 mL of TOP was injected at 80 °C in an Ar atmosphere followed by the injection of 0.5 mL of 0.2 M S in ODE solution at 300 °C. This solution was immediately cooled down to 150 °C to avoid the further growth of CdS QDs. To this solution, 8 μmoles of copper stearate solution of ODE (1 mL) was added, and the reaction mixture was annealed for several hours to obtain the Cu doped CdS QDs. Samples were washed with a hexane/methanol mixture and precipitated using acetone.

8.4. Results and discussion:

Cu doped CdS QDs were synthesized using colloidal methods as discussed in detail in the experimental section. Briefly, the QDs were obtained by first synthesizing undoped QDs in presence of appropriate ligands at high temperature and cooling it down to about 150 ^{0}C before the addition of Cu precursor that was subsequently followed by the overcoating of the host semiconductor. The overcoating of the host semiconductor was carried out to overcome the challenge of inserting the dopant into core of the QD.[16] This was further verified by etching the obtained sample with a small amount of hydrogen peroxide and measuring the ICP-OES as well as the optical properties. ICP-OES measurements obtained after thorough washing of the QDs show that the ratio of Cu/Cd atoms has not changed drastically suggesting the presence of Cu in the interior of the QD.

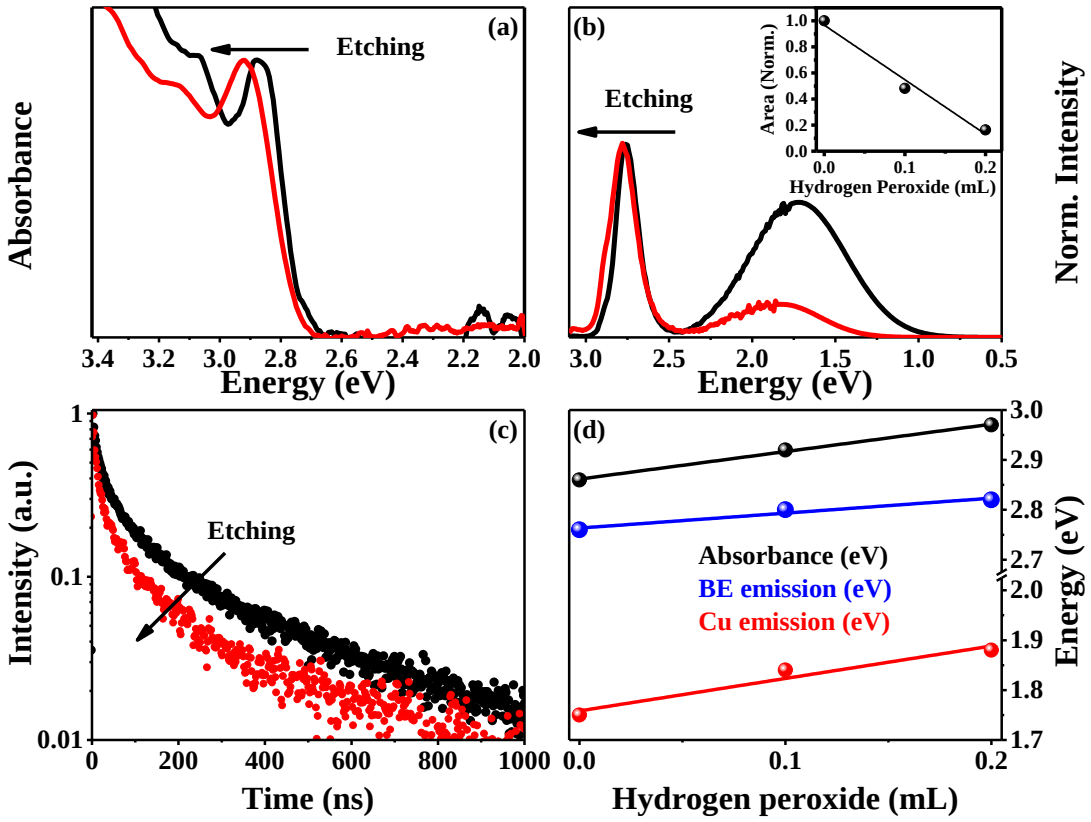

Figure 8.1. *Absorption, Steady state PL Spectra and TrPL Spectra of Cu doped CdS QDs before and after the etching experiment using Hydrogen Peroxide.*

Further, the location of the Cu in these doped QDs was obtained using controlled etching of the surface of the QDs using hydrogen peroxide. 2 mmol of hydrogen peroxide was slowly added to 10^{-5} mmol of Cu doped CdS QDs in hexane solution. The absorption spectra (shown in Figure 8.1(a)) obtained before and after the addition of hydrogen peroxide clearly shows a blue shift of the absorption spectra suggesting that the size of the QDs has decreased. However, the steady state and TrPL Spectra (Figures 8.1(b) and 8.1(c)) shows the presence of Cu related emission in the sample even after the etching of the surface of the QD, though slightly blue shifted due to smaller crystallite size. The shift in the energy of the absorption, band edge emission and Cu related emission upon addition of hydrogen peroxide is shown in Figure 8.1(d). Since the Cu emission is sensitive to the surface of the QD, the emission intensity decays more rapidly with the addition of etching agent as observed in Figure 8.1(b). Additionally, the increase in the fast component as seen from the TrPL data (Figure 8.1(c)) on etching the surface of QD and decrease in the QY of the QDs (inset to Fig. 8.1(b)) indicates the increase in trap states on the surface of the QD. Nevertheless, in spite of removal of the

surface of the QD, the presence of Cu related emission as well as presence of Cu in ICP-OES analysis suggests that Cu was not solely present in the surface of the QDs. The amount of Cu incorporated into the QDs as determined by ICP-OES measurement (about 1%) is lower than the stoichiometric amount of Cu added during the reaction (about 4%) as expected.

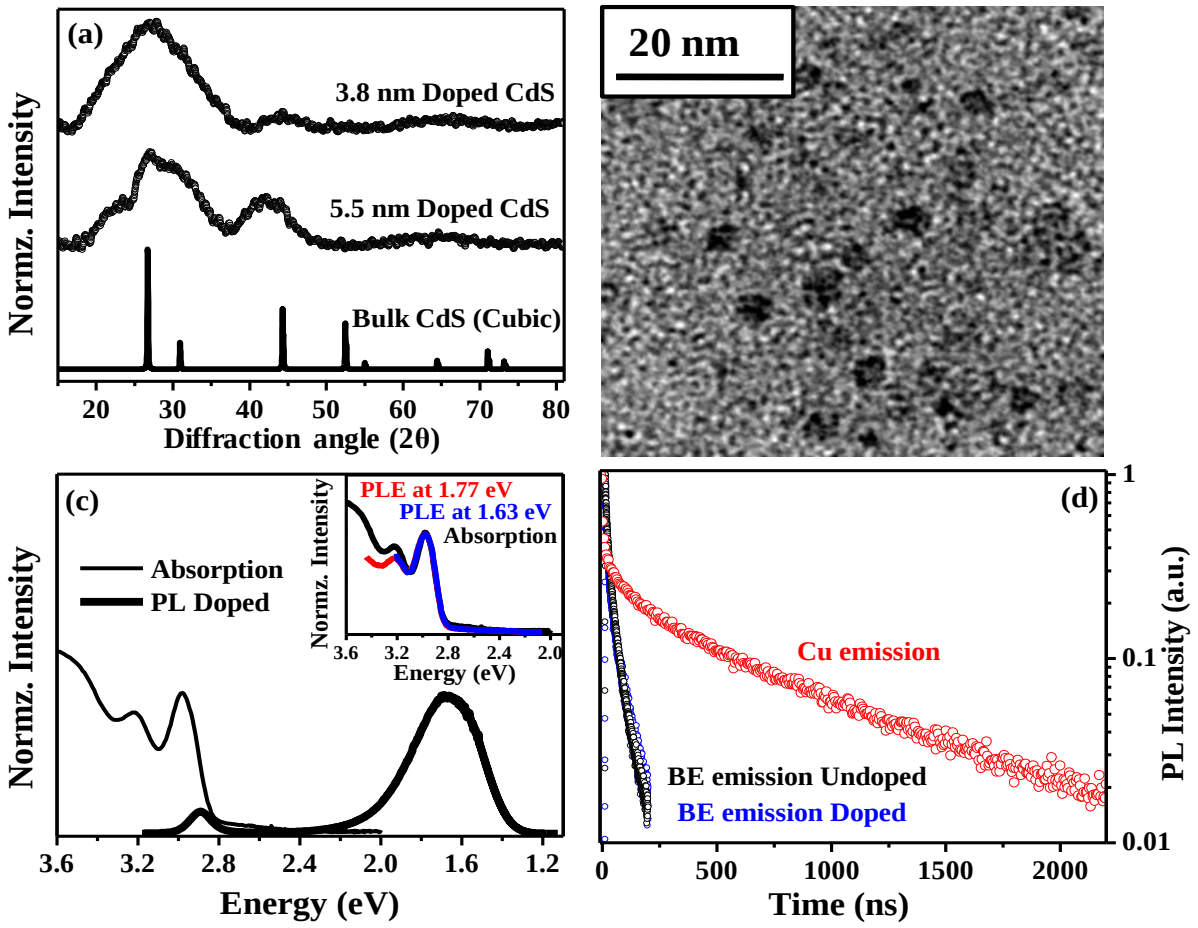

Figure 8.2. ***(a)*** *XRD patterns of bulk zinc blende CdS as well as the QD experimental (open circles) patterns of 3.8 nm and 5.5 nm particle CdS QDs.* ***(b)*** *Typical TEM image showing the formation of spherical particles of 3.8 nm particles. The inset shows the selected area electron diffraction pattern of these QDs showing the crystallinity of these particles.* ***(c)*** *Typical absorption (thin line) and PL data (thick line) of Cu doped CdS QDs. The inset shows the PLE data collected at different emission energies in the Cu emission region along with the absorption* ***(d)*** *Typical lifetime decay plots collected at band edge energy (black line) and at Cu related emission peak (red line).*

Typical XRD pattern as well as the TEM image of Cu doped CdS QDs are shown in Figures 8.2(a) and 8.2(b) respectively. XRD pattern clearly show the formation of CdS QDs when compared to the bulk data obtained from Inorganic Crystal Structure Database. However, the pattern was broadened (shown in Figure 8.2(a)) due to their small size and the

size of the particles were determined using the Scherrer formula. TEM measurements on the same samples is shown in Figure 8.2(b) and is found to have an average size of about 3.9 nm. It is important to note that the size of the QDs obtained by this procedure for both doped and undoped samples was found to be similar implying that the size and crystal structure have not changed after doping Cu.

The optical properties of these materials were measured using absorption and steady state and TrPL as shown in Figures 8.2(c) and 8.2(d). As expected the absorption of the QDs is blue shifted with respect to the bulk due to their small size. However, it is interesting to note that PL emission peak is drastically red shifted since the spectrum is dominated by the Cu related emission and band edge emission is largely suppressed. The origin of the Cu related emission has been extensively discussed in earlier literature reports[19-21, 25] and is concluded to be due to the coupling of the conduction band-edge to the level associated with the Cu impurity. Additionally, the large bandwidth of the Cu related emission has also been extensively investigated[25] and is concluded to arise from the intrinsic nature of this emission. Similar to these reports, PLE spectra measured at various energies of the Cu related emission is found to be exactly similar to the absorption spectra as shown in the inset to Figure 8.2(c) suggesting that the origin of the band width of the Cu emission is independent of the size distribution. The typical lifetimes of the band edge emission peak and the Cu related emission are shown in Figure 8.2(d) and it is interesting to note that while the lifetime of the band edge emission is of the order of 30-60 ns, Cu related emission is stable in the excited state for upto a 1000 ns, confirming that the peak is not due to the surface states and is due to the weak spatial overlap between the CB electron wave function and the localized Cu state.

Both TOP and oleic acid are used as ligands during the synthesis of CdS QDs. Oleic acid is known to passivate the electron traps on the CdS QD surface as studied in **Chapter 6**. The Cu related emission thus obtained in CdS QDs is observed to possess a QY of upto 35% with lifetimes in the range of 0.8 to 1 μs as well as wide energy range emission acting as a bridge between the visible and NIR regions. Additionally, since the Cu related emission arises due to a transition from conduction band of the host to the Cu *d* level, this emission can be tuned as a function of size even within the same material, thus retaining all the advantages of these materials while fine-tuning the peak energy to meet the needs of the specific application. Typical absorptions and emission for various sizes of CdS QDs are shown in Figure 8.3(a)

with emission maxima varying from 1.9 eV to 1.35 eV. The PL QY of these materials was found to be between 25-35% in the NIR region. While these characteristics are useful for broad band phosphor materials, thermal stability would be essential for practical uses as phosphor materials. Hence, we heated both toluene solution of these materials as well as thin films over a period of about 6 hours to 100 ^{o}C while retaining the film or solution at any given temperature for about an hour. The results of these experiments are shown in Figures 8.3(b) and 8.3(c) for a solution and thin film respectively. The normalized area under each of the plot is plotted in Figure 8.3(d) and from the figure it is evident that the material is relatively unaltered upto 100 ^{o}C in solution and loses only about 20% of the emission QY in case of thin films. This extraordinary thermal stability and thermal reversibility is found to be unlike other previously reported Cu doped materials thus making them ideal materials for several applications.

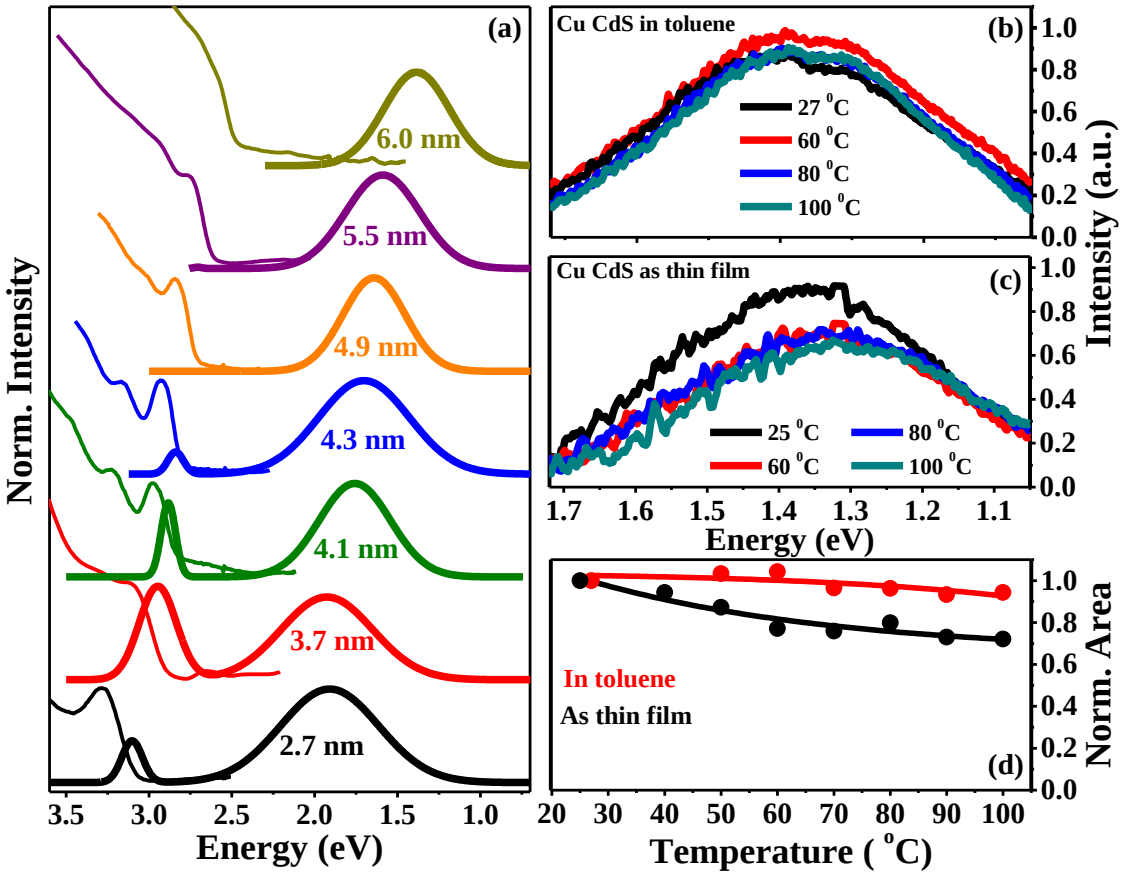

Figure 8.3. (a) *Typical absorption (thin line) and PL plots (thick line) of different sizes of Cu doped CdS QDs. Thermal stability obtained by heating the sample and collecting the Cu related emission at high temperature for* ***(b)*** *a toluene solution of doped QDs and* ***(c)*** *thin film of doped QDs.* ***(d)*** *The normalized PL area plotted as a function of temperature both for solution (red dots) and thin film (black dots).*

8.5. Conclusions:

We observe that Cu doped CdS QDs can be synthesized with high QY and broad band emission with single exponential decay of the emission by using oleic acid as a ligand which is known to passivate the electron traps on CdS QD surface. The Cu related emission of these materials, for the case of CdS QDs lie in the NIR energy range that bridges the gap between visible and IR region. Using this systematic study, we have optimized the QY of the Cu related emission in these materials to about 35%. We have also studied the thermal stability of this emission and found it to be surprisingly stable upto 100 ^{o}C thus making these materials ideal for phosphor applications.

Section II

Visible Photo Responsive Cu and Fe co-doped ZnS Quantum Dots

8.6. Abstract:

Upon doping Fe in Cu doped ZnS QDs, a broad absorption band in visible region was observed. The doping in these QDs is shown to have a high photo-response in the visible region unlike their undoped counterparts that is only effective in the UV region leading to light sensing applications.

8.7. Introduction:

Photo detectors with UV-visible-NIR spectral response gained a great attention due to their various applications in image sensing, communication and environmental monitoring.[26, 27] Here, in this section, we focus on potential materials for visible photo detectors. Crystalline Si is one of the most studied system that has been used for visible light detection.[28] But it has its own limitations e.g. its absorption remains weak over the entire spectrum, only exceeding 10^4 cm^{-1} at 500 nm.[29] Oxide semiconductors were found to be good candidates to replace Si in many electrical devices.[30] Oxide semiconductor based devices are transparent due to their very high band gap and so limited to UV light detection.[31] Efforts were made to improve the visible light response of these oxide semiconductors to some extent with the help of a polymer material as photo absorbing layer.[32] One of the other ways of make use of these oxide materials is by mixing with semiconductor QDs.[33] Doping (p-type) in NiO results in visible light sensing.[34] Other than these oxide materials, there are an extensive reports on the UV based photo detectors which are based on high band gap materials such as ZnO and ZnS nano structures.[35-37] Semiconductor materials like CdS,[38] ZnTe[39] and In_2S_3[40] show visible photo response while InGaAs,[41] InAs[42] and Cd_3P_2[43] are good for NIR light detection. However, most of these materials are toxic in nature especially those suitable in the visible and NIR spectral window. Hence, the search for developing visible light sensitive materials made up of earth abundant, low toxic and less expensive is still ongoing.

Among the variety of approaches studied, one of the approaches of attaining visible light sensitive materials is by altering the properties of UV absorbing materials like ZnO and ZnS such that they show visible photo response. It was shown in the literature that doping into ZnO and TiO_2 strongly affects their band gap.[44, 45] In this section, we tuned the optical properties of high band gap material ZnS by co-doping with Cu and Fe and show that it can be used as low toxic visible light response material.

8.8. Experimental section:

8.8.1. Materials:

CuI, Iron acetylacetonate, zinc acetate, zinc stearate, S powder, DDT, oleic acid (90%), oleylamine (70%), TOP (90%) and ODE (90%) were purchased from Sigma-Aldrich. Hexane, methanol and acetone were obtained from SD Fine chemicals. All the purchased chemicals were used without any further purification.

0.2 M zinc oleate was prepared by heating 367 mg of zinc acetate to 200 ^{o}C in presence of 1.13 g of oleic acid and 7 mL of ODE to from a clear solution. Once zinc oleate is formed, the reaction mixture is allowed to cool down to room temperature. Approximately, 3 mL of oleylamine is added to the reaction mixture to prevent the solidification of zinc oleate solution at room temperature.

ZnS was obtained by mixing 6 mL of zinc oleate with 2.5 mL of DDT and 2 mL of oleic acid at room temperature.

8.8.2. Synthesis of Cu and Fe co-doped ZnS QDs:

0.1 mmol (19 mg) of CuI, 0.1 mmol (35 mg) of Iron acetylacetonate and10 mL of oleylamine were degassed in a three-necked flask for one hour at 80 ^{o}C and then the reaction mixture was back-filled with Ar. The temperature of the reaction was raised to 250 ^{o}C where 2 mL of TOP was swiftly injected into the reaction mixture. Then, the reaction mixture was annealed for two hours at this temperature. After two hours, ZnS solution was added to the reaction mixture in a drop-wise manner three times in regular intervals of 45 minutes. After addition of complete ZnS solution into the reaction mixture, the reaction mixture was annealed for 4-5 hours till the reaction mixture turns into thick black coloured solution. The sample was washed using hexane/methanol mixture and then precipitated by adding excess of acetone. The undoped ZnS QDs were prepared by simply mixing Zinc stearate and S in ODE at 270 ^{o}C.

8.8.3. Dark and photo response measurements of undoped and co-doped QDs:

I-V characteristics of undoped ZnS and Cu and Fe co-doped ZnS QDs were measured with Solar simulator (Newport, model: 91160-1000, 300W Xe lamp) equipped with AM 1.5G filter

with the simulated light intensity adjusted to 100 mW cm^{-2}. The sample is coated on a ITO substrate and the Au electrodes were used as contacts from the sample to the source meter.

8.9. Results and discussion:

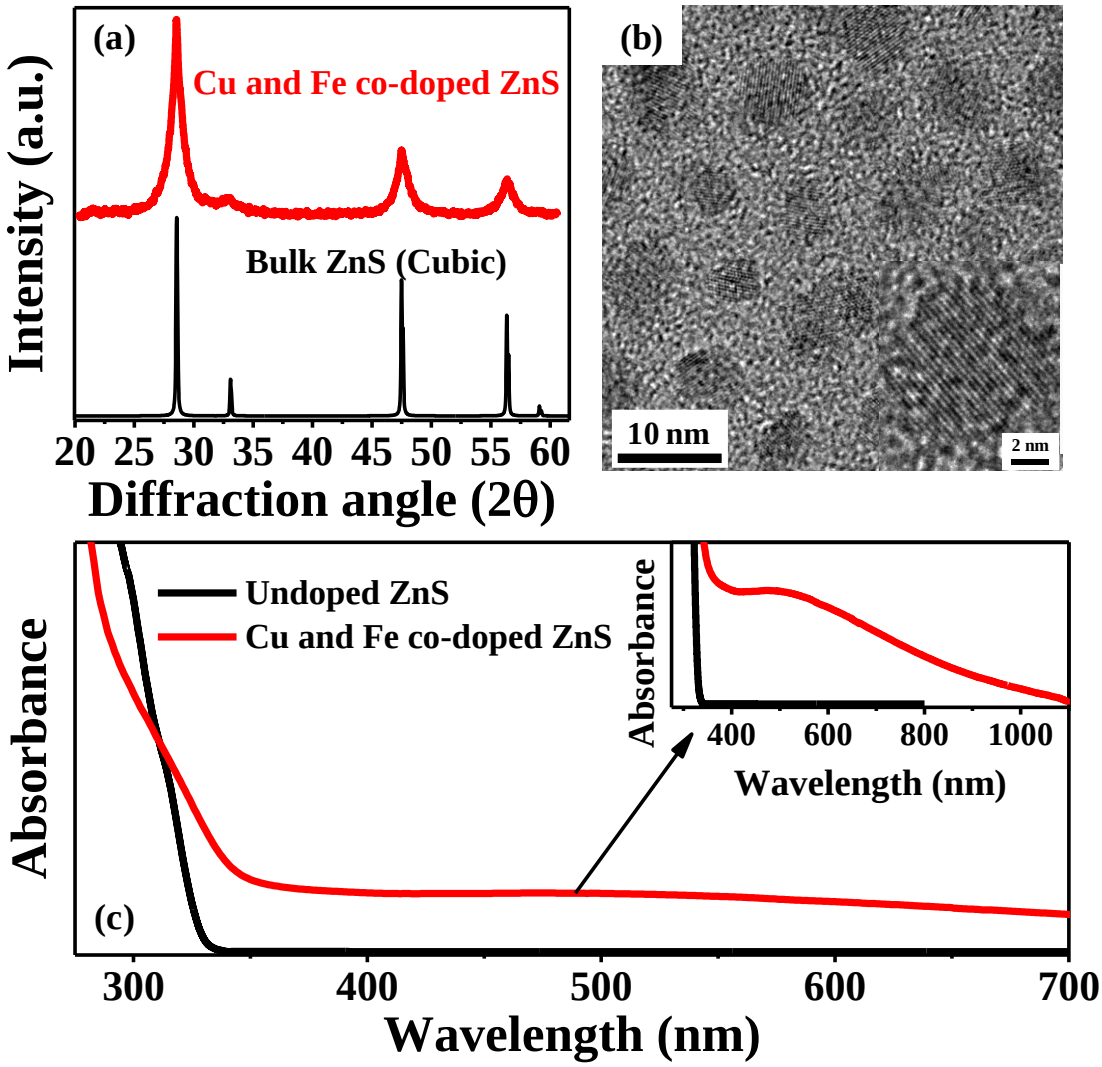

Figure 8.4. (a) *XRD pattern of Cu and Fe co-doped ZnS QDs along with the bulk cubic ZnS pattern.* ***(b)*** *TEM image of Cu and Fe co-doped ZnS QDs. Inset shows the high-resolution TEM image of the co-doped QDs* ***(c)*** *Absorption spectra of the undoped and co-doped ZnS QDs and the inset shows the magnified portion of the spectrum of the co-doped QDs in the visible region.*

Cu and Fe co-doped QDs were synthesized by adding ZnS precursor to the solution containing Cu and Fe in presence of oleylamine as explained in experimental section. The formation of the QDs was first confirmed by XRD as shown in Figure 8.4(a). The XRD pattern of the formed sample matches well with the bulk cubic ZnS. Though XRD does not confirm the doping of

Cu or Fe into ZnS lattice, elemental analysis (ICP-OES) shows the presence of Cu (6%) and Fe (5%) in the doping regime. The presence of broad peaks in the XRD pattern of doped dots compared to the bulk XRD pattern as shown in Figure 8.4(a) suggests the formation of very small particles. The formation of small particles was further confirmed from TEM image as shown in Figure 8.4(b). The size of the particles is estimated to be around 5-6 nm and the size distribution of the particles is small as observed from the figure. The crystallinity of the particles is also observed from the high resolution TEM image which is shown as an inset of Figure 8.4(b). Figure 8.4(c) shows the optical characterization of the undoped and co-doped ZnS QDs. The undoped ZnS QDs (black line in the figure) show a band gap in the UV regime as expected for ZnS which is a high band gap material. On the other hand, the co-doped sample (red line) shows an extra band in the visible regime around 600 nm along with the similar absorption band in the UV region. This can be clearly seen in the inset of this figure. The origin of this extra visible band is not clear at this moment. These doped dots contain the absorption band (shorter wavelength) similar to the case of undoped dots and this might be due to the inherent nature of the co-doped dots with two absorption bands or it may be just due to the presence of undoped portion present in the sample.

The main aim of this section is to measure the photo response of these doped dots. We have performed the I-V measurements on the undoped and co-doped samples as shown in Figure 8.5 and the device details are given in the experimental section. Figures 8.5(a) and 8.5 (b) show the I-V characteristics of undoped and co-doped ZnS QDs in dark and with the illumination of light. It can be observed that both the undoped and co-doped dots show the enhancement of current when they are illuminated with the Xe lamp compared to dark response. The photo-response is similar to observations in literature as well as in the case of undoped ZnS in UV region.

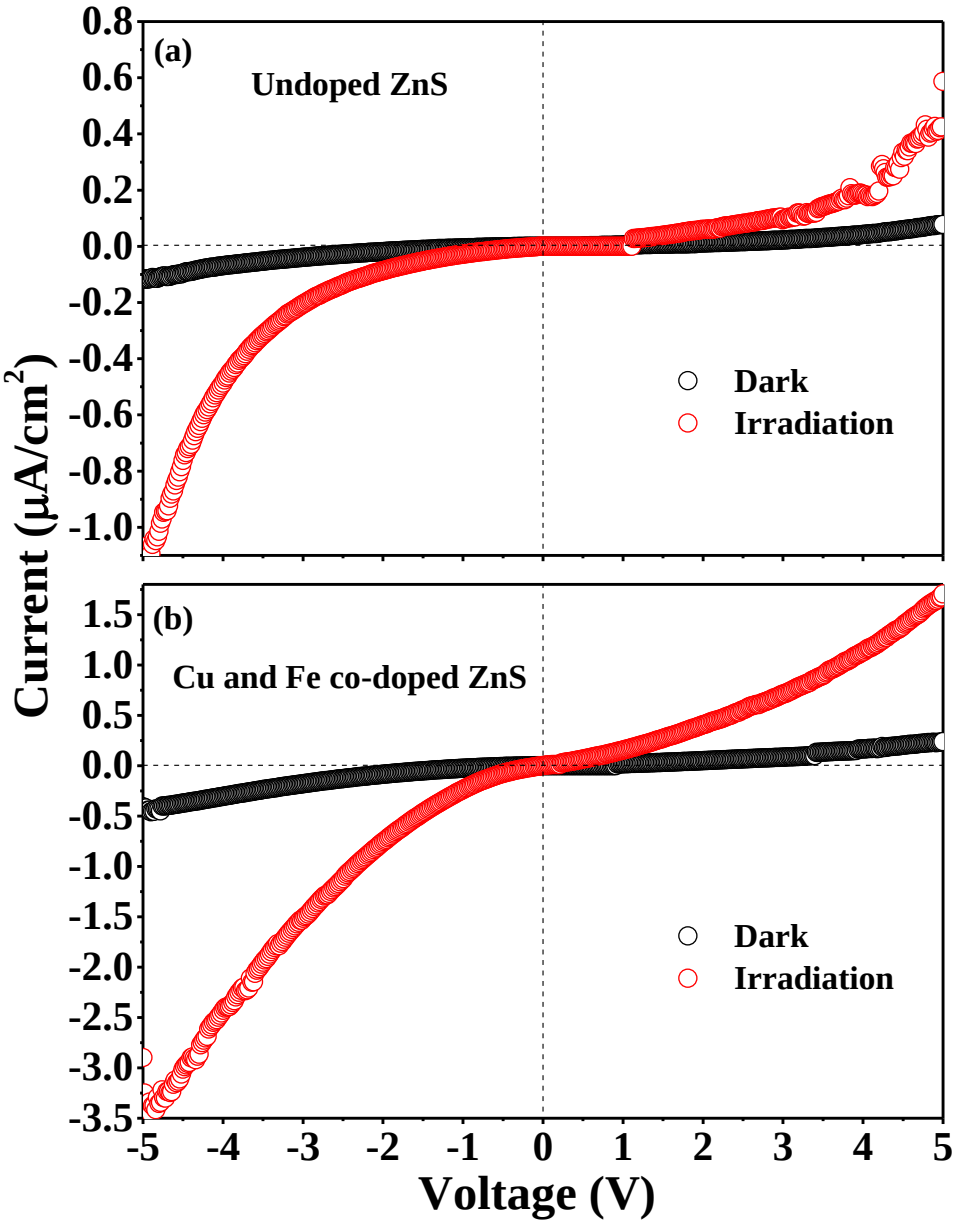

Figure 8.5. *The I-V characteristics of* ***(a)*** *undoped and* ***(b)*** *co-doped QDs in dark and with the irradiation of light using Xe lamp.*

However, there exists an extra visible absorption band in the co-doped QDs which is not present in the undoped QDs. To find out whether there is any contribution of this visible absorption band to the photo response of these co-doped QDs (shown in Figure 8.5(b)), we have measured their photo response by using cut off filters which blocks the light of shorter wavelengths as shown in Figure 8.6. A 450-nm filter only allows the light of wavelengths greater than 450 nm.

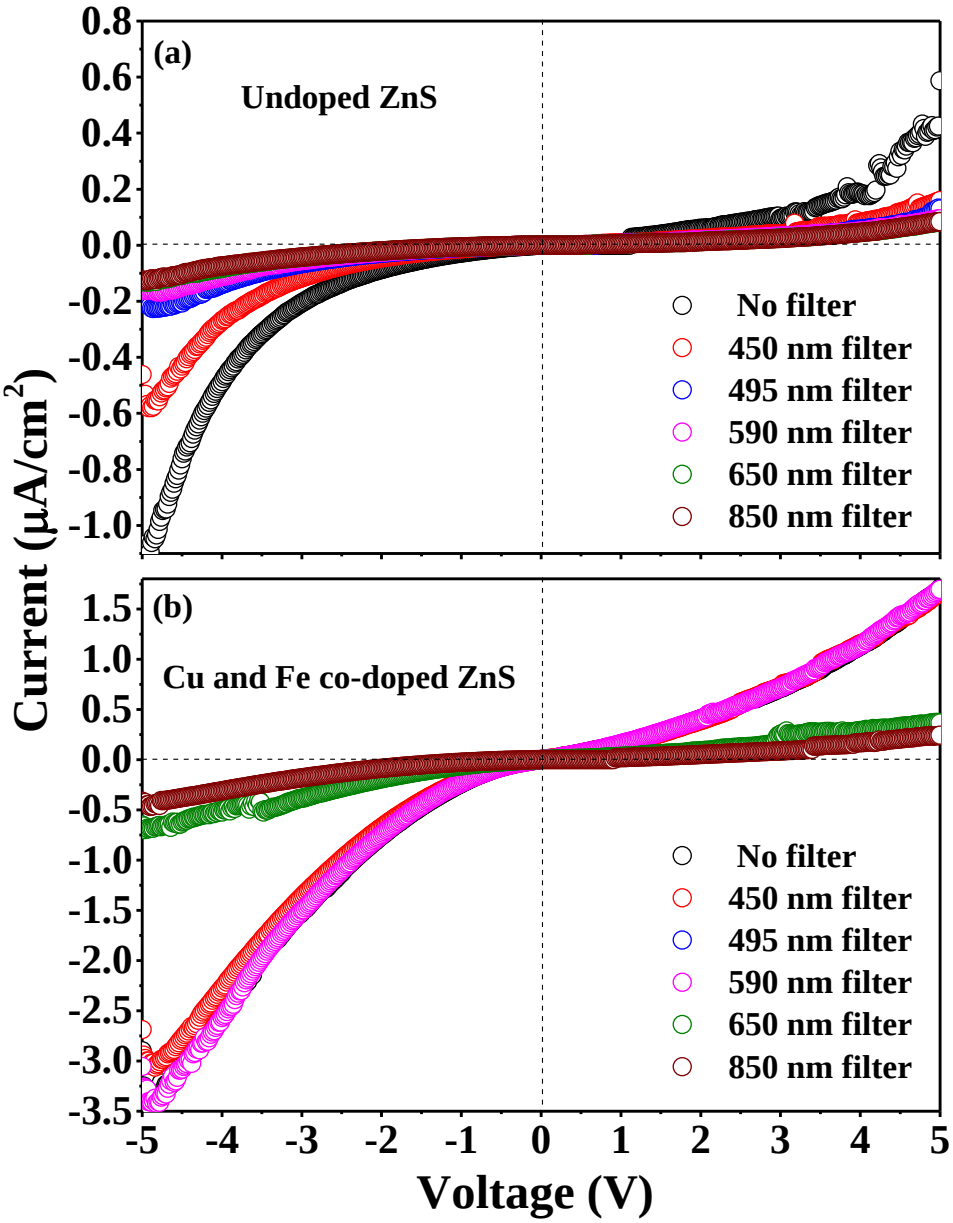

Figure 8.6. *The phot response of* ***(a)*** *undoped and* ***(b)*** *co-doped QDs by using different cut off filters.*

In case of undoped QDs, the photo current gradually decreases with increasing the wavelength of cut off filters as shown in Figure 8.6(a). There is a decrease in photo response even with a 450 nm-filter and it decreases further with increase in the wavelength of the cut off filters. This suggests that undoped ZnS QDs are effective only in UV regime. On the other hand, the co-doped QDs show photo response in the visible region also as shown in Figure 8.6(b). The photo response is almost unchanged even with the use of 590-nm filter but

thereafter it diminishes. This shows that these Cu and Fe co-doped ZnS QDs can be good candidates for visible light detection.

8.10. Conclusions:

Cu and Fe co-doped ZnS QDs are successfully synthesized. The co-doping results in an extra visible absorption band. The co-doped QDs show both UV and visible photo response whereas their undoped counterparts are only effective in the UV region. These co-doped QDs can be potential candidates for non-toxic and environmentally benign visible photo detectors.

Bibliography:

[1] Z. Chen, L. Zhang, Y. Sun, J. Hu, D. Wang, *Adv. Funct. Mater.* **2009**, *19*, 3815.

[2] H. Q. Wang, M. Batentschuk, A. Osvet, L. Pinna, C. J. Brabec, *Adv. Mater.* **2011**, *23*, 2675.

[3] A. Shalav, B. S. Richards, T. Trupke, K. W. Kramer, H. U. Gudel, *Appl. Phys. Lett.* **2005**, *86*, 013505.

[4] W. Van Sark, A. Meijerink, R. E. I. Schropp, J. A. M. Van Roosmalen, E. H. Lysen, *Sol. Energy Mater. Sol. Cells* **2005**, *87*, 395.

[5] J. Qiao, L. Duan, L. Tang, L. He, L. Wang, Y. Qiu, *J. Mater. Chem.* **2009**, *19*, 6573.

[6] G. Qian, Z. Zhong, M. Luo, D. Yu, Z. Zhang, Z. Y. Wang, D. Ma, *Adv. Mater.* **2008**, *21*, 111.

[7] Y. Yang, R. T. Farley, T. T. Steckler, S. H. Eom, J. R. Reynolds, K. S. Schanze, J. Xue, *Appl. Phys. Lett.* **2008**, *93*, 163305.

[8] L. Han, F. Song, S. Q. Chen, C. G. Zou, X. C. Yu, J. G. Tian, J. Xu, X. Xu, G. Zhao, *Appl. Phys. Lett.* **2008**, *93*, 11110.

[9] N. Tessler, V. Medvedev, M. Kazes, S. H. Kan, U. Banin, *Science* **2002**, *295*, 1506.

[10] M. J. Panzer, V. Wood, S. M. Geyer, M. G. Bawendi, V. Bulovic, *J. Disp. Tech.* **2010**, *6*, 90.

[11] C. C. Lin, R. S. Liu, *J. Phys. Chem. Lett.* **2011**, *2*, 1268.

[12] N. Pradhan, X. Peng, *J. Am. Chem. Soc.* **2007**, *129*, 3339.

[13] S. Kim, B. Fisher, H. J. Eisler, M. Bawendi, *J. Am. Chem. Soc* **2003**, *125*, 11466.

[14] T. Franzl, J. Muller, T. A. Klar, A. L. Rogach, J. Feldmann, D. V. Talapin, H. Weller, *J. Phys. Chem. C* **2007**, *111*, 2974.

[15] A. Avidan, D. Oron, *Nano Lett.* **2008**, *8*, 2384.

[16] N. Pradhan, D. Goorskey, J. Thessing, X. Peng, *J. Am. Chem. Soc.* **2005**, *127*, 17586.

[17] N. Pradhan, D. M. Battaglia, Y. Liu, X. Peng, *Nano Lett.* **2007**, *7*, 312.

[18] D. Chen, R. Viswanatha, G. L. Ong, R. Xie, M. Balasubramaninan, X. Peng, *J. Am. Chem. Soc.* **2009**, *131*, 9333.

[19] N. S. Karan, D. D. Sarma, R. M. Kadam, N. Pradhan, *J. Phys. Chem. Lett.* **2010**, *1*, 2863.

[20] R. Viswanatha, S. Brovelli, A. Pandey, S. A. Crooker, V. I. Klimov, *Nano Lett.* **2011**, *11*, 4753.

[21] B. B. Srivastava, S. Jana, N. Pradhan, *J. Am. Chem. Soc.* **2011**, *133*, 1007.

[22] R. Xie, X. Peng, *J. Am. Chem. Soc.* **2009**, *131*, 10645.

[23] P. N. Tananaev, S. G. Dorofeev, R. B. Vasil'ev, T. A. Kuznetsova, *Inorg. Mater.* **2009**, *45*, 347.

[24] X. Michalet, F. F. Pinaud, L. A. Bentolila, J. M. Tsay, S. Doose, J. J. Li, G. Sundaresan, A. M. Wu, S. S. Gambhir, S. Weiss, *Science* **2005**, *307*, 538.

[25] S. Brovelli, C. Galland, R. Viswanatha, V. I. Klimov, *Nano Lett.* **2012**, *12*, 4372.

[26] G. Konstantatos, E. H. Sargent, *Nat. Nanotechnol.* **2010**, *5*, 391.

[27] G. Konstantatos, J. Clifford, L. Levina, E. H. Sargent, *Nat. Photonics* **2007**, *1*, 531.

[28] S. Mridha, D. Basak, *J. Appl. Phys.* **2007**, *101*, 083102.

[29] C. M. Herzinger, B. Johs, W. A. McGahan, J. A. Woollam, W. Paulson, *J. Appl. Phys.* **1998**, *83*, 3323.

[30] T. Sakai, H. Seo, S. Aihara, M. Kubota, N. Egami, D. Wang, M. Furuta, *Jpn. J. Appl. Phys.* **2012**, *51*, 010202.

[31] T. H. Chang, C. J. Chiu, S. J. Chang, T. Y. Tsai, T. H. Yang, Z. D. Huang, W. Y. Weng, *Appl. Phys. Lett.* **2013**, *102*, 221104.

[32] H.-W. Zan, W.-T. Chen, H.-W. Hsueh, S.-C. Kao, M.-C. Ku, C.-C. Tsai, H.-F. Meng, *Appl. Phys. Lett.* **2010**, *97*, 221104.

[33] X. Liu, X. Yang, M. Liu, Z. Tao, Q. Dai, L. Wei, C. Li, X. Zhang, B. Wang, A. Nathan, *Appl. Phys. Lett.* **2014**, *104*, 113501.

[34] J. Mallows, M. Planells, V. Thakare, R. Bhosale, S. Ogale, N. Robertson, *ACS Appl. Mater. Interfaces* **2015**, *7*, 27597.

[35] X. Wang, Z. Xie, H. Huang, Z. Liu, D. Chen, G. Shen, *J. Mater. Chem.* **2012**, *22*, 6845.

[36] L. Hu, J. Yan, M. Liao, H. Xiang, X. Gong, L. Zhang, X. Fang, *Adv. Mater.* **2012**, *24*, 2305.

[37] O. Game, U. Singh, T. Kumari, A. Banpurkar, S. Ogale, *Nanoscale* **2014**, *6*, 503.

[38] H. Li, X. Wang, J. Xu, Q. Zhang, Y. Bando, D. Golberg, Y. Ma, T. Zhai, *Adv. Mater.* **2013**, *25*, 3017.

[39] Z. Liu, G. Chen, B. Liang, G. Yu, H. Huang, D. Chen, G. Shen, *Opt. express* **2013**, *21*, 7799.

[40] X. Xie, G. Shen, *Nanoscale* **2015**, *7*, 5046.

[41] H. Tan, C. Fan, L. Ma, X. Zhang, P. Fan, Y. Yang, W. Hu, H. Zhou, X. Zhuang, X. Zhu, *Nano-Micro Letters* **2016**, *8*, 29.

[42] J. Miao, W. Hu, N. Guo, Z. Lu, X. Zou, L. Liao, S. Shi, P. Chen, Z. Fan, J. C. Ho, *ACS Nano* **2014**, *8*, 3628.

[43] C. Yang, H. Pan, S. Liu, S. Miao, W.-H. Zhang, J. Jie, X. Xu, *Chem. Commun.* **2015**, *51*, 2593.

[44] H. Qin, W. Li, Y. Xia, T. He, *ACS Appl. Mater. Interfaces* **2011**, *3*, 3152.

[45] S. Kouser, S. R. Lingampalli, P. Chithaiah, A. Roy, S. Saha, U. V. Waghmare, C. N. R. Rao, *Angew. Chem. Int. Ed.* **2015**, *54*, 8149.

List of Publications

1) Study of Surface and Bulk Electronic Structure of II-VI Semiconductor Nanocrystals Using Cu as a Nanosensor.

G Krishnamurthy Grandhi, Renu Tomar and R. Viswanatha

ACS Nano **2012,** *6*, 9751.

2) Tunable Infrared Phosphors Using Cu Doping in Semiconductor Nanocrystals: Surface Electronic Structure Evaluation.

G Krishnamurthy Grandhi and R. Viswanatha

J. Phys. Chem. Lett. **2013**, *4*, 409.

3) Cu Doping in Ligand Free CdS Nanocrystals: Conductivity and Electronic Structure Study.

G Krishnamurthy Grandhi, K. Swathi, K.S. Narayan and R. Viswanatha

J. Phys. Chem. Lett. **2014**, 5, 2382.

4) Understanding the Role of Surface Capping Ligands in Passivating the Quantum Dots Using Copper Dopants as Internal Sensor.

G Krishnamurthy Grandhi, Arunkumar M. and R. Viswanatha

J. Phys. Chem. C **2016**, *120*, 19785.

5) Demystifying Complex Quantum Dot Heterostructures Using Photo-generated Charge Carrier Delocalization.

G Krishnamurthy Grandhi and R. Viswanatha

Manuscript submitted.

6) Low Temperature Dynamics of Surface and Bulk Electronic Structure of Quantum Dots.

G Krishnamurthy Grandhi, Renu Tomar and R. Viswanatha

Manuscript under preparation.

1.2. Doping in bulk semiconductors-Addendum

(At the end of the second paragraph in the section 1.2 (page no. 10))

Optically active doping in II-VI bulk semiconductors:

Mn doping into II-VI semiconductors was also widely studied which is known to alter the electronic structure of the host materials.[89-91] Mn doping into ZnO mainly affect the absorption properties of the material.[89] Mn doping into ZnS results in a PL emission at 2.1 eV which is due to $^4T_1$ to $^6A_1$ transition of dopant energy levels.[90] Dopants such as Ge and V also affect the optical properties of II-VI semiconductors. For example, Ge doping into CdTe leads to appearance or enhancement of two new bands at 0.91 eV and 0.81 eV and suppresses the 1.40 eV band which is usually present in undoped CdTe. This is due to compensation of deep Cd donor levels with the doping.[92] The doping in II-VI semiconductors also alter the band gap of host material. It was found that Al and Sb doping also alter the band gap of CdTe thin films where the band gap of CdTe decreases with increase in the dopant concentration.[93] Similarly, varying the concentration of Ag dopants results in band gap tuning in ZnSe.[94]

Bibliography:

[89] T. Mizokawa, T. Nambu, A. Fujimori, T. Fukumura, M. Kawasaki, *Phys. Rev. B* **2002**, *65*, 085209.

[90] M. Godlewski, S. Yatsunenko, M. Zalewska, A. Kłonkowski, T. Strachowski, W. Łojkowski, in *Solid State Phenomena, Vol. 128*, Trans Tech Publ, **2007**, pp. 123.

[91] I. P. McClean, C. B. Thomas, *Semicond. sci. Technol.* **1992**, *7*, 1394.

[92] U. Pal, P. Fernandez, J. Piqueras, N. V. Sochinskii, E. Dieguez, *J. Appl. Phys.* **1995**, *78*, 1992.

[93] A. A. J. Al-Douri, F. Y. Al-Shakily, M. F. A. Alias, A. A. Alnajjar, *Adv Cond Matter Phys.* **2010**, *2010*, 974684(1-5).

[94] Y. Xi, L. El Bouanani, Z. Xu, M. A. Quevedo-Lopez, M. Minary-Jolandan, *J. Mater. Chem. C* **2015**, *3*, 9781.

1.3. Doping in semiconductor QDs-Addendum

(Just after the main heading of section 1.3 (page no. 10))

Overview of the optically active doping in II-VI semiconductor QDs:

Intentional doping of foreign atoms can be useful in altering the host QD properties. The doping into QDs is of greater interest for the fundamental and advanced research. Among these dopants, transition metal ion doped QDs were widely studied by various research groups. The presence of dopants tune the magnetic, electrical and optical properties of the host semiconductor QD material.

Among these transition metal dopants, Mn doping has been one of the widely-studied system for nearly two decades[3,50,52,55,70] due to its constant PL emission energy around 560 nm irrespective of the host band gap. The Mn emission occurs due to the interaction of photo-excited host material with the dopant levels though mechanism is not clearly understood.[69] Also, the Mn emission peak is expected to be narrow in width as it occurs between two atomic states. However, relatively broader Mn PL peak is observed. It was earlier shown that the broadness of the Mn PL peak arises due to the vibronic coupling of these two states.[69] Recent studies show that the Mn emission can be tuned from 480-580 nm by varying the strain around the Mn centre.[95,96] This suggests that the broad Mn emission observed earlier is mainly due to presence of Mn centres of different strain values. Over the years, PL QY of the Mn dopant reached more than 50%[58,70] and also the synthetic techniques were modified to achieve the high quality Mn doped QDs on the gram-scale.[70] Meanwhile, Cu doping in II-VI semiconductors also has been widely studied where Cu introduces the dopant levels in between CB and VB of host.[60,73,75] The emission mechanism of Cu dopant emission is different from that of Mn dopant and this will be discussed in detail in the following subsections. Other optical dopants such as Ag, Cr and Ni[67,72] also introduce mid-gap states and gives rise to the dopant emission though they are not as widely investigated as Mn and Cu.

Bibliography:

[3] P. K. Santra, P. V. Kamat, *J. Am. Chem. Soc.* **2012**, *134*, 2508.

[50] R. N. Bhargava, D. Gallagher, X. Hong, A. Nurmikko, *Phys. Rev. Lett.* **1994**, *72*, 416.

[52] D. J. Norris, N. Yao, F. T. Charnock, T. A. Kennedy, *Nano Lett.* **2001**, *1*, 3.

[55] F. V. Mikulec, M. Kuno, M. Bennati, D. A. Hall, R. G. Griffin, M. G. Bawendi, *J. Am. Chem. Soc.* **2000**, *122*, 2532.

[58] N. Pradhan, D. Goorskey, J. Thessing, X. Peng, *J. Am. Chem. Soc.* **2005**, *127*, 17586.

[60] P. N. Tananaev, S. G. Dorofeev, R. B. Vasil'ev, T. A. Kuznetsova, *Inorg. Mater.* **2009**, *45*, 347.

[67] S. Jana, B. B. Srivastava, S. Jana, R. Bose, N. Pradhan, *J. Phys. Chem. Lett.* **2012**, *3*, 2535.

[69] R. Beaulac, P. I. Archer, S. T. Ochsenbein, D. R. Gamelin, *Adv. Funct. Mater.* **2008**, *18*, 3873.

[70] B. B. Srivastava, S. Jana, N. S. Karan, S. Paria, N. R. Jana, D. D. Sarma, N. Pradhan, *J. Phys. Chem. Lett.* **2010**, *1*, 1454.

[72] S. Jana, G. Manna, B. B. Srivastava, N. Pradhan, *Small* **2013**, *9*, 3753.

[73] B. B. Srivastava, S. Jana, N. Pradhan, *J. Am. Chem. Soc.* **2011**, *133*, 1007.

[75] R. Viswanatha, S. Brovelli, A. Pandey, S. A. Crooker, V. I. Klimov, *Nano Lett.* **2011**, *11*, 4753.

[95] A. Hazarika, A. Pandey, D. D. Sarma, *J. Phys. Chem. Lett.* **2014**, *5*, 2208.

[96] A. Hazarika, A. Layek, S. De, A. Nag, S. Debnath, P. Mahadevan, A. Chowdhury, D. D. Sarma, Phys. *Rev. Lett.* **2013**, *110*, 267401.